INFORMATION TO USERS

This manuscript has been reproduced from the microfilm master. UMI films the text directly from the original or copy submitted. Thus, some thesis and dissertation copies are in typewriter face, while others may be from any type of computer printer.

The quality of this reproduction is dependent upon the quality of the copy submitted. Broken or indistinct print, colored or poor quality illustrations and photographs, print bleedthrough, substandard margins, and improper alignment can adversely affect reproduction.

In the unlikely event that the author did not send UMI a complete manuscript and there are missing pages, these will be noted. Also, if unauthorized copyright material had to be removed, a note will indicate the deletion.

Oversize materials (e.g., maps, drawings, charts) are reproduced by sectioning the original, beginning at the upper left-hand corner and continuing from left to right in equal sections with small overlaps. Each original is also photographed in one exposure and is included in reduced form at the back of the book.

Photographs included in the original manuscript have been reproduced xerographically in this copy. Higher quality 6" x 9" black and white photographic prints are available for any photographs or illustrations appearing in this copy for an additional charge. Contact UMI directly to order.

UMI®

Bell & Howell Information and Learning
300 North Zeeb Road, Ann Arbor, MI 48106-1346 USA
800-521-0600

STUDY OF DRIVER-SEAT INTERACTIONS AND ENHANCEMENT OF VEHICULAR RIDE VIBRATION ENVIRONMENT

Xuting Wu

A thesis

in

the Department

of

Mechanical Engineering

Presented in Partial Fulfillment of the Requirements
for the Degree of Doctor of Philosophy
at Concordia University
Montréal, Québec, Canada

December 1998

ABSTRACT

STUDY OF DRIVER-SEAT INTERACTIONS AND ENHANCEMENT OF VEHICULAR RIDE VIBRATION ENVIRONMENT

Xuting Wu, Ph.D.
Concordia University, 1998

Prolonged exposure to vehicular vibration and shocks has been related to discomfort, reduced work efficiency and various health and safety risks for the drivers, specifically for the off-road vehicle drivers. Enhancement of shock and vibration environment of such vehicles involves characterization of vibration environment, biodynamic response of the driver, design and analysis of secondary suspension, and seating dynamics. Relationships between biodynamic measures are derived through analysis of measured data and selected biodynamic models. The response measures exhibit high sensitivity to variations in subject characteristics and test conditions. The magnitude of such variations can be significantly reduced by representing 'to-the-body' biodynamic characteristics in terms of apparent mass (APMS) and by identifying a range of test conditions applicable to off-road vehicle driving. It is further shown that normalized APMS correlates well with the 'through the body' biodynamic function, expressed in terms of seat-to-head transmissibility (STHT). A synthesis of reported data, applicable within the identified range of conditions, is performed to propose a range of idealized biodynamic response characteristics. A three degree-of-freedom biodynamic model of the occupant is developed using measured 'to-the-body' and 'through-the-body' response characteristics. The model parameters are identified through solution of a constrained optimization function comprising magnitude and phase components of both response functions. The validity of the proposed model is demonstrated by comparing its response with the range of idealized values and measured data.

Occupant-seat interactions are investigated through measurement and analysis of distribution of contact force and area. The results are utilized to propose a nonlinear and asymmetric seat cushion model incorporating body hop motion and cushion bottoming

under high magnitude excitations. The proposed analytical model is validated using laboratory measured data. A nonlinear suspension seat model is further developed to incorporate asymmetric force-velocity and nonlinear force-deflection characteristics of the damper and elastic end-stops, respectively. A combined human-suspension seat model is finally derived upon integrating the proposed occupant, cushion and suspension models. The validity of the coupled model is thoroughly examined under harmonic and stochastic vibration excitations of different classes of vehicles. The results show that the proposed model can serve as an effective design and analysis tool for assessment of seating dynamic comfort and whole-body vibration exposure of vehicle drivers.

The results of a comprehensive parametric study clearly revealed that attenuation of continuous and shock-type excitations pose conflicting design requirements. It is thus proposed to develop suspension design for optimal attenuation of continuous vibration, while the severity of end-stop impacts caused by shock-type excitations be minimized through design of optimal buffers. The suspension performance under continuous and shock excitations is assessed in terms of Seat Effective Amplitude Transmissibility (SEAT) and Vibration Dose Value (VDV) ratio, respectively. Two different optimization problems are formulated to minimize the SEAT and VDV ratios. The first optimization problem is solved to achieve optimal stiffness and damping properties of the suspension, while the peak dynamic deflection is constrained to account for occasional end-stop impacts. The second optimization problem is solved to derive optimal properties of the end-stop buffers. The results suggest that soft and lightly damped suspension with low degree of damping asymmetry coupled with low friction and large mass can enhance vibration isolation performance. Thick and soft elastic buffers with linear stiffness characteristics result in low VDV ratio response. Although a thick buffer increases the frequency of impacts slightly, its low stiffness tends to reduce the severity considerably. The proposed design with optimal suspension and buffer parameters yields considerable reduction in both SEAT and VDV ratio response under selected classes of excitations.

ACKNOWLEDGEMENTS

I am sincerely grateful to my supervisors, Dr. Subhash Rakheja and Dr. Paul-Émile Boileau, for their initiation of the project and their constant guidance and dedication throughout the thesis work. Their valuable advice and contributions have helped to make the final appearance of this thesis.

I would like to acknowledge the support provided by Mr. Danius Juras in the experimental setups. The assistance provided by Ms. Susan Molloy in data digitization is further appreciated. I thank all the friends and colleagues who voluntarily participated in my experiments as test subjects.

I wish to acknowledge the contribution of various researchers whose data have been employed in this study. I am especially grateful to the Human Factors Research Unit, ISVR, University of Southampton, for allowing me to use some of the experimental data on suspension seat end-stop impacts.

Financial support provided by the Institut de recherche en santé et en sécurité du travail du Québec (IRSST) scholarship, FCAR scholarship, Concordia External Grant Holder Doctoral Scholarship, and Concordia International Tuition Fee Remission Award are gratefully acknowledged.

The encouragement and understanding of my wife, Xiaohong, make the completion of this thesis possible. Her essential assistance in the final stage is further acknowledged. I dedicate this thesis to her.

TABLE OF CONTENTS

CHAPTER 3

WHOLE-BODY BIODYNAMICS: DEVELOPMENT OF HUMAN BODY MODEL

CHAPTER 4

DEVELOPMENT OF A SEAT CUSHION MODEL THROUGH STUDY OF DYNAMIC PRESSURE DISTRIBUTION AT THE HUMAN-SEAT INTERFACE

CHAPTER 5

MODEL DEVELOPMENT OF HUMAN-SUSPENSION SEAT SYSTEM

CHAPTER 6

STEADY-STATE VIBRATION PERFORMANCE OF HUMAN-SUSPENSION SEAT SYSTEM

CHAPTER 7

ANALYSIS OF DRIVER-SUSPENSION SEAT SYSTEM UNDER END-STOP IMPACTS

CHAPTER 8

CONCLUSIONS AND RECOMMENDATIONS FOR FUTURE WORK

LIST OF FIGURES

LIST OF TABLES

LIST OF ABBREVIATIONS AND SYMBOLS

ABBREVIATIONS

APMS	Apparent mass
DPMI	Driving-point mechanical impedance
EBS	Erect back supported
ECA	Effective Contact Area
ENS	Erect back not supported
FFT	Fast Fourier Transform
HP	High pass
IP_{max}	maximum ischium pressure
ISO	International Standard Organization
LP	Low pass
PSD	Power spectral density
rmq	Root-mean-quad
rms	Root-mean-square
SAE	Society of Automotive Engineers
SDOF	Single-degree-of-freedom
SEAT	Seat Effective Amplitude Transmissibility
STHT	Seat-to-head transmissibility
VDV	Vibration dose value
WBVVS	Whole-Body Vehicular Vibration Simulator

SYMBOLS

ω	angular frequency (rad/s)
χ	parameter vector
β	scaling factor
λ, ψ	weighting factor
ζ, ζ_1, ζ_2	damping ratio
α_0	damper inclination angle at mid-ride position (degree)
γ_1, γ_2	reduction factor
ω_{n1}, ω_{n2}	natural angular frequency (rad/s)
$a(j\omega)$	complex driving point acceleration
a_1, a_2, a_3, a_4	parameters associated with nonlinear cushion force
$a_H(j\omega)$	complex head response acceleration
$a_{w,rms}$	weighted rms acceleration (m/s^2)
B	horizontal distance between the attachment points of damper (m)
c, c_1, c_2, c_3	damping coefficient (Ns/m)
c_c	cushion damping coefficient (Ns/m)
c_{eq}	equivalent viscous damping (Ns/m)
c_s	suspension damping coefficient (Ns/m)
d	half of suspension free travel (m)
d_m, $d_m^{(t)}$, $d_m^{(b)}$,	half of maximum suspension travel (m)
F	driving-point force (N)
$F(j\omega)$	Complex Force

$f(y)$	nonlinear cushion force (N)
F_0	magnitude of friction force (N)
F_1, F_2, F_3	forces acting between model masses (N)
F_b	buffer force (N)
F_c	cushion force (N)
f_c	cut-off frequency (Hz)
F_{c0}	static load on cushion (N)
F_{ce}	cushion elastic force (N)
F_d	damper force (N)
F_f	friction force (N)
f_n, f_{n1}, f_{n2}	natural frequency (Hz)
f_p	Primary resonant frequency (Hz)
F_s	suspension spring force (N)
$H(j\omega)$	complex seat-to-head transmissibility
$h^{(t)}, h^{(b)}$	displacement lag due to buffer hysteresis (m)
H_0	mid-ride position (m)
H_p	Band-limiting filter
H_w	Network weighting filter
j	complex phaser
k_1, k_2, k_3	spring rate (N/m)
$k_{b1}^{(b)}, k_{b2}^{(b)}, k_{b3}^{(b)}, k_{b4}^{(b)}$	bottom buffer stiffness coefficients
$k_{b1}^{(t)}, k_{b2}^{(t)}, k_{b3}^{(t)}, k_{b4}^{(t)}$	top buffer stiffness coefficients
k_{c1}, k_{c3}	cushion stiffness coefficients

k_s	suspension spring rate (N/m)
$M(j\omega)$	complex apparent mass
m_0, m_1, m_2, m_3	mass (kg)
m_s	suspension mass (kg)
p	asymmetry factor
$T(j\omega)$	complex seat-to-head transmissibility
t, t_1	time (s)
T_b	Buffer thickness (m)
T_c	Cushion thickness (m)
U	objective function
U_M	error resulting from apparent mass
U_T	error resulting from seat-to-head transmissibility
v	velocity (m/s)
v_1, v_2	transition velocities (m/s)
W_k	Weighting function in vertical direction
x_0, x_1, x_2, x_3, x_s	model displacement response
X_0, X_1, X_2, X_3, X_S	Laplace transformation of x_0, x_1, x_2, x_3, x_s
y	deflection of seat cushion (m)
y_0	static deflection of seat cushion (m)
y_1	threshold of cushion bottoming (m)
$Z(j\omega)$	Complex driving-point mechanical impedance
z_s, $\dot{z}_s$	relative displacement and velocity of suspension

CHAPTER 1

INTRODUCTION AND SCOPE OF RESEARCH

1.1 Off-Road Vehicle Vibration and Their Effects on Operators

Vehicle drivers are invariably exposed to whole-body vibration and shocks, arising primarily from the tire-terrain interactions. Of particular concern are operators of off-road vehicles, such as agricultural tractors, forestry vehicles, construction vehicles, *etc.*, who are constantly exposed to severe vibration and shocks caused by vehicle moving over rough terrains. Exposure to such vehicular vibration and shocks has been known to interfere with the driver's comfort, working efficiency and health. The chronic health problems, caused by prolonged exposure to such vibration in the 0.5 – 80 Hz frequency range, include: low back pain, spinal disorders, abdominal pain, digestive and vision problems, *etc.* [1].

In view of severe health and safety risks posed by exposure to vibration and shock environment of off-road vehicles, there has been an increased emphasis towards ride quality improvement by minimizing the levels of vibration transmitted to the driver. Improvement in ride quality of off-road vehicles through primary suspension, cab suspension and seat suspension have been investigated by various researchers [2, 3, 4]. Most of these studies have concluded that implementations of primary suspension and cab suspension require complex alterations in vehicle design. Furthermore, a primary suspension would be impractical in vehicles carrying frame-mounted equipment. The dynamic response of the seat and its suspension, thus plays a critical role in enhancing the ride vibration environment of off-road vehicles.

1.2 Control of Vehicle Vibration Transmitted to Drivers through Suspension Seats

The ride environment of off-road vehicles comprises comprehensive magnitudes of low frequency vibration along all three translational and rotational axes. The flow of such vibration to the operator occurs through the feet, seat back and seat cushion. It has been reported that the component of vertical vibration on the seat usually is the highest after the frequency and the axis weightings are applied. Off-road vehicles, due to their interactions with uneven terrains, are known to yield high magnitudes of longitudinal and lateral vibrations, which are comparable to those of vertical vibration [1]. Upon recognising high magnitudes of translational and rotational vibration, a concept in multi-axis seat vibration isolator has been proposed in the early 80's [5]. The commercial suspension seats, employed in heavy road and off-road vehicles, however, are designed to attenuate vibration in the vertical mode only, since the attenuation of vibration along all the other axes needs complex suspension mechanisms, which would increase the cost and reduce the reliability of the products.

The vertical mode suspension seats are known to yield vibration isolation superior to that of the conventional seats, since the suspensions are designed to achieve their natural frequency well below the frequency of dominant off-road vehicle vibration. Because the vertical vibration of off-road vehicles, invariably, predominate in the 2 – 3.25 Hz frequency range, suspension seats are designed to be soft with natural frequencies below 1.5 Hz to achieve vibration isolation. The low stiffness or low natural frequency of the seat is realized upon integrating additional restoring elements below a relatively hard seat cushion, which is primarily intended to provide adequate body support and body weight distribution. The suspension mechanisms, invariably, consist of

either mechanical or air spring, and an energy dissipating element for resonant vibration suppression. Figure 1.1 illustrates a comparison of acceleration transmissibility of a suspension seat with that of a conventional metal spring and foam seat, loaded with an identical human subject. It may be seen that the suspension seat attenuates vibration above about 3 Hz, while a conventional foam seat provides attenuation of vibration only at frequencies above about 5 Hz. A suspension seat also provides considerably superior isolation of vibration than the foam seat, specifically in the 2 to 12 Hz frequency range. A suspension seat is thus ideally suited for off-road and heavy road vehicles where predominant vertical vibration occur within 1 to 15 Hz frequency range. A suspension seat, however, amplifies vehicle vibration in the vicinity of its resonant frequency, which may occur in the 1 – 2 Hz frequency range. The suitability of a suspension seat for a given vibration environment thus depends on whether this amplification can be adequately offset by the attenuation of vibration occurring at higher frequencies.

Suspension seats, invariably, exhibit resonance at frequencies well below 2 Hz, while the travel is mostly limited to 100 mm in order to minimise the interference with control tasks to be performed by the driver. The maximum travel in some suspension seats, such as forklift truck seats, is limited to only 40 to 50 mm. The low suspension stiffness coupled with limited travel, yields considerable end-stop impacts when the input motion is sufficiently large to cause the suspension to reach the end of its travel. Conventional suspension seats use rubber buffers to reduce the severity of such end-stop impacts. The considerably high stiffness characteristics of these rubber buffers cause high magnitude resonant oscillations of the suspension and thus transmit high levels of shock and vibration to the driver. The vibration isolation performance of a suspension seat thus further relies on

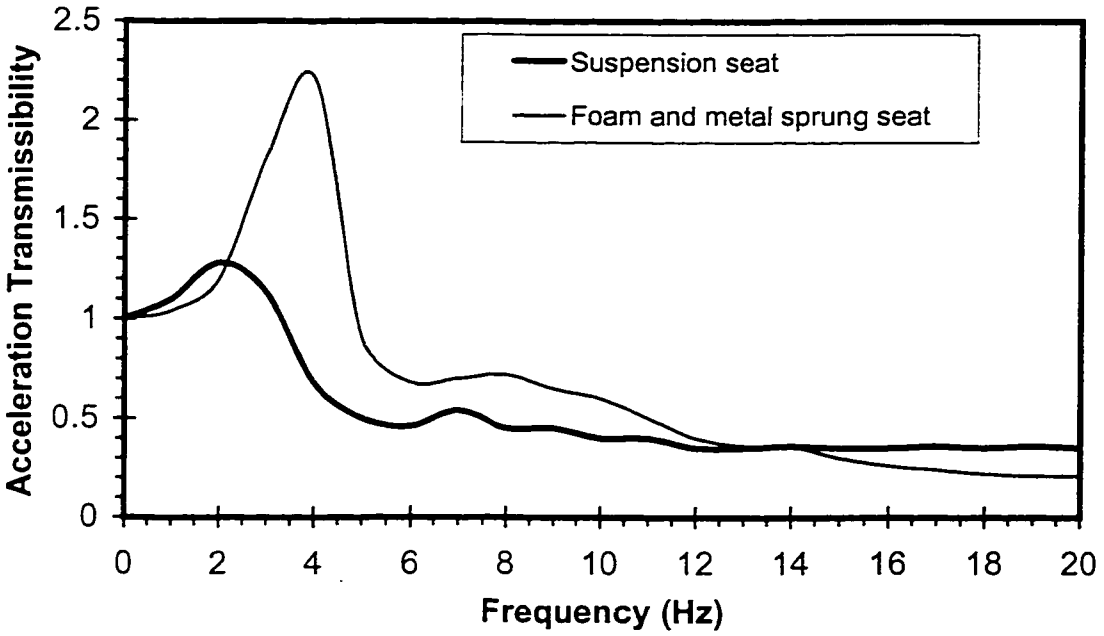

Figure 1.1: Comparison of acceleration transmissibility of a suspension seat with that of a foam and metal sprung seat [1].

the frequency and severity of end-stop impacts. The frequency of end-stop impacts is of considerable concern for both off-road and heavy road vehicle applications. Wheeled off-road vehicles with large diameter and soft tires yield frequent bottoming of suspension due to interactions with highly uneven terrains. Modern heavy road vehicles are designed with relatively low natural frequency wheel or primary suspension to reduce the magnitudes of dynamic tire loads transmitted to pavements and to achieve enhanced isolation of road induced vibration. The dynamics of low natural frequency suspension seat coupled with that of the low natural frequency primary suspension have resulted in increased frequency of end-stop impacts in seat suspension systems. The frequency of end-stop impacts in such vehicles increases considerably under vehicle operation on rough roads and roads with certain discontinuities, such as urban roads.

End-stop impacts in a suspension seat cause high levels of shock and vibration arising from impacts, and thus driver discomfort. In a field survey of the whole-body vibration experienced by tractor drivers, Stiles [6] reported that 45% of seats increase the acceleration levels experienced by the driver. Much of the increase was attributed to the end-stop impacts. The drivers of certain vehicles indicated preference for an unsuspended seat due to high severity of end-stop impacts. Burdoff and Swuste [7] measured the isolation of eleven different suspension seats in the laboratory under standardised vehicle vibration spectra and also in vehicles driving over typical surfaces. The results showed that 19 of 24 transmissibility measurements performed in vehicles were greater than the corresponding transmissibilities measured in the laboratory. The study concluded that laboratory measurements of dynamic response of suspension seats do not provide an adequate basis for predicting their performance in the field. The discrepancies between

laboratory and field measurements were mostly attributed to non-stationarity of vehicular motions and relatively high crest factors, defined as the ratio of peak acceleration to its rms value, of vehicular motions. The presence of shock motion with high crest factor may cause more frequent occurrence of end-stop impacts than those occurring during laboratory tests.

The dynamic performance characteristics of various passive suspension seats have been investigated in few studies through laboratory or field measurements, and development and analysis of linear and nonlinear analytical models [5, 7, 8]. A limited number of active and semi-active suspension seat concept have also been explored to enhance the steady-state vibration isolation performance [9, 10, 11]. The dynamics of end-stop impacts and their contributions to overall vibration attenuation performance of suspension seats, however, have not yet been explored. The lack of such studies may be attributed to the complexities associated with end-stop impacts and severe design constraints associated with suspension seats.

In a recent study, Boileau [8] established that consideration of end-stop impacts poses contradictory design requirements for suspension seats. Some designs of rubber buffers in conventional suspension seats induce severe end-stop impacts, and the standards concerning testing of suspension seat end-stop impacts do not yet exist. In Europe, a major consortium of both research institutes and seat manufacturers have recently initiated a study with objectives of developing test methods for suspension seat end-stop impacts, improving buffer and suspension design and finally reducing the shock and vibration transmitted to the driver body.

Many studies have further established that the dynamics of the seated human body contributes considerably to the overall performance of seats [12, 13, 14]. Earlier studies,

however, were performed using passive loads assuming negligible contribution of the biodynamic response behavior of the seated subjects. A number of experimental studies on suspension seats have thoroughly investigated the contributions due to the human driver [14, 15]. The validity of the results derived from such studies, however, is limited due to extensive inter- and intra-subject variations and the use of limited number of subjects. Some recent studies have also attempted development of coupled human-seat models to study the contributions due to seated driver. Although a number of analytical model representations of seated body have been proposed based upon measured biodynamic response characteristics, many concerns have been raised on the validity of these models. The need to develop credible human body models has thus been emphasized.

1.3 Scope of the Dissertation Research

The design and analysis of suspension seats can be effectively performed using modeling and simulation techniques to examine the suspension's behavior under known excitations. The design optimization techniques can be further applied to determine optimal design parameters necessary to achieve an adequate compromise between the performance associated with attenuation of continuous steady state vibration and prevention of severe end-stop impacts. The modeling and simulation based design approach, however, requires consideration of the biodynamic response of the human body. It has been established that the human body behaves similar to a rigid mass under vertical vibration at excitation frequencies below 2 Hz [12]. At higher frequencies, the human body exhibits complex biodynamic response to vibration and contributes

considerably to the overall performance of the coupled human-seat system. Several seated human body models have been reported in the literature. Majority of these models, however, were developed while attempting to match the measurements of biodynamic response functions either 'to the body (i.e. driving-point mechanical impedance and apparent mass) [12, 16, 17] or 'through the body' (seat-to-head transmissibility and seat-to-body segment transmissibility) [18, 19, 20]. For a complex system like the human body, it is desirable to develop a model on the basis of multiple system input-output relationships to enhance the uniqueness of the model and to reflect the body dynamics as close as possible. Only few models have been attempted on the basis of satisfying both driving-point mechanical impedance or apparent mass and seat-to-head transmissibility [8, 21, 22]. However, these models also included some biomechanical data and were based on biodynamic response functions for which the determination of both functions often implied different experimental conditions. The dynamic responses presented in different functions may not reveal the same information of the human biodynamic system, which is highly variable under different test conditions. As a result, large discrepancies between the simulated model responses and the collected data have been shown to exist. Furthermore, studies on possible relationships between the biodynamic functions involved and the proper structures of the model do not yet exist.

A vertical suspension seat is usually modeled as a two-degrees-of-freedom dynamical system, where the properties of seat cushion, suspension spring and end-stop buffer are simplified as linear elements [5, 8] and Coulomb friction force is represented by ideal characteristics. The suspension damper is either considered as an element of constant velocity squared damping coefficient, or variable damping coefficients

incorporating bleed and blow-off stages. In both models, symmetric force-velocity characteristics of dampers have been assumed. The asymmetric damper characteristics in compression and rebound may cause variations in the mid-ride position of the suspension sprung mass under excitations of different magnitudes. Such variations in the mid-ride position from the preset position can cause more frequent and more severe end-stop impacts. Furthermore, the elastic end-stops in previous models have often been regarded as springs of linear stiffness. This approximation can be considered sufficient when the end-stop buffers experience only small deformations during occasional impacts. The force-deflection characteristics of elastic end-stops, in general, exhibit progressively hardening properties and hysteresis [23]. Large deflection of the buffer caused by either high magnitude excitation or repeated impacts can thus lead to significant errors.

Many suspension seats employ softer compression buffers and relatively stiff rebound buffers. The severity of impacts with the rebound buffers is thus considerably high. Under such end-stop impacts, the seated driver's body may lose contact with the seat cushion during upward motion. The cushion may experience bottoming, as the body falls back on the seat. While the linear cushion model, employed in earlier studies, might be considered appropriate under low magnitude vibration, it may cause large discrepancies between analytical and test results. Therefore it seems essential to develop a comprehensive seat cushion model incorporating such nonlinearities and to combine such a model with an appropriate human-suspension seat model.

Once the combined human-suspension seat model is developed, the optimal suspension seat design characteristics under continuous steady state vibration can be realized by minimizing the frequency weighted rms acceleration at the driver-seat

interface under given excitation spectra, defined in various standards, by limiting the relative displacement response of the suspension within a predefined range. Secondly, optimization of end-stop rubber buffer properties may be achieved to reduce the severity of end-stop impacts by using vibration excitation levels sufficiently large to cause successive end-stop impacts. Since the conditions involving the occurrence of end-stop impacts involve contradictory suspension design requirements to those applying without such impacts, dampers with variable damping coefficients may be needed to reach the required compromise under the combined vibration excitation conditions.

1.4 Objectives of the Dissertation Research

From the review of reported studies briefly discussed above, it is apparent that study of seating dynamics and suspension design necessitate appropriate considerations of both steady-state vibration and shock excitations. The application of reported analytical models are limited due to lack of appropriate models for the human body, seat cushion, end-stop buffers and suspension damping. The primary objective of this dissertation research is thus formulated to develop a combined human-suspension seat model, which could be effectively used to study the transmission of vertical vibration and shocks to the seated driver. The model, incorporating nonlinear characteristics of the cushion, damper, buffers and human body dynamics could be employed to derive optimal suspension design to achieve an adequate compromise between both steady-state vibration and end-stop impacts performance. The specific objectives of the research are formulated as follows, which also comply with some of the recommendation for future work outlined in [8]:

(a) Derive generalized biodynamic response characteristics, including driving point mechanical impedance, apparent mass and seat-to-head transmissibility, through systematic synthesis of the measured data reported by various researchers;

(b) Analyze the influence of various test variables and contributing factors on the biodynamic response characteristics, and define test conditions similar to those most likely to be encountered in off-road vehicle driving;

(c) Establish the relationships between the 'to the body' and 'through the body' biodynamic functions and explore the possibility to develop a human body model based on satisfying both types of functions;

(d) Measure 'to the body' and 'through the body' biodynamic response functions applicable to seated subjects under test conditions representative of off-road vehicle driver vibration environment and develop a human body model based on the data;

(e) Develop a seat cushion model through systematic investigation on the dynamic pressure distribution at the driver-seat interface;

(f) Develop a combined human-suspension seat model with particular emphasis on the nonlinear asymmetric properties of suspension damper, rubber buffer, and seat cushion;

(g) Compare the response characteristics of the combined human-suspension seat model with the experimental results to determine the validity of the model;

(h) Perform parametric sensitivity analyses to determine primary contributing factors influencing the suspension performance under steady-state vibration and shock excitations;

(i) Perform design optimization to achieve minimum vibration transmission under specific vibration excitation spectra, and the optimal buffer force-deflection characteristics and hysteresis to minimize the severity of end-stop impacts;

(j) Propose design guidance for suspension seat parametes and end-stop buffer properties.

1.5 Thesis Organization

This dissertation is organized into eight chapters describing systematic developments in realizing the above objectives. The literature is reviewed in appropriate chapters highlighting the research contributions on the various subjects. Chapter 2

presents the results of a complete review of published data on whole-body biodynamic response. The influence of various factors on the biodynamic responses is investigated. A data synthesis is performed to define the range of idealized biodynamic response characteristics under conditions representative of off-road vehicle driving. Chapter 3 presents the review of some human body models and discusses the various biodynamic response functions. A seated human body model is proposed based on measured data representing 'to the body' and 'through the body' response functions, obtained simultaneously under a predefined set of test conditions.

The effects of whole-body vertical vibration on the characteristics of dynamic human-seat interface pressure distribution are investigated in Chapter 4, to enhance an understanding of the driver-seat interface force-motion relationships. Based on the results, a nonlinear seat cushion model is proposed and validated. A combined non-linear human-suspension seat model is developed and validated in Chapter 5. The model is further utilised in Chapters 6 and 7 to optimise suspension properties, seat cushion properties and end-stop buffer properties, in order to achieve an adequate compromise between the steady-state vibration attenuation and end-stop impacts prevention performance characteristics. The optimum suspension seat for steady-state vibration attenuation under given random excitations is investigated in Chapter 6, through parameter sensitivity analysis and optimization techniques. This 'optimum suspension seat' is further used to investigate the effects of end-stop buffer force-deflection characteristics and buffer damping on end-stop impacts in Chapter 7. Finally, the highlights of the dissertation research, conclusions and the recommendations for future studies are presented in Chapter 8.

CHAPTER 2

WHOLE-BODY BIODYNAMICS: A SYNTHESIS OF THE REPORTED DATA

2.1 Introduction

Attenuation of whole-body vehicular vibration transmitted to the occupants necessitates a thorough understanding of various factors, including occupants' response to vibration, the manner of vibration transmission through the body, and seating considerations. It has been established that the human-seat system performance is affected not only by the seat design, but also by the biodynamics of the driver, as illustrated in Figure 2.1. The characterization of the biodynamic response of the seated human body under vertical vibration is of particular interest, since the seated posture and vertical vibration direction are those most likely to be involved in several vibration environments, including vehicle driving.

The biodynamic response behavior of the human body subjected to whole-body vibration may be characterized using three different biodynamic functions. Two of these functions have often been used interchangeably to describe 'to the body' force-motion relationship at the human-seat interface, namely the driving-point mechanical impedance (DPMI) and the apparent mass (APMS). The DPMI relates the driving force and resulting velocity response at the driving point, and is given by:

$$Z(j\omega) = \frac{F(j\omega)}{v(j\omega)} \tag{2.1}$$

where $Z(j\omega)$ is the complex DPMI, and $F(j\omega)$ and $v(j\omega)$ are the driving force and response velocity at the driving point, respectively. ω is the angular frequency in rad/s and

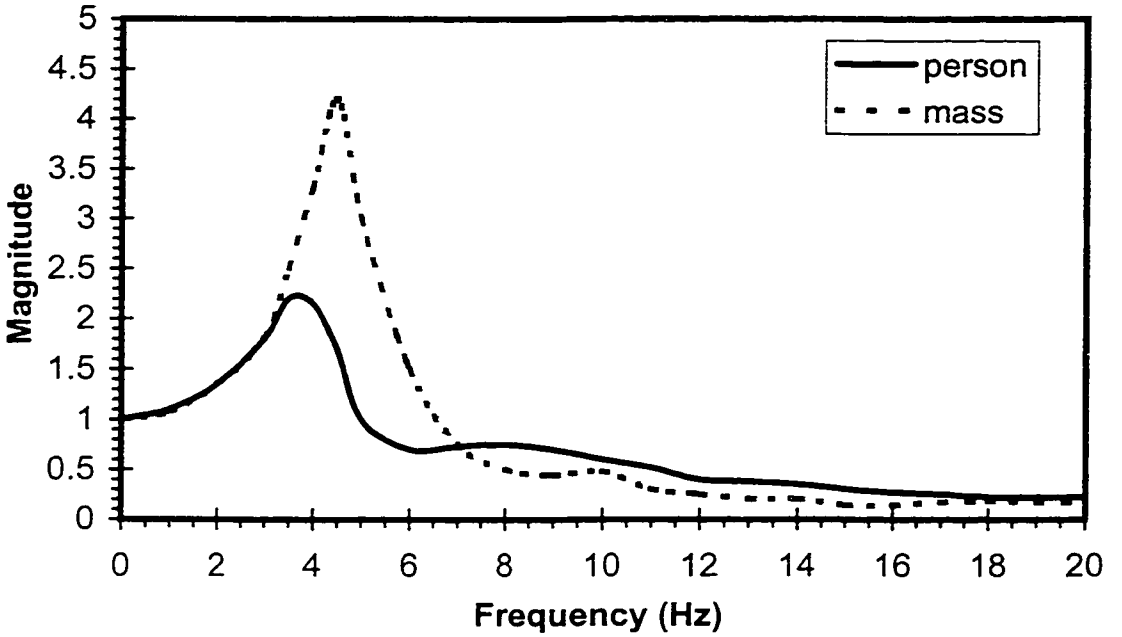

Figure 2.1: Comparison of vertical vibration transmissibility magnitude of a foam and metal spring seat loaded with a person and a rigid mass of equivalent weight [1].

$j=\sqrt{-1}$ is the complex phasor. The APMS relates the driving force and the resulting acceleration response, and is related to the DPMI by:

$$M(j\omega)=\frac{F(j\omega)}{a(j\omega)}=\frac{Z(j\omega)}{j\omega} \tag{2.2}$$

where $M(j\omega)$ is the apparent mass and $a(j\omega)$ is the driving point response acceleration. The magnitude of APMS has a simple physical interpretation that it is equal to the static mass of the human body supported by the seat at very low frequencies, when the human body effectively acts as a rigid mass. The acceleration response and the driving force thus remain in phase at low frequencies. The magnitude of DPMI can be obtained by multiplying the APMS by the angular frequency, thus tending to make the resonant peaks appear more apparent at high frequencies, than if they were represented in term of APMS. From the definitions of DPMI and APMS, it is apparent that DPMI leads the APMS by a constant 90^0 phase angle.

The other biodynamic response function may be referred to as 'through the body' biodynamic function, and is termed as seat-to-head transmissibility (STHT), which describes the vibration transmission through the body from seat to head, and is expressed as:

$$H(j\omega)=\frac{a_{\mathrm{H}}(j\omega)}{a(j\omega)} \tag{2.3}$$

where $H(j\omega)$ is the complex seat-to-head transmissibility function and $a_{\mathrm{H}}(j\omega)$ is head response acceleration. At low frequencies, the motion at the human-seat interface $a(j\omega)$ is transmitted directly to the head due to effectively rigid mass behavior of the human body, leading to unity value of transmissibility magnitude and zero phase difference.

The above three functions have been employed to characterize the human biodynamic response by performing measurements under a variety of test conditions. Based on the measured data, a number of biodynamic models have been proposed in the literature for the purpose of estimating the magnitudes of the forces transmitted to particular subsystems within the body (*e.g.* the spine), and/or establishing potential damage mechanisms, and/or assessing the tolerance to vibration under exposure to intensive vibration levels [1]. Majority of the measurement conditions employed in several investigations, however, can not be considered representative of those likely to prevail while driving heavy road and off-road vehicles. Since the biodynamic response of the human body subjected to vibration is strongly related to a wide range of intrinsic (*e.g.* body mass and posture) and extrinsic (*e.g.* vibration type, intensity and frequency) variables, the applicability of a proposed biodynamic model to driving situations may be questioned without analyzing the test conditions used for deriving the data on which the model relies.

In this chapter, the published data on whole-body biodynamic response characteristics are thoroughly reviewed together with the test conditions. The influence of various factors on the biodynamic responses are investigated on the basis of published literature. Based on the analysis, a set of test conditions applicable to heavy vehicle drivers is defined and a data synthesis is performed while retaining only the data derived under the corresponding conditions. From the data synthesis, a range of most probable values is defined that should ideally be used for the development of a human body model, applicable in off-highway driving situations.

2.2 Review of Published Data on Whole-Body Biodynamic Response

The vertical biodynamic response characteristics of the seated human body reported in the literature were thoroughly reviewed in terms of the postural constraints, excitation levels, number of subjects, and frequency range. As expected, the test conditions and the response values were observed to vary significantly among the various investigations. In many of the earlier studies, such as those conducted by Coermann [12], Suggs *et al.* [16], Vogt *et al.* [24] and Miwa [25], the number of subjects included was usually small and there were few considerations of the many factors, such as seated postures, subject characteristics, vibration excitations, *etc.* In some studies, the feet of the subjects were either not supported or supported but not vibrated [21, 25]. In other cases, the excitation magnitudes used in deriving the data were significantly higher than those which could be expected in most common situations. Some studies were conducted under increasing steady-state acceleration in a centrifuge to investigate the non-linearity of the human body under increasing gravity [21]. As for subject population, some studies employed men, women and children as subjects [17], and many studies employed subjects of significantly different weight. Although all these studies have contributed greatly to gain an understanding of human biodynamic response, the results could not be grouped to derive a generally acceptable response behavior due to excessive variations in test conditions. Several data sets reported in the literature in terms of APMS, DPMI and STHT are identified in Table 2.1. The different test conditions are categorized in terms of subject characteristics, excitation type, magnitude and frequency range, and postural constraints. Although the vibration response characteristics of the human subjects have

Table 2.1: Characterization of published data on whole-body biodynamic response.

Authors	Subject			Excitation			Posture	Reported Functions
	Number	Sex	Mass (kg)	Type	Level	Frequency Range		
Coermann [12]	8	Male	70-99	Sine	0.1 g 0.2 g 0.3 g	1 – 20 Hz	Standing; Sitting with feet not supported, no backrest	Mean DPMI magnitude and phase, Mean STHT magnitude
Edwards and Lange [40]	2	Male	77 and 84	Vertical Sine	0.2g – 0.5 g	1 - 20 Hz	Supine; Lateral; Standing	Individual DPMI
Vogt, Coermann and Fust [24]	10	Male	79 (mean)	Sine	0.5 g with increased gravity of 1g, 2g, 3g	2 –15 Hz	Erect sitting, loosely restrained, feet supported, but not vibrated	Mean DPMI magnitude and phase, Mean STHT magnitude
Suggs, Abrams and Stikeleather [16]	11	Male	58-90	Vertical Sine	0.10 in peak-peak	1.75-10 Hz	Sitting upright hands in lap feet supported no backrest	Mean DPMI magnitude and phase
Miwa [25]	5	Male	50-76	Sine	0.1g rms	3 – 200 Hz	Standing; Kneeling; Sitting erect and relaxed, feet not vibrated	Mean DPMI magnitude and phase

Table 2.1 (continued)

Authors	Subject			Excitation			Posture	Reported Functions
	Number	Sex	Mass (kg)	Type	Level	Frequency Range		
Griffin, Lewis, Parsons and Whitman [46]	112	56 males 28 females 28 children		Sine	1 ms^{-2} rms	4 and 16 Hz	Sitting, increasing height of footrest	Mean STHT magnitude and phase
Griffin, Lewis, Parsons and Whitman [46]	36	18 males 18 females		Sine	1 ms^{-2} rms	1 – 100 Hz	Sitting, increasing height of footrest	Mean STHT magnitude and phase
Griffin, Lewis, Parsons and Whitman [46]	1	Male	68	Swept sine and Discrete sine	1 ms^{-2} rms	1 – 100 Hz	Sitting, with and without footrest	STHT magnitude and phase
Mertens [21]	9	6 males 3 females	57–90	Vertical Sine	0.4 g rms with increased gravity of 1g, 2g, 3g, and 4g	2 – 20 Hz	Upright sitting with feet not supported	Mean DPMI magnitude and phase STHT magnitude and phase

Table 2.1 (continued)

Authors	Subject			Excitation			Posture	Reported Functions
	Number	Sex	Mass (kg)	Type	Level	Frequency Range		
Sandover [45]	6		52.7-87.2	Random	1,2, 2.3 ms^{-2} rms	1 - 25 Hz	Erect with various conditions of feet and arms	Individual APMS magnitude and phase
Donati & Bonthoux [27]	15	Male	49-74	Sine sweep, Broad band random	1.6 ms^{-2}	1 – 10 Hz	Erect, feet supported, hands on steering wheels	Mean DPMI magnitude and phase
Fairley and Griffin [43]	1	Male	63	Vertical Gaussian random	1 ms^{-2} rms	0.25 – 20 Hz	Sitting, no backrest, feet supported/not supported, soft/hard seat	APMS magnitude and phase
Fairley and Griffin [44]	8	Male	57 – 85	Vertical Random	1 ms^{-2} rms	0.25 – 20 Hz	normal posture, feet supported and vibrated	Individual APMS magnitude and phase
Hinz and Seidel [28]	4	male	56 – 83	Vertical Sine	1.5 and 3.0 ms^{-2} rms	2 – 12 Hz	Moderately erect sitting	Mean DPMI magnitude and phase Mean STHT magnitude and phase

Table 2.1 (continued)

Authors	Subject			Excitation			Posture	Reported Functions
	Number	Sex	Mass (kg)	Type	Level	Frequency Range		
Paddan and Griffin [34]	12	Male	58-81	Vertical Gaussian Random	1.75 ms^{-2} rms	Up to 25 Hz	Two postures: Sitting with backrest; Sitting without backrest	Mean STHT magnitude
Fairley and Griffin [17]	8	Male	57–85	Vertical Random	0.25, 0.5, 1.0, 2.0 ms^{-2} rms	Up to 20 Hz	4 seated postures: Normal; Upright erect; Upright, tense; Upright back supported; Feet supported on footrest moving with platform	Mean APMS magnitude APMS magnitude and phase for one subject only
Fairley and Griffin [17]	60	24 males 24 females 12 children	Not reported	Vertical Random	1.0 ms^{-2} rms	Up to 20 Hz	Upright, no backrest, footrest vibrating, hands in lap	Individual APMS magnitude and phase
Fairley and Griffin [41]	8	Male	57 – 85	Fore-aft Lateral	0.2, 1, 2 ms^{-2} rms	0.25-20Hz	Sitting, back supported/not supported	Individual APMS magnitude and phase
Smith [42]	5	3 males 2 females	64 – 86	Sine and quasi random	1 and 2 ms^{-2} rms	3 – 21 Hz	sitting upright with back support and constraint	Mean DPMI magnitude

Table 2.1 (continued)

Authors	Subject			Excitation			Posture	Reported Functions
	Number	Sex	Mass (kg)	Type	Level	Frequency Range		
ISO CD 5982 [22]	39		51–94	sinc	1 - 2 ms^{-2} rms	0.5 – 31.5 Hz	Vaguely defined, 10 persons had feet supported by footrest moving with seat, various restraint systems	Mean DPMI magnitude and phase Mean STHT magnitude and phase
Holmlund, Lundstrom, Lindbergh [29]	30	15 males 15 females	57– 92 54–93	Sinc	0.5, 0.7, 1.0, 1.4 ms^{-2} rms	2 – 100 Hz	Relaxed and erect upper body	Mean DPMI magnitude and phase
Seidel [30]	37	males	49-103	Random spectra (earth moving machine)	0.7, 1.0, 1.4 ms^{-2}	0 – 20 Hz	Hard seat without backrest, Feet supported and vibrated	Mean DPMI magnitude
Boileau and Rakheja [31]	7	Males	75.4 mean	Sine sweep and broad band random	1, 1.5, 2.0 ms^{-2} rms	0 – 10 Hz	Erect sitting with back support Erect sitting without back support	Mean DPMI magnitude and phase
Zimmermann and Cook [35]	30		77.6	Sinc	1 ms^{-2}	4.5 – 16 Hz		Mean STHT magnitude

been measured under carefully controlled conditions in each of these studies, considerably different test conditions have been employed by different researchers. These differences in test conditions, though not all of them were clearly stated in some studies, can be considered as the primary reason for the large variations among the reported biodynamic response characteristics. It is thus essential to examine the influence of various test conditions before attempting to define a range of most probable values applicable to a particular situation.

2.3 Factors Influencing Magnitude of APMS or DPMI

Influence of some of the factors on the biodynamic measurements have been investigated in many studies [8, 17, 21, 25-31]. Table 2.2 lists the factors, which have been considered in most of the studies. The reported data are reviewed to identify the influence of those factors, which are discussed in the following subsections.

Table 2.2: Factors influencing the biodynamic response characteristics.

Subject characteristics:	**Vibration characteristics:**
Posture (back support, backrest inclination, muscle tension, feet and hand support; seated and standing); Body mass;	Type (*e.g.* sine, random, real vehicle floor spectra); Magnitude (*e.g.* rms, peak amplitude); Frequency (*e.g.* range)

2.3.1 Influence of seated posture on APMS and DPMI magnitude

Posture has been shown to have an influence on the biodynamic response characteristics. The posture of a seated person is related with the orientation of the lower

back, the contact with the backrest and the backrest inclination. The limbs position can also affect the biodynamic response. Muscle tension (*e.g.* sitting normally, erect or tense, and relaxed) is often cited as a possible cause of alterations in biodynamic response [17]. Since the contributions due to posture and muscle tension may not easily be distinguished, it appears appropriate to include the discussion of muscle tension in this section. Furthermore, the biodynamic data were reported on the basis of either APMS or DPMI in different studies. The measured data sets are thus presented in terms of both functions in this section in order to compare different data sets, and demonstrate the different trends arising from the two functions which may affect the analysis.

Miwa [25] measured the human DPMI corresponding to kneeling, sitting and standing postures. Under the sitting posture, the subjects sat on a vertical vibrator with feet hanging free, except in one test where the effect of a static footrest was investigated. Based on the mean value of five subjects, it was observed that the DPMI magnitude without a footrest was larger than that with a footrest over the entire frequency range investigated (3 - 200 Hz).

As to the effect of sitting erect and relaxed, the DPMI magnitude under erect sitting posture at two resonant frequencies (around 7 Hz and 15 Hz, respectively) was observed to be larger than that for relaxed posture [25]. The influence of sitting erect and relaxed has also been demonstrated [30], involving a group of 37 subjects. The subjects sat on a hard seat without backrest, with feet supported and vibrated on a footrest. The two postures were defined as relaxed posture with hands placed on a steering wheel, and erect posture with a straight back and the arms crossed in front of the chest. The mean DPMI magnitudes corresponding to two mass groups (60-70 kg and 70-80 kg) and two

different postures are shown in Figure 2.2. For both postures, DPMI response exhibits peaks near 5 Hz, 7 Hz and 13 Hz. The relaxed posture, however, yields significantly lower magnitude of DPMI than the erect posture at frequencies above 4 Hz. The first resonant frequency established from DPMI data occurred at higher frequencies with the erect posture than that with relaxed posture. When the data sets were converted to APMS, the shift of first resonance frequency is shown more clearly, as shown in Figure 2.3. With a relaxed posture, the resonant frequency, as seen from APMS data, is at around 3.7 Hz and with an erect posture the resonance frequency is near 5 Hz. It can be postulated that the erect posture with high muscle tension increases the stiffness of human body, and thus the resonant frequency.

The influence of a backrest and variations in its inclination angle has been investigated by Boileau and Rakheja [31], involving a total of 7 male subjects. The subjects sat on a rigid seat with an inclined adjustable backrest and feet were supported on the vibrator. Three postures were defined as: (i) sitting erect with only lower back in contact with the backrest, referred to as 'ENS' posture; (ii) sitting erect with most of the back in contact with the backrest, referred to as 'EBS' posture; (iii) sitting erect with most of the back in contact with the backrest while the backrest is inclined at an angle of 14 degrees to the vertical, referred to as 'EBS14' posture. The mean DPMI magnitude, illustrated in Figure 2.4, reveals significant influence of the seated posture. An ENS posture yields higher DPMI magnitude over the entire frequency range and a higher resonant frequency than those observed for the EBS posture. With an inclination angle of the backrest, the EBS14 posture yields a higher resonant frequency and higher DPMI

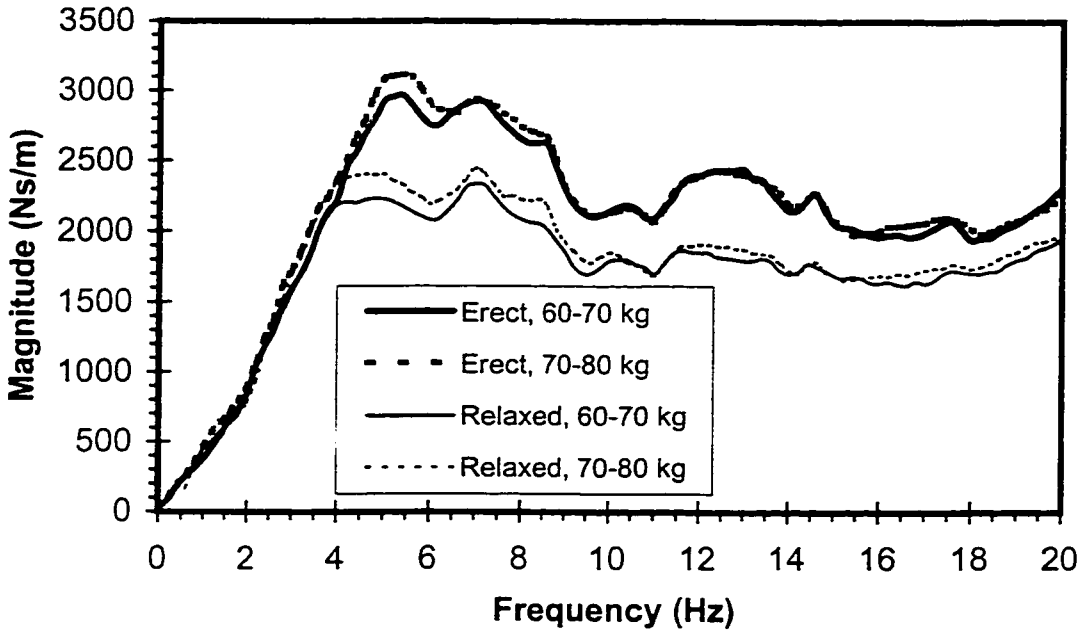

Figure 2.2: Effects of subject posture and body mass on the mean magnitude of driving-point mechanical impedance [30].

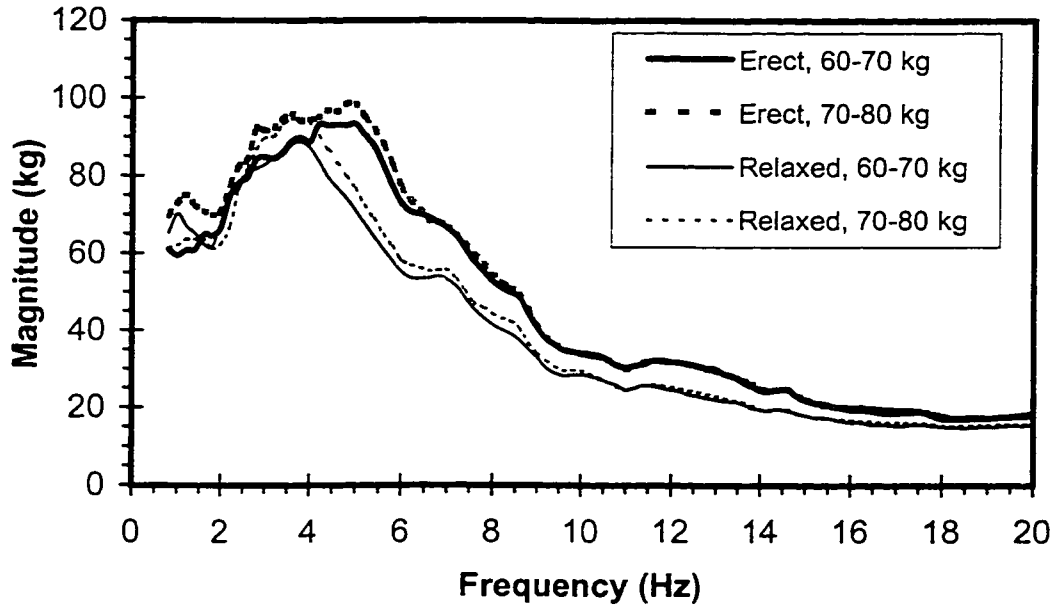

Figure 2.3: Effects of subject posture and body mass on the equivalent magnitude of apparent mass (converted from [30]).

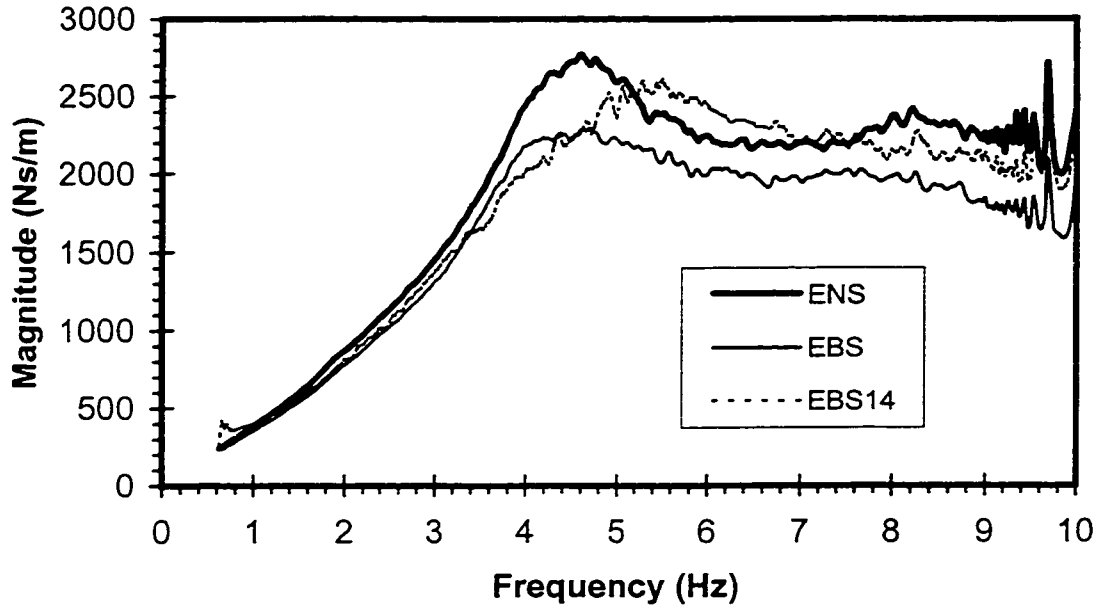

Figure 2.4: Effect of seated posture on magnitude of driving-point mechanical impedance under sinusoidal excitation (2 m/s² rms) [31].

magnitude at frequencies above 4.5 Hz than those observed for the EBS posture, where the backrest remains vertical.

It can be therefore generally concluded that the DPMI and APMS magnitude appears to be higher for feet not supported than if the feet are supported, and the ENS posture usually yields higher DPMI and APMS magnitude than the relaxed and/or EBS posture. Although some studies have considered different hand and arm postures, such as crossed in front of chest, resting on lap or resting on a steering wheel, the influence of these factors on the DPMI or APMS has not been reported. Since the hand-arm accounts for only a small percentage of body weight, the considerations of hand positions is thus assumed insignificant compared to seated posture, body mass and vibration excitation magnitude.

2.3.2 Influence of subject mass on DPMI and APMS magnitude

The DPMI or APMS of seated body is strongly affected by the body weight. Fairley and Griffin [17] reported the APMS of 60 seated subjects including men, women and children in the vertical axis, which revealed large scatter in the data due to the large variations in the subject masses. The magnitude of data scatter, however, was greatly reduced when the individual curves were normalized with respect to the static seated mass of each subject. The DPMI characteristics, reported by Seidel [30] for a total of 37 male subjects assuming an erect seated posture, was grouped into four sets based upon different ranges of subject mass, namely subject groups with less than 60 kg mass (9 subjects); with mass between 60-70 kg (11 subjects); with mass between 70-80 kg (14 subjects); and with a mass higher than 80 kg (3 subjects). Figure 2.5 illustrates the mean

magnitude of DPMI (averaged across all exposure conditions) for subjects in different mass ranges. For all the four mass groups, the primary resonant frequency ranges from 4.5 to 5.5 Hz, while the groups with higher mass revealed lower resonant frequency frequency. The peak magnitude of DPMI corresponding to the primary resonant frequency also increased for groups with higher mass range. Figure 2.6 illustrates the same data sets converted into APMS, which clearly illustrates considerably larger differences in the peak APMS magnitudes for different mass groups. The difference in the primary resonant frequency, however, is nearly vanished. It can thus be concluded that the resonant magnitude increases considerably and the resonant frequency decreases slightly with an increase in subject mass.

2.3.3 Influence of magnitude of excitation on APMS and DPMI magnitude

The biodynamic response characteristics of the seated human body under varying levels of whole body vibration have been investigated in several studies. Fairley and Griffin [17] reported the APMS of eight male subjects exposed to four magnitudes of vibration (0.25, 0.5, 1.0 and 2.0 ms^{-2} rms). For all eight subjects, the primary resonant frequency appeared to decrease with increase in magnitude of vibration. Holmlund *et al.* [29] also reported DPMI magnitude for a group of 15 male subjects exposed to different excitation levels, with relaxed and erect sitting posture, as shown in Figure 2.7. It can be observed that both the mean impedance magnitude and the two resonant frequencies decrease with increasing vibration level. This may be attributed to 'softening' of the human body under higher levels of vibration excitation. These observations are further supported by the studies performed by Seidel [30]. Different studies, however, have

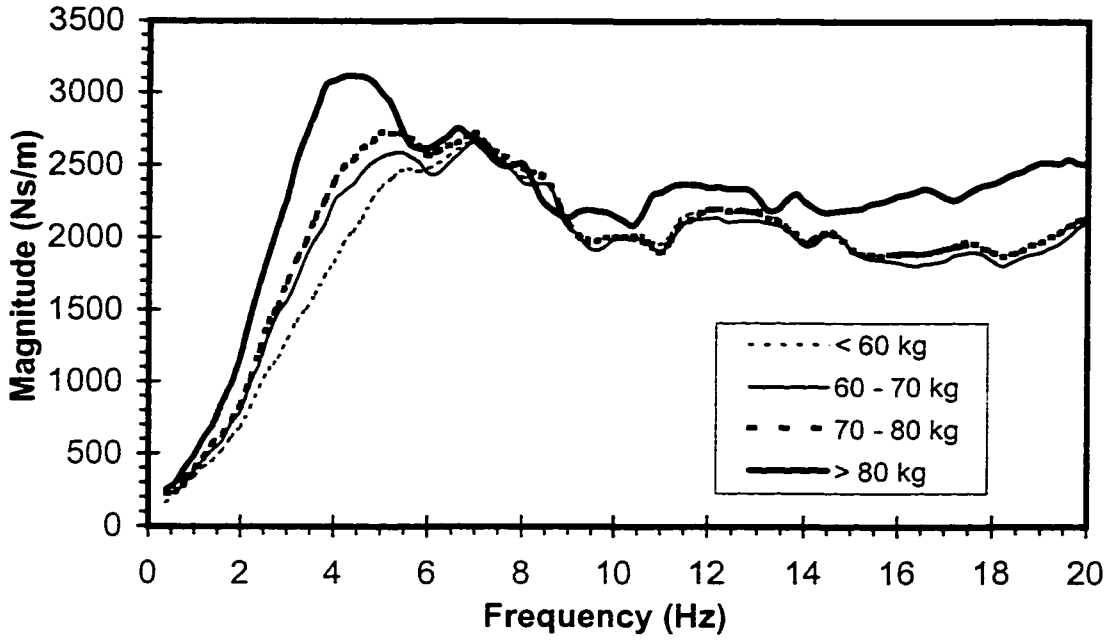

Figure 2.5: Effect of subject body mass on the magnitude of driving-point mechanical impedance [30].

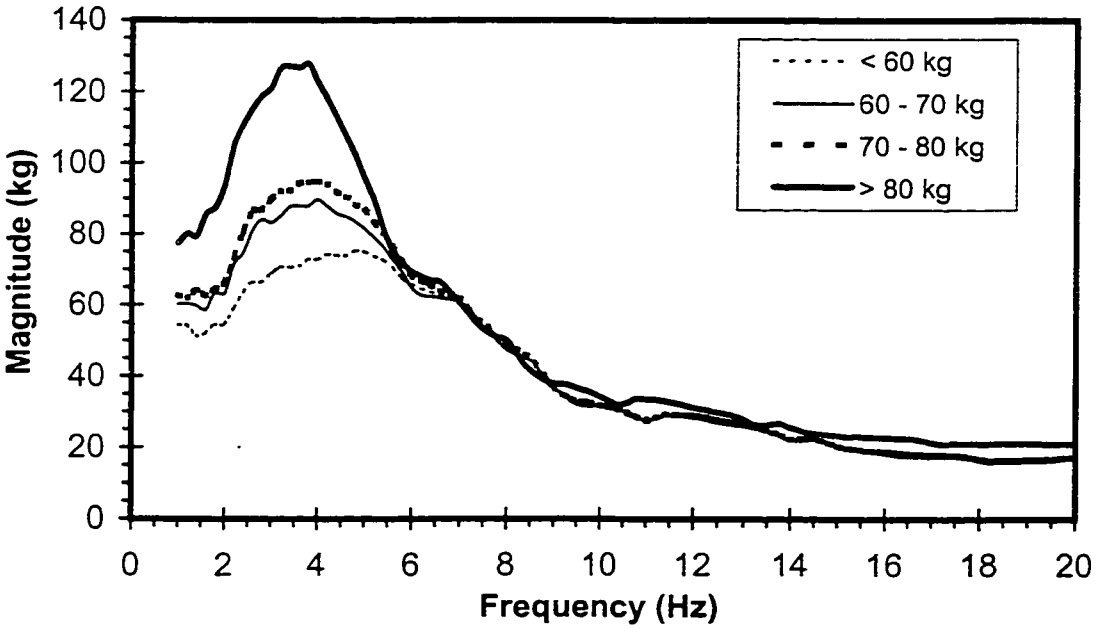

Figure 2.6: Effect of subject body mass on the magnitude of apparent mass [30].

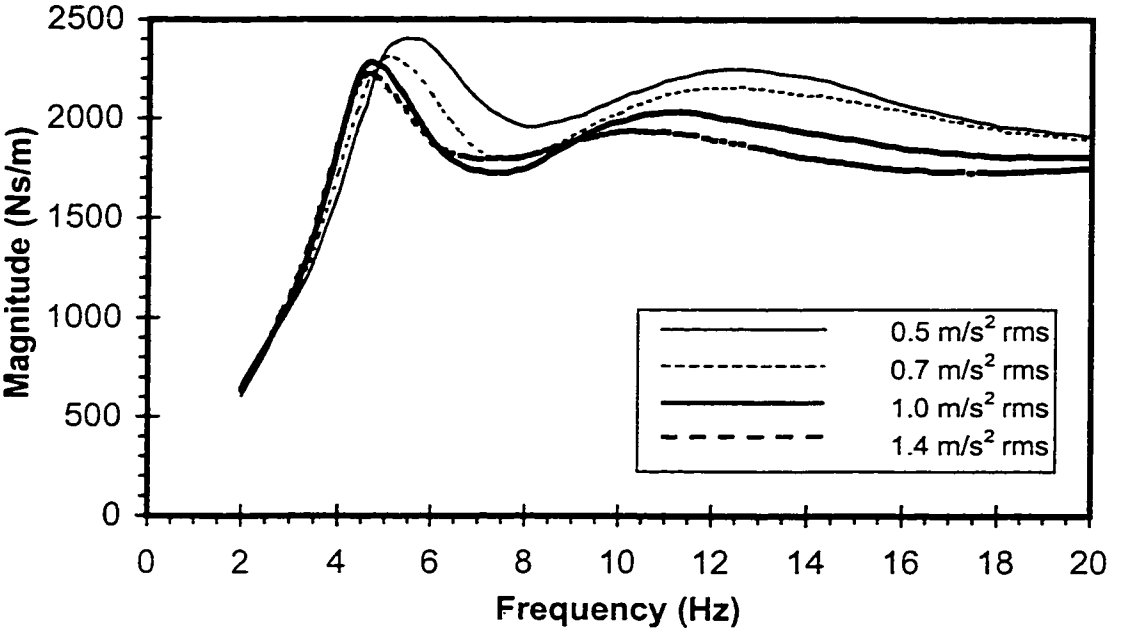

Figure 2.7: Effect of excitation level on magnitude of driving-point mechanical impedance for male subjects [29].

reported considerably different quantitative variations in DPMI with varying magnitudes of excitations. The mean DPMI data acquired for four male subjects exposed to sinusoidal vibration (2 - 12 Hz) of two different magnitudes (1.5 and 3.0 ms^{-2} rms), as shown in Figure 2.8, have been reported by Hinz and Seidel [28]. Figure 2.9 illustrates the corresponding APMS magnitude data derived from the reported DPMI data.

The results show that the peak DPMI magnitude decreases by 21.6% from 3700 to 2900 Nsm^{-1}, when excitation magnitude is increased from 1.5 to 3.0 ms^{-2} rms. In the experiment conducted by Holmlund *et al.* [29], peak DPMI magnitude decreases only by 7.1% from 2390 to 2220 Nsm^{-1}, when the excitation magnitude increases from 0.5 to 1.4 ms^{-2} rms. The dependency of DPMI or APMS magnitude on the magnitude of vibration excitations suggests nonlinear response behavior of the human body. The above studies may further suggest that the biodynamic response behavior becomes increasing nonlinear under higher levels of excitations. When the excitation levels vary within a narrow range, the human response to vibration may be considered nearly linear, as observed from Figure 2.7. The mean DPMI data reported by Boileau and Rakheja [31] for a total of 7 subjects maintaining an ENS posture exposed to three different levels of sinusoidal excitations (1.0, 1.5 and 2.0 ms^{-2} rms) is further examined to verify the above observation. Although the mean DPMI, shown in Figure 2.10, reveals a slight decrease in the primary resonant frequency, the peak magnitude reduces by only 3.2%, from 2786 to 2699 Nsm^{-1}, when the excitation level increases from 1.0 to 2.0 ms^{-2} rms. This observation also holds true for the data obtained under EBS postures.

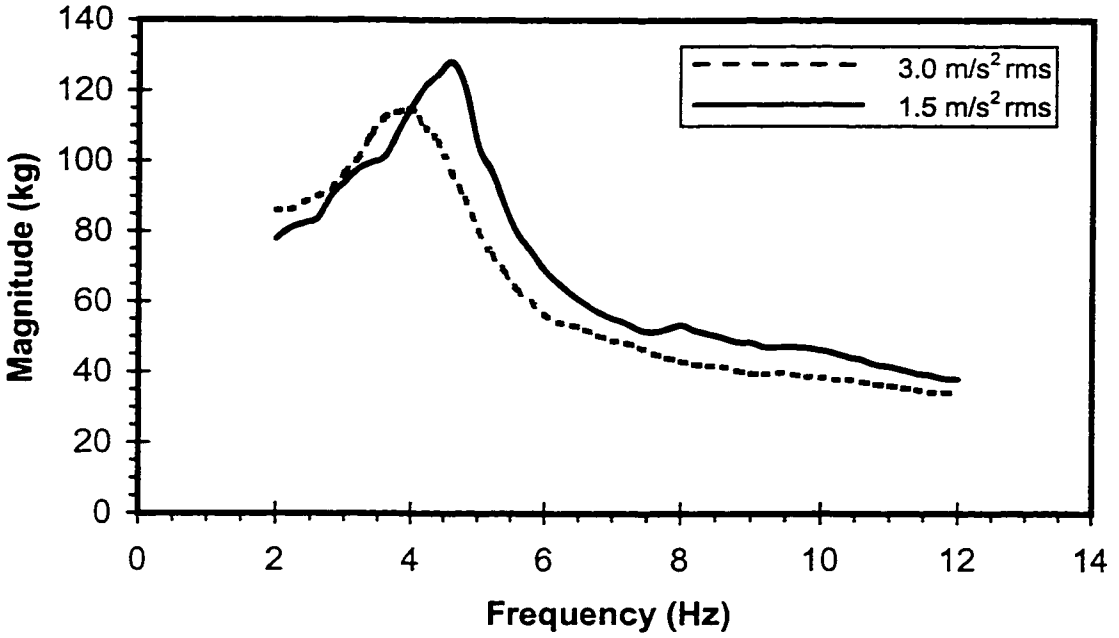

Figure 2.8: Effect of excitation level on magnitude of apparent mass [28].

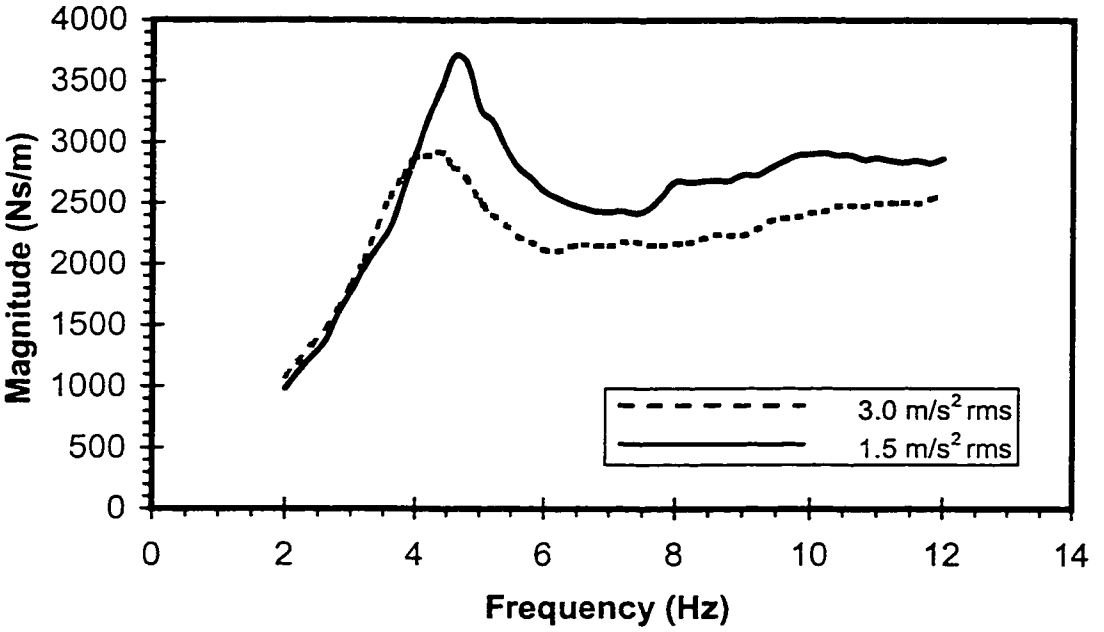

Fgiure 2.9: Effect of excitation level on magnitude of equivalent driving-point mechanical impedance (converted from from [28]).

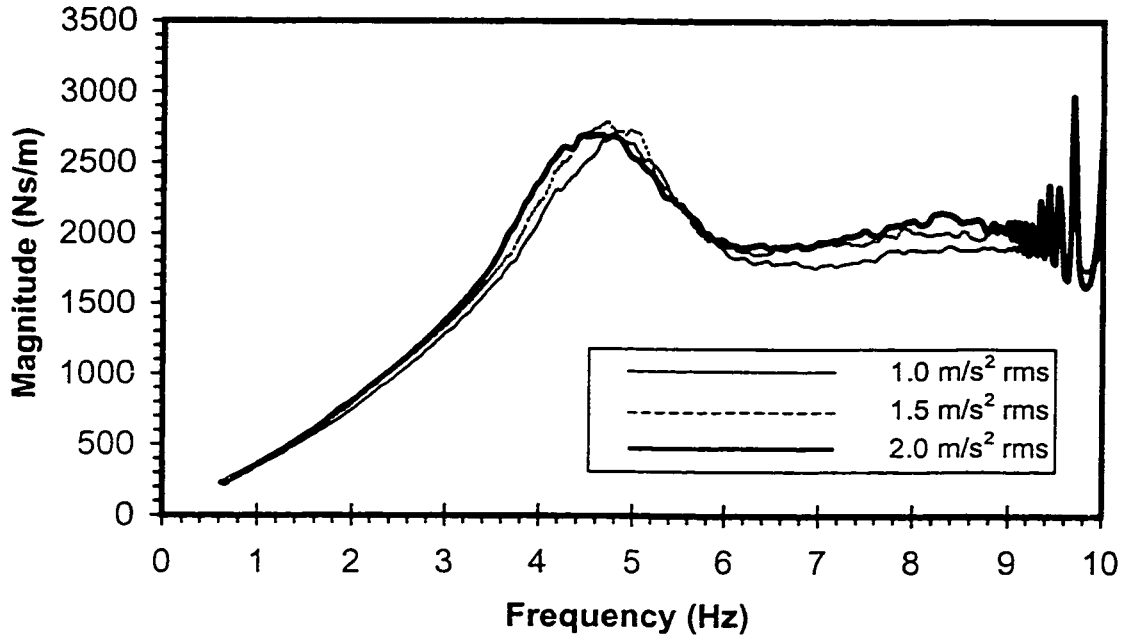

Figure 2.10: Effect of excitation level on magnitude of driving-point mechanical impedance with subject maintaining an ENS posture [31].

2.3.4 Influence of type of vibration excitation

The possible influence of type of vibration excitation on the DPMI magnitude has been investigated by Donati and Bonthoux [27] and Boileau [8]. Donati and Bonthoux exposed 15 male subjects to both sinusoidal and broad band random vibration excitations. For both of the vibration stimuli the frequency band was restricted to 1-10 Hz frequency range and the rms level of the acceleration was held at 1.6 ms^{-2}. The statistical analysis of the measured data showed that different stimuli did not affect the DPMI magnitude significantly except in the vicinity of primary resonant frequency, where sinusoidal excitations resulted in DPMI greater than that obtained under random motion. Boileau [8] investigated the influence of four types of excitation signals, including sinusoidal sweep and broad-band random excitations in the 1.0 to 2.0 ms^{-2} rms range, and four random excitation classes defined for off-road vehicles [32, 33]. The DPMI data were averaged over various vibration excitation levels for different postures. It was concluded that the DPMI magnitude vary only slightly for all the excitation signals and the seated postures considered in the study. It was thus suggested that the DPMI characteristics determined under sinusoidal or broad-band random vibration of similar magnitudes can be conveniently applied for off-road vehicle vibration.

2.4 Factors Influencing Magnitude of STHT

Although the influence of various factors on the DPMI and APMS have been studied extensively, only few studies have reported their influence on the seat-to-head vibration transmissibility of the seated subjects [26, 28, 34-37]. The lack of reported studies on seat-to-head vibration transmissibility may be attributed to complexities

associated with measurement of acceleration response of the human head. Some observations, however, may be made on the influence of various factors from the limited number of reported studies.

2.4.1 Influence of seated posture on STHT magnitude

The changes in seated posture, muscle tension, back support, and head and limb position may have the most significant influence on the STHT magnitude. Griffin *et al.* [26] investigated the STHT of a single subject assuming eight different postures ranging from 'slouched' to 'erect', and five head positions ranging from looking 50^0 down to looking 50^0 up under sinusoidal excitations of 1.0 ms^{-2} rms in the 0 to 50 Hz frequency range. The erect posture resulted in increase in the STHT magnitude at all frequencies above 3 Hz, and approximately 4 to 1 increase in the range of 15 - 25 Hz. The slouched posture, however, resulted in STHT magnitude well below unity at frequencies above 3 Hz. In the same study, the mean transmissibility determined for 18 male subjects, revealed that a stiff posture resulted in increased STHT magnitude at frequencies above 6 Hz, and lower STHT magnitude at frequencies below 6 Hz, when compared to those obtained for a relaxed posture. It has also been reported that increased muscle tension results in higher STHT from 5 to 10 Hz.

Cooper [37] investigated the influence of head angle on STHT up to 30 Hz, while controlling the posture of spine. It was found that raising or lowering the head increased the pitch vibration of the head, which contributes considerably to the vertical motion of the head. Paddan and Griffin [34] investigated the influence of leaning against a rigid backrest when evaluating STHT through experiments involving 12 subjects. The mean

STHT response characteristics of 12 subjects with and without backrest support are illustrated in Figure 2.11. The results clearly show that contact with a backrest yields significant increase in the transmission of vertical vibration at frequencies above 4.5 Hz. The contact with the backrest also increases the resonance frequency from 4.2 Hz to 6.2 Hz. It is probable that some of the increase is associated with different orientation of the head and neck, and the vibration transmission from backrest.

Some studies have also reported that the pelvis orientation could affect STHT magnitude [35, 38]. A footrest may further affect the STHT since it influences the seated posture, muscle tension, and the area of contact between the vibration input and the body. The STHT measurements performed by Griffin *et al.* [26] revealed that presence of a footrest (normal height) or its absence (legs hanging free) do not influence the STHT considerably. It is expected that any change in arm position or any other factor which causes a general posture change will affect the STHT response. This can be considered as the main reason for larger variations in STHT data between individuals and results reported by different researchers.

2.4.2 Influence of subject mass or body size on STHT

Only few studies have explored the influence of variation in the body mass and size on the STHT magnitude. A definite influence of such variations, however, could not be established due to considerable variations in the measured response of individuals. Some studies have concluded that increased mass or increased body size can be associated with lower STHT magnitude over a wide frequency range [39].

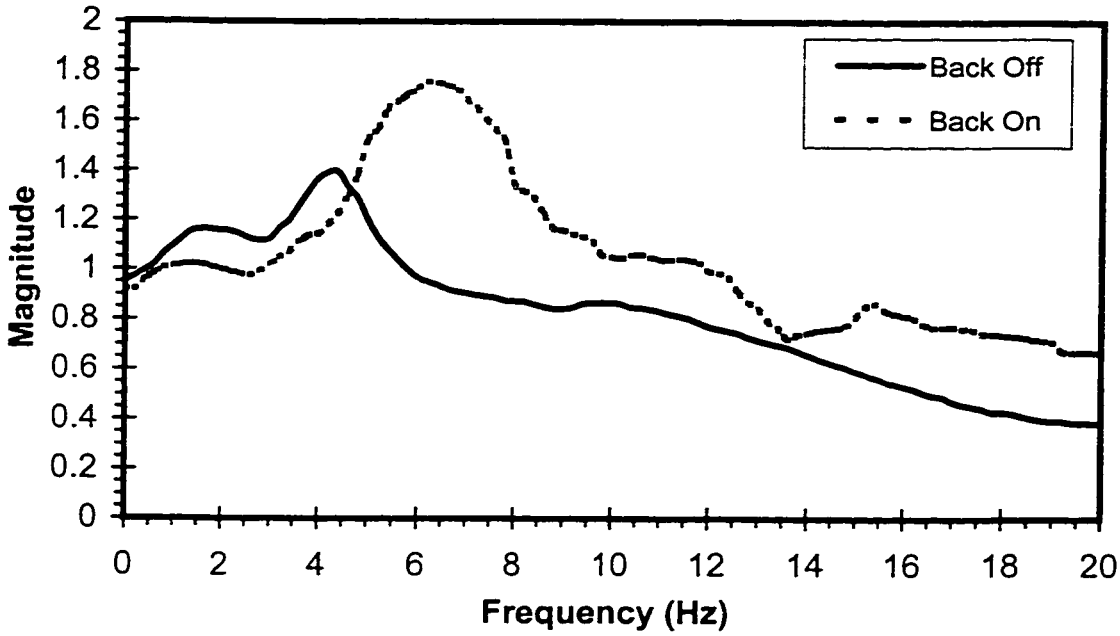

Figure 2.11: Effect of contact with a rigid flat backrest on the mean seat-to-head transmissibility of 12 subjects [34].

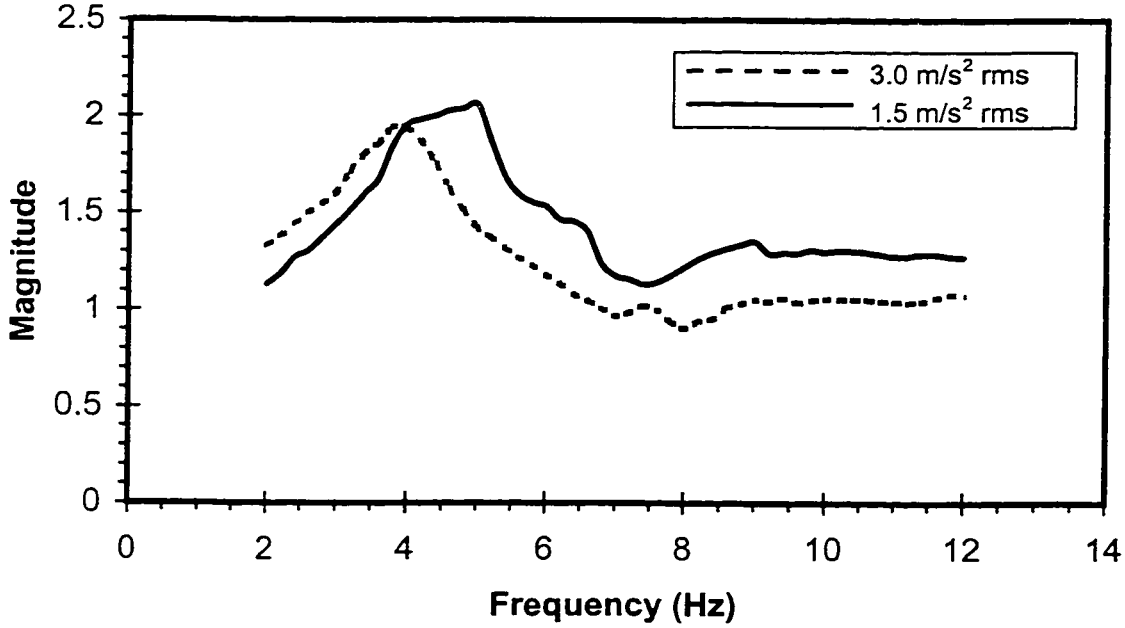

Figure 2.12: Effect of excitation level on mean magnitude of seat-to-head transmissibility of 4 subjects [28].

2.4.3 Influence of excitation magnitude

Few studies have concluded that the dynamic response of the seated body varies with magnitude of vibration excitation [26, 28]. The influence of the excitation magnitude on the STHT, however, is small, when compared with the contributions due to inter- and intra-subject variations. Variations in back support and head inclination are known to cause greater effects on STHT than that caused by variations in magnitude of the vibration. High levels of vibration excitations, however, can cause a significant change in STHT, though it is difficult to point out whether the change is caused by the non-linearity of the human body or the subject's voluntary control of the dynamic response of the body in order to reduce discomfort experienced under high levels of vibration.

Figure 2.12 illustrates the mean STHT of 4 male subjects under sinusoidal excitations of 1.5 and 3.0 ms^{-2} rms acceleration [28]. The influence of excitation level on the STHT appears to be significant and very similar to that observed for APMS (Figure 2.8). The primary resonant frequency and resonant magnitude decrease with increasing vibration intensity. The higher levels of excitation yield lower magnitudes of APMS and STHT at frequencies above 4 Hz, and higher values at frequencies below 4 Hz. When the excitation level is increased from 1.5 to 3.0 ms^{-2}, the primary resonant frequency established from STHT is reduced significantly from 5.0 to 3.8 Hz, and the resonant magnitude is reduced from 2.06 to 1.94.

2.5 Definition of Criteria for Developing Generalized Values for Biodynamic Response Functions

In view of the significant influence of some of the test conditions on the biodynamic response functions, it has been suggested that any attempt to define generalized values to characterize the biodynamic magnitude and phase response functions of the body would not be appropriate unless it could be defined specifically for a particular application or over a limited and well defined range of conditions.

In an earlier attempt to define generalized values for the biodynamic response of the body, an ISO 5982 Draft document [22] had proposed DPMI and STHT magnitude and phase characteristics of the human body based on a synthesis (*i.e.* combination and average) of various data sets reported by different investigators for the seated and standing individuals. The proposed values, particularly with regard to DPMI, were subsequently found to deviate quite considerably from those which would likely apply under conditions involving feet and postural constraints, and vibration excitation levels more typical of those likely to prevail in commonly encountered situations such as vehicle driving. It was thus postulated that the synthesis performed in defining the standardized values in the ISO CD 5982 perhaps included data sets, which were generated under too different and broad range of conditions, not representative of those in commonly encountered situations such as vehicle driving. In an effort to provide an understanding of the biodynamic response behavior of the seated body under commonly encountered work vibration environments, there was a need to use commonly available published data to define a range of most probable or idealized values to characterize the magnitude and phase responses of the concerned biodynamic functions under a particular range of conditions applicable to the situation considered.

As part of this study, a range of idealized values is defined for the DPMI, APMS and STHT of subjects maintaining an erect seated posture without backrest support, while the feet are supported and vibrated. The range of idealized values of the different biodynamic functions are determined by combining and averaging various data sets selected from the reported literature. The selected data sets, however, are limited only to those for which the reported experimental conditions include the specified posture and involve vibration excitation levels lower than or equal to 5 ms^{-2}. Such conditions can be broadly associated with those prevailing while driving particular types of vehicles, principally those employed in off-road applications. By extending the frequency span of interest to cover the range from 0.5 to 20 Hz and by incorporating the most recently available data, this synthesis may be considered to constitute a follow-up of a previous work initiated by Boileau [8] and has been reported in [89]. The data sets satisfying all of the following requirements were thus selected for the synthesis:

- Data sets specifying either individual or group mean subject mass of the test subject population, with attempt to limit the range of individual body masses to within 49 to 94 kg, corresponding to the range for which the most numerous number of data sets are available;

- Data sets on DPMI or APMS acquired with feet supported and vibrated, although this condition was considered irrelevant for STHT;

- Data sets acquired under vibration excitation amplitudes below 5 ms^{-2} rms, with the nature of the excitation specified as either sinusoidal or random;

- Data sets acquired under vibration excitations including spectral components within the 0.5 to 20 Hz frequency range;

- Data sets acquired under vibration excitations constrained to the vertical direction;

- Data sets acquired with subject population clearly identified, with particular analysis of those sets based on single subject;

- Data sets reporting the subject posture as being erect seated without backrest support, irrespective of the hands position.
- Data sets reporting either the magnitude, or both the magnitude and phase of the biodynamic response functions were included for the synthesis.

2.6 Selection of the Published Data on DPMI and APMS

The published data sets are initially selected based on the criteria defined in Section 2.5. Data sets presenting anomalous behavior, which may be caused by unreported differences in experimental conditions, subject populations, postural constraints, and vibration excitations used by the various investigators, are further removed on the basis of the standard deviation analysis. The remaining data sets are retained for the synthesis and for defining the most probable or idealized values applicable to the seated human body under the specified conditions.

2.6.1 Data selection based on predefined criteria

Of a total of 22 data sets identified for DPMI or APMS, summarized in Table 2.1, eight were rejected on the basis of selection rules outlined in Section 2.5. These included the data reported by Coermann [12], Edwards and Lange [40], Vogt *et al.* [24], Miwa [25], Mertens [21], Fairley and Griffin [17, 41], and Smith [42]. These data sets are excluded due to two primary factors: (i) subjects' feet neither supported nor vibrated; and (ii) certain test conditions, such as subject mass, and posture, not reported. The unreported information of the total body mass of the test subjects is the main reason for not having considered the mean normalized APMS data reported in Fairley and Griffin [17], which otherwise is regarded as a very valuable data set in view of the significantly large subject population involved (60 subjects including 24 men, 24 women and 12 children). The

characteristics related to the subject population, excitation and response function reported for each of the remaining data sets are summarized in Table 2.3, as they relate to the raw data considered for the synthesis on DPMI and APMS. While all of these data sets reported either DPMI or APMS magnitude, only twelve provided the corresponding phase information between the force and motion variables.

Among the data sets complying with the selection rules, a distinction is made in Table 2.3 for some data sets, which although reported by the same authors, were generated using different types and/or levels of excitations. Such is the case in the study by Hinz and Seidel [28] in which mean APMS data is reported for two levels of sinusoidal excitations, 1.5 and 3.0 ms^{-2}, hereafter referred to as H&S-1.5 and H&S-3.0, respectively. Suggs *et al* [16] reported mean DPMI data while using a constant displacement sinusoidal excitation but without exceeding an acceleration of 3.5 ms^{-2} rms within the frequency range considered. Donati and Bonthoux [27], and Boileau and Rakheja [31] reported mean DPMI data under both sinusoidal and random excitations of equivalent levels, 1.6 ms^{-2} in the former study while the latter included an average of data acquired at fixed magnitudes ranging from 1.0 to 2.0 ms^{-2}. These data sets are further identified as D&B-sine, D&B-random, B&R-sine and B&R-random in this study.

Seidel [30] reported mean DPMI data grouped according to the mass range of the population of subjects involved in the experiments. These data sets, referred to as Seidel 60-70 and Seidel 70-80, represent the mean values of DPMI measured under a fixed range of vibration amplitudes, using subject population with mass ranging from 60 to 70 kg and 70 to 80 kg, respectively. The data by Holmlund *et al.* [29] represents the total group average based on mean normalized DPMI values reported using 15 female and 15

Table 2.3: Characterization of data sets considered for mechanical impedance and apparent mass.

Authors	Subject			Excitation			Reported Functions
	Number	Sex	Mass	Type	Level	Frequency Range	
Suggs, Abrams and Stikeleather [16]	11	Male	58-90 kg	Sine	2.54 mm peak-peak	1.75-10 Hz	Mean DPMI magnitude and phase
Sandover [45]	6		52.7- 87.2 kg	Random	1 ms^{-2} rms	1 - 25 Hz	Individual APMS magnitude and phase
Donati and Bonthoux [27]	15	Male	49-74 kg	Sine sweep	1.6 ms^{-2}	1 – 10 Hz	Mean DPMI magnitude and phase
Donati and Bonthoux [27]	15	Male	49-74 kg	Broad band random	1.6 ms^{-2}	1 – 10 Hz	Mean DPMI magnitude and phase
Fairley and Griffin [43]	1	Male	63 kg	Gaussian random	1 ms^{-2} rms	0.25 – 20 Hz	APMS magnitude and phase
Fairley and Griffin [44]	8	Male	57 – 85 kg	Random	1 ms^{-2} rms	0.25 – 20 Hz	Individual APMS magnitude and phase
Hinz and Seidel [28]	4	Male	56 – 83 kg	Sine	1.5 ms^{-2} rms	2 – 12 Hz	Mean DPMI magnitude and phase
Hinz and Seidel [28]	4	Male	56 – 83 kg	Sine	3.0 ms^{-2} rms	2 – 12 Hz	Mean DPMI magnitude and phase
ISO CD 5982 [22]	39		51 – 93.8 kg	Sine	1 - 2 ms^{-2} rms	0.5 – 31.5 Hz	Mean DPMI magnitude and phase
Holmlund, Lundstrom and Lindbergh [29]	15 15	Men Women	57 – 92 kg 54 – 93 kg	Sine	0.5, 0.7, 1.0, 1.4 ms^{-2} rms	2 – 100 Hz	Mean DPMI magnitude and phase
Seidel [30]	11	Males	60-70 kg	Random	0.7, 1.0, 1.4 ms^{-2}	0 – 20 Hz	Mean DPMI magnitude
Seidel [30]	14	Males	70-80 kg	Random	0.7, 1.0, 1.4 ms^{-2}	0 – 20 Hz	Mean DPMI magnitude
Boileau and Rakheja [31]	7	Males	75.4 kg	Sine sweep	1, 1.5, 2.0 ms^{-2} rms	0 – 10 Hz	Mean DPMI magnitude and phase
Boileau and Rakheja [31]	7	Males	75.4 kg	Broad band random	1, 1.5, 2.0 ms^{-2} rms	0 – 10 Hz	Mean DPMI magnitude and phase

male subjects under constant excitation level of 0.5 ms^{-2}. Two APMS data sets, acquired under the same conditions, reported by Fairley and Griffin [43, 44], are considered: one representing a single subject data (referred to as F&G-1983), while the other is obtained by averaging individual data reported for 8 subjects (referred to as F&G-1986). The data extracted from the ISO CD 5982 [22] represents by itself a synthesis of various data sets having been reported under specific conditions. The curves are said to apply to subjects under excitation levels of 1 to 2 ms^{-2}, although it is admitted that the acceleration amplitudes were not specified by the authors for some of the studies considered, and it is not clear exactly which data sets were considered in the synthesis. The data is said to apply to seated subjects with an upright body position, although it is admitted that posture was often vaguely defined in the studies considered and that it generally included subjects with feet hanging free. As for the data referred to as Sandover [45], it represents an average of six individually reported APMS data.

Figure 2.13 presents a comparison of the DPMI magnitude in the 0.5 to 20 Hz frequency range derived from the 14 reported data sets identified in Table 2.3. These data sets are also presented by their equivalent APMS magnitude in Figure 2.14. The corresponding phase data related to the DPMI response is presented in Figure 2.15. The APMS phase data is not presented since, by definition, it would only differ from DPMI phase by a constant phase angle of 90°. Although the conditions pertaining to these data sets are reported to lie within the common bounds established from the selection rules, significant variations, which may be more apparent in specific frequency ranges, are observed among the data. An examination of Figures 2.13 and 2.14 further reveals significantly larger variations among the reported DPMI magnitude. In contrast, the

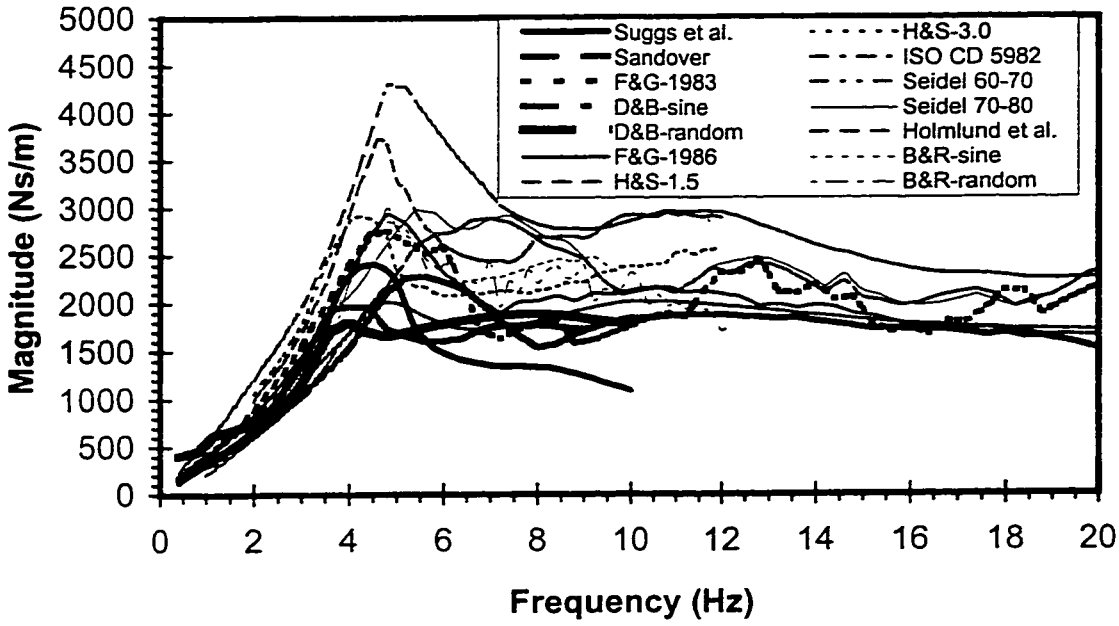

Figure 2.13: A comparison of magnitudes of driving-point mechanical impedance reported under defined conditions.

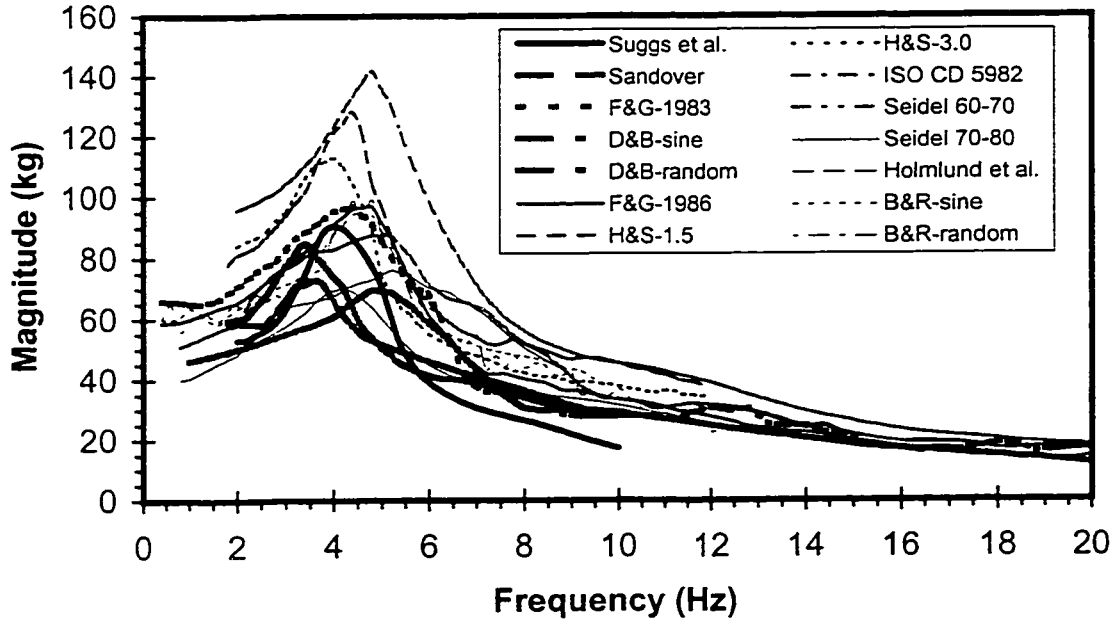

Figure 2.14: A comparison of magnitudes of apparent mass reported under defined conditions.

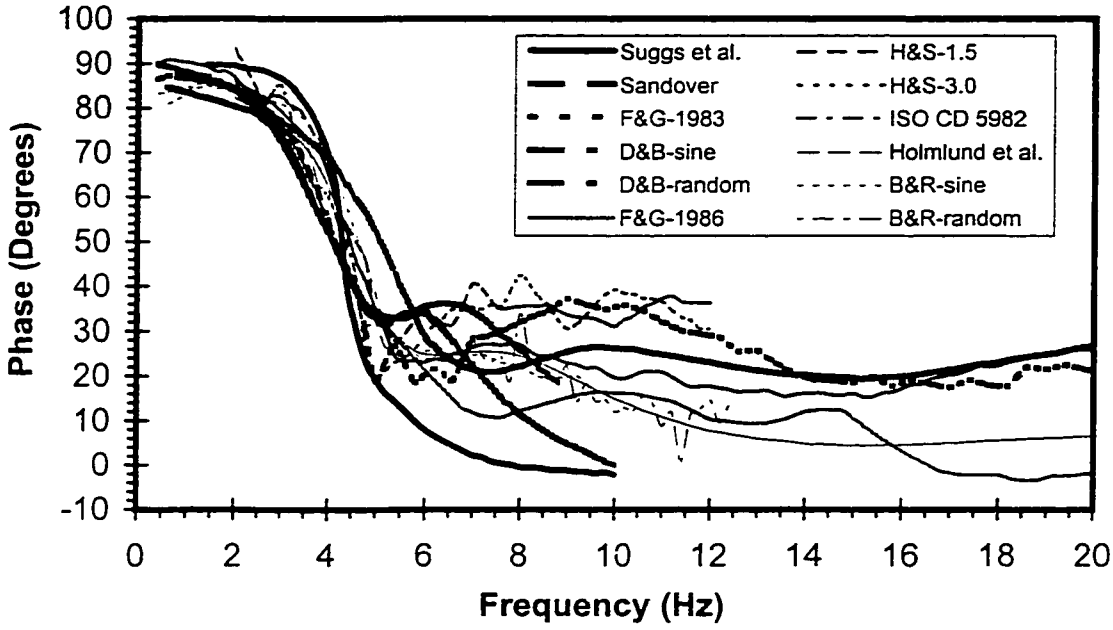

Figure 2.15: A comparison of driving-point mechanical impedance phase response reported under defined conditions.

APMS magnitude data sets appear to be relatively closer, particularly at higher frequencies, since the frequency dependence present in the DPMI function is eliminated when APMS function is employed. It can be observed that by presenting the measured results in terms of either DPMI or APMS, different trends can be noted, which may affect the analysis. The merits and demerits of these two functions in demonstrating measured biodynamic data, although very important, have never been addressed in the literature. This fundamental issue is thus explored in Chapter 3 in an attempt to identify a desirable biodynamic function.

2.6.2 Data selection based on analysis of the standard deviation

Although all of the identified data sets were extracted from studies in which the reported conditions satisfied most of the previously defined selection rules, it is difficult to establish the sources of variability between the various data sets. While every effort was made to restrict the range of experimental conditions to those defined by the selection rules, there most certainly remained unreported differences in experimental procedures, subject populations, postural constraints, and types and levels of vibration excitations used by the various investigators. These differences could also have contributed to the observed variations between the data sets. Although it would be impossible to entirely eliminate these sources of variation when considering data originating from different studies, their relative influence may be minimized while performing the synthesis by rejecting the data presenting anomalous behavior and retaining only those data sets for which similar trends may be observed.

In an effort to show the extent of the variations between the various data sets and to identify which should be excluded from the synthesis, the standard deviation on the mean values is computed as a function of frequency for different combinations of data sets. The combination presenting the least variation (*i.e.* lowest standard deviation) over the broadest frequency range is subsequently retained for the synthesis and for defining the most probable or idealized values applicable to the seated human body under the specified conditions.

An examination of the various DPMI data sets, illustrated in Figure 2.13, reveals that the majority of the curves show certain important trends. Majority of the data sets exhibit dominant peak in the 4 to 6 Hz frequency range, followed by a decline and a second weakly apparent peak within the 10 to 14 Hz frequency range. While the absolute magnitudes observed in various studies clearly differ, most curves show similar trends or at least have their magnitudes within close bounds except for a few isolated data sets. Such is the case for the ISO CD 5982 [22] data which definitely forms an outlier over most of the frequency range. The proposed values are generally much higher than those provided by the other data sets, particularly near the primary resonant frequency. This apparent overestimation of the impedance magnitude compared to those reported in several other studies has also been reported by Holmlund *et al.* [29]. There have been suspicions that this might be due to the fact that the ISO CD 5982 data perhaps applies more closely to subjects with feet hanging freely than to those with feet supported. Hinz and Seidel's data [28] reported under an excitation level of 1.5 ms^{-2} (H&S-1.5) is also observed to follow trends similar to that of the ISO CD 5982 data: the magnitude is considerably higher than those for most of the other data sets over most of the frequency

range considered. The data reported by Hinz and Seidel [28] under 3.0 ms^{-2} (H&S-3.0) presents also some concerns with respect to the other data sets in constituting a potential outlier towards the lower and higher extremities of the frequency range considered. Another anomaly is observed with Suggs *et al.* data [16] at frequencies above approximately 6 Hz, where the reported magnitude is considerably lower than the other data sets. The pattern showing a continued decrease in magnitude with frequency contradicts that observed for most other data sets in a similar frequency range. Finally, the data reported by Seidel *et al.* [30], identified as Seidel 60-70 and Seidel 70-80, may be considered to be somewhat anomalous in that both data sets show peak magnitude occurring at a frequency ranging from 6 to 8 Hz, which is distinctly higher than the 4 to 6 Hz range established from most of the other data sets. While most data sets indicate a decrease in magnitude within the 6 to 8 Hz frequency range, followed by a subsequent increase at higher frequencies, these two data sets with peaks occurring in the 6 to 8 Hz frequency range contradict with the generally observed trends.

An examination of the selected data sets expressed in terms of APMS (Figure 2.14), generally reveals variations of considerably lesser degree amongst the various data sets, when compared to the corresponding variations among the DPMI data appearing in Figure 2.13. This is particularly evident towards higher frequencies, although the spread may appear broader at low frequencies. Generally, the data sets on DPMI magnitude identified as forming outliers or presenting anomalies are also found to present such particularities when presented in terms of the APMS. For three of these data sets, however, the anomaly may appear to be more or less obvious depending on whether the data is presented in terms of DPMI or APMS. This is the case for H&S-3.0 data, which

exhibits considerable deviations from the majority of the other data at lower frequencies, when presented in terms of the APMS. In contrast, Seidel 60-70 and Seidel 70-80 data sets are observed to follow more closely the trends prescribed by the majority of APMS curves than those established on the basis of DPMI.

A quantitative analysis is further performed in an effort to identify the definite outliers. The standard deviations of the DPMI magnitude are computed for different combinations of the data sets. Figure 2.16 presents the distribution of the standard deviation computed as a function of frequency for five different combinations of data sets of DPMI magnitude. The first combination involves all the 14 data sets identified in Table 2.3, while subsequent cases gradually exclude some of the data sets identified as showing anomalies with respect to majority of the data. The exclusion of data sets reported by ISO CD 5982, H&S-1.5 and Suggs *et al.* yields considerably lower standard deviation over most of the frequency range concerned. The results further show the standard deviation of combinations excluding H&S-3.0, Seidel 60-70 and Seidel 70-80 data sets. The most significant standard deviation, in general, is observed to occur in the 4 to 6 Hz frequency range, indicating that the most important variability amongst the studies occur at frequencies near the main body resonance. The results presented in Figure 2.16 suggest that the exclusion of the above data sets (ISO CD 5982, H&S-1.5, H&S-3.0, Suggs *et al.*, Seidel 60-70 and Seidel 70-80) leads to a probable combination, which exhibit least deviation amongst various data sets in the entire frequency range.

The standard deviations of the APMS magnitude established from various combinations of data sets, identified in Table 2.3, are presented in Figure 2.17, as a

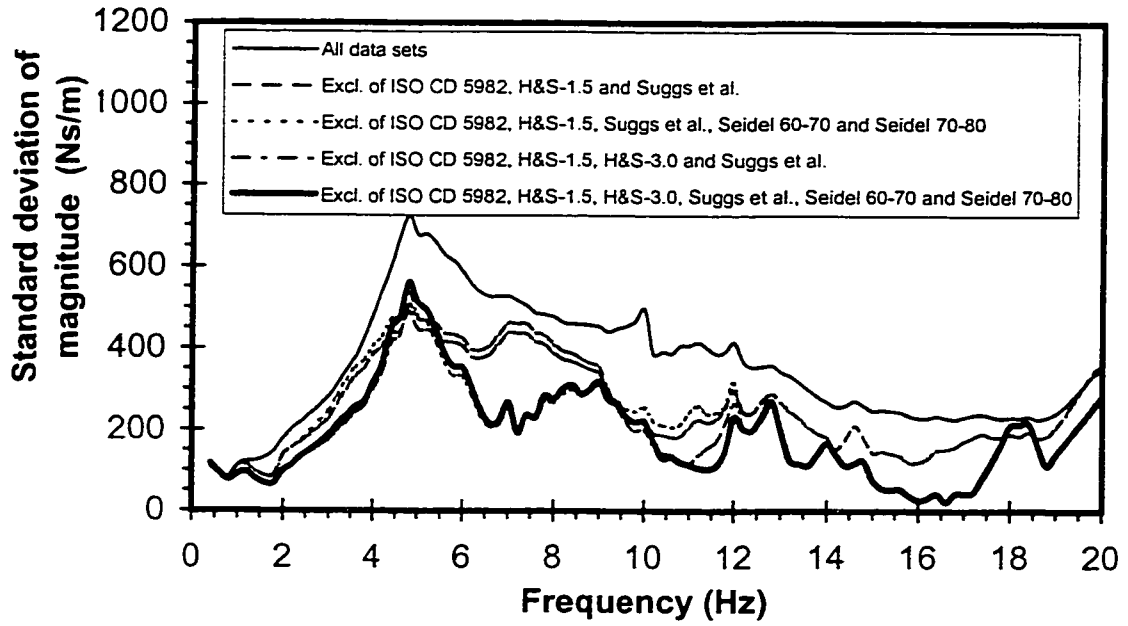

Figure 2.16: Absolute value of standard deviation on mean magnitude of driving-point mechanical impedance computed for various combinations of data.

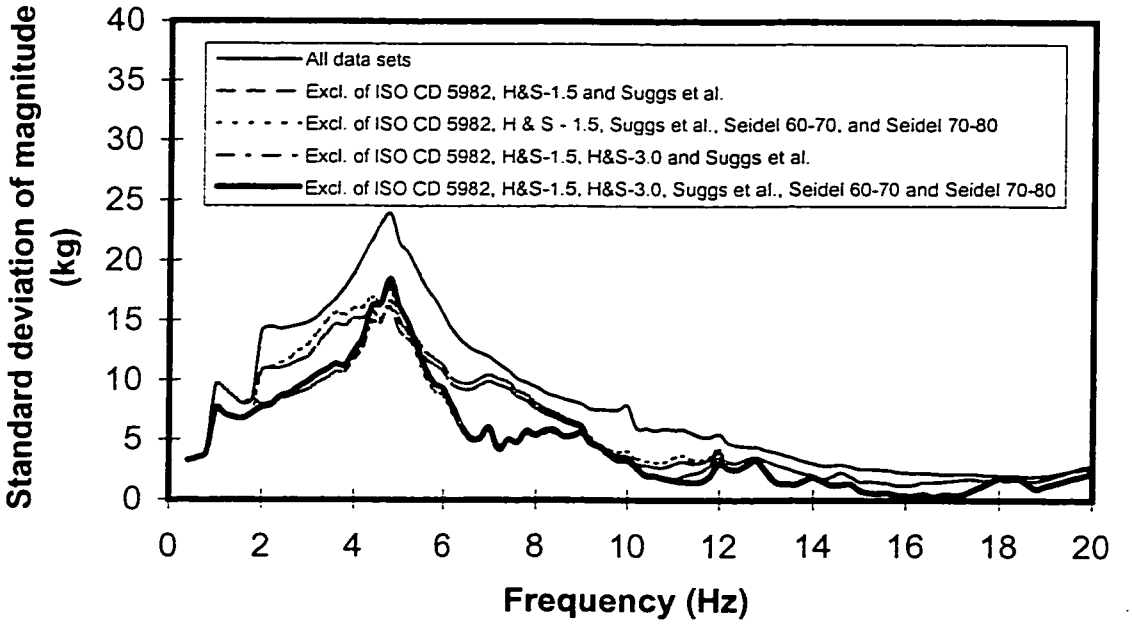

Figure 2.17: Absolute value of standard deviation on mean magnitude of apparent mass computed for various combinations of data.

function of the vibration frequency. The results suggest that the exclusion of the above data sets yield limited degree of variation amongst the data.

The comparison of the selected data sets of DPMI phase, illustrated in Figure 2.15, reveals a relatively consistent pattern. The DPMI phase is approximately 90° at very low frequencies, which asymptotically approaches 0° at higher frequencies. While most data sets exhibit generally good agreement in the phase response up to approximately 5 Hz, large differences are observed to arise at higher frequencies. The phase data sets presented in Figure 2.15 show that only two of the twelve data sets exhibit important differences with respect to the rest of the data sets. These include the data reported by Suggs *et al.* [16] and Donati & Bonthoux [27] under random excitation (D&B-random). The DPMI phase response in both cases approaches zero at a frequency less than 10 Hz, while the rest of the data sets indicate a more gradual decrease in phase response with frequency.

Following the procedure applied for defining the most probable values of DPMI and APMS magnitudes, the data sets presenting apparent deviations from majority of the data sets are excluded to derive the most probable values of DPMI phase. Moreover, a further selection rule is introduced calling for exclusion of the phase data whenever such data was produced concurrently with the magnitude information, which was excluded from the synthesis. This selection rule suggests that the phase information cannot be applied, if the corresponding magnitude response is considered inapplicable, since both are determined under identical conditions. In contrast, the inapplicability or unavailability of phase information does not imply the exclusion of corresponding magnitude information owing to the difficulties in performing proper phase measurements and to

the fact that poor phase information does not impede the value of magnitude information. Applying the above stated selection rules to the phase data presented in Figure 2.17 results in exclusion of the data sets referred to as ISO CD 5982, Suggs *et al.*, H&S-1.5 and H&S-3.0. D&B-random data is also excluded in view of its considerable deviations with respect to most other data sets. The final selection based on the remaining seven data sets is further justified by the standard deviation shown in Figure 2.18. The results show relatively small standard deviation, when the above data sets are excluded.

2.7 Selection of the Reported Data on Vertical STHT

The reported data sets on vertical STHT were initially selected based on the predefined criteria, and the standard deviation of various combinations was performed to identify a suitable combination.

2.7.1 STHT data selection based on predefined criteria

A total of 10 data sets on the vertical STHT of the seated human body were identified from the published studies, based on the selection rules described in Section 2.5. Two sets reported by Griffin *et al.* [46] were rejected, since the mass information of the test subjects was not specified. The number of subjects used, and the nature and level of vibration excitations employed in each of the remaining data sets are summarized in Table 2.4. While all the studies reported STHT magnitude, only five provided the corresponding phase information. Majority of the data was acquired using sinusoidal excitation with vibration levels usually much higher than those used for defining DPMI or APMS. While the levels used for DPMI or APMS were most often maintained below 2

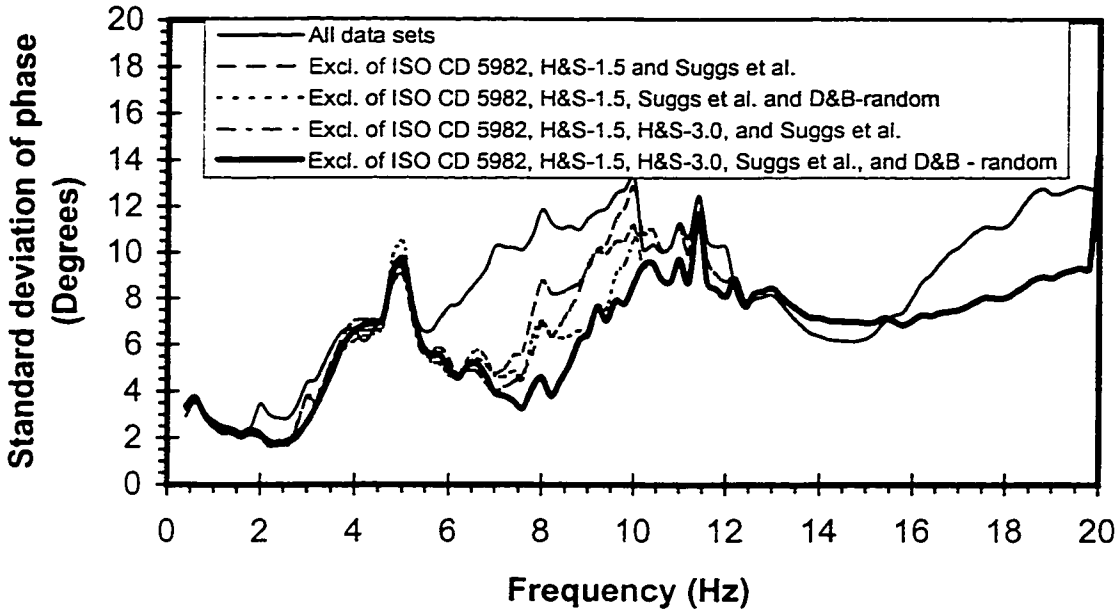

Figure 2.18: Absolute value of standard deviation on the mean phase angle of driving-point mechanical impedance computed for various combinations of data.

Table 2.4: Characterization of data sets considered for seat-to-head transmissibility.

Authors	Subject			Excitation			Reported Functions
	Number	Sex	Mass	Type	Level	Frequency Range	
Coermann [12]	1	Male	84 kg	Sine	<5 ms^{-2} rms	1 – 20 Hz	Magnitude
Vogt, Coermann and Fust [24]	10	Male	70 kg (mean)	Sine	5 ms^{-2} rms	2 –15 Hz	Mean magnitude
Mertens [21]	9	6 males 3 females	57 – 90 kg	Sine	4 ms^{-2} rms	2 – 20 Hz	Mean magnitude and phase
Hinz and Seidel [28]	4	Male	56 – 83 kg	Sine	1.5 ms^{-2} rms	2 – 12 Hz	Mean magnitude and phase
Hinz and Seidel [28]	4	Male	56 – 83 kg	Sine	3.0 ms^{-2} rms	2 – 12 Hz	Mean magnitude and phase
Paddan and Griffin [34]	12	Male	70.8 kg (mean)	Gaussian Random	1.75 ms^{-2} rms	Up to 25 Hz	Individual magnitude and phase
ISO CD 5982 [22]	50		75 kg (mean)	Sine	1 - 2 ms^{-2} rms	0.5 – 31.5 Hz	Mean magnitude and phase
Zimmermann and Cook [35]	30		77.6 kg (mean)	Sine	1 ms^{-2}	4.5 – 16 Hz	Mean magnitude

ms^{-2}, the majority of STHT data were acquired under levels ranging from 1.5 to 5.0 ms^{-2}.

Most of the data sets identified in Table 2.4 were obtained using a large number of subjects, except for that reported by Coermann [12], which relates to only one subject. Hinz and Seidel [28] reported mean STHT data under two different levels of excitations, 1.5 ms^{-2} and 3.0 ms^{-2} (referred to as H&S-1.5 and H&S-3.0), using 4 subjects. The values reported by Mertens [21] and considered in this study are the mean of data obtained from superposition of a static acceleration of 1 g, representing normal gravity, and of a dynamic vibration level of 4 ms^{-2}. Vogt *et al* [24] were amongst the earliest investigators to provide mean data complying with the selection rules, while Paddan and Griffin [34] (P&G-1988) were amongst the latest. Zimmermann and Cook [35] recently published mean data on the STHT established using 30 subjects, although the data was reported only at specific discrete frequencies between 4.5 and 16 Hz, while the corresponding phase information was not provided. Although such data, referred to as Z&C-1997, is provided for different pelvic orientations, only that defined for the neutral position is considered in this study. The data proposed in the ISO CD 5982 [22] presents a synthesis of various data sets and is said to represent the mean transmissibility of 50 subjects with mean mass of 75 kg exposed to vibration excitation levels between 2 and 4 ms^{-2}. It is generally admitted that, in some of the studies considered for deriving the ISO CD 5982 curves, the vibration excitation levels and the body position were not specified. The synthesis did not distinguish between values pertaining to the sitting and standing body positions.

Figure 2.19 presents a comparison of the STHT magnitude data derived from the various data sets identified in Table 2.4, while Figure 2.20 presents a comparison of the

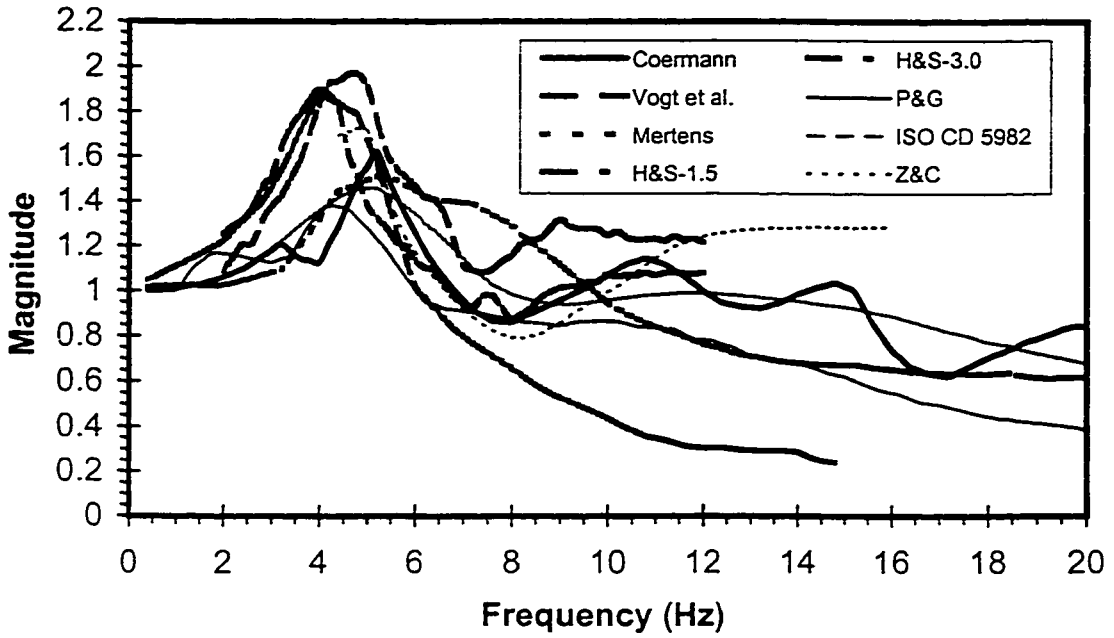

Figure 2.19: A comparison of the magnitudes of the seat-to-head transmissibility reported under the defined conditions.

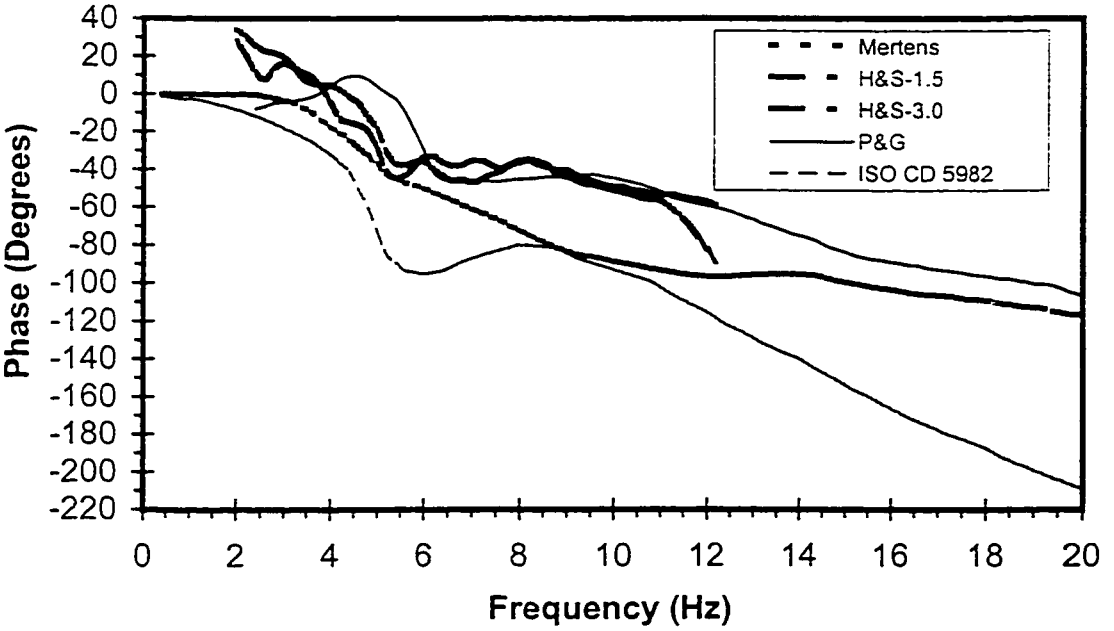

Figure 2.20: A comparison of the seat-to-head transmissibility phase angles reported under the defined conditions.

corresponding phase data, whenever available. In comparison with the data on DPMI and APMS, significantly fewer data sets are available on STHT, while more variations are found to exist between the various data sets over most of the frequency range considered. This may be expected in view of the complexities associated with the measurements. Furthermore the function, being a transfer function through the body, is relatively more sensitive to some of the experimental conditions, mainly subject posture, than the APMS or DPMI.

2.7.2 STHT data selection based on standard deviation

Similar to the selection of data sets on DPMI and APMS, the standard deviation on the mean values of STHT is computed as a function of frequency for different combinations of data. The combination presenting the least variation (*i.e.* lowest standard deviation) over the broadest frequency range is subsequently retained for the synthesis and for defining the most probable or idealized values applicable to the seated human body under the specified conditions.

From analysis of the data sets shown in Figure 2.19, the pattern regarding STHT magnitude indicates a dominant peak occurring within the 4 to 6 Hz frequency range, corresponding to primary whole-body resonance. This is usually followed by a gradual decrease of STHT magnitude with frequency, although some data sets indicate potential secondary peaks at frequencies above 10 Hz. The frequency at which the peak transmissibility occurs is seen to vary amongst the data sets, as does the peak magnitude itself. In all cases, the transmissibility magnitude is larger than unity at frequencies below approximately 6 Hz, while there is a tendency for the magnitude to drop below 1.0 at

frequencies above 6 Hz. Exceptions to these trends are seen with H&S-1.5 and H&S-3.0. While the former indicates a transmissibility magnitude greater than 1.0 over the entire frequency range considered, the latter is only seen to decrease below 1.0 over a very limited frequency range. Zimmermann and Cook's data (referred to as Z&C) is also observed to present discrepancies at frequencies above 10 Hz by indicating a gradual amplification of vibration with frequency, while most other data sets show a gradual attenuation over a similar frequency range. Finally, Vogt *et al.* [24] data constitutes a definite outlier at frequencies above 6 Hz by presenting a very rapid drop in STHT magnitude with frequency as opposed to a more gradual decrease for most other data sets.

Figure 2.21 presents the standard deviation on the mean values of STHT magnitude computed for different combinations of the data sets. Considering the entire frequency range, the combination of data which generally involves lesser degree of variation at most frequencies is that based on only four data sets, which exclude those by H&S-1.5, H&S-3.0, Vogt *et al.* and Z&C. The five data sets on the STHT phase response, shown in Figure 2.20, indicate a general pattern with most curves showing a 0° phase angle at low frequency followed by a gradual decrease in phase angle as the frequency is increased. Applying the data synthesis selection rule defined in Subsection 2.6.2 to the effect that phase data should be excluded whenever magnitude data is rejected results in further exclusion of H&S-1.5 and H&S-3.0 data sets. Consequently, only three data sets are made available to define the STHT phase information. These are the data reported by Mertens [21], Paddan and Griffin [34] and that proposed in ISO CD 5982 [22].

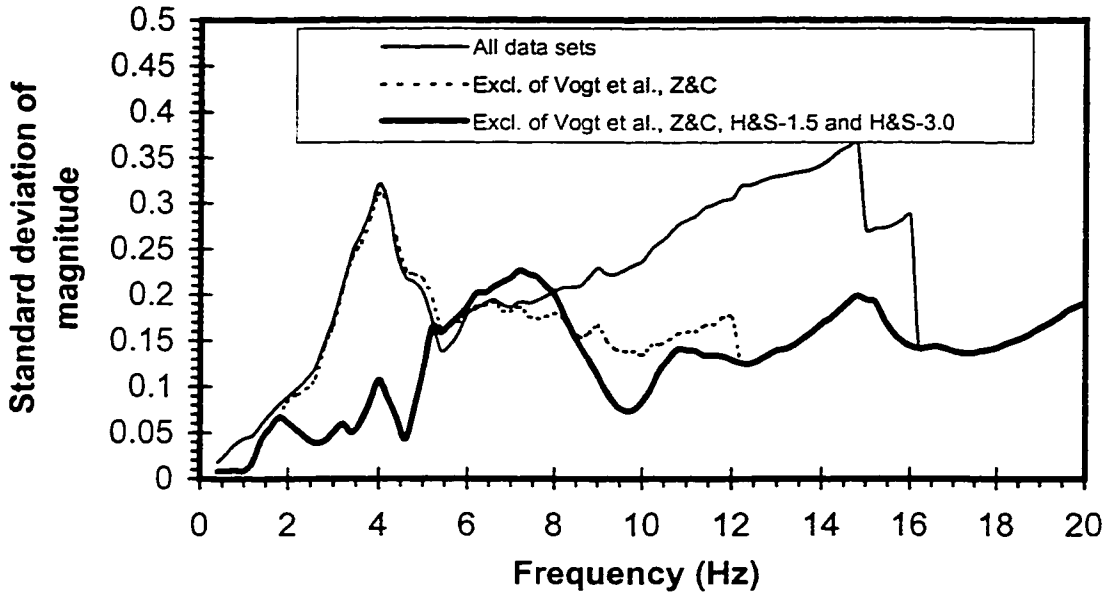

Figure 2.21: Absolute value of standard deviation on mean magnitude of the seat-to-head transmissibility computed for various combinations of data

2.8 Definition of a Range of Idealized Values

The unexplained differences in biodynamic response characteristics emerging from different studies serve to justify the exclusion of outliers or data sets, which present peculiar behavior with respect to generally observed trends established from majority of the studies. Since the aim of this study is to define idealized values under very specific range of conditions, the exclusion of any particular data set should not be interpreted as a value judgment on the quality of the reported data, but more as an indication that the particular conditions under which the data was acquired perhaps do not comply with the prescribed conditions. While every effort was made to consider only the data for which the reported conditions would closely match with those established by the selection rules, the possibility of particular conditions, either unreported or misinterpreted, could have led to the observed discrepancies.

The range of idealized or most probable values characterizing the biodynamic response of the seated body under the particular conditions is derived in the 0.5 to 20 Hz frequency range, by simply averaging of the selected data sets, upon removal of the outliers, and by smoothing and creating envelopes about the mean values. Smoothing is accomplished from successive piecewise approximations using a fixed number of points while creating an overlap. Any data that fall within the range of idealized values defined by the envelope curves may be considered to be acceptable representation of the biodynamic response functions of the seated human body under the specific conditions defined.

2.8.1 Range of idealized values of DPMI and APMS

Upon exclusion of the data sets identified in Section 2.6 for DPMI and APMS magnitudes, the synthesis of the data sets within the most desired combinations are illustrated in Figures 2.22 and 2.23, respectively. The synthesis is based on 8 data sets identified as Sandover, F&G -1983, D&B-sine, D&B-random, F&G -1986, Holmlund *et al.*, B&R-sine, and B&R-random. The figures show the smoothened envelopes of maximum and minimum values derived from the data reported in various studies as a function of the vibration frequency. The mean values of the data sets considered, indicated in the figures as central bold solid lines, relate to the idealized values, which may be considered for biodynamic modeling or other applications. For completion, the smoothened envelopes formed from the computations of standard deviation on the mean values are also included in the figures. Overall, the figures represent data acquired with 65 different subjects whose mass ranges from 49 to 93 kg, with mean value close to 70 kg. The excitation levels used for generating these data are observed to vary between 0.5 and 2.0 ms^{-2} rms, with a slightly higher proportion of subjects submitted to sinusoidal than to random excitations. While the mean smoothened DPMI magnitude curve shows a peak occurring at 4.8 Hz, that for APMS is more towards 4.4 Hz. In both cases, the envelopes formed from the standard deviation on the mean follow very closely those formed from maximum and minimum values. The coefficient of variation (*i.e.* ratio of standard deviation to the mean) is relatively the same for DPMI and APMS magnitudes, except at lower frequencies (<1.5 Hz), where the variation is considerably larger when the data is treated in terms of DPMI than that in terms of APMS.

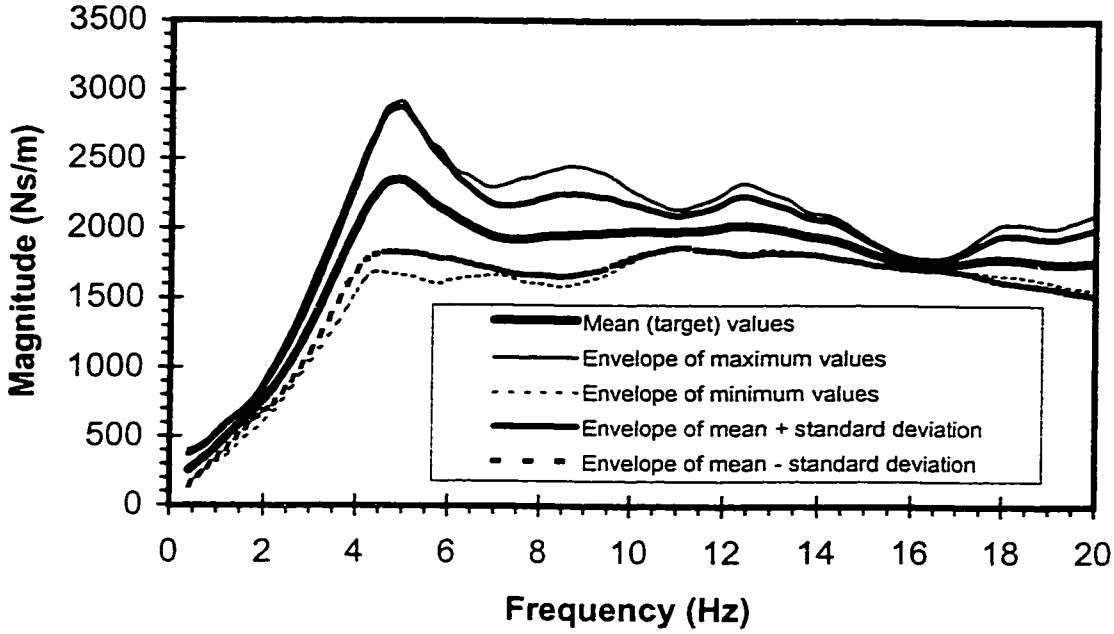

Figure 2.22: Driving-point mechanical impedance data envelope contours of idealized magnitude values under the defined conditions.

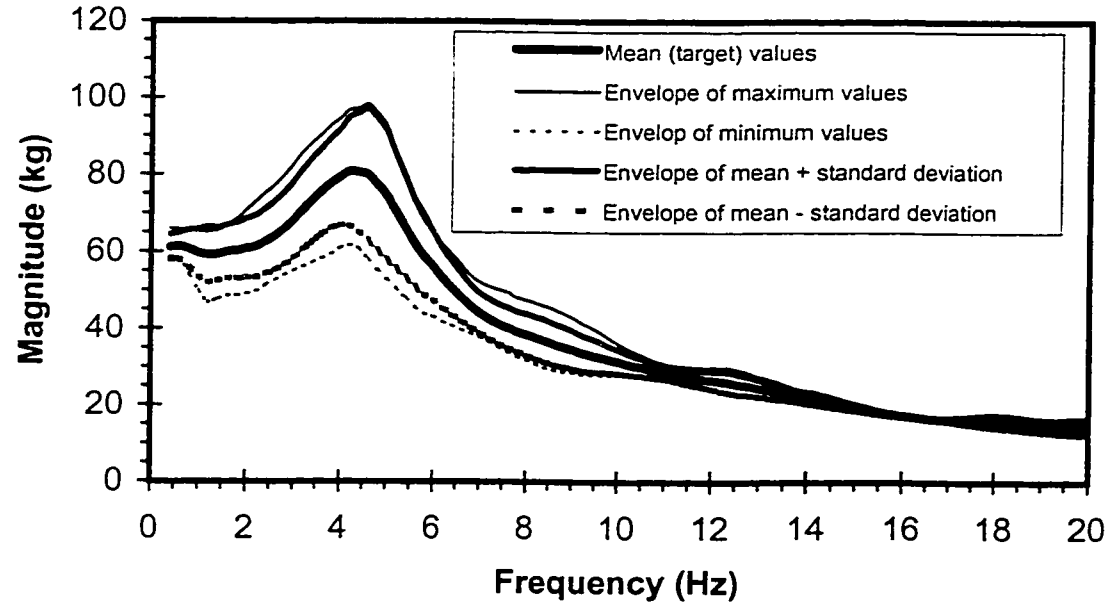

Figure 2.23: Apparent mass data envelope contours of idealized magnitude values under the defined conditions.

It has to be pointed out that there were relatively few data sets available to perform the data synthesis at frequency above 10 Hz. Among the 8 data sets employed in defining the range of idealized values, three of them were measured up to 10 Hz, and another was measured up to 12.5 Hz. Therefore, there are only four data sets appearing between 12.5 Hz and 20 Hz and this may explain the narrowness of the envolope at such frequencies.

With regard to the DPMI phase, the exclusion of the data sets identified in Subsection 2.6.2, resulted in a synthesis based on 7 data sets, including Sandover, F&G-1983, D&B-sine, F&G-1986, Holmlund *et al.*, and B&R-sine and B&R-random. The results, shown in Figure 2.24, indicate a significant broadening of the error or coefficient of variation at frequencies above 8 Hz, owing to the considerable discrepancies between the data sets. Overall, these data are established with same subject population and excitation levels used for defining DPMI and APMS magnitude, with the exception that a considerably higher proportion of subjects were subjected to sinusoidal than to random excitations.

2.8.2 Range of Idealized values of STHT

Finally the synthesis of the data on STHT presented in Figures 2.25 and 2.26 for magnitude and phase is based on four and three data sets, respectively. The synthesis includes data sets reported by Mertens [21], Paddan and Griffin [34] and ISO CD 5982 [22]. The data reported by Coermann [12] is the fourth data set considered for STHT magnitude. Overall, 72 subjects are involved in generating the data reported in these studies with mass ranging from 57 to 90 kg. The largest population of subjects is that

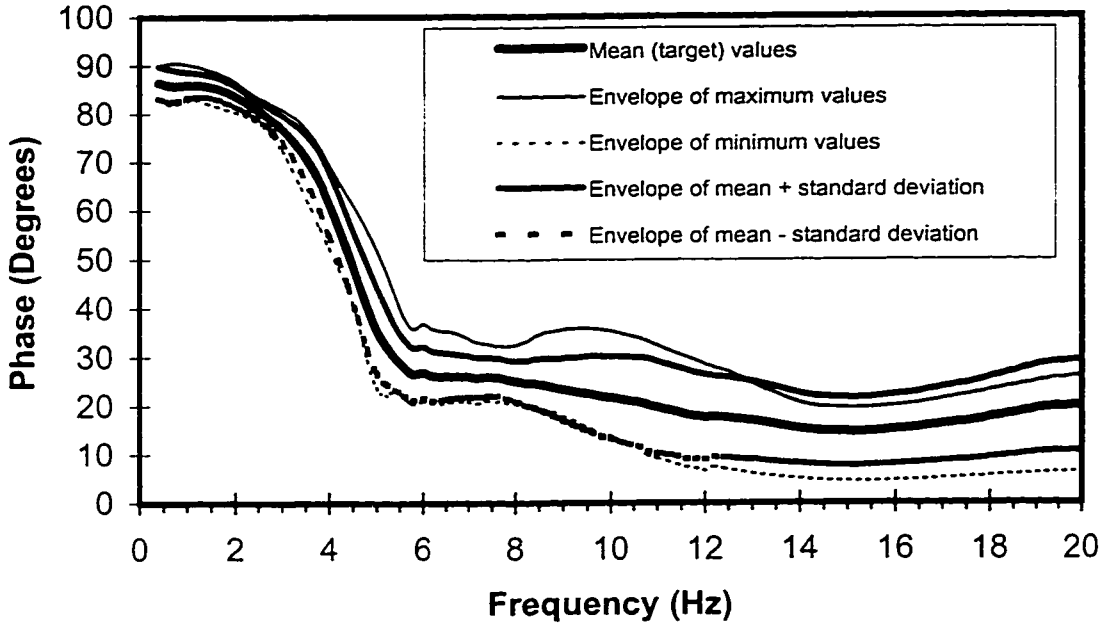

Figure 2.24: Driving-point mechanical impedance data envelope contours of idealized phase values under the defined conditions.

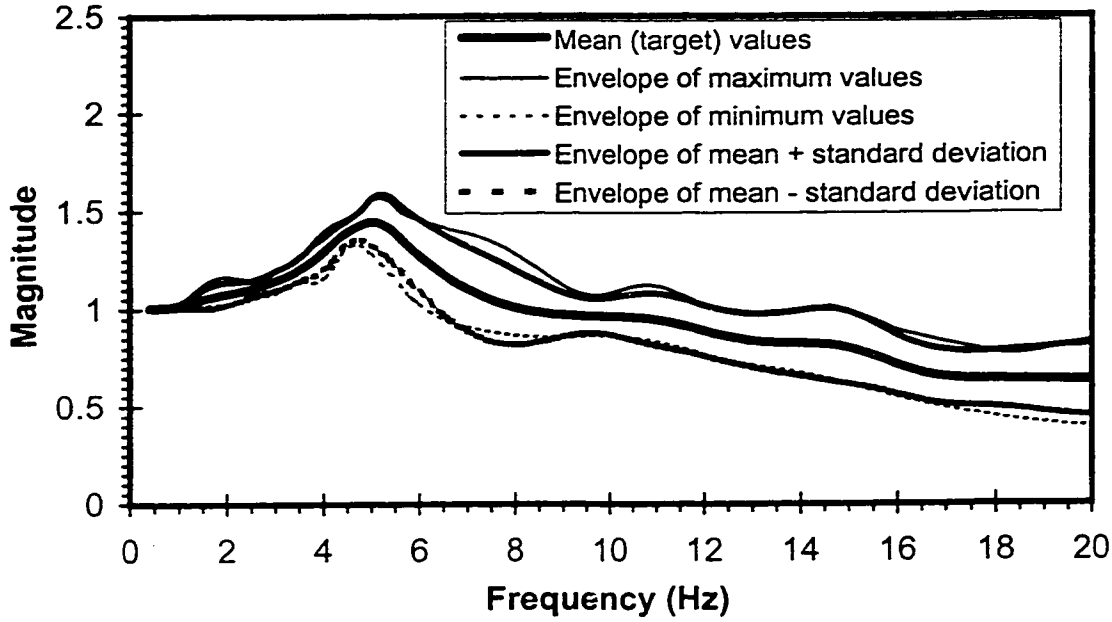

Figure 2.25: Seat-to-head transmissibility data envelope contours of idealized magnitude values under the defined conditions.

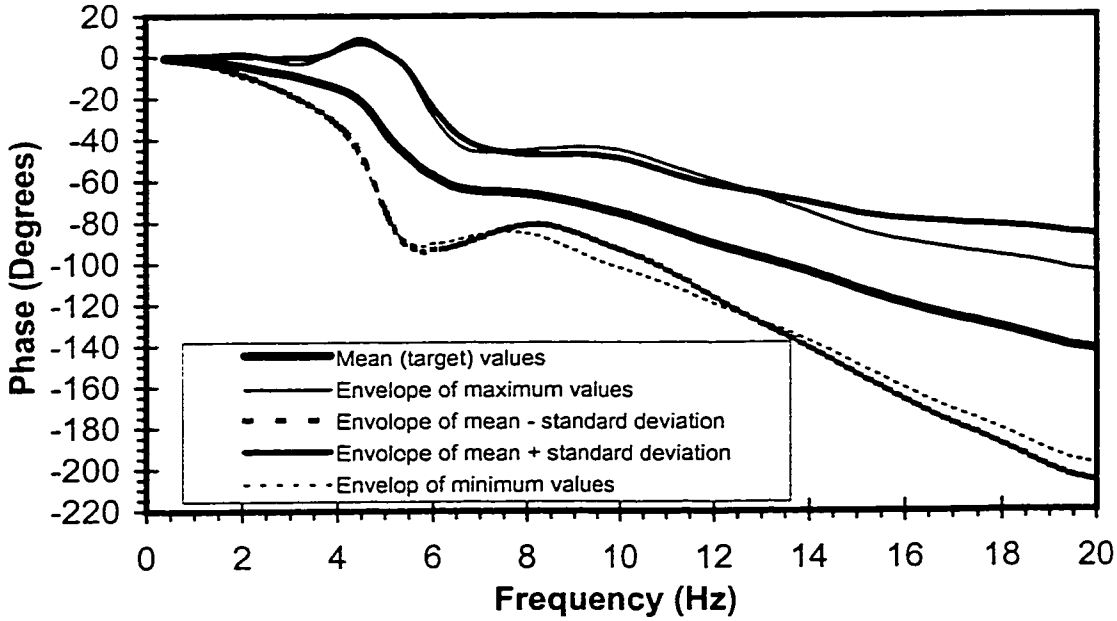

Figure 2.26: Seat-to-head transmissibility data envelope contours of idealized phase values under the defined conditions.

reported in the ISO CD 5982 [22], which involves 50 out of the 72 subjects. The excitation levels used in these studies are observed to vary between 1.75 and 5 ms^{-2}, with a considerably higher proportion of subjects reported to have been submitted to sinusoidal than to random excitations. It should be noted that the data sets, which are considered to satisfy the selection rules, are the same as those used in a previous study [8], in which the analysis had been limited to an upper frequency of 10 Hz. From the results of the synthesis, shown in Figure 2.25, it can be observed that peak STHT magnitude is expected to occur at a frequency of 5.1 Hz, which is slightly different from the resonant frequencies of 4.8 and 4.4 Hz, estimated from the DPMI and APMS idealized values, respectively.

In view of the uncertainties associated with the inclusion of the ISO CD 5982 data as part of the final data synthesis on STHT, a comparison was further made of the mean synthesized values reported in Figures 2.25 and 2.26 with those which would have resulted by not considering the ISO CD 5982 data. The results, shown in Figure 2.27, indicate that the effect of not including the ISO CD 5982 data while computing the mean STHT magnitude is almost negligible; while the effect appears to be considerably more important on phase. Furthermore, the exclusion of the ISO CD 5982 data from the synthesis does not prevent the resulting mean phase information to fall within the envelope of values previously defined while retaining this data set (Figures 2.25 and 2.26). On that basis, it is concluded that the range of the idealized STHT values computed while retaining the ISO CD 5982 data would not be altered in any significant manner by not considering this data set.

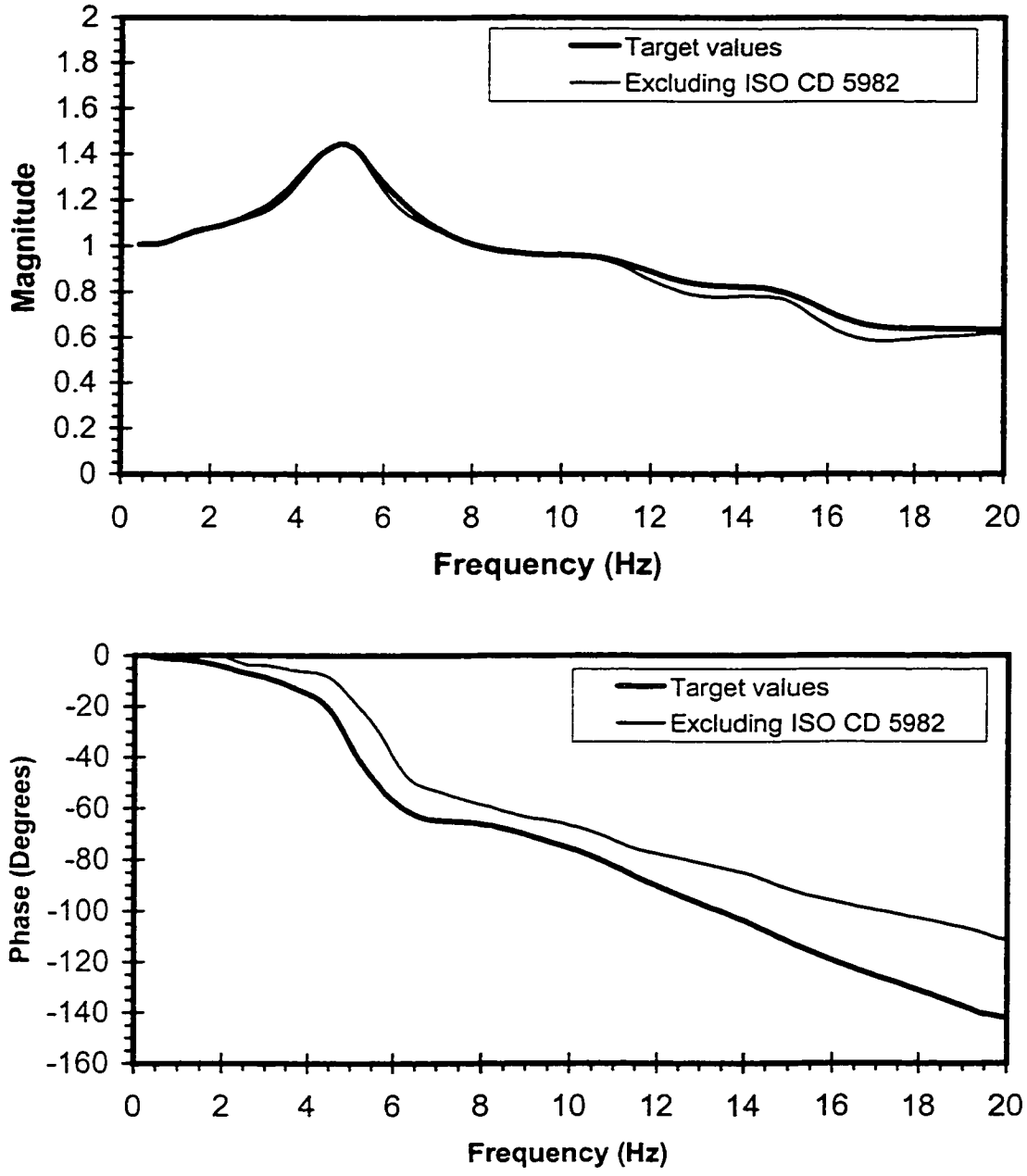

Figure 2.27: Comparison of proposed mean (target) values of seat-to-head transmissibility with those excluding ISO CD 5982.

The very limited number of available data sets employed in defining the idealized range of STHT (4 data sets for magnitude and 3 data sets for phase, all up to 20 Hz) may result in an envelope which is too narrow at certain frequency ranges. The mean, upper and lower bounds, and the standard error corresponding to the range of most probable values of each of the smoothened biodynamic response functions are also summarized in Tables 2.5 to 2.7 at central frequencies of one-third octave bands between 0.5 and 20 Hz.

2.9 Summary

The human body exhibits highly complex biodynamic response, which is affected by many factors, including subject posture, mass, and vibration magnitude and frequency. While body size and mass can influence the DPMI and APMS, the changes in seated posture often yield the largest variations. Erect posture yields significantly higher resonant frequency and magnitude of DPMI than that obtained for relaxed and back supported postures. Feet and hand position can also have a large influence on the DPMI and APMS. An increase in the subject mass yields significant increase in the magnitude at resonance, and a decrease in the resonant frequency as observed from the peak DPMI and APMS response. An increase in excitation level causes both the resonant frequency and corresponding magnitude of DPMI to shift towards lower values. However, these variations are observed to be significant only if the vibration levels vary over a wide range. The variations in DPMI under high levels of vibration excitation may be due to either the non-linearity of the human body or the voluntary change of the posture.

Variations in STHT of an individual are primarily caused by changes in body posture, and head and limbs positions. Both erect posture and 'looking up' head position

Table 2.5: Target and range of idealized driving-point mechanical impedance of the seated human body under the defined conditions.

Frequency (Hz)	Magnitude (Ns/m)				Phase (degrees)			
	Lower limit	Mean (target)	Standard error	Upper limit	Lower limit	Mean (target)	Standard error	Upper limit
0.5	148	254	116	400	83	86	3	90
0.63	218	304	95	425	82	86	3	90
0.8	266	359	86	471	82	86	3	91
1	310	424	87	539	83	86	3	90
1.25	356	493	88	607	83	86	2	90
1.6	490	627	71	703	82	85	2	89
2	614	768	93	893	80	84	2	87
2.5	758	947	132	1141	79	81	2	84
3.15	1131	1429	212	1732	69	75	3	80
4	1541	2002	316	2389	52	61	7	69
5	1663	2346	522	2908	24	36	9	52
6.3	1635	2065	298	2404	20	26	5	36
8	1605	1939	274	2392	20	25	4	32
10.0	1756	1981	196	2273	14	22	8	35
12.5	1828	2023	211	2327	7	18	8	27
16.0	1710	1750	37	1791	4	15	7	20
20.0	1552	1755	239	2099	6	20	9	26

Table 2.6: Target and range of idealized apparent mass of the seated human body under the defined conditions.

Frequency (Hz)	Magnitude (kg)				Phase (degrees)			
	Lower limit	Mean (target)	Standard error	Upper limit	Lower limit	Mean (target)	Standard error	Upper limit
0.5	58.7	61.2	3.2	65.9	-7	-4	3	0
0.63	58.0	61.4	3.5	65.8	-8	-4	3	0
0.8	53.8	60.6	5.0	65.6	-8	-4	3	1
1	49.8	59.6	6.2	65.2	-7	-4	3	0
1.25	46.9	59.2	7.2	65.2	-7	-4	2	0
1.6	48.5	60.0	7.0	66.7	-8	-5	2	-1
2	49.0	60.8	7.6	70.6	-10	-6	2	-3
2.5	51.2	62.6	8.5	75.2	-11	-9	2	-6
3.15	56.0	70.7	10.4	85.6	-21	-15	3	-10
4	61.0	79.3	12.4	94.6	-38	-28	7	-21
5	52.8	74.5	16.6	92.3	-66	-54	9	-38
6.3	41.9	53.2	7.7	61.9	-69	-64	5	-54
8	31.9	38.5	5.4	47.4	-69	-65	4	-58
10.0	27.8	31.5	3.1	36.1	-76	-68	8	-55
12.5	23.4	25.9	2.7	29.8	-83	-72	8	-63
16.0	17.0	17.4	0.4	17.8	-85	-75	7	-70
20.0	12.5	14.1	1.9	16.9	-84	-70	9	-64

Table 2.7: Target and range of idealized seat-to-head transmissibility of the seated human body under the defined conditions.

Frequency (Hz)	Magnitude				Phase (degrees)			
	Lower limit	Mean (target)	Standard error	Upper limit	Lower limit	Mean (target)	Standard error	Upper limit
0.5	1.00	1.01	0.01	1.02	-1.2	-0.6	0.8	0.0
0.63	1.00	1.01	0.01	1.02	-1.9	-1.0	1.3	0.0
0.8	1.00	1.01	0.01	1.02	-2.4	-1.2	1.7	-0.0
1	1.01	1.02	0.01	1.03	-2.8	-1.5	1.9	-0.1
1.25	1.02	1.03	0.02	1.06	-3.4	-1.8	2.3	-0.1
1.6	1.02	1.06	0.05	1.14	-5.6	-2.9	3.8	-0.2
2	1.03	1.08	0.06	1.16	-8.4	-4.3	5.8	-0.2
2.5	1.04	1.10	0.05	1.15	-11.8	-6.3	6.3	-0.6
3.15	1.11	1.16	0.05	1.22	-20.5	-9.7	9.4	-3.4
4	1.16	1.29	0.09	1.36	-32.5	-15.0	18.5	4.2
5	1.28	1.45	0.12	1.56	-72.9	-35.6	38.4	3.8
6.3	0.99	1.23	0.19	1.44	-93.0	-59.8	30.3	-34.1
8	0.87	1.01	0.19	1.28	-81.5	-66.3	19.0	-45.3
10.0	0.86	0.96	0.09	1.08	-93.1	-75.6	26.5	-45.1
12.5	0.74	0.86	0.13	0.99	-121.2	-93.2	29.8	-62.1
16.0	0.55	0.71	0.15	0.89	-166.1	-119.5	41.0	-89.0
20.0	0.40	0.63	0.18	0.84	-206.3	-142.2	55.8	-104.3

can cause significant increase in vibration transmitted to the head. Contact with the backrest increases the transmission of vibration at above 4.5 Hz and the primary resonance frequency. The primary resonance frequency and resonance magnitude decrease when vibration intensity is increased considerably.

The reported data on DPMI or APMS, and STHT exhibit excessive variations, which are attributed to variations in the test conditions, and inter- and intra-subject variations. A synthesis of reported data thus can not be performed without carefully specifying the criteria with regards to the body posture, subject population and excitation magnitude and frequency components. Selection rules are thus formulated to represent the vehicular vibration environment. The data sets satisfying these rules are selected for synthesis to identify a most probable values of biodynamic functions. By excluding outliers based on standard deviation analysis, a synthesis of the selected data was performed and smoothened envelope contours encompassing the mean values of the selected data were constructed in the 0.5 to 20 Hz frequency range to characterize the DPMI, APMS and STHT of the seated subjects with feet supported, and exposed to vibration excitation levels lower than 5 ms^{-2}. The synthesis is based on 8 data sets for DPMI and APMS magnitudes, and 7 data sets for the phase response. The idealized curves on STHT are based on considerably fewer data sets: four for the magnitude and three for the phase. The data that fall within the proposed range of idealized values are considered to provide acceptable representation of the seated human body's biodynamic response behavior under the specific range of conditions.

CHAPTER 3

WHOLE-BODY BIODYNAMICS: DEVELOPMENT OF HUMAN BODY MODEL

3.1 Introduction

The biodynamic response characteristics of the seated human body in terms of 'to the body' and 'through the body' functions can be described by either the DPMI or APMS, and the STHT functions. The DPMI or APMS functions describe the force-motion relationship at the driving-point of the body, while STHT relates to the transmission of vibration through the body. Majority of the human body models, reported in the literature, are derived upon curve-fitting the DPMI or APMS data, while neglecting the physiological structure of the body [16, 17]. Such models, based upon curve-fitting algorithm, may not be considered unique. The uniqueness of the human body models may be enhanced by satisfying both the DPMI/APMS and STHT data during model development. Only three of the reported models have been derived using this approach, in conjunction with curve-fitting or multi-variable optimization techniques [8, 21, 22]. These models, however, have not been successful in satisfying both the measured DPMI/APMS and STHT data. Furthermore, the models either are unnecessarily complex, or yield considerable discrepancies between the model response and measured data. The poor agreements between the model response and measured data may be attributed to these primary facts: (i) the models were derived by simply curve-fitting the DPMI/APMS and STHT data, without investigating analytically the possible relationships between the biodynamic functions; (ii) the data used to derive the biodynamic response functions have often been derived from a synthesis of reported data, while the test conditions related to

synthesized STHT data may be different from those related to synthesized DPMI/APMS data (variations in test conditions are known to strongly influence the biodynamic response characteristics, as discussed in Chapter 2); and (iii) all three models have attempted to incorporate biomechanical data, resulting in complex models which may not be necessary to investigate seating dynamics.

In order to derive a reliable seated body model that can satisfy both biodynamic functions, it is extremely vital to enhance an understanding of the possible relationship between the two types of functions. It is also necessary to identify a possible model structure from the measured biodynamic response. Finally, it is essential to consider the measured biodynamic response characteristics in terms of both DPMI/APMS and STHT functions, using the same subject population and common test conditions. The measured response characteristics, however, must correlate well with the range of idealized values established from the data synthesis performed in Chapter 2, while the model development may be attempted based on the measured data. A reasonable correlation between the model response and measured data, if attained, will validate the proposed modeling approach and lead to a somewhat unique solution. A poor correlation will only indicate that two functions considered in the study are not representative of the biodynamic behavior of the seated body.

In this chapter, the principles for developing a biodynamic model representing the seated body dynamics, while operating off-road vehicles, are discussed. The relationship between APMS and STHT functions are derived based upon both experimental data and theoretical analysis. An appropriate function describing the driving-point force-motion relationship is proposed for modeling consideration. The DPMI/APMS and STHT data to

be used in the model development were measured under the predefined test conditions, and validated by comparing with the target values established in the data synthesis in Chapter 2. A seated body model is proposed and the model parameters are estimated to satisfy both the measured APMS and STHT data. The human body model developed in this chapter will eventually be combined with the seat cushion model to be developed in Chapter 4 and seat suspension model to be developed in Chapter 5, to investigate the human-suspension seat performance under different types of excitations.

3.2 Principles for Deriving Biodynamic Models for the Seated Body

Based on the discussions in Section 3.1, the principles for deriving biodynamic models for the seated body are summarized as follows:

- The model should be based on both DPMI or APMS and STHT data measured using the same subject group under predefined test conditions representing typical vibration work conditions of off-road vehicle drivers, as defined in Chapter 2;

- The degrees of freedom and the structure of the model should be based on the general trends observed from the measured biodynamic data, and available models, instead of knowledge of anatomy and anthropometry;

- The model should be derived by mathematically curve-fitting the data sets presented in terms of the above biodynamic functions, while consideration of the biomechanical data should be avoided due to associated uncertainties and complexities;

- Masses in the model thus do not need to correspond with any specific body segment mass. The head motion, however, must be derived from the vibration response of the representative indicated mass, while the mass value may not correspond to the human head mass.

3.3 Discussions on Biodynamic Response Functions

Both the DPMI and APMS can be used to describe the force-motion relationship at the human-seat interface. The researchers have thus used either one of these functions,

depending upon their preferences or conveniences. For example, ISO CD 5982 [22] refers strictly to DPMI data, while Sandover [45] and Fairley and Griffin [17, 41, 43, 44] have extensively used the APMS function. The benefits and limitations of using either function in presenting the biodynamic data, however, have not been addressed in the literature. It is generally assumed that both functions describe the force-motion relationships equivalently, since they are related by definition. Some differences of significant importance, however, have been observed, when biodynamic data is presented in terms of the two functions. The most significant difference occurs in estimation of the body's primary resonant frequency, as discussed in Section 2.6. It should be noted that the primary resonant frequency is taken as the frequency at which peak magnitude of the function considered occurs. It is therefore essential to study the relationship between the two functions in order to select an adequate representation of the driving-point force-motion function for the model development. Since the APMS and STHT characteristics shown in Figures 2.8 and 2.12 reveal considerable similarities, both functions may be considered to describe the same dynamic characteristics of the body. A theoretical link between these two functions, however, has not yet been explored.

3.3.1 Analysis of measured DPMI and APMS functions

The DPMI and APMS data reported in the literature were thoroughly analyzed to identify the desirable response function to be used and to perform a synthesis for deriving the idealized response characteristics. An analysis of 14 data sets, acquired under a similar range of test conditions, revealed extensive variations in the DPMI and APMS magnitude, as illustrated in Figures 2.13 and 2.14. Various APMS data sets, however,

revealed relatively less variations in the primary resonant frequency, while the range of primary resonant frequency was observed to be much wider on the basis of DPMI data (from 4.0 to 7.0 Hz). On the basis of the 14 data sets shown in Figures 2.13 and 2.14, the standard deviation on the mean value of the primary resonant frequency of the human body, are computed and listed in Table 3.1 when presented in terms of both DPMI and APMS.

Table 3.1: Variation in the primary resonant frequency of the human body derived from data sets reported by different researchers in terms of DPMI and APMS.

Functions	Mean (Hz)	Standard Deviation (Hz)	Range (Hz)
DPMI	4.89	0.77	4.0 - 7.0
APMS	4.51	0.51	3.6 - 5.4

It can be observed that the DPMI demonstrates larger variations in both standard deviation and range of primary resonant frequency of the human body than the APMS. The DPMI data sets further yield a higher mean value of primary resonant frequency than that derived from the APMS data sets. The same trend is also observed when the results obtained within a single study using a group of subjects are compared. The magnitudes of DPMI and APMS of a group of seven subjects under sine sweep excitation of 1 ms^{-2} rms in the 0 to 10 Hz frequency range are illustrated in Figures 3.1 and 3.2 [8]. The measured data was attained for all subjects maintaining an identical posture of upright upper body without back support and with feet supported and vibrated. It can be observed that large variations exist among the group of subjects even under identical test conditions, which are mostly attributed to the inter-subject variability. The results show relatively large variations in the DPMI at frequencies above 4 Hz, and in APMS data at frequencies

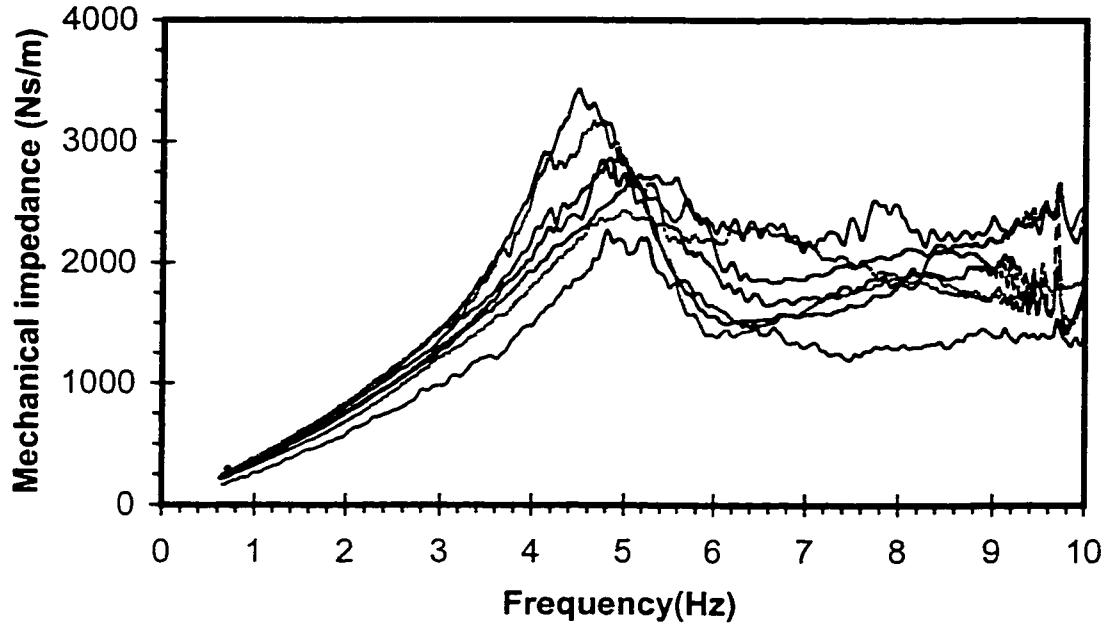

Figure 3.1: The magnitude of driving-point mechanical impedance of seven subjects measured under sine sweep excitation of 1 m/s² rms with an ENS posture.

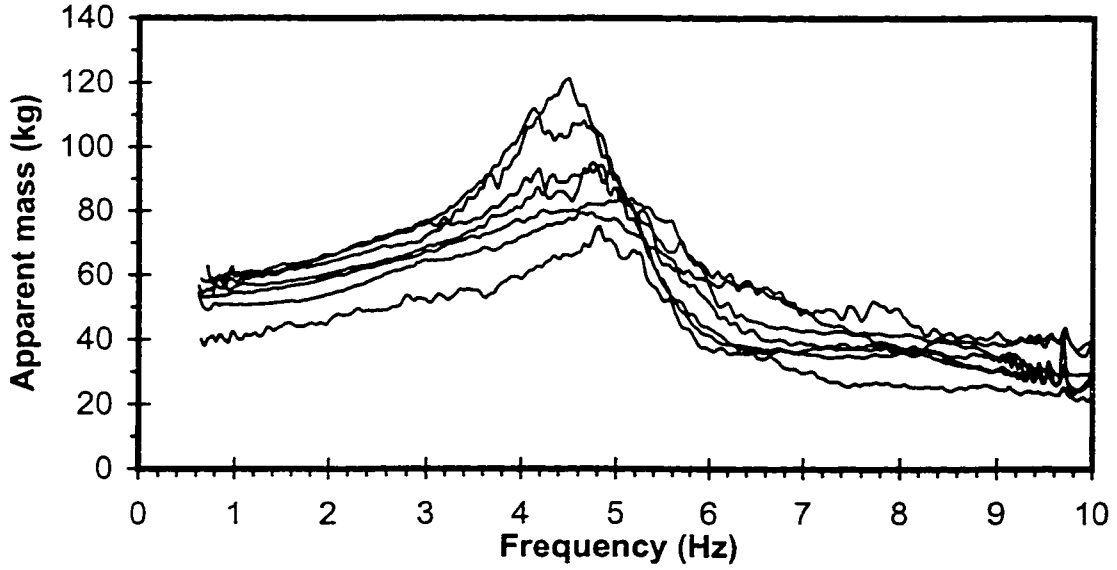

Figure 3.2: The magnitude of apparent mass of seven subjects measured under sine sweep excitation of 1 m/s² rms with an ENS posture.

below 5 Hz. The response in terms of APMS tends to limit the spread between subjects' data and show slightly closer primary resonant frequencies than those observed from the DPMI. Again, it can be noticed that the DPMI yields higher mean primary resonant frequency than the APMS. The mean, standard deviation and range of the primary resonant frequencies derived from the measured DPMI and APMS data are summarized in Table 3.2. The results show trends similar to those observed in Table 3.1, though the standard deviation and range of primary resonant frequency of the subjects are considerably lower, which is due presumably to the identical test conditions pertaining to this data set. The variations, presented in Table 3.2, are therefore mainly attributed to the inter-subject variability. Nevertheless, it would appear that the APMS function perhaps yields more consistent primary resonant frequency than DPMI among a group of subjects.

Table 3.2: Variations in primary resonant frequency of the human body using data sets measured with a group of seven subjects [8].

FUNCTIONS	Mean (Hz)	Standard Deviation (Hz)	Range (Hz)
DPMI	4.84	0.22	4.5 - 5.4
APMS	4.75	0.17	4.5 - 5.0

The variations in whole-body resonant frequency prediction from the DPMI and APMS functions, are further investigated through analysis of reported biodynamic models. A total of four biodynamic models, reported in the literature and shown in Figure 3.3, are considered for the analysis [12, 16, 17, 47]. The equations of motion for the four selected models are then derived to define the modulus and phase expressions of the DPMI and APMS of the models. The expressions derived for the DPMI and APMS

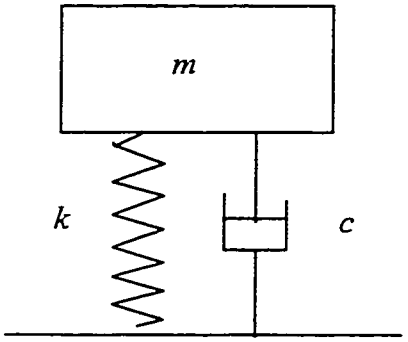

Coermann [12]

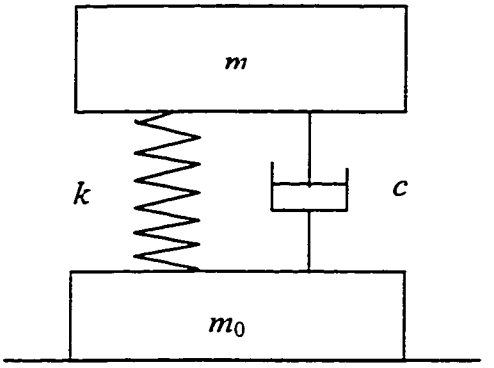

Fairley and Griffin [17]

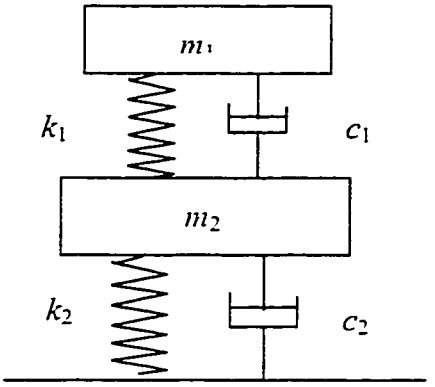

Allen [47]

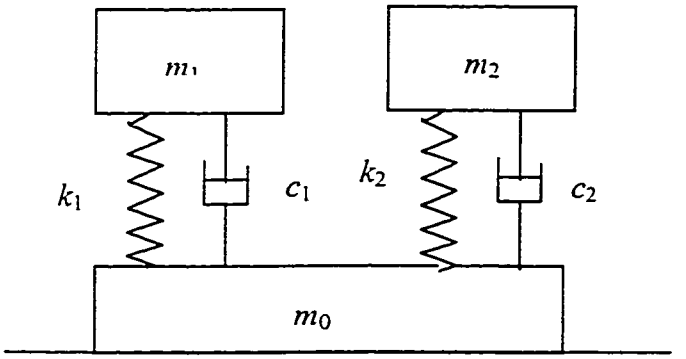

Suggs *et al* [16]

Figure 3.3: Selected biodynamic models.

magnitude and phase response characteristics are summarized in Table 3.3. Various model variables are defined in Table 3.4.

These expressions may be used to determine the primary resonant frequency, corresponding to peak value of the APMS or DPMI functions by means of numerical computations. The biodynamic models subject to inherent differences in the human body characteristics can be represented by variations in parameters such as mass, stiffness and damping coefficients. ±20% variations are assumed for all the parameters to determine the sensitivity of the primary resonant frequency (f_p) to variations in the model parameters. The primary resonant frequency with an increase or a decrease of 20% of a parameter is calculated when other parameters are kept equal to the nominal values defined for each model, as listed in Table 3.4. f_n describes the undamped natural frequency of single DOF models proposed by Coermann [12] and Fairley and Griffin [17]. f_{n1} and f_{n2} are the two natural frequencies of the two DOF models proposed by Allen [47] and Suggs *et al.* [16]. The mass, stiffness and damping parameters are represented by (m, m_1, m_2), (k, k_1, k_2), and (c, c_1, c_2), respectively, as indicated in Figure 3.3. The damping ratio of the SDOF models is represented by ζ, while ζ_1 and ζ_2 describe the uncoupled damping ratios of the two DOF model, proposed by Allen [47], and expressed as:

$$\zeta_1 = \frac{c_1}{2m_1\omega_{n1}} \qquad \zeta_2 = \frac{c_2}{2m_2\omega_{n2}} \tag{3.1}$$

For models with more than one parameter of the same type, all the similar parameters are varied by the same amount (±20%) for each computation. For example, a variation of +20% in mass means that all the three masses in Suggs *et al*'s model are

Table 3.3: Expressions for magnitude and phase of DPMI and APMS of the four models.

FUNCTIONS	APMS	DPMI
Model	$M(\omega)=\sqrt{\frac{\lvert A(\omega)\rvert^2+\lvert B(\omega)\rvert^2}{\lvert C(\omega)\rvert^2+\lvert D(\omega)\rvert^2}}$ $\varphi(\omega)=a\tan\frac{B(\omega)}{A(\omega)}-a\tan\frac{D(\omega)}{C(\omega)}$	$Z(\omega)=\omega M(\omega)=\omega\sqrt{\frac{[A(\omega)]^2+[B(\omega)]^2}{[C(\omega)]^2+[D(\omega)]^2}}$ $\varphi(\omega)=\frac{\pi}{2}+a\tan\frac{B(\omega)}{A(\omega)}-a\tan\frac{D(\omega)}{C(\omega)}$
Coermann [12]	$A(\omega)=mk$ $B(\omega)=mc\omega$ $C(\omega)=k-m\omega^2$ $D(\omega)=c\omega$	
Fairley and Griffin [17]	$A(\omega)=(m+m_0)k-m_0m\omega^2$ $B(\omega)=(m+m_0)c\omega$ $C(\omega)=k-m\omega^2$ $D(\omega)=c\omega$	
Allen [47]	$A(\omega)=(m_1+m_2)k_1k_2-(m_1c_1c_2+m_2c_1c_2+m_1m_2k_2)\omega^2$ $B(\omega)=(m_1+m_2)(c_1k_2+c_2k_1)\omega-m_1m_2c_2\omega^3$ $C(\omega)=k_1k_2-(m_1k_2+m_2k_1+m_1k_1+c_1c_2)\omega^2+m_1m_2\omega^4$ $D(\omega)=(c_1k_2+c_2k_1)\omega-(m_1c_2+m_2c_1+m_1c_1)\omega^3$	
Suggs *et al* [16]	$A(\omega)=(m+m_1+m_2)k_1k_2+mm_1m_2\omega^4-[(m+m_1+m_2)c_1c_2+m(m_1k_2+m_2k_1)+m_1m_2(k_1+k_2)]\omega^2$ $B(\omega)=(m+m_1+m_2)(k_1c_2+k_2c_1)\omega-[m(m_1c_2+m_2c_1)+m_1m_2(c_1+c_2)]\omega^3$ $C(\omega)=k_1k_2-(m_1k_2+m_2k_1+c_1c_2)\omega^2+m_1m_2\omega^4$ $D(\omega)=(c_1k_2+c_2k_1)\omega-(m_1c_2+m_2c_1)\omega^3$	

increased by 20%, and the corresponding primary resonant frequency is expressed as $f_{(m+20\%)}$. While the primary resonant frequency of the nominal model is represented by f_p, the sensitivity of the resonant frequency to variation in the model parameters is derived upon considering ±20% variations in all the model parameters. The total variation or sensitivity, Δf_p, is defined as the square root of sum of squares of variations in the primary resonant frequency caused by the variations in each parameter or each type of parameters:

$$\Delta f_p = [(f_p - f_{m-20\%})^2 + (f_p - f_{m+20\%})^2 + (f_p - f_{k-20\%})^2 + (f_p - f_{k+20\%})^2 + (f_p - f_{c-20\%})^2 + (f_p - f_{c+20\%})^2]^{\frac{1}{2}} \quad (3.2)$$

Table 3.4: Parameters of the selected models.

Model	Nominal model parameters
Coermann [12]	f_n=6.3 Hz, k=131181 Nm^{-1}, ζ=0.57, m=83.72 kg
Fairley and Griffin [17]	m=45.6 kg, m_0=6 kg, ζ=0.475, c=1360 Nsm^{-1}, f_n=5 Hz
Allen [47]	m_1=5.0kg, ζ_1 =0.05, f_{n1}=17.0 Hz, m_2=50.0kg, ζ_2 =0.3, f_{n2}=5.0 Hz
Suggs *et al.* [16]	m_0=6 kg, m_1=36.4 kg, m_2=18.6 kg, k_1=25968 Nm^{-1}, k_2=41549 Nm^{-1}, c_1=485 Nsm^{-1} , c_2=884 Nsm^{-1}

The primary resonant frequencies corresponding to variations in each parameter and the total variation of the primary resonant frequency resulting from the variations of all the parameters, Δf_p, for all the four models are listed in Table 3.5. The primary resonant frequencies computed from DPMI are consistently higher than those derived from APMS. An increase in the mass parameter(s) tends to reduce the primary resonant frequency, while an increase in the stiffness parameter(s) tends to increase the primary resonant frequency for both the DPMI and the APMS. The variations in the damping coefficient(s), however, yield somewhat contradictory variations in the primary resonant

frequencies derived from DPMI and APMS. An increase in the damping coefficient(s) tends to increase the primary resonant frequency derived from the DPMI, and decrease that from the APMS. This analysis supports the previous conclusions drawn from the experimental data to the effect that the APMS tends to yield smaller variations in the primary resonant frequency than the DPMI, and the DPMI yields higher primary resonant frequency than the APMS. It can be concluded that the wide variations in the primary resonant frequency is inherent in the biodynamic measure based upon DPMI. Since the primary resonant frequency is of greatest interest in the study of human biodynamic response to vibration, the averaging based on APMS seems to be more appropriate in both the data synthesis and the experimental data processing for a group of subjects. The averaging based on DPMI is more likely to cover trends than would otherwise appear using the APMS, due to the larger variations in the primary resonant frequency, resulting from individual differences in subject characteristics.

Table 3.5: Variations in primary resonant frequency caused by model parameter variations.

MODEL	Coermann [12]		Fairley and Griffin [17]		Allen [47]		Suggs *et al* [16]	
FUNCTION	DPMI	APMS	DPMI	APMS	DPMI	APMS	DPMI	APMS
f_p (Hz) (nominal parameters)	8.2	5.2	5.6	4.2	4.9	4.5	4.2	3.9
$f_{m-20\%}$ (Hz)	10.6	5.7	6.7	4.6	5.6	5.0	4.7	4.3
$f_{m+20\%}$ (Hz)	6.9	4.9	5.0	4.0	4.5	4.2	3.8	3.6
$f_{k-20\%}$ (Hz)	8.6	4.6	5.4	3.7	4.5	4.0	3.8	3.4
$f_{k+20\%}$ (Hz)	8.3	5.9	5.9	4.8	5.3	5.0	4.6	4.3
$f_{c-20\%}$ (Hz)	7.1	5.5	5.2	4.4	4.8	4.6	4.2	4.0
$f_{c+20\%}$ (Hz)	11.3	5.0	6.4	4.1	5.0	4.4	4.3	3.8
Δf_p (Hz)	4.4	1.1	1.6	0.9	1.0	0.9	0.9	0.8

At very low excitation frequencies when the body is effectively rigid, the APMS of the body is equal to its static mass supported by the seat. The APMS can be conveniently normalized to the static mass supported by the seat to reduce the extent of variations attributed to the body mass. Other advantages of presenting results in terms of APMS include that APMS can be obtained directly from the signals provided by accelerometers and force transducers, and the mass cancellation or mass correction is quite simple, since the APMS of a rigid seat is ideally a constant value equal to the static mass, and the phase angle is nearly zero within a wide frequency range. It is therefore recommended that the APMS be used to describe the 'to the body' biodynamic response characteristics of the human body and for defining the objective function for parameter estimation.

3.3.2 Analysis of the relationship between APMS and STHT

The APMS and STHT relate to 'to the body' and 'through the body' functions, respectively. Although not related by definition, the similarities between the APMS and STHT, have been clearly evident especially in view of the primary resonant frequency (Figures 2.8 and 2.12). A definite relationship between the magnitudes of the two functions can also be established, when APMS is normalized with respect to the body mass. The equations of motion, formulated for the four models, shown in Figure 3.3, are further analyzed to derive expressions for the normalized APMS and STHT magnitude and phase functions. Table 3.6 summarizes the derived expressions for normalized APMS, and STHT functions. The normalization of APMS was realized upon dividing the APMS magnitude by the total mass of the model. Although the models do not describe a

Table 3.6: Expressions for magnitude and phase of the normalized APMS and STHT of the selected models.

	Normalized APMS	**STHT**
Model	$Normalized\ M(\omega) = \sqrt{\frac{[A(\omega)]^2 + [B(\omega)]^2}{[C(\omega)]^2 + [D(\omega)]^2}}$ $\varphi(\omega) = \tan^{-1}\left[\frac{B(\omega)}{A(\omega)}\right] - \tan^{-1}\left[\frac{D(\omega)}{C(\omega)}\right]$	$H(\omega) = \sqrt{\frac{[A(\omega)]^2 + [B(\omega)]^2}{[C(\omega)]^2 + [D(\omega)]^2}}$ $\varphi(\omega) = \tan^{-1}\left[\frac{B(\omega)}{A(\omega)}\right] - \tan^{-1}\left[\frac{D(\omega)}{C(\omega)}\right]$
Coermann [12]	$A(\omega) = k$ $\quad B(\omega) = c\omega$ $C(\omega) = k - m\omega^2$ $\quad D(\omega) = c\omega$	$A(\omega) = k$ $\quad B(\omega) = c\omega$ $C(\omega) = k - m\omega^2$ $\quad D(\omega) = c\omega$
Fairley and Griffin [17]	$A(\omega) = k - \frac{m_0 m}{m_0 + m}\omega^2$ $\quad B(\omega) = c\omega$ $C(\omega) = k - m\omega^2$ $\quad D(\omega) = c\omega$	$A(\omega) = k$ $\quad B(\omega) = c\omega$ $C(\omega) = k - m\omega^2$ $\quad D(\omega) = c\omega$
Allen [47]	$A(\omega) = k_1k_2 - (c_1c_2 + \frac{m_1m_2}{m_1 + m_2}k_2)\omega^2$ $B(\omega) = (c_1k_2 + c_2k_1)\omega - \frac{m_1m_2}{m_1 + m_2}c_2\omega^3$ $C(\omega) = k_1k_2 - (m_1k_2 + m_2k_1 + m_1k_1 + c_1c_2)\omega^2 + m_1m_2\omega^4$ $D(\omega) = (c_1k_2 + c_2k_1)\omega - (m_1c_2 + m_2c_1 + m_1c_1)\omega^3$	$A(\omega) = k_1k_2 - c_1c_2\omega^2$ $B(\omega) = (c_1k_2 + c_2k_1)\omega$ $C(\omega) = k_1k_2 - (m_1k_2 + m_2k_1 + m_1k_1 + c_1c_2)\omega^2 + m_1m_2\omega^4$ $D(\omega) = (c_1k_2 + c_2k_1)\omega - (m_1c_2 + m_2c_1 + m_1c_1)\omega^3$
Suggs *et al.* [16]	$A(\omega) = k_1 - [\frac{c_1c_2}{k_2} + \frac{(m + m_1)m_2}{m + m_1 + m_2}\frac{k_1}{k_2} + \frac{(m + m_2)m_1}{m + m_1 + m_2})]\omega^2 + \frac{mm_1m_2}{m + m_1 + m_2}\frac{1}{k_2}\omega^4$ $B(\omega) = (c_1 + c_2\frac{k_1}{k_2})\omega - [\frac{(m + m_1)m_2}{m + m_1 + m_2}\frac{c_1}{k_2} + \frac{(m + m_2)m_1}{m + m_1 + m_2}\frac{c_2}{k_2}]\omega^3$ $C(\omega) = k_1 - (m_1 + m_2\frac{k_1}{k_2} + \frac{c_1c_2}{k_2})\omega^2 + \frac{m_1m_2}{k_2}\omega^4$ $D(\omega) = (c_1 + c_2\frac{k_1}{k_2})\omega - (\frac{m_1c_2 + m_2c_1}{k_2})\omega^3$	$A(\omega) = k_1$ $B(\omega) = c_1\omega$ $C(\omega) = k_1 - m_1\omega^2$ $D(\omega) = c_1\omega$

direct biomechanical representation of the head, the extreme mass response is considered to describe the transmission of motion through the body model. Certain similarities between the normalized APMS and the STHT can be directly observed from the expressions summarized in the table. The single DOF model, proposed by Coermann [12], yields identical expressions for both STHT and normalized APMS, which suggests the measurement of either APMS or STHT will provide identical biodynamic characteristics of the human body. The similarity between the two functions, however, is less apparent when the order of the model is increased. On the basis of the derived expressions, the degree of similarity between the normalized APMS and STHT expressions of the selected models can be expressed in the following order: Coermann, Fairley and Griffin, Allen and Suggs *et al.*

The frequency response characteristics of both the normalized APMS and STHT for the four selected models are illustrated in Figure 3.4. The magnitude and phase characteristics of both the functions for the single DOF model, proposed by Coermann [12] are identical, as expected from the expressions. The Fairley and Griffin model [17] also yields almost identical results in the normalized APMS and STHT magnitudes over the entire frequency range, while identical phase response only up to 5 Hz. Since the normalized APMS function tends to suppress the magnitude of APMS at higher frequencies, the magnitude corresponding to the second resonant frequency of higher order models, in general, tends to be considerably lower for that function. The model proposed by Allen [47] yields similar magnitudes of normalized APMS and STHT only at frequencies below 10 Hz, while the STHT magnitude response exhibits a significant second resonance at 17.7 Hz. It should be noted that APMS relates to the force-motion

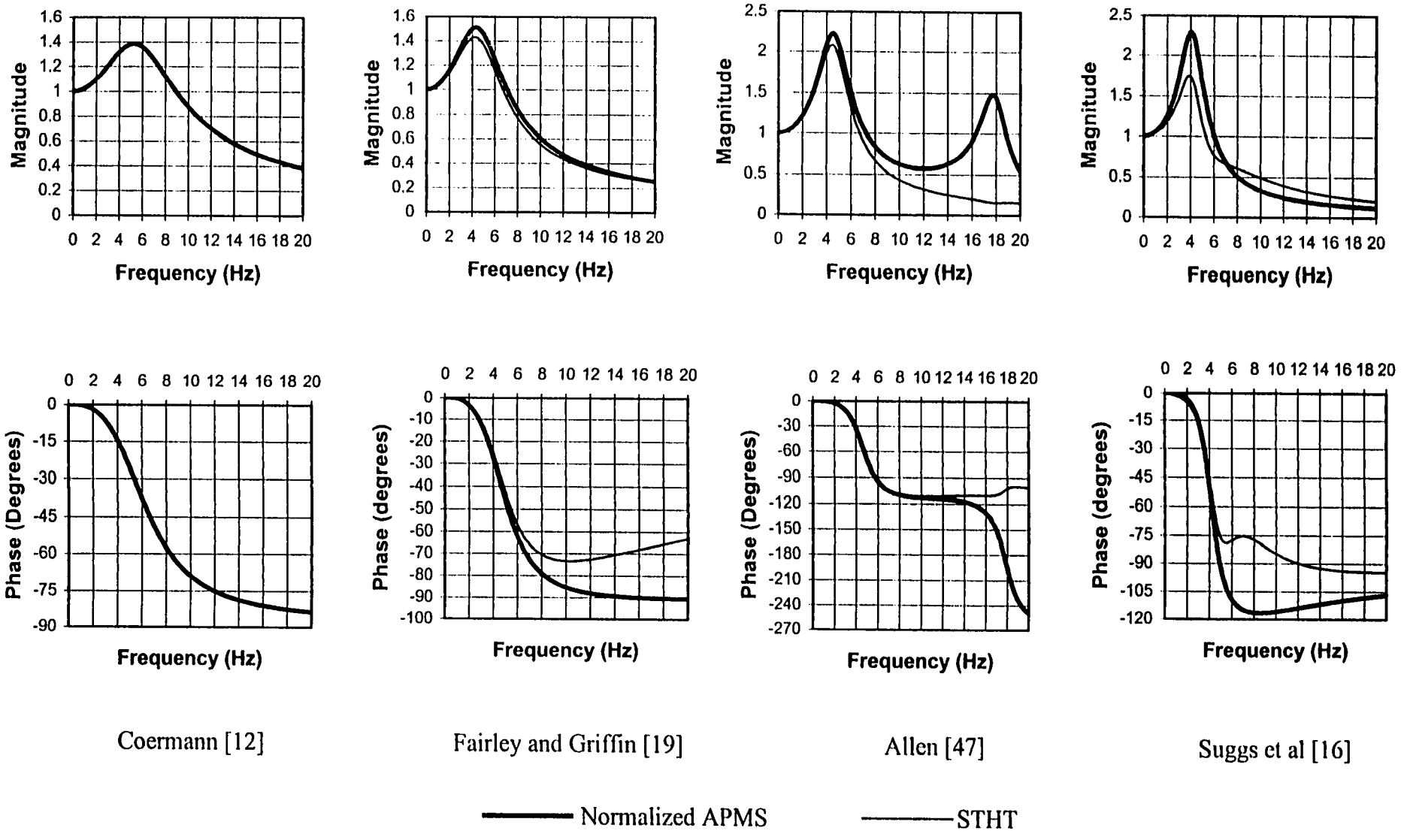

Figure 3.4: Magnitudes and phases of both normalized APMS and STHT for the four biodynamic models.

ratio divided by square of the frequency. The APMS thus diminishes at higher frequencies. At excitation frequencies below 10 Hz, the phase response of the normalized APMS and STHT derived from Allen's model are almost identical. The results derived from the Suggs *et al*'s model yield relatively large difference between the magnitudes of the normalized APMS and STHT in the vicinity of the primary resonant frequency, while both functions exhibit identical frequency corresponding to peak magnitudes. At higher frequencies, however, both functions approach similar values in magnitude. The corresponding phase response of the two functions around the primary resonance are found to be quite similar. Although certain differences between the magnitude and phase characteristics of the normalized APMS and STHT of the higher order models exist, the primary resonant frequencies derived from these two functions are almost identical for all the models. The primary resonant frequencies derived from the STHT, APMS and DPMI functions for all the models are summarized in Table 3.7 using the nominal model parameter values presented in Table 3.4.

An eigenvalue analysis of the selected models is further performed to identify their primary damped resonant frequencies. For all the four models, the STHT and APMS functions yield almost identical primary resonant frequencies, which are considerably different from those derived from the DPMI function. The reported studies have invariably identified the primary resonant frequencies from the peak magnitude of the biodynamic function considered. The results clearly show that such prediction can differ considerably depending upon the function considered. The results of eigenvalue analysis, also listed in Table 3.7, show that the primary resonant frequencies predicted from STHT and APMS functions are more likely to represent the primary resonant frequency of the

body, which is inherent body characteristics, and should not change by using different biodynamic functions. On the other hand, the primary resonant frequencies, predicted from DPMI, tend to differ considerably from the primary resonant frequency derived from eigenvalue analysis, and thus is considered to be less accurate in predicting the inherent primary resonant frequency. These results suggest that if a model is to be based on both driving-point force-motion relation transfer function and vibration transmission function, APMS and STHT functions should be selected. Attempts to use DPMI along with STHT would result in wide discrepancies in response predictions, specifically for predicting the primary resonant frequency. Furthermore, the results also suggest that it is possible to develop a seated body model with relatively lower degrees-of-freedom, on the basis of analytical functions and measured data.

Table 3.7: Comparison of primary resonant frequencies of the selected models derived from different functions.

	Primary resonant frequency (Hz)			
MODEL	Coermann [12]	Fairley and Griffin [17]	Allen [47]	Suggs *et al.* [16]
Eigenvalue analysis	5.2	4.4	4.6	4.1
STHT magnitude	5.2	4.3	4.5	4.0
APMS magnitude	5.2	4.2	4.5	3.9
DPMI magnitude	8.2	5.6	4.9	4.2

3.4 Measurement of APMS and STHT

From the review of reported measured data and various studies, it has been established that many factors influence the biodynamic response of the human body. For the purpose of developing a reliable model based on both APMS and STHT functions, one has to ensure that the differences arising from possible variations in the test conditions and the subjects are minimized while measuring the data. An attempt is made

to measure both functions under identical laboratory test conditions and for the same group of subjects in order to limit any variations, which may arise from application of different experimental conditions. On the basis of the measured data, a biodynamic model is attempted using the principles described in Section 3.2.

3.4.1 Experimental set-ups

A whole-body vehicular vibration simulator (WBVVS) was used to provide the necessary excitations for measurement of the biodynamic response characteristics of a group of subjects. The WBVVS can simulate whole-body vibration environment of a wide range of vehicles, with maximum displacement of 20 cm. A resonance search test had been performed and it was found that the WBVVS has a nearly flat frequency response at excitation frequencies below 20 Hz [8]. Emergency safety switches were provided to the subject and the operator to stop the WBVVS in case of an emergency.

A rigid seat with a height of 424 mm was constructed, with a seat pan (406 mm wide and 410 mm deep) and a backrest (406 mm wide and 508 mm high) made of 6.35 mm thick aluminum plates. The rigid seat was supported and mounted on a force platform (20 mm thick), which was fixed to the WBVVS using four load cells (30 mm thick) of strain-gage type. Therefore, the total seated height of the subject from the WBVVS platform was 474 mm. The dimensions of the seat were selected based on the suggested values given in SAE J1163 [48], which describes operator seat location for off-road work machines, SAE J899 [49], which defines operator's seat dimensions for off-road self-propelled work machines, and SAE J826 [50], which suggests devices for use in defining and measuring vehicle seating accommodation. The total mass of the seat and

force platform was 23.5 kg. The output of each load cell was connected to a summing junction to achieve a direct measure of the total force. An accelerometer was attached on the seat pan to measure the acceleration transmitted to the human body. The resonant frequency of the load cell-seat system, when loaded with a 65 kg rigid mass, was measured as approximately 30 Hz, which was well above the upper frequency limit 20 Hz of interest in this study. A bite-bar, proposed as the most convenient device for measuring head motion [1], was designed and assembled by fixing an accelerometer to a rigid bar with a diameter of 10 mm and a length of 200 mm. The total mass of the bite-bar was less than 50 g. Both the accelerometer on the seat pan and on the bite-bar were *KISTLER Translational Angular PiezoBEAM* system (model 8832), which can simultaneously measure translational and angular vibration.

A white noise signal was used to drive the WBVVS. The signal had a flat PSD spectrum up to 30 Hz. Through calibration and tuning, the WBVVS generated two acceleration levels: 1 ms^{-2} rms and 2 ms^{-2} rms. During the test, the subjects were requested to put their hands on the steering wheel but without leaning against it, rest feet flat on the vibration platform and look forward at a fixed point on the front wall. The subjects were asked to assume two postures, *i.e.* sitting erect with only the lower portion of the back in contact with the backrest (ENS posture) and sitting erect with most of the back in contact with the backrest (EBS posture). The bite-bar was held between the teeth (close to the corner of the mouth) with the accelerometer at a location about 100 mm to the right of the mid-sagittal plane at mouth level. Before each test, the experimenter directed the properly seated subject to rotate the bite-bar until the sensitivity axis of the accelerometer was vertical.

Six male subjects participated in the experiment. The characteristics of the test subject population are listed in Table 3.8. The ages of the subjects range from 24 to 43 years and the height from 1.65 to 1.76 m (mean height 1.72 m). Sitting mass is the subject's mass supported by the seat pan, while standing mass is the total mass of the subject. The subjects fall within the mass range of 58 to 73 kg with a mean mass of 64.2 kg. The percentage of subject mass resting on the seat pan (mass ratio) differs from subject to subject.

Table 3.8: Characteristics of the test subject population.

Subject	Age (years)	Height (m)	Mass (kg) standing	Mass (kg) sitting	Mass ratio
S	24	1.75	68.5	55	0.80
R	43	1.68	58	48.5	0.84
C	34	1.76	63.5	55	0.87
D	29	1.74	63.5	47	0.74
Z	37	1.73	73	61	0.84
K	34	1.65	58.5	54	0.92

All the subjects who participated in the experiments had no previous record of low back pain. They were thoroughly informed on the contents of the experiments prior to the testing and were requested to sign a consent form. The duration of vibration exposure for any given test did not exceed 90 seconds. The acceleration time histories of vibration on the seat pan and the vertical and pitch head vibrations measured using the bite-bar were recorded to allow pitch motion correction. The vertical acceleration signals from the seat pan accelerometer and from the bite-bar accelerometer were also directly connected to a B&K 2035 dual channel signal analyzer to monitor the STHT response. The vertical acceleration signal from the seat pan and the force signal from the load cells

were directly connected to another B&K 2035 dual channel FFT analyzer to obtain the APMS response.

3.4.2 Analysis of measured APMS data

The APMS of the seated subjects, was derived upon performing inertia correction of the measured force data. The measured dynamic force comprises components due to the biodynamic response of the seated body, and the inertia forces due to rigid seat and the force platform. The apparent mass, $m(s)$, of the seated body is thus derived as:

$$m(s) = M(s) - m_{seat}(s) \tag{3.3}$$

Where m(s) is the APMS of human body, M(s) is the total measured APMS of the human-seat system and m_{seat}(s) is the APMS of the rigid seat and the force platform alone, which, ideally, should be a constant real value. The correction defined by Equation (3.3) was performed at each frequency within the range of interest.

Figures 3.5 to 3.8 illustrate the magnitudes of measured APMS of six different subjects seated with EBS and ENS postures and subject to two excitation levels (1 and 2 ms^{-2} rms). Although similar trends are observed among the data obtained for different subjects, large inter-subject variations can also be observed. The inter-subject variability, however, is significantly reduced when the influence of body mass is eliminated by normalizing the magnitude of APMS with respect to the individual sitting mass as shown in Figures 3.9 to 3.12. The results show that an ENS posture yields larger inter-subject variability than the EBS posture under both excitation levels. This difference is mostly attributed to the inability of subjects to maintain a constant stable posture, when an ENS posture is assumed. Under all four test conditions, similar trends can be observed for

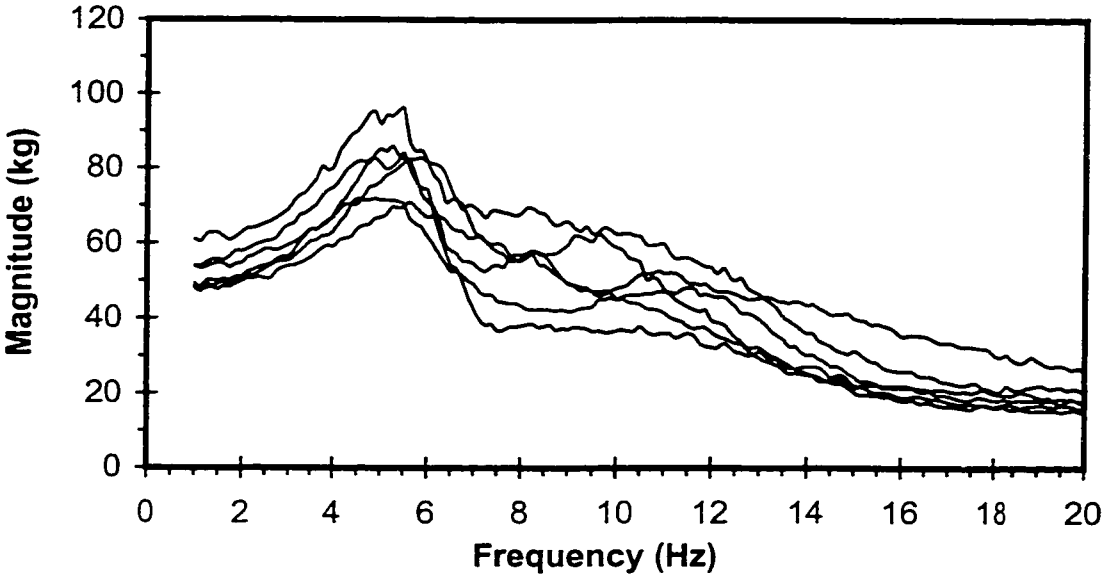

Figure 3.5: The measured apparent mass of six subjects under EBS posture and 1 m/s² rms acceleration excitation.

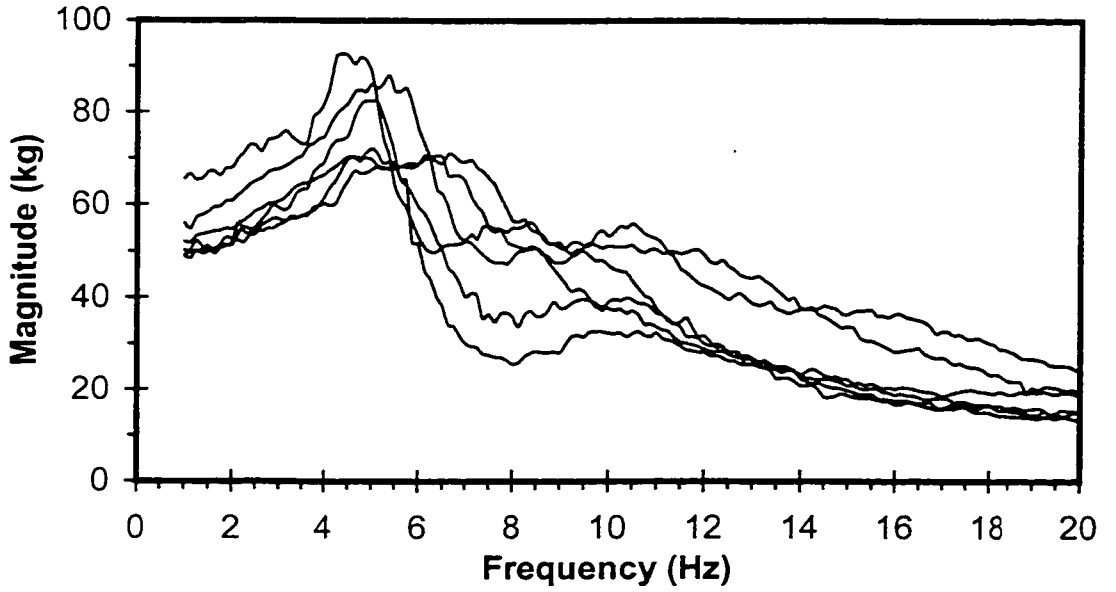

Figure 3.6: The measured apparent mass of six subjects under ENS posture and 1 m/s² rms acceleration excitation.

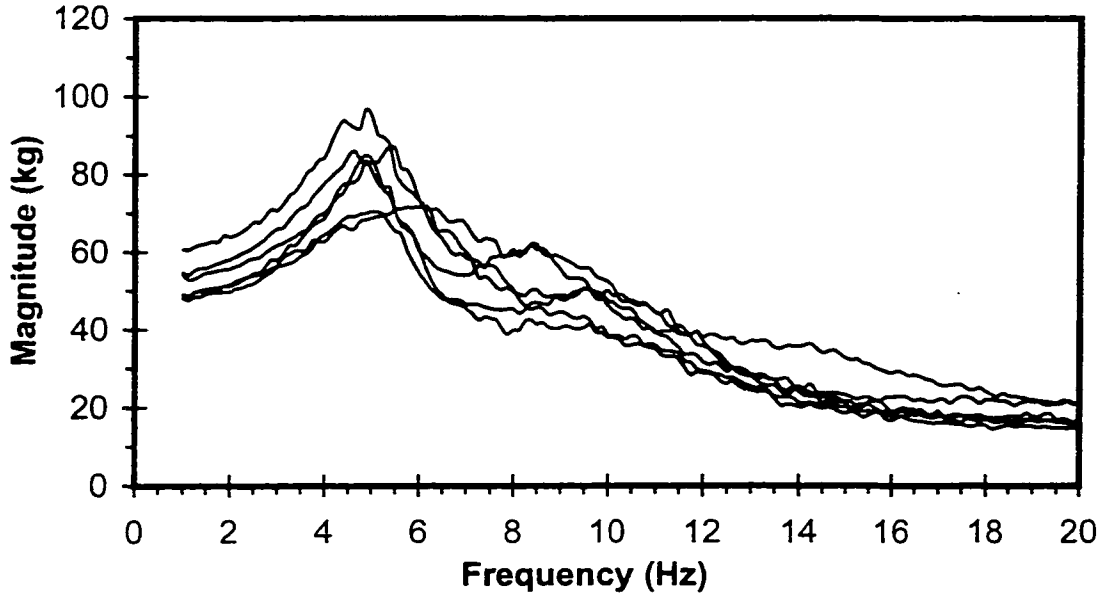

Figure 3.7: The measured apparent mass of six subjects under EBS posture and 2 m/s² rms acceleration excitation.

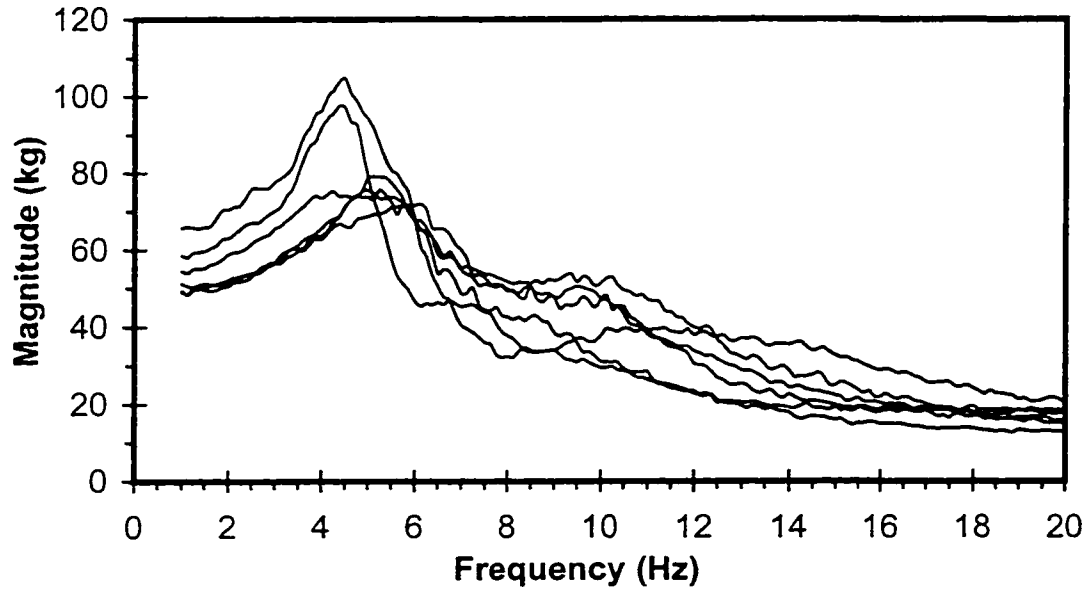

Figure 3.8: The measured apparent mass of six subjects under ENS posture and 2 m/s² rms acceleration excitation.

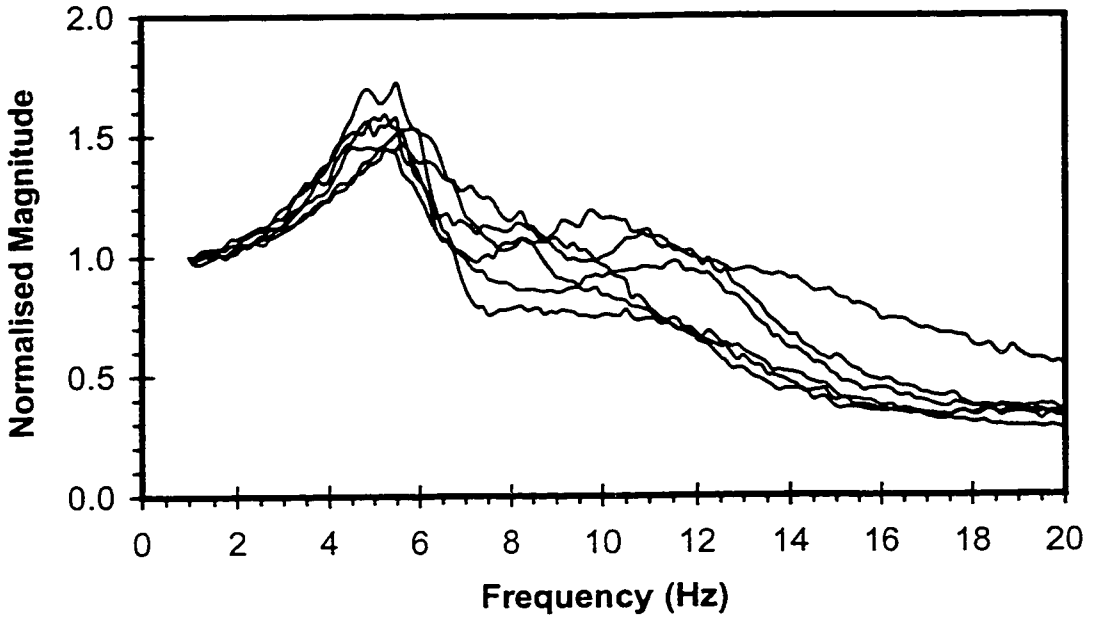

Figure 3.9: The normalized apparent mass of six subjects measured under EBS posture and 1 m/s² rms acceleration excitation.

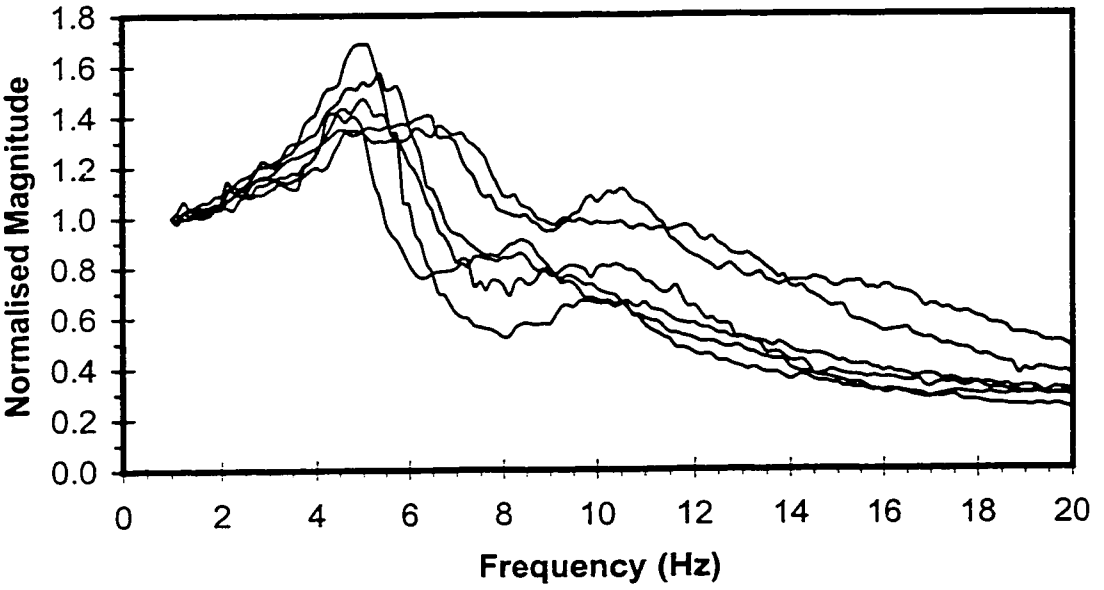

Figure 3.10: The normalized apparent mass of six subjects measured under ENS posture and 1 m/s² rms acceleration excitation.

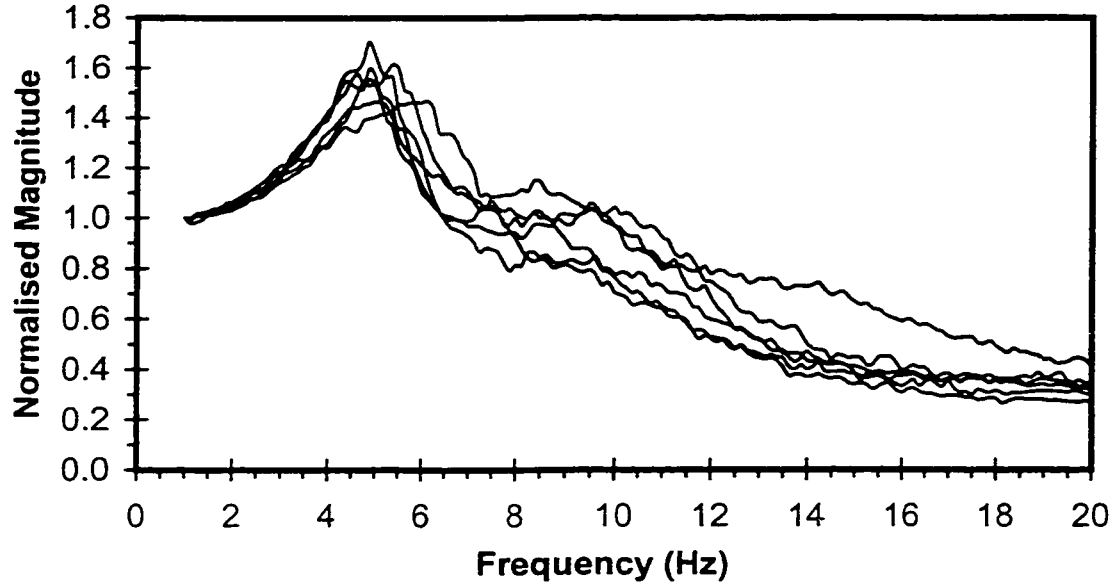

Figure 3.11: The normalized apparent mass of six subjects measured under EBS posture and 2 m/s² rms acceleration excitation.

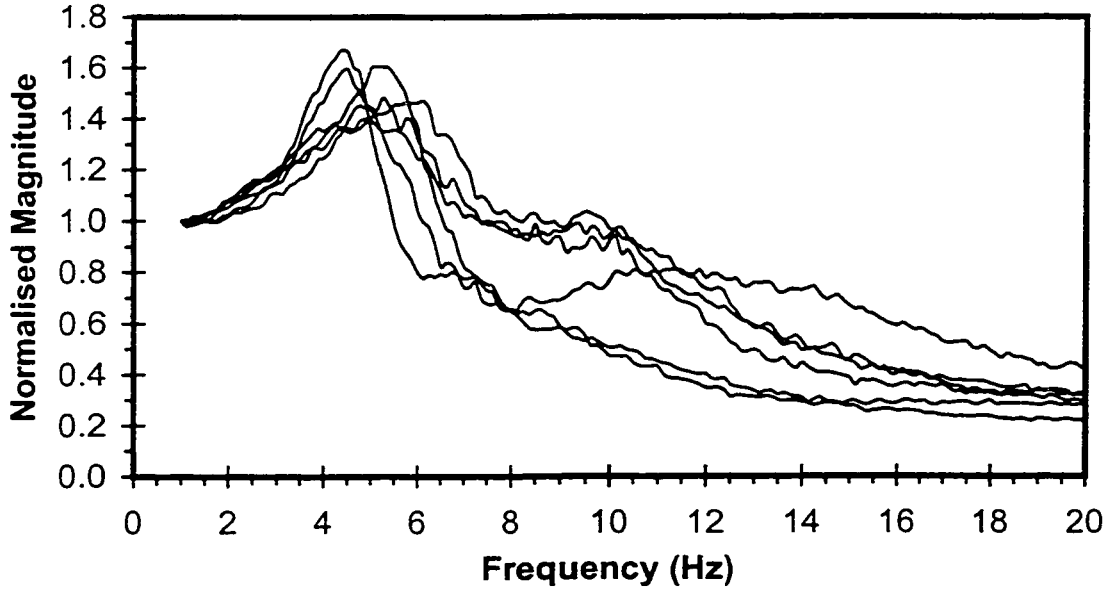

Figure 3.12: The normalized apparent mass of six subjects measured under ENS posture and 2 m/s² rms acceleration excitation.

individual subjects, with two apparent resonant peaks arising in the vicinity of 5 Hz and 10 Hz, respectively.

In an attempt to investigate the influence of the seated posture and excitation levels on the APMS data, analyses of variance (F-test) were performed at various discrete frequencies in the 0.5-20 Hz frequency range. The results of the F-test did not indicate significant postural and excitation level effects on the APMS magnitude within the frequency range investigated. Lower significance levels associated with a change in the seated posture, however, were obtained in almost entire frequency range. The lowest significance level (p=0.11) was obtained at a frequency of 11.5 Hz under 2 ms^{-2} rms excitation. These results indicate that changing from an ENS posture to an EBS posture has a greater influence on the mean APMS magnitude than that caused by increasing the excitation level from 1 ms^{-2} rms to 2 ms^{-2} rms. The significance of postural and excitation level effects were also evaluated using the F-test in a recent study [31]. The study reported significant postural effect (p<0.05), while no significant effect associated with excitation magnitude was yielded. The contradictory conclusions with respect to the postural effect may be attributed to the different biodynamic functions considered in the reported and present studies, and certain differences in the test conditions. Since the APMS function reveal considerably smaller variations between the different data sets, arising from different subject characteristics and test conditions than the DPMI function, analyses of variance based upon DPMI may yield higher significance levels.

In view of the potential influence of the seated posture on the APMS data, the data sets measured under two excitation levels with the subjects assuming an ENS posture are combined to define the mean APMS magnitude and phase response of seated

subjects (n=12), as illustrated in Figure 3.13, where the upper and lower bounds of the data are also indicated by the envelope curves. The resonance in the vicinity of 5 Hz has been reported in almost all the studies on either APMS or DPMI of the seated body, which is generally associated with the resonance of the chest structure. This has also been supported by visual observations and subjective response of the subjects [51], as well as by the observations made during this study. The second resonant peak, however, was not apparent in several reported data sets. Holmlund *et al.* [29] reported the second resonance near 11.5 Hz on the basis of measuring DPMI of 15 male subjects in a sitting posture. Subjects sat on a rigid seat pan and positioned their feet on an adjustable footrest. The footrest was adjusted such that the lower legs were vertical and the upper legs were horizontal (*i.e.* the thighs being well in contact with the seat pan). During the tests, they had noticed the resonance of the subjects' bottom at a frequency corresponding to the second resonance peak. Smith [42] reported a second resonant peak occurring between 10 and 13 Hz, and speculated that the generation of the second resonance was primarily due to lack of a footrest and the resulting increased loading of the legs against the seat pan. Furthermore, Fairley and Griffin [17] had also concluded that the APMS of the body above 10 Hz increased when the height of the moving footrest was reduced, since this induced an increased seated height and contact of the thighs with the seat pan.

The influence of variations in thigh contact may also explain the apparent discrepancy between these results and those reported in [31]. The mean APMS magnitude is further compared with that obtained in [31] through measurements performed in the same laboratory, as shown in Figure 3.14. The primary differences between the test conditions employed in two studies included different dimensions of the

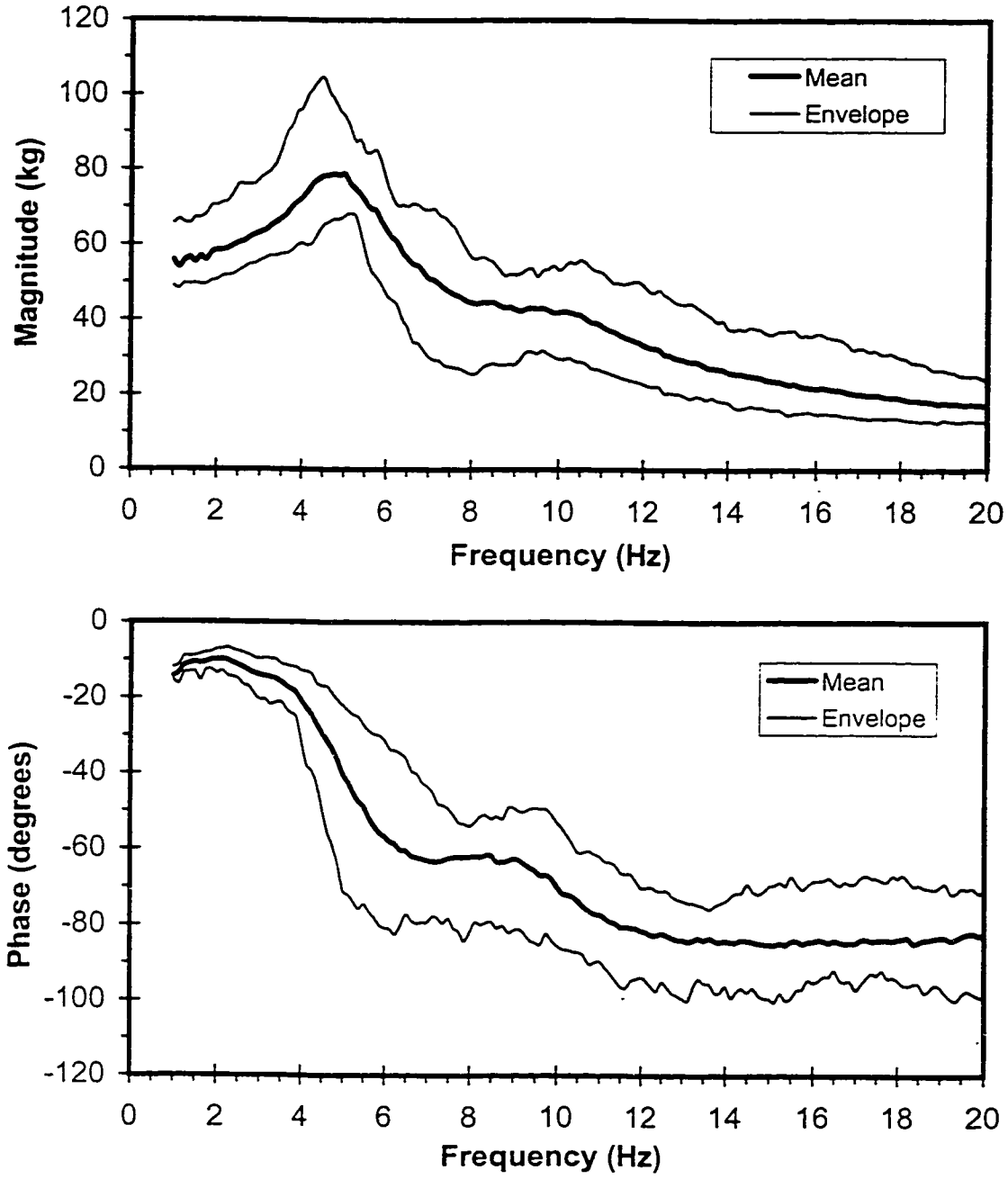

Figure 3.13: The mean and maximum and minimum envelopes of apparent mass of six subjects under ENS posture.

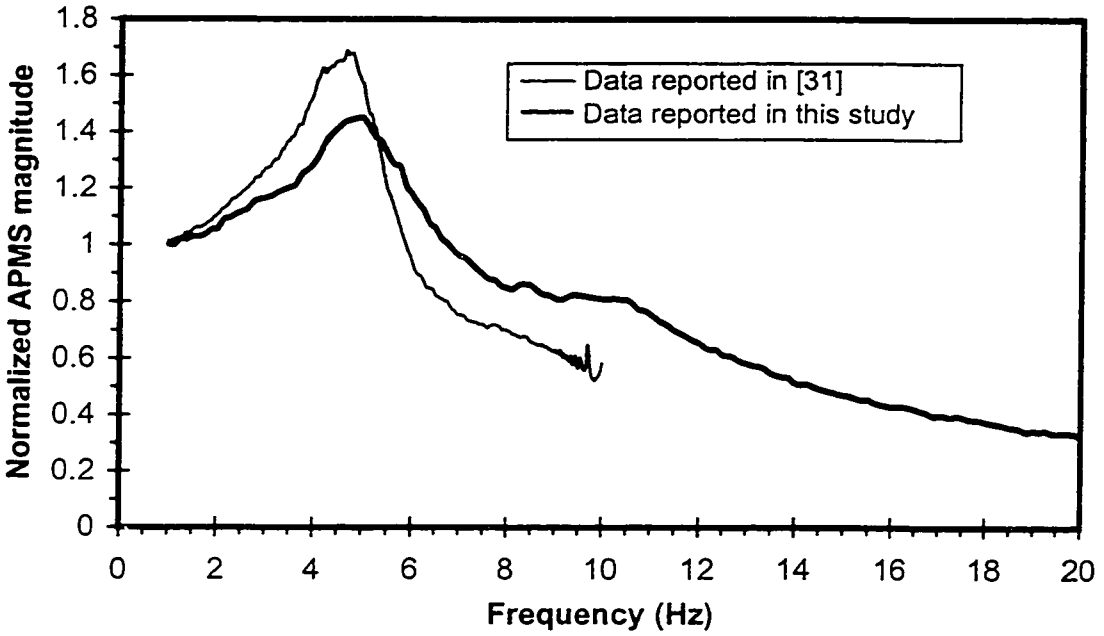

Figure 3.14: Comparison of mean normalized apparent mass magnitude measured under ENS posture with that reported in [31].

seat pan and mean body mass. The present study employed a seat pan with depth of 410 mm and seat height of 478 mm, while the reported study employed pan depth of only 254 mm with seat height of 474 mm. The present study also employed subjects with lower mean mass (64.2 kg versus 75.4 kg), a shorter subject group (mean height: 1.72 m versus 1.75 m) and higher excitation levels (1.0 and 2.0 ms^{-2} rms unweighted versus weighted). Since the subjects were requested to sit with the lower portion of the back in contact with the backrest, the shorter subjects would most likely sit on a deeper pan with relatively larger thigh contact area leading to a larger proportion of the body weight supported by the seat. The present study thus resulted in a higher mean value of the body mass ratio supported by the seat (84%) when compared to that obtained in the reported study (74%), even though the mean subject mass was lower. The mean normalized APMS obtained upon averaging across the two magnitudes were used to compare the different trends demonstrated in the two studies in order to minimize the contribution due to variations in the subject mass (see Figure 3.14). The reported data reveals a relatively higher peak at a slightly lower resonant frequency, when compared to the mean APMS data obtained in this study.

3.4.3 Analysis of the measured STHT data

The measured STHT response characteristics, in general, reveal considerably larger variations among the data sets reported in different studies [52], and even within subjects participating in the same study [34], as discussed earlier in Section 2.4. It has been stated that intra- and inter-subject variability can be quite significant and that a change in seated posture can cause considerable variation in STHT than that may be

caused in APMS [1]. The STHT magnitude of six subjects was measured under various test conditions, the results of which are illustrated in Figures 3.15 to 3.18. From the data, it can be observed that the ENS posture yields larger variations among different subjects than the EBS posture, under both excitation levels. For the EBS posture, peak STHT magnitude can be observed to occur between 5 and 10 Hz. The results suggest that the use of a backrest can increase the vibration transmission over a wide frequency range. This observation is also supported by the results reported by Paddan and Griffin [34] as illustrated in Figure 2.11. Under an ENS posture, however, the STHT magnitudes for several subjects tend to fall below unity at all frequencies above 5 Hz, while others show values constantly in excess of unity up to 20 Hz with the exception of a dip in the 4-4.5 Hz frequency range.

It should be noted that the vertical vibration of the head measured using a bite-bar located at the corner of the mouth includes the contributions due to both the vertical vibration of cervical vertebrae and the pitch motion of the head. The measured data thus needs to be appropriately corrected for the pitch motion. Assuming small pitch angle, the corrected vertical STHT can be estimated from [53]:

$$H_c(s) = H(s) + H_{pitch}(s) \cdot \ell_x \tag{3.4}$$

where $H_c(s)$ is the corrected complex STHT function; $H(s)$ is the complex STHT function measured using the bite-bar and the platform vibration, and $H_{pitch}(s)$ is the measured complex pitch STHT function derived as the ratio of bite-bar pith acceleration to the vertical seat acceleration. ℓ_x is the estimated distance from the bite-bar (*i.e.* the corner of the mouth) to the center of the cervical vertebrae (C7), which may differ from subject to subject. This distance varied from 0.11 m to 0.13 m, with a mean value of 0.125 m, for

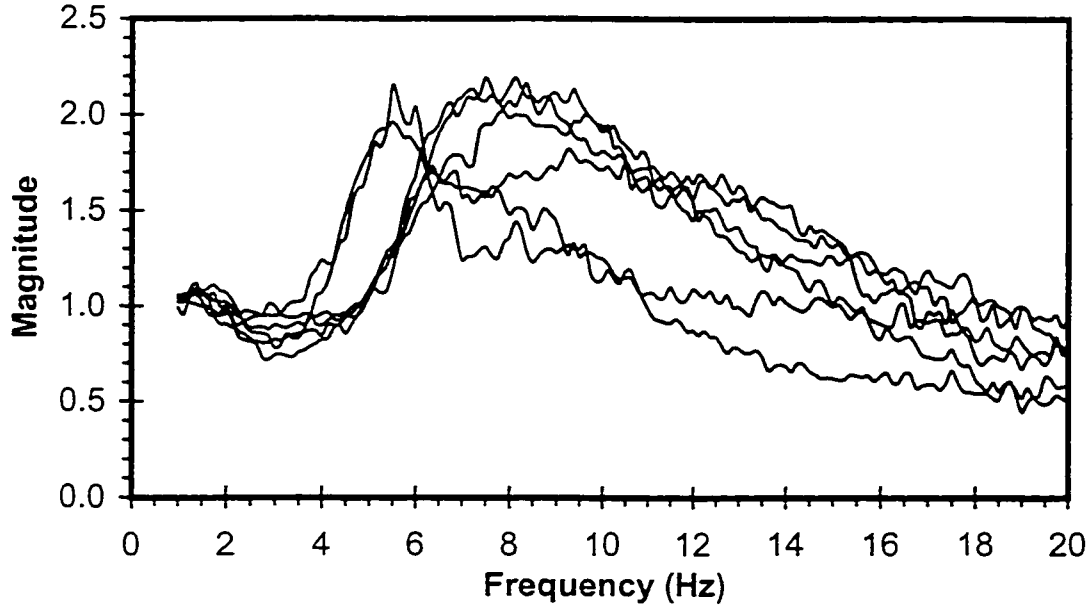

Figure 3.15: The measured seat-to-head transmissibility of six subjects under EBS posture and 1 m/s² rms acceleration excitation.

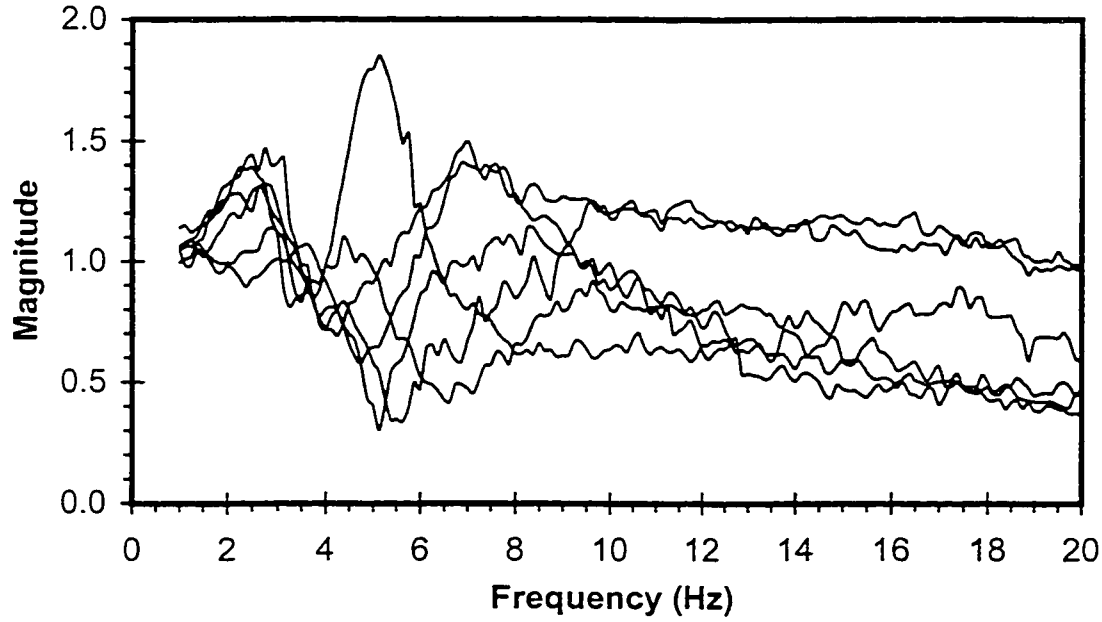

Figure 3.16: The measured seat-to-head transmissibility of six subjects under ENS posture and 1 m/s² rms acceleration excitation.

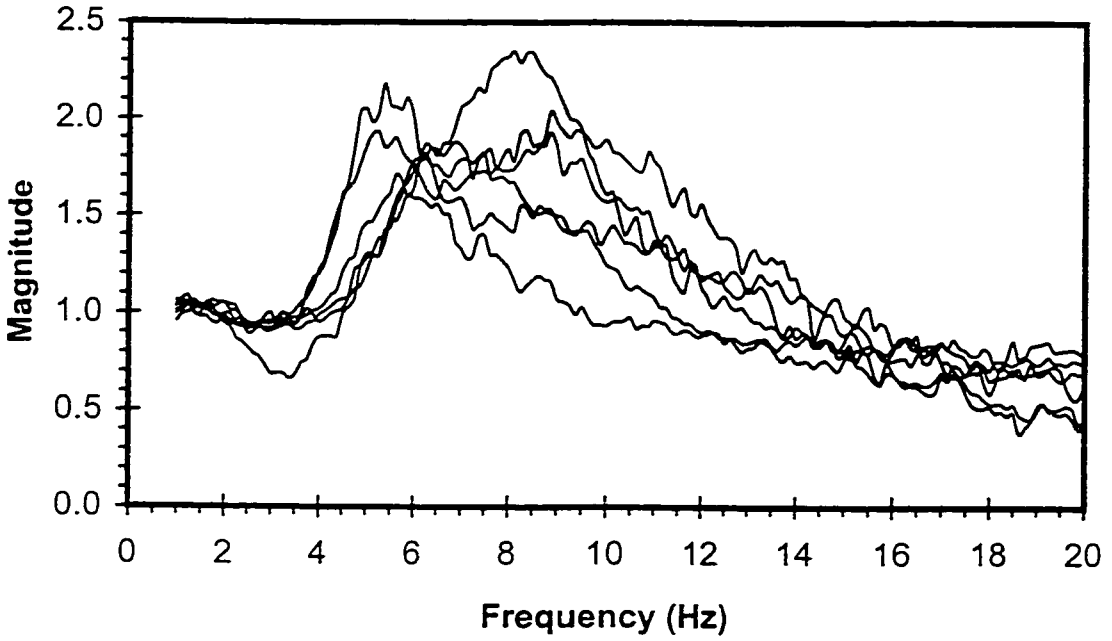

Figure 3.17: The measured seat-to-head transmissibility of six subjects under EBS posture and 2 m/s² rms acceleration excitation.

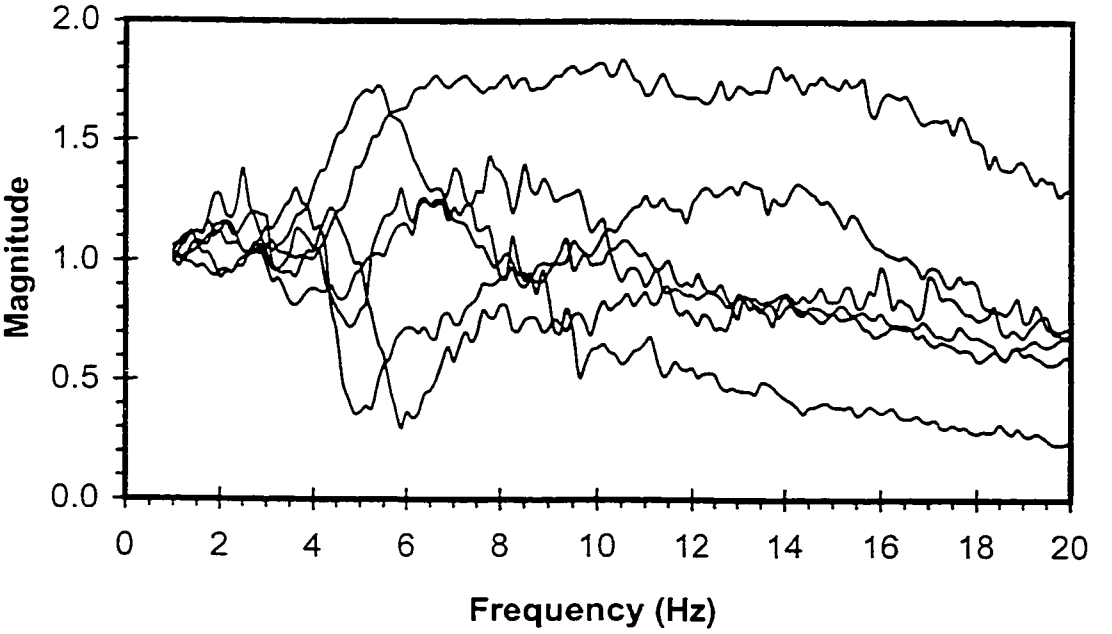

Figure 3.18: The measured seat-to-head transmissibility of six subjects under ENS posture and 2 m/s² rms acceleration excitation.

the group of six subjects considered in the study, compared with the range of 0.1 - 0.2 m, with a mean value of 0.14 m, for a group of eight subjects employed by Matsumoto and Griffin [53].

The measured STHT data is corrected for pitch vibration of the head using Equation (3.4). The corrected magnitude and phase response of the six subjects assuming an ENS posture are illustrated in Figures 3.19 and 3.20, respectively, for 1 and 2 m/s^{-2} rms acceleration excitations. Compared with the APMS data measured under the same test conditions (Figures 3.6 and 3.8), larger inter-subject variability can be observed among the corrected STHT data sets. This may demonstrate that the STHT is considerably more sensitive to the involuntary changes in seated posture. An apparent peak in STHT magnitude appears in the vicinity of 5 Hz for most of the subjects. This primary resonance of the body has been reported repeatedly by various researchers and considered to be caused by the chest structure resonance. While it can be observed that majority of the magnitude curves fall below unity at higher excitation frequencies, specifically under 2 ms^{-2} rms excitation level, some of the curves remain above unity in most of the frequency range. An analysis of variance (F-test) was performed to determine the excitation level effects on the STHT magnitude. The results showed insignificant influence of variation in excitation levels on the STHT magnitude. The STHT data measured under two excitation levels are thus combined to form the STHT magnitude and phase values to be used in the model development. Figure 3.21 illustrates the mean STHT magnitude and phase response and the corresponding upper and lower bound envelopes.

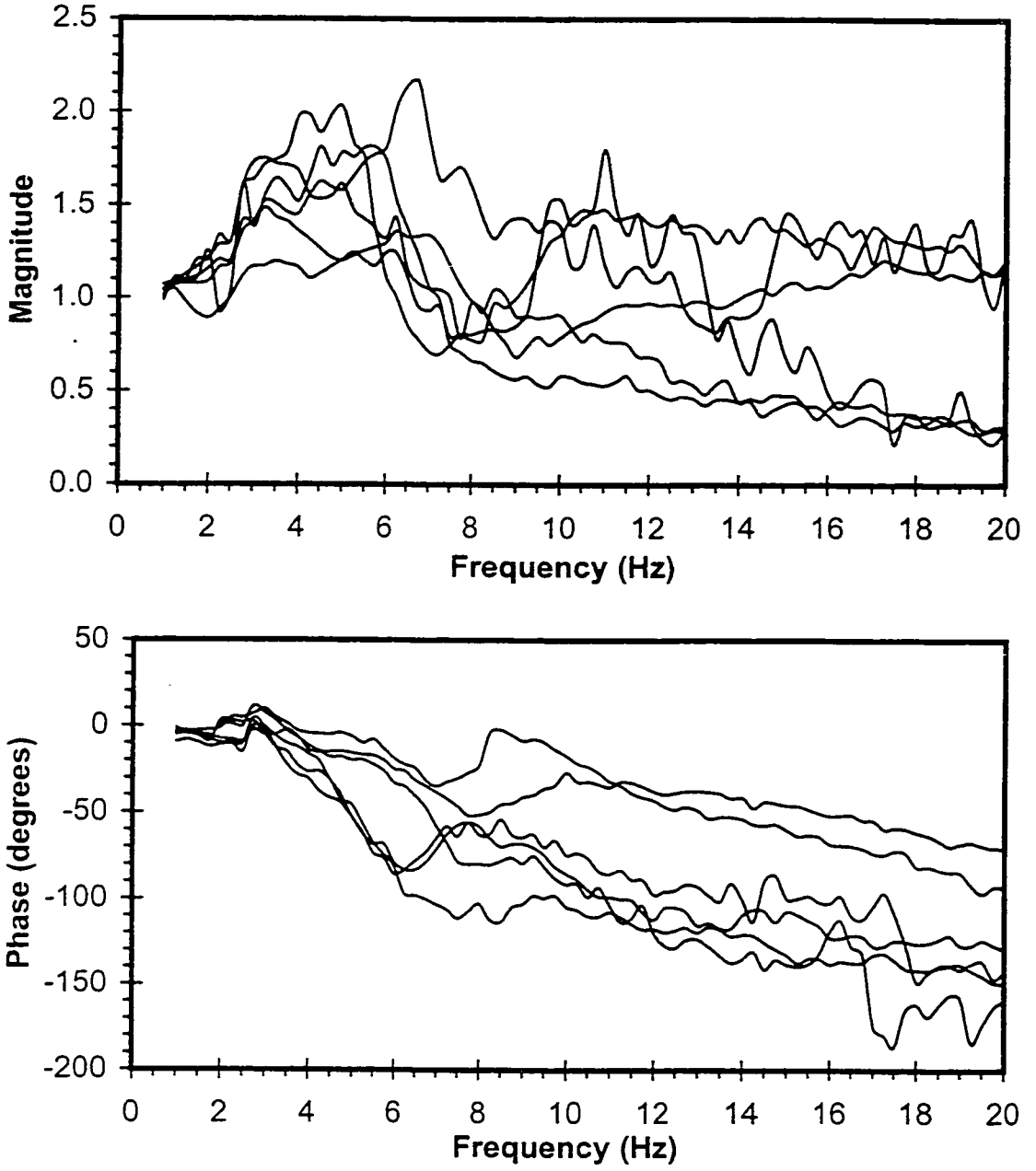

Figure 3.19: The corrected seat-to-head transmissibility of six subjects under ENS posture and 1 m/s² rms acceleration excitation.

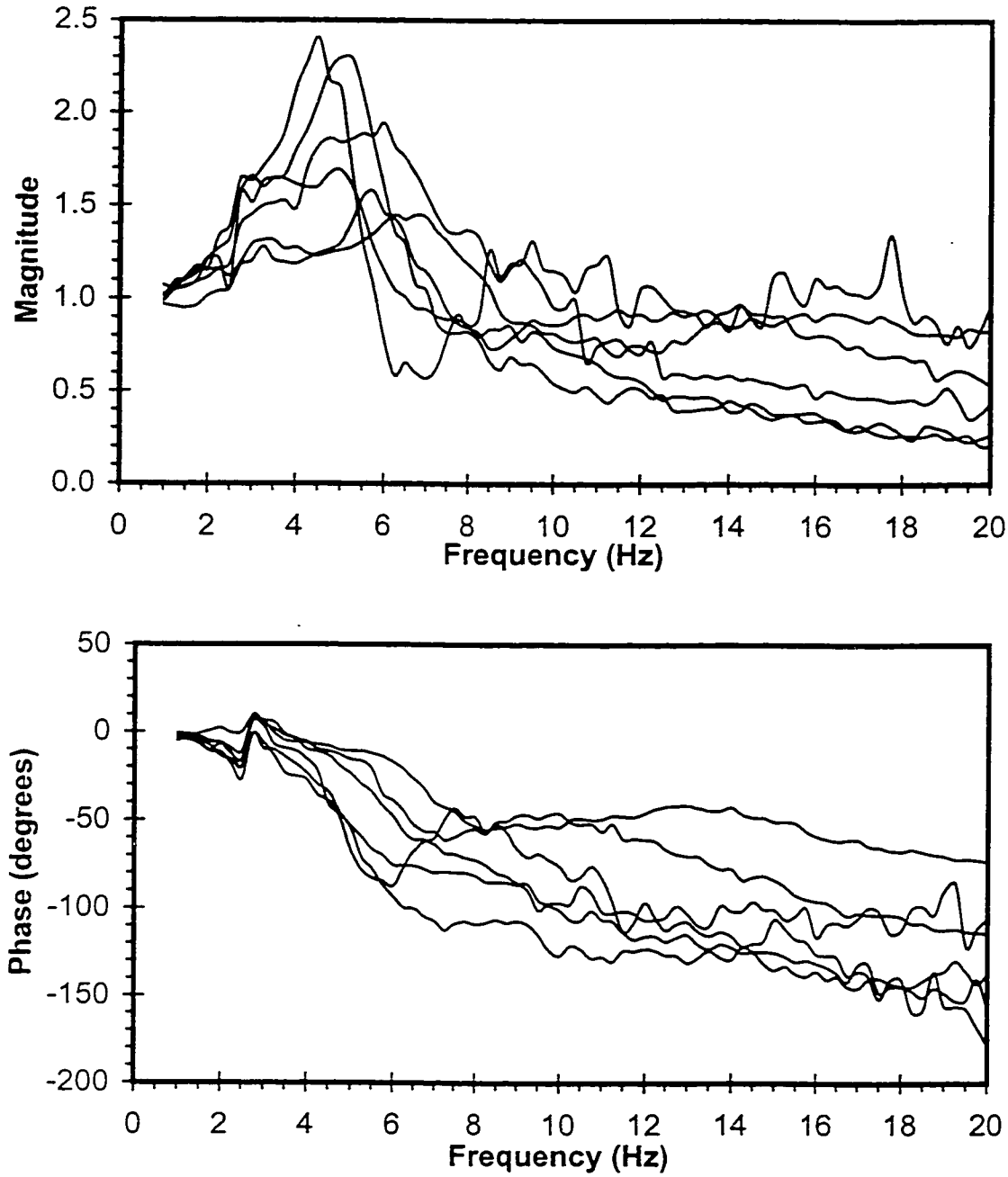

Figure 3.20: The corrected seat-to-head transmissibility of six subjects under ENS posture and 2 m/s² rms acceleration excitation.

3.5 Comparison of Experimental Results with Range of Idealized Values

The mean APMS and STHT data for the ENS posture, averaged over excitation levels of 1 and 2 ms^{-2} rms (illustrated in Figures 3.13 and 3.21, respectively), are compared with those derived from the synthesis performed on the various data sets reported under ENS posture. Figures 3.22 and 3.23 illustrate the comparison of mean and range of measured magnitude and phase response with those derived from synthesis of reported data in Chapter 2. The measured mean APMS magnitude demonstrates trend similar to those observed from the synthesized data, and falls well within the range of idealized values below 9 Hz. At frequencies above 9 Hz, the mean measured data is greater than the synthesized data. This may be partly attributed to two factors: (i) the mean measured APMS magnitude response exhibits a second resonant peak near 10 Hz due to increased thigh contact with the large seat pan used in this study, while some of the reported data sets included in the data synthesis do not show such a second peak; and (ii) there are relatively few data sets available to perform the data synthesis at higher frequencies above 10 Hz, as described in Section 2.8. The range of idealized values at frequencies between 12.5 Hz and 20 Hz includes only four data sets, and thus yield considerable narrowness of the envelope in this frequency range. A close agreement between the mean measured APMS phase and the range of idealized synthesized phase can be observed in Figure 3.22.

The mean measured STHT magnitude agrees well with the range of idealized values only at frequencies above 8 Hz. At lower frequencies, however, the measured mean STHT magnitudes are observed to be larger than the upper bound of the idealized values, more particularly at frequencies between 2.5 and 6 Hz. Again, these discrepancies

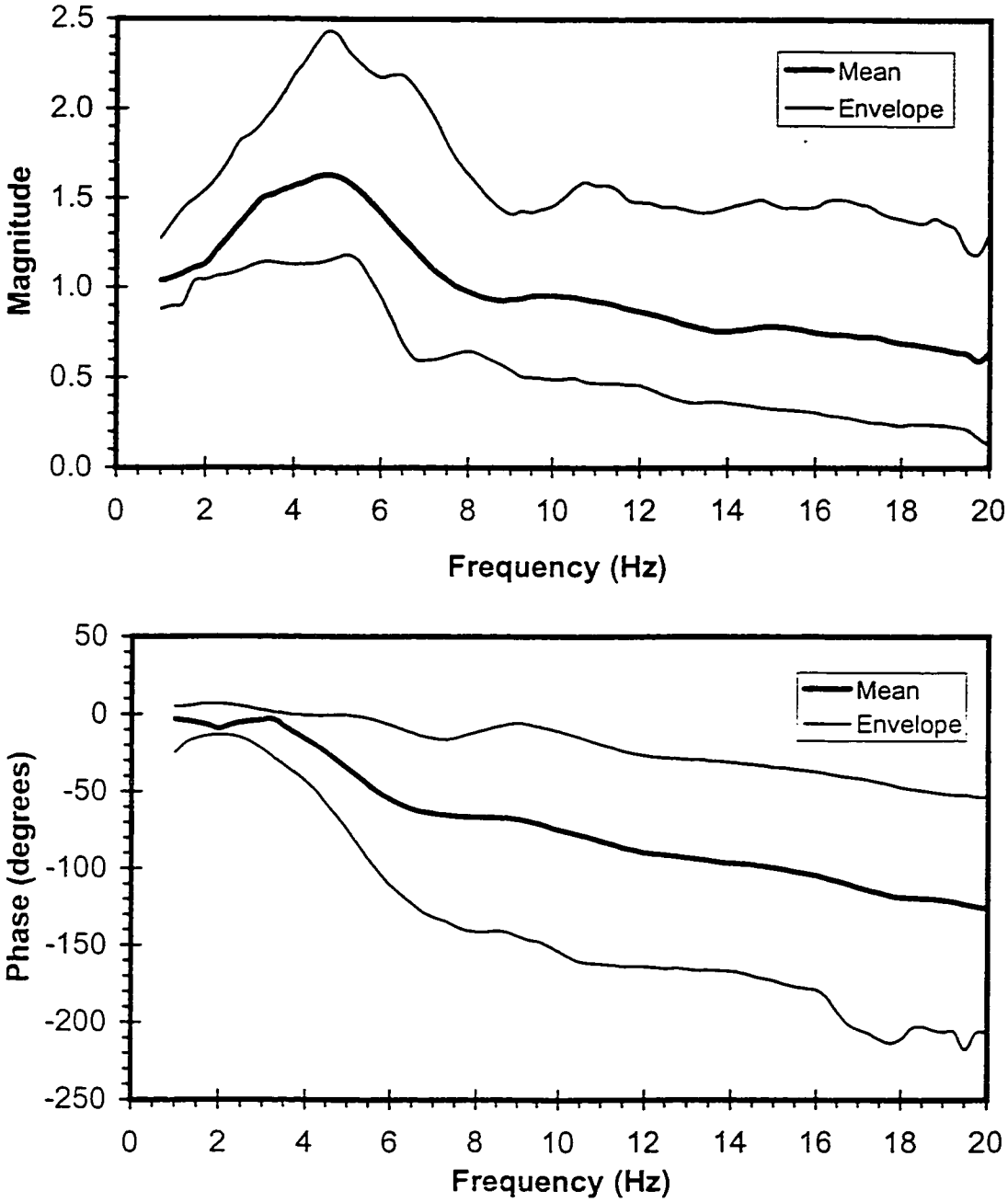

Figure 3.21: The mean and maximum and minimum envelopes of corrected seat-to-head transmissibility of six subjects under ENS posture.

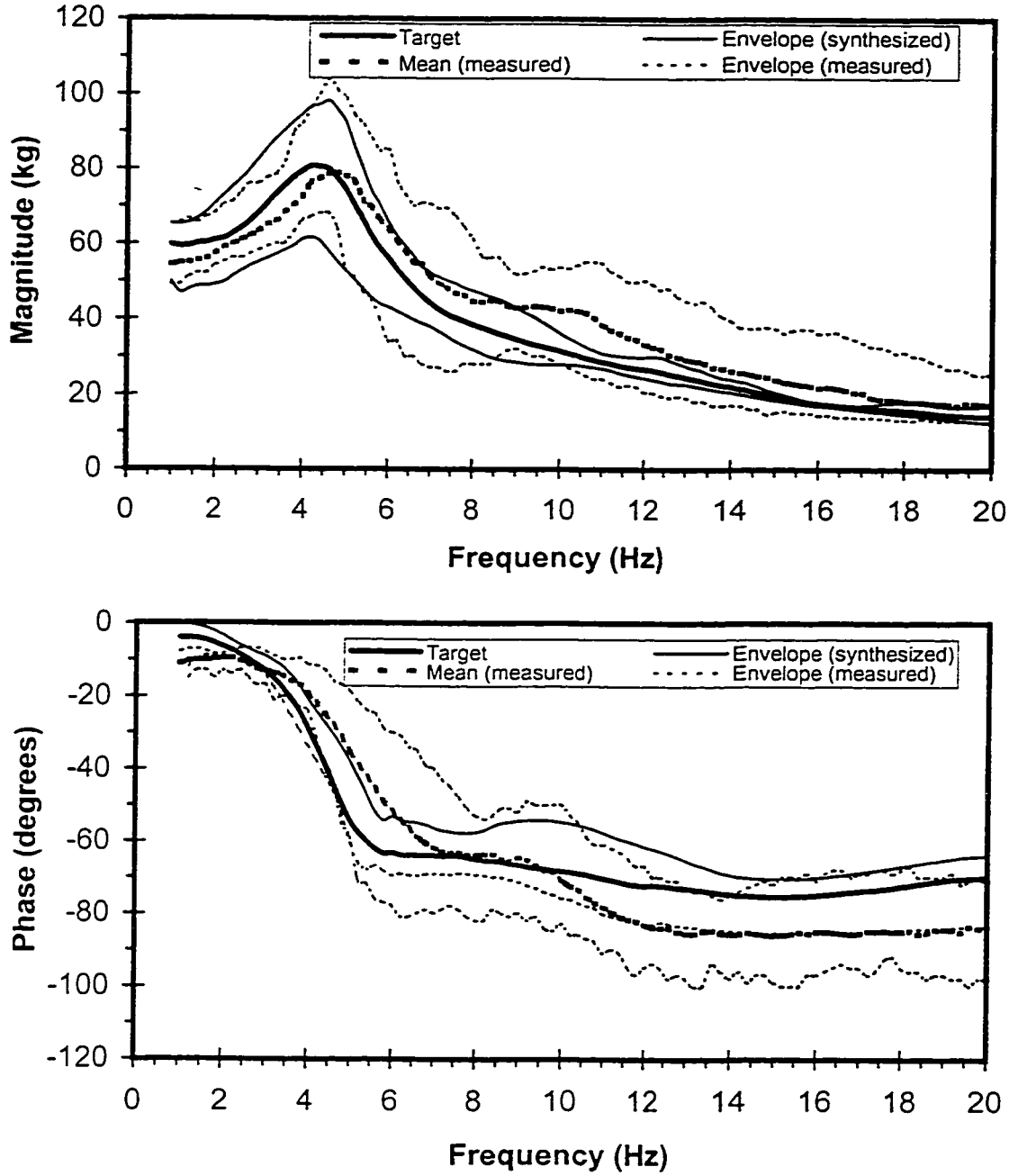

Figure 3.22: A comparison of the measured mean APMS for the ENS posture obtained under excitation levels of 1 and 2 m/s² rms with those derived from the synthesis of reported data sets.

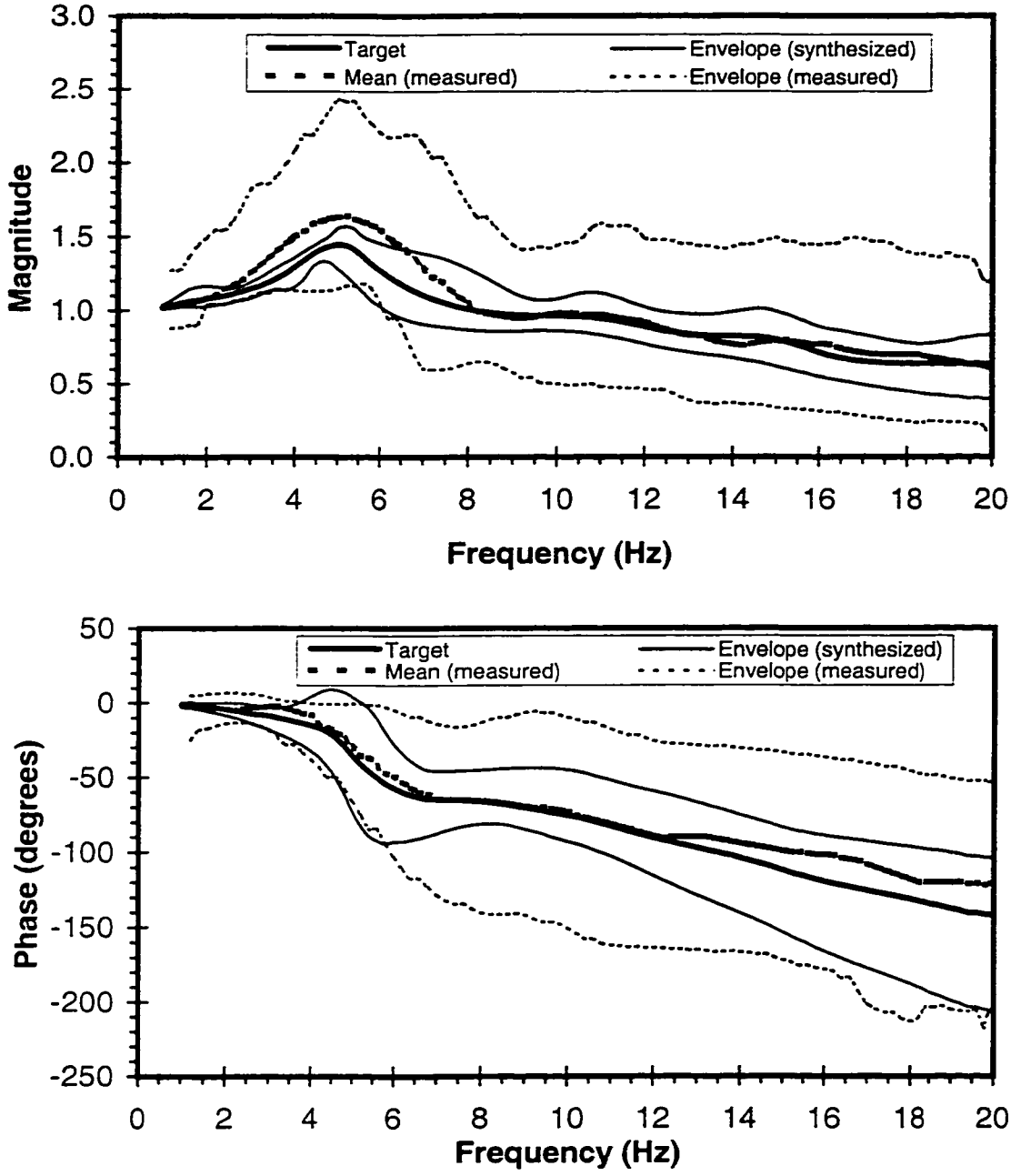

Figure 3.23: A comparison of the measured mean STHT for the ENS posture obtained under excitation levels of 1 and 2 m/s² rms with those derived from the synthesis of reported data sets.

can partly be explained by the very limited number of available data sets employed in defining the idealized range of STHT. The four data sets used in defining the range of idealized STHT may result in an envelope which is too narrow. Similar to APMS phase response, the mean measured STHT phase response also agrees well with the synthesized phase.

The primary resonant frequency and the peak magnitudes derived from the synthesized and measured data are further compared in Table 3.9. The measured APMS and STHT data show excellent agreement in terms of primary resonant frequency (5 Hz), while the same pair of values obtained from the data synthesis shows large variation (4.4 and 5.1 Hz, respectively). This may be sufficient to show that for the same subject population and test conditions, the APMS and STHT functions can yield similar primary resonant frequencies, while the difference in predicting primary resonant frequency from synthesized APMS and STHT may be due to wide range of different test conditions employed. For this reason, it may be more appropriate to define a model based on the measured data, instead of synthesized values. In addition to the analytical discussions on the APMS and STHT functions (Section 3.3), the results may further suggest that it is in practice possible to develop a seated human body model based on both the APMS and STHT data.

Table 3.9: Comparison of primary resonant frequency and peak magnitude obtained from the data synthesis and the experiment.

	Synthesized		**Measured**	
	Primary resonant frequency (Hz)	Peak Magnitude (Normalized)	Primary resonant frequency (Hz)	Peak Magnitude (Normalized)
APMS	4.4	80 kg (1.33)	5.0	78 kg (1.42)
STHT	5.1	1.45	5.0	1.64

3.6 Development of Human Driver Model

Since the proposed human body model is to be used in the study of seating dynamics, the structure should be simple and the number of degrees-of-freedom should be low for its convenient use. Various mechanical models reported in the literature and specifically those illustrated in Figure 3.3, with number of degrees-of-freedom ranging from 1 to 4, were evaluated. The effectiveness of these models in describing the measured APMS and STHT functions were further evaluated. Based upon these preliminary evaluations, a three degrees-of-freedom model was attempted to approximate the human body dynamic responses in terms of both APMS and STHT functions. The model parameters were identified through minimizing an error function comprising measured and model response in terms of magnitude and phase characteristics of APMS and STHT.

3.6.1 Proposed model structure of the seated human body

The proposed three degree-of-freedom model, shown in Figure 3.24, comprises four masses, coupled by linear elastic and damping elements. The masses m_1 to m_3 are introduced with an objective to describe the biodynamic behavior related to two resonant peaks observed in the APMS and STHT magnitude response near frequencies of 5 Hz and 10 Hz, respectively. The lower mass m_0 is introduced to increase the flexibility for tuning the model parameters without increasing the number of degrees-of-freedom. This mass specifically affects the APMS response with only negligible effect on the STHT response. The response of mass m_2 is considered to represent the head response for computing the STHT. Although the model may be related to the biomechanical structure

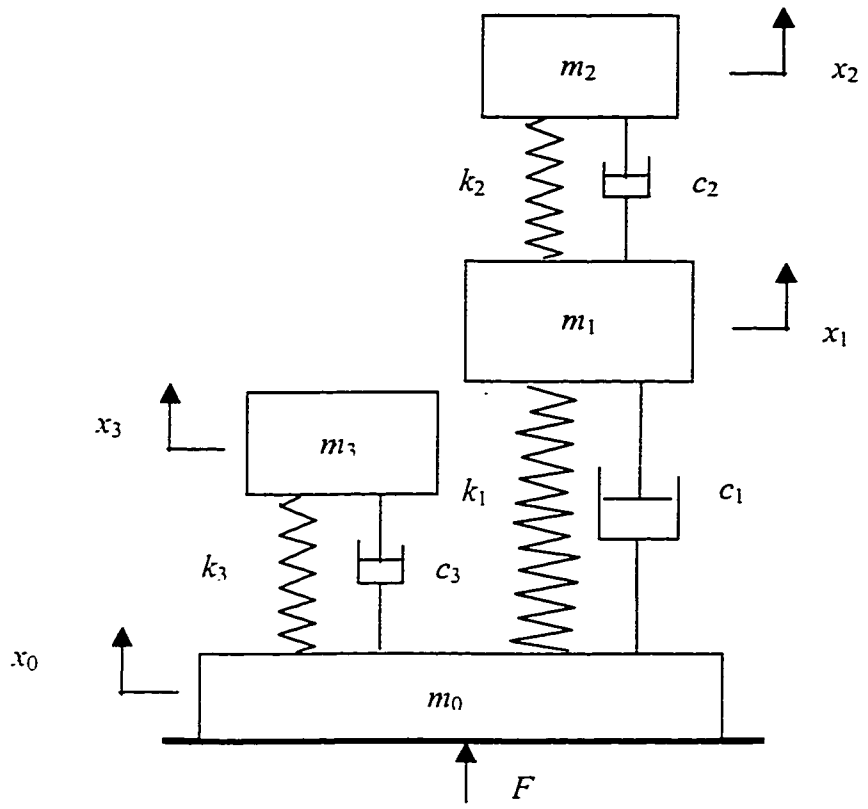

Figure 3.24: Proposed human biodynamic model.

of the human body to provide a better understanding, this approach may introduce severe limit constraints on the parameters leading to parameter uncertainties and complex minimization problem. The model is developed on the basis of experience obtained from examinations of various reported mechanical models, while the biomechanical correlation is not at all attempted. The equations of motion of the model shown in Figure 3.24 are formulated as follows:

$$\begin{cases} m_1\ddot{x}_1 + c_1(\dot{x}_1 - \dot{x}_0) + k_1(x_1 - x_0) + c_2(\dot{x}_1 - \dot{x}_2) + k_2(x_1 - x_2) = 0 \\ m_2\ddot{x}_2 + c_2(\dot{x}_2 - \dot{x}_1) + k_2(x_2 - x_1) = 0 \\ m_3\ddot{x}_3 + c_3(\dot{x}_3 - \dot{x}_0) + k_3(x_3 - x_0) = 0 \end{cases} \tag{3.5}$$

where m_i, c_i and k_i (i=1, 2, 3) are the masses, damping coefficients and stiffness coefficients, respectively, of the model.

Laplace transform of Equations (3.4) yields the following expressions for the transfer function, where each function relates to the ratio of a mass response to the base motion:

$$\begin{cases} \dfrac{X_1(s)}{X_0(s)} = \dfrac{(c_1 s + k_1)(m_2 s^2 + c_2 s + k_2)}{\Delta(s)} \\ \dfrac{X_2(s)}{X_0(s)} = \dfrac{(c_1 s + k_1)(c_2 s + k_2)}{\Delta(s)} \\ \dfrac{X_3(s)}{X_0(s)} = \dfrac{c_3 s + k_3}{m_3 s^2 + c_3 s + k_3} \end{cases} \tag{3.6}$$

where

$$\Delta(s) = [m_1 s^2 + (c_1 + c_2)s + (k_1 + k_2)](m_2 s^2 + c_2 s + k_2) - (c_2 s + k_2)^2 \tag{3.7}$$

The STHT response of the model is computed from:

$$T(s) = \frac{X_2(s)}{X_0(s)} \tag{3.8}$$

The APMS response is derived from the resultant force at mass m_0 and the driving-point acceleration $\ddot{x}_0$. The resultant force F at the lower mass can be computed from the equation of motion for mass m_0:

$$m_0\ddot{x}_0 + c_1(\dot{x}_0 - \dot{x}_1) + c_3(\dot{x}_0 - \dot{x}_3) + k_1(x_0 - x_1) + k_3(x_0 - x_3) = F \tag{3.9}$$

The solution of Equation (3.5) and (3.9) yields:

$$F = m_0\ddot{x}_0 + m_1\ddot{x}_1 + m_2\ddot{x}_2 + m_3\ddot{x}_3 \tag{3.10}$$

The APMS response of the model can then be derived as follows:

$$M(s) = \frac{F(s)}{s^2 X_0(s)} = m_0 + m_1\frac{X_1(s)}{X_0(s)} + m_2\frac{X_2(s)}{X_0(s)} + m_3\frac{X_3(s)}{X_0(s)} \tag{3.11}$$

3.6.2 Estimation of model parameters

A parametric optimization technique was used to determine the model parameters. An objective function was defined to minimize the error between the computed and the measured values of the two biodynamic response functions over a specific frequency range. The objective function is defined as the weighted sum of the squared magnitude and phase errors associated with the APMS or STHT functions, respectively, and expressed as:

$$U(\chi) = \quad \text{minimize}[\,\alpha U_M(\chi) + \beta U_T(\chi)] \tag{3.12}$$

where $U_M(\chi)$ and $U_T(\chi)$ are sum of squared errors resulting from APMS and STHT, respectively, given by:

$$\begin{cases} U_M(\chi) = \lambda\sum_{i=1}^{N}\left\{\left[\,|M(\omega_i)| - |M_t(\omega_i)|\,\right]\right\}^2 + \sum_{i=1}^{N}\left\{\left[\,|\phi_M(\omega_i)| - |\phi_{Mt}(\omega_i)|\,\right]\right\}^2 \\ U_T(\chi) = \psi\sum_{i=1}^{N}\left\{\left[\,|T(\omega_i)| - |T_t(\omega_i)|\,\right]\right\}^2 + \sum_{i=1}^{N}\left\{\left[\,|\phi_T(\omega_i)| - |\phi_{Tt}(\omega_i)|\,\right]\right\}^2 \end{cases} \tag{3.13}$$

where $M(\omega_i)$ and $\varphi_M(\omega_i)$ are the magnitude and phase of the APMS response of the model corresponding to excitation frequency ω_i. $M_t(\omega_i)$ and $\varphi_{Mt}(\omega_i)$ are the corresponding measured values. $T(\omega_i)$ and $\varphi_T(\omega_i)$ are the magnitude and phase of the STHT response of the model, and $T_t(\omega_i)$ and $\varphi_{Tt}(\omega_i)$ are the corresponding measured values. N is the number of discrete frequencies selected in the 0.5 to 20 Hz frequency range. χ is a vector of model parameters to be identified, expressed as:

$$\chi = \{m_0, m_1, m_2, m_3, c_1, c_2, c_3, k_1, k_2, k_3\}^T \qquad (3.14)$$

where 'T' designates the transpose. λ and ψ are weighting factors used in the APMS and STHT error functions, respectively, to ensure somewhat comparable contributions of magnitude and phase errors in the objective function. Since the range of APMS magnitude and phase over the frequency range of interest are in the same order, the weighting factor λ is selected as 1. The magnitude of STHT varies in the 0.5 to 1.4 range, which is considerably smaller than its phase range of 0° to -120° over the frequency range of interest. The weighting factor ψ is thus assumed a value of 10^4 to emphasize the contribution due to STHT magnitude. α and β are weighting factors on the APMS and STHT errors. Since driver APMS is critical in seating dynamics, α was given a value of 10 to put more emphasis on the error arising from APMS data.

The minimization problem expressed in Equation (3.12), is solved subject to constraints applied on the total model mass. Since the mean measured data is related to mean body mass of 53.4 kg, supported by the seat, a limit constraint is defined to allow the total mass to vary within a narrow band (± 4%), such that:

$$51.4\,kg \le \sum_0^3 m_i \le 55.4\,kg; \qquad (3.15)$$

The optimization function is further subject to the following parameter constraints:

$$\begin{aligned} &m_0 > 0; \quad m_1 > 0; \quad m_2 > 0; \quad m_3 > 0 \\ &k_1 > 0; \quad k_2 > 0; \quad k_3 > 0 \\ &c_1 > 0; \quad c_2 > 0; \quad c_3 > 0 \end{aligned} \tag{3.16}$$

3.6.3 Model parameter values

The constrained optimization problem, defined in Equations (3.12) through (3.16), is solved using *MATLAB* software package [54]. The solutions were obtained for different starting values of the parameter vector χ, and the resulting model parameters were examined to obtain optimal values and minimum error of the objective function. Different optimization runs corresponding to different starting values converged to similar values of model parameter and the error function. The model parameters, thus identified. are summarized below:

$m_0 = 3.5$ kg

$m_1 = 42.6$ kg	$k_1 = 45644$ N/m	$c_1 = 1305$ Ns/m
$m_2 = 2$ kg	$k_2 = 29087$ N/m	$c_2 = 91$ Ns/m
$m_3 = 5.7$ kg	$k_3 = 26617$ N/m	$c_3 = 155$ Ns/m

$$\sum_{i=0}^{3} m_i = 53.8 kg$$

The analytical model of the seated body is evaluated to derive the response characteristics in terms of STHT and APMS, using Equations (3.8) and (3.11), respectively. The computed response characteristics are compared with the measured response, as shown in Figures 3.25 and 3.26, to examine the effectiveness of the proposed

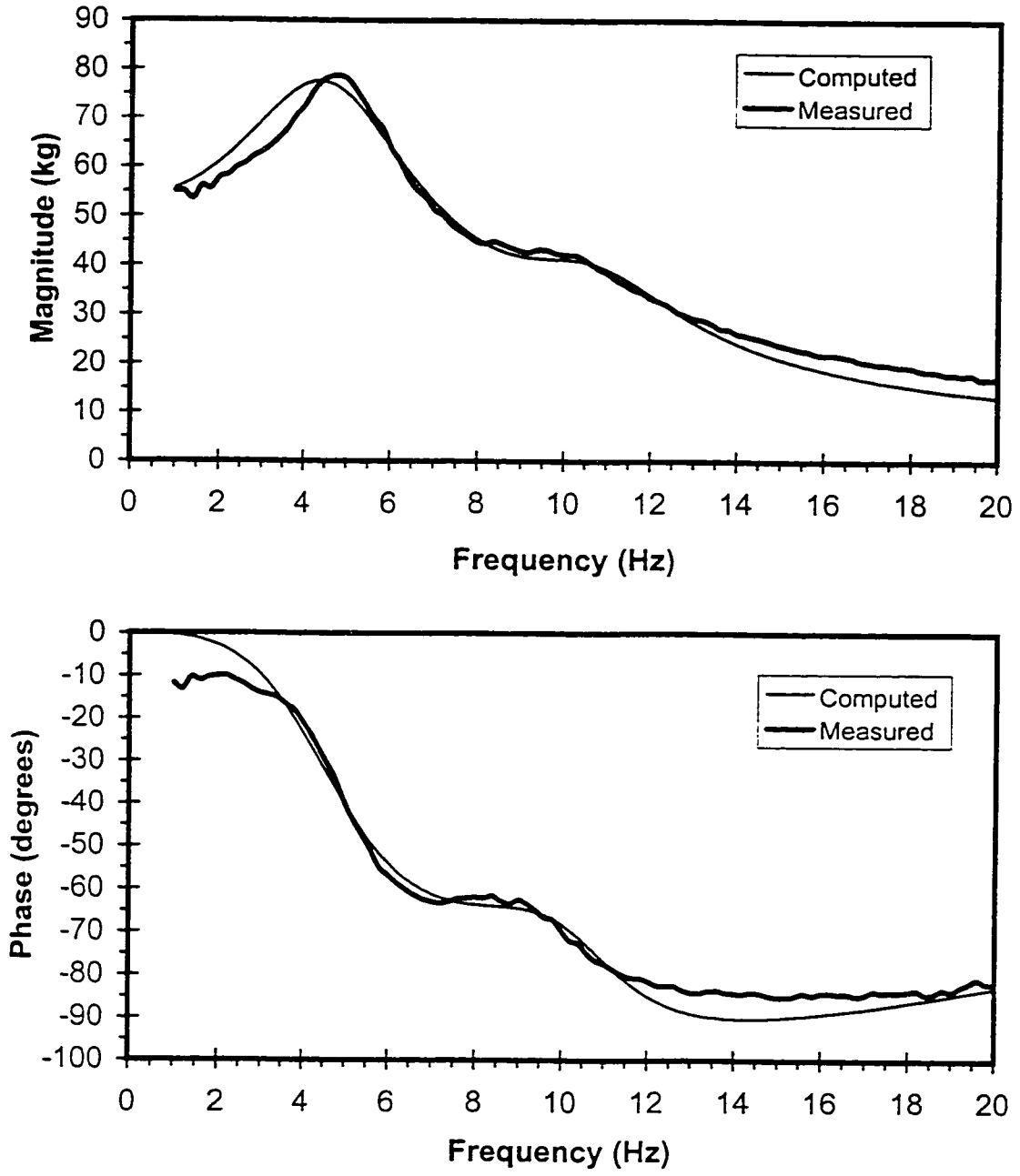

Figure 3.25: Comparison of the computed apparent mass with the measured data.

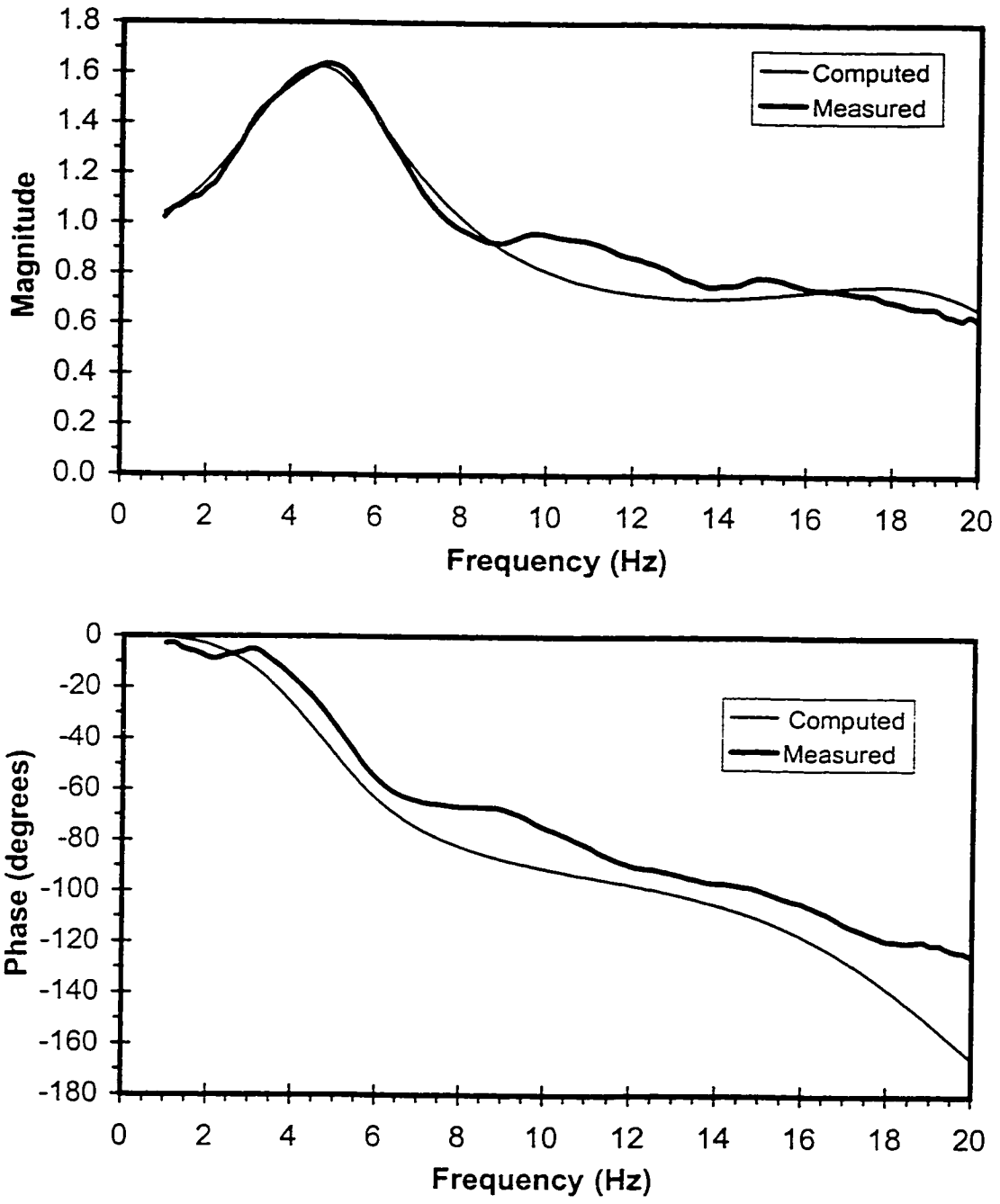

Figure 3.26: Comparison of the computed seat-to-head transmissibility with the measured data.

model. The results, in general, show a reasonably good agreement between the measured and computed response characteristics. While the APMS magnitude and phase response, computed from the model, correlates very well with the measured data, the STHT response exhibits some error at frequencies above 7 Hz. The computed APMS function reveals two resonant peaks in the vicinity of 5 Hz and 10 Hz, which are quite consistent from the measured data. The resonance in the vicinity 5 Hz is primarily associated with the deflection modes of coupled subsystem comprising m_1 and m_2, while the resonance near 10 Hz is associated with deflection mode for the mass m_3. The STHT is solely attributed to the dynamic response due to subsystem comprising m_1 and m_2. Similar to the measured data, the computed STHT function reveals a resonance near 5 Hz. The second resonant peak near 10 Hz, however, is not apparent in the computed STHT response.

The STHT magnitude response reveals a slight peak near 18 Hz, which is attributed to the second deflection mode of the subsystem comprising m_1 and m_2. The measured data does not reveal a peak near this frequency. Among the four target curves, the model provides a poorest fit with the measured STHT, which was given the lowest weighting in the optimization function. An eigenvalue analysis shows that the damped primary resonant frequency is at 4.6 Hz, which is slightly lower than 5 Hz, at which the maximum APMS and STHT magnitudes of the measured data occur.

3.7 Summary

A seated human body model is required for the study of seating dynamics. For uniqueness of the model, it may be desirable to include both DPMI/APMS, which describe 'to' the body or force-motion relationship at the driving point, and STHT data, which describe 'through' the body or vibration transmission function, in the model development. In order to

validate the adequacy of this modeling approach, a relationship between the biodynamic functions is investigated. The study showed that 'to' and 'through' the body response can be best described by APMS and STHT functions. Both functions yield similar values of primary resonant frequencies. In view of wide inter-subject variations and variation in the test conditions employed in different studies, both the functions were measured in the laboratory under identical test conditions, and using same subject group.

The discussions on the DPMI and APMS functions, based on both experimental data and theoretical analysis, suggest that the APMS might be a better function than DPMI in that the APMS function tends to show less variations in terms of the primary resonant frequency among a group of data sets derived either from data synthesis or from laboratory measurements. A close agreement between the normalized APMS and STHT functions has been established analytically in terms of the primary resonant frequency of seated body and the magnitude. This conclusion, together with that observed from the laboratory measurements, showed that the APMS and STHT data measured under same test conditions and with the same subject population indeed agrees well in terms of the primary resonant frequency. A three degrees-of-freedom linear human body model is proposed and its parameters are estimated using optimization techniques. Reasonable agreement was observed between the model response and the measured APMS and STHT data, which validates the modeling procedure and provides a reliable seated body model. The seated body model will be further used to study the performance characteristics of coupled human-seat system under various vibration excitations.

CHAPTER 4

DEVELOPMENT OF A SEAT CUSHION MODEL THROUGH STUDY OF DYNAMIC PRESSURE DISTRIBUTION AT THE HUMAN-SEAT INTERFACE

4.1 Introduction

The vibration related discomfort characteristics of off-road vehicle drivers is strongly related to various seat design factors, including posture, the range and ease of adjustments and ride vibration environment. The driver comfort has been further related to the pressure distribution at the interface between the human body and the seat support surfaces. The occurrence of high local pressure at the human-seat interface is known to cause soft tissue deformation leading to restricted blood and nutrient flows, and thus human discomfort [55]. Some studies performed on the human subjects seated in a static environment have concluded that inadequate pressure distribution can cause tissue anoxia and skin ulceration among the paralyzed patients with lack of sensitivity in the weight-bearing areas, and discomfort and rapid fatigue among the healthy subjects [56-59]. A study conducted by Sanders and McCormick [60] proposed that for healthy seated subjects, the body weight should be uniformly distributed over the buttocks area with minimal weight under the thighs, since the high pressure at the soft tissues of the thighs yields considerable discomfort and reduced working efficiency. The comfort requirements of the vehicle seats, involving postural support and vibration attenuation, are different from those of the other seats. The influence of seat cushion designs on the seating comfort and driver posture has been evaluated through a number of subjective and objective studies. A study performed by Ng *et al.* [61] reported that an adequate driver-seat support could reduce the stresses in muscles of the back, buttocks, and legs

caused by prolonged sitting during daily driving activities. The muscles experience increased static loading in an attempt to restore stability under poor seating posture, thereby contributing to increased driver discomfort and fatigue. Bowers-Carnahan *et al.* [62] performed a subjective survey of the heavy-duty truck operators to identify their seat design preferences and specific ailments experienced by the drivers. While lower back pain, neck pain, muscle stiffness, and sore buttocks and legs were identified as the most commonly reported ailments, most of the drivers identified the need for improvements in the seat cushion design. Thakurta *et al.* [63] evaluated the seating comfort related to various seat zones through subjective studies and correlated the comfort assessments to measured driver-seat interface pressure under static loads. The subjective evaluations of the four specific zones including shoulders, lumbar, ischium tuberosities, and thighs showed good correlation with the measured pressure distribution. A considerably significant correlation was established between the interface pressure and the subjective evaluations for the lumbar and ischium support areas. While these studies have reported the pressure distribution at the human-seat interface under static environment, the characteristics of the pressure distribution under whole-body vibration have not been widely reported. The latter is considered to relate more closely with vehicle seating comfort than static pressure distribution.

The polyurethane foam widely used in seat cushion design has complex mechanical properties and the ride comfort is closely related with these properties [64]. The effect of the composition, density and thickness of polyurethane foam and the effect of sample shape and seat cover on vibration transmission have also been studied [65, 66, 67]. The polyurethane foam seats have highly nonlinear visco-elastic properties

depending upon the excitation vibration magnitude and frequency content, the seated posture and subjects' physical characteristics [14]. A linear seat cushion model, however, has been employed in majority of the simulation studies on seating dynamics [5, 8, 68, 69], by representing the visco-elastic properties of the cushion along the vertical axis with an equivalent linear spring and a parallel linear viscous damper. Such a model has been used to predict the vibration transmitted to the human body and to investigate the optimum seat cushion parameters so as to minimize the vibration exposure of the seated driver for given vibration excitation spectra. Although the linear cushion model provides good representation of polyurethane foam seats when the magnitude of input vibration is low, it will produce large error when the magnitude of input vibration is large. Furthermore, the model cannot account for two phenomena which may occur under high levels of excitations leading to suspension seat end-stop impacts: (i) cushion may bottom out; and (ii) the body may hop. A nonlinear and representative cushion model is thus needed to account for these two phenomena. The development of a seat cushion model may require systematic identification of its force-deflection and force-velocity characteristics, distribution of static and dynamic forces at the driver-seat interface and force-motion relationship for the human driver.

In this study, the effect of whole-body vertical vibration on the characteristics of dynamic human-seat interface pressure distribution is investigated using both a rigid and a soft seat to enhance an understanding of the force distribution and driver discomfort related to cushion design. The magnitude of peak pressure and the characteristics of pressure distribution including ischium pressure, effective contact area and contact force,

are specifically analyzed as functions of the magnitude and frequency of vertical vibration. Based on the results, a nonlinear seat cushion model is proposed and validated.

4.2 Pressure Distribution Measurement

Various methods have been proposed during the past three decades to perform qualitative and quantitative measurements of pressure at the human-seat and human-bed interface. Swearingen *et al.* [70] obtained a qualitative measure of the sitting pressure using an absorbent paper placed over inked corduroy cloth. The density of the ink transfer provided a measure of pressure intensity. Lindan [56] developed the "bed of nails and springs", comprising nails and springs placed at 1 cm intervals over a hard board, to quantify the interface pressure through measurement of spring deflection. Frisina [71] developed a measurement system using the principle of pressure-controlled chemical reaction. The measurement method, however, was reported to be quite sensitive to temperature variations. Mooney [72] developed a flexible and pressurized pneumatic cell to measure the external pressure using the principle of differential pressure based contact sensor. A pressure evaluation pad (PED), comprising a 12×12 matrix of pneumatically controlled contact switches based upon the similar principle, was developed by Garber *et al.* [73] to carry out relative assessments of various wheelchair cushions. Optical sensors [57], capacitive [74] and strain-gauge [75] based pressure transducers have also been employed to measure pressure distribution between the human body and different surfaces. Most of the systems, however, have been limited in their applications to measure the human-seat interface pressure distribution on curved elastic surfaces due to the large size of the available sensors. The visco-elastic properties of the human-seat

interface are significantly altered when such measurement systems using large size sensors are used on soft and curved cushion surfaces. Furthermore, the rigid interface created by the relatively large size pressure transducers results in artificially high pressure loading on the tissues and poor resolution of the measured data. Accurate measurement of pressure distribution in the vicinity of ischial tuberosities requires a closely spaced grid of thin, miniature and flexible sensors. A number of flexible and thin-film resistive and capacitive pressure sensors have thus been developed to perform the measurements on flexible and curved surfaces. Piché *et al.* [76] developed a flexible pressure sensing matrix using thin film force-sensing resistors to measure the dynamic pressure distribution at the man-machine interface. Gurram *et al.* [77] performed the study of dynamic grip-pressure distribution at the hand-handle interface of a vibrating hand-held power tool using both resistive sensors developed by Piché *et al.* [76] and capacitive pressure sensors developed by NOVEL Inc (Beichstraβe 8, 8000 München 40, Germany). The study performed using 20 sensors mounted on the subject hand demonstrated that the resistive sensors yield considerable measurement errors due to large hysteresis associated with the force sensing resistors. Such is not the case with the capacitive sensors developed by NOVEL inc., which were thus used in this study in conjunction with the signal conditioning, data acquisition and the signal analysis system, known as the PLIANCE system.

4.2.1 Description of the PLIANCE system

The PLIANCE system comprises a pressure sensing mat of 256 flexible capacitive sensors, an analyzer with an analogue amplifier and a control/interface

module, and a data acquisition system. The sensing matrix comprises sensors arranged in 16 rows and 16 columns, molded within a mat of flexible material of thickness less than 2 mm. The distance between the centers of two successive sensors in a row or a column is 24.5 mm, and each sensor has a dimension of 10 mm × 10 mm. The spacing between the sensors placed either in a row or a column is 14.5 mm and the effective area of the sensing mat is thus 39.2×39.2 cm^2. The analyzer samples the sensor matrix during a measurement and transfers the data to a personal computer through the serial interface. The sampling rate of the entire measurement system is 21.2 Hz. The measured data is simultaneously displayed in color-coded graphics, which can be stored or output to other software packages for further analyses.

4.2.2 Experimental design of pressure distribution measurement

The distribution of pressure at the human-seat interface under vertical vibration has been investigated for a rigid and a soft automotive seat. The rigid seat had been used in the APMS and STHT measurements and described in Subsection 3.4.1. The seat pan and backrest were adjusted to be flat and vertical, respectively, during the experiments. The soft automotive seat consists of a 430 mm × 500 mm foam cushion with a thickness of 114 mm fixed to a rigid frame. The seat pan and backrest angles were also adjusted to flat and vertical, respectively. The soft seat height was adjusted to 432 mm, compared with the height of the rigid seat, 478 mm. The seats were installed on the WBVVS described in Subsection 3.4.1 to perform the measurements under controlled vertical vibration.

The PLIANCE seat pressure mat was installed on the seat pan and an accelerometer was mounted at the seat base to measure the vibration excitation. The measurements were performed under sinusoidal excitations of two different magnitudes (1 ms^{-2} rms and 2 ms^{-2} rms) and different frequencies (1, 2, 2.5, 3, 4, 4.5, 5, 6, 8 and 10 Hz). The measurements under the low magnitude vibration (1 ms^{-2} rms) were initiated at an excitation frequency of 1 Hz, which was gradually increased to selected frequencies. The measurements at the lowest frequency of 1 Hz, however, could not be performed under 2 ms^{-2} rms acceleration due to safety constraints imposed on the maximum displacement of the WBVVS. The measurements under the higher acceleration were thus initiated at 2 Hz instead of 1 Hz.

A population of six subjects participated in the experiments, with mass ranging from 47.9 kg to 94.9 kg, as listed in Table 4.1. This range lies close to the subject mass range of 49 kg to 94 kg, defined in Section 2.5 for performing the data synthesis. During the measurements, the subjects were requested to sit on the sensing mat, which was taped on the seat surface, with their ischium tuberosities being located near a line marked on the sensing mat. The line was 100 mm from the seatback to ensure the ischium tuberosities and the thighs being well within the effective sensing area. The subjects kept sitting erect either with backrest (EBS) or without backrest (ENS), as required, with hands on the lap and feet supported on the vibrating floor. They were advised to maintain a balanced and consistent posture during the tests. These postures were slightly different from the ENS and EBS postures defined in Subsection 3.4.1 in that the lower portion of the subject back was not in contact with the backrest. For the convenience of discussion,

the two postures are still referred to as the ENS posture and the EBS posture. Each measurement was performed twice and the data was examined for repeatability.

Table 4.1: Characteristics of subjects participating in the experiments on dynamic pressure distribution measurements.

Subject	A	B	C	D	E	F
Height (m)	1.60	1.73	1.60	1.73	1.63	1.72
Mass (kg)	47.9	54.6	58.1	76.5	78.7	94.6

4.3 Analysis of the Interface Pressure Distribution

The distribution of human-seat interface pressure on both the rigid and soft seats under static and dynamic seating environments was acquired under different postures for each subject. The measured data was analyzed to yield static and dynamic pressure distribution contours, dynamic ischium pressure, effective contact area and contact force at the human-seat interface under different excitation frequencies, excitation magnitudes, and seated postures. It is observed that the dynamic pressure under dynamic seating is significantly higher than that obtained under static seating. Although the dynamic pressure distribution obtained using all subjects reveal a similar pattern, the pressure values under a given vibration excitation differ greatly from one subject to another. The EBS posture generally induces more force near the tailbone than the ENS posture, which usually yielded higher pressure values in the vicinity of ischial tuberosities. Under vibration excitation, the maximum variations of the ischium pressure and the effective contact area on the soft seat are yielded around the resonant frequency of the human-seat system. Increased excitation magnitude causes increased maximum ischium pressure and maximum effective contact area around the resonant frequency of the human-seat system.

The results have been reported and analyzed in two papers [77, 78]. While the inter-subject variability and the effect of posture have been discussed in these two papers, this chapter mainly focuses on results measured with a single subject (subject D) under one posture (ENS), except where stated, to reveal the general trends of dynamic pressure distribution and lead to the development of a seat cushion model.

4.3.1 Static pressure distribution contour maps

Figure 4.1 illustrates the typical three dimensional maps of the interface pressure measured at the surfaces of the rigid and the soft seats under static seating conditions. The results show that sitting on a rigid surface yields dominant pressure distribution within the ischium region with peak pressure occurring in the vicinity of the ischial tuberosities. The high interface pressure peaks observed with the rigid seat are expected to cause fatigue and discomfort over prolonged sitting [74]. The resulting effective human-seat contact area is thus quite small and the magnitude of pressure under the thighs is relatively negligible. The interface pressure distribution obtained for a soft seat, however, is considerably different. The seated weight is more or less uniformly distributed over a considerably larger sitting area and the peak interface pressure is significantly lower than that encountered on a rigid seat. The maximum static pressure, however, still appears in the vicinity of ischial tuberosities. The soft seat with low level peak interface pressure can thus be expected to reduce driver fatigue and discomfort caused by the local concentration of interface pressure.

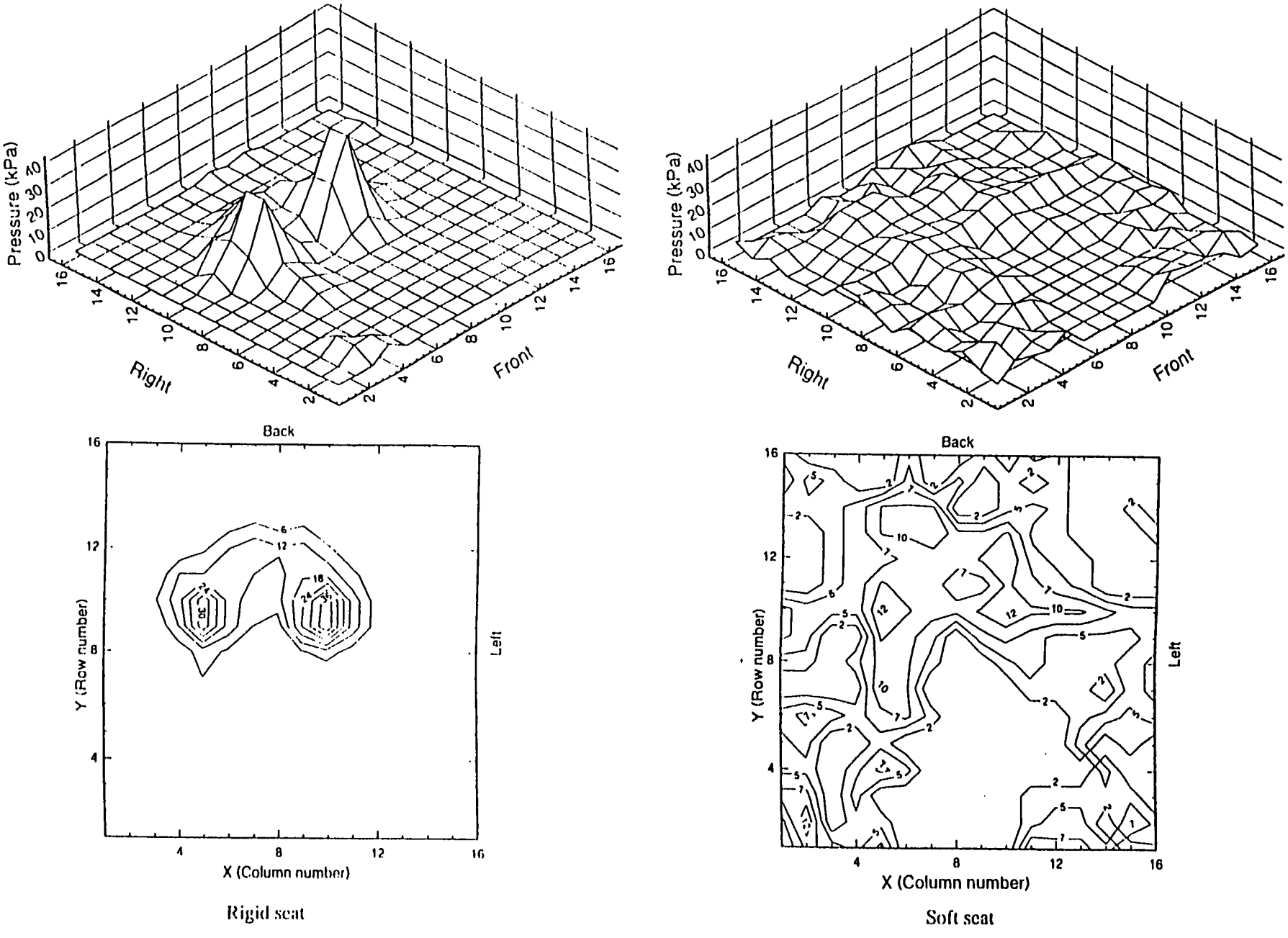

Figure 4.1: Static interface pressure distribution measured on the rigid and the soft seat surfaces.

4.3.2 Time histories of dynamic ischium and thigh pressures

Since the interface pressure is mostly concentrated in the vicinity of the tuberosities, an examination of the dynamic pressure distribution in this region can provide considerable insight into the design requirements for the seat cushions. The magnitude of ischium pressure is strongly related to the properties of seating surface, posture, magnitude and frequency of vibration excitation and the resonant frequency of the coupled seat-human system. The time histories of typical ischium pressure measured on the rigid and soft seat surfaces are illustrated in Figures 4.2 under both static and dynamic conditions (Subject D, ENS posture). The results were obtained under two sinusoidal excitation magnitudes (1 ms^{-2} rms and 2 ms^{-2} rms acceleration) at different frequencies (5 Hz for the rigid seat; and 2.5 Hz for the soft seat). The two different frequencies were selected corresponding to respective resonant frequencies of the coupled rigid and soft seat-human systems. The ischium pressure on a rigid seat surface approaches its peak value near 5 Hz, attributed to the fundamental resonance of the seated subject. The measurements performed with the soft seat revealed peak ischium pressure under vibration excitations in the 2.5 - 3.0 Hz range, attributed to the resonance of the coupled seat-human system, as illustrated in Figure 4.3. The figure presents the acceleration transmissibility of the soft seat coupled with a human subject. The results show peak response in the 2.5-3.0 Hz frequency range. The pressure time histories presented in Figure 4.2 show that the static ischium pressure measured on the rigid seat is almost 6 times that of the pressure measured on the soft seat for the same subject. The dynamic ischium pressure oscillates at the respective frequencies of excitations, and the magnitude of pressure varies considerably with the magnitude of excitation for both

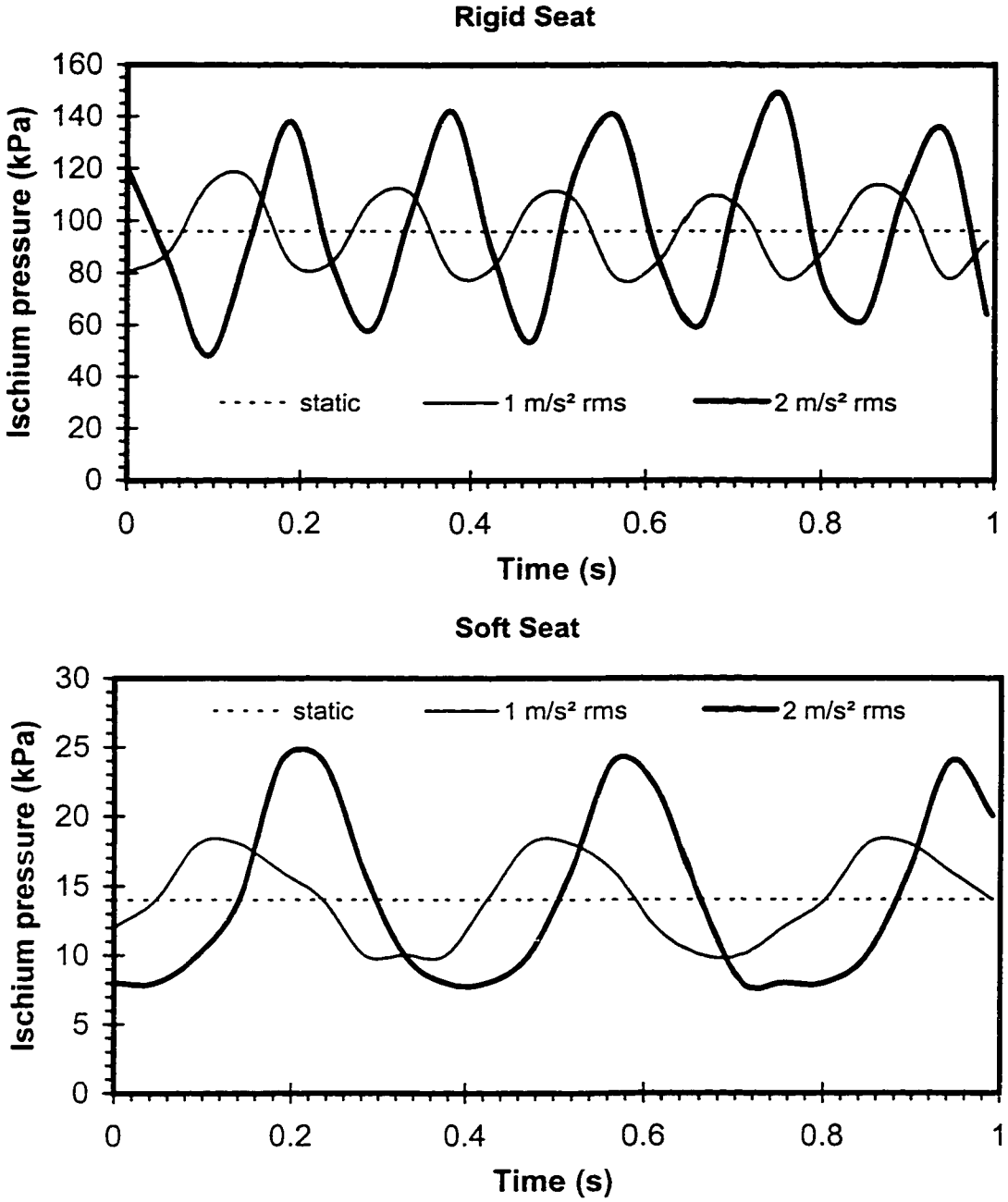

Figure 4.2: Typical time histories of dynamic and static ischium pressure measured on the rigid and the soft seats.

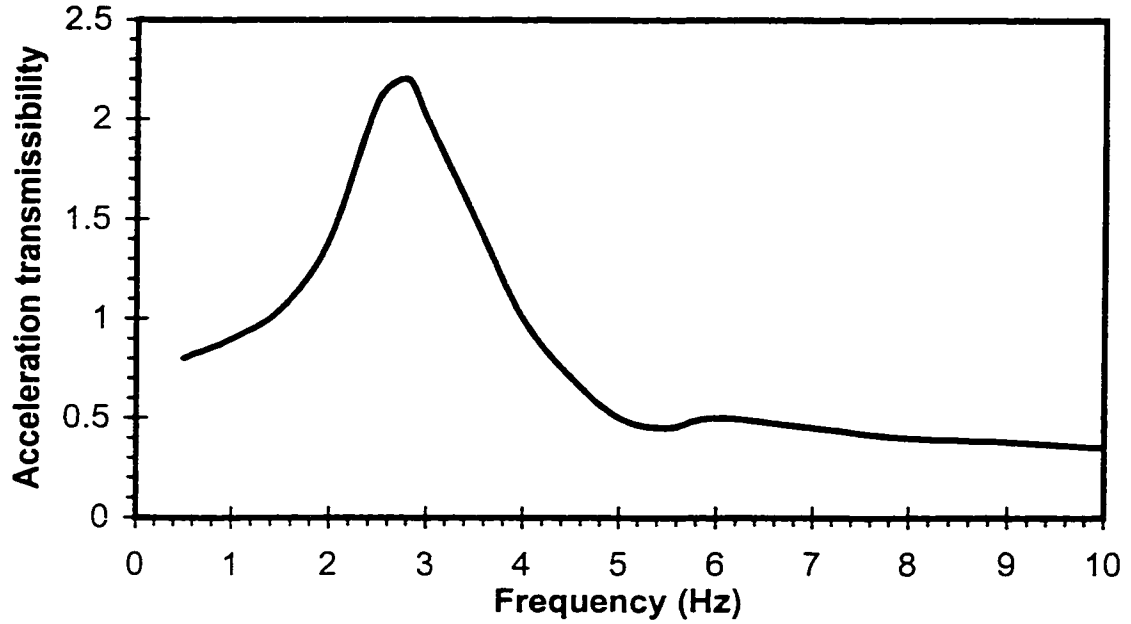

Figure 4.3: Acceleration transmissibility of the coupled human-soft seat system with a subject of 75 kg (excitation: sinusoidal, 0.5 to 10 Hz, 1 m/s² rms acceleration).

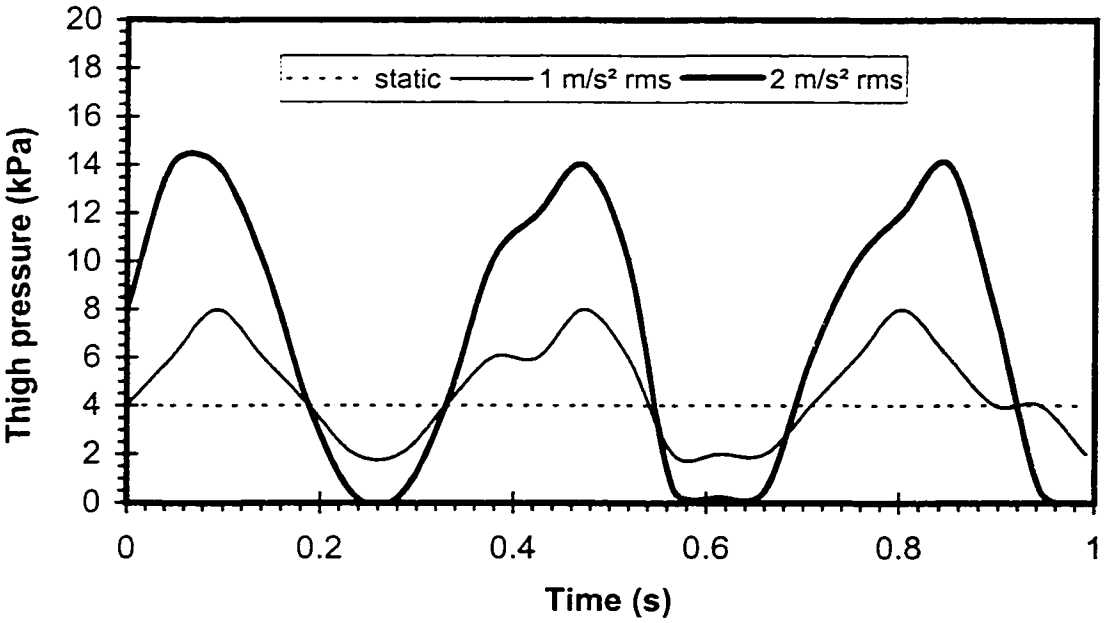

Figure 4.4: Typical time histories of the thigh pressure measured on the soft seat at an excitation frequency of 2.5 Hz (subject D, ENS posture).

seating surfaces. While the rigid seat exhibits almost symmetric variations in the ischium pressure, the soft seat yields considerable asymmetry in the ischium pressure variation with respect to time. The peak ischium pressure on a soft seat tends to increase significantly under compression, and decrease only slightly under rebound. The degree of asymmetry increases with increase in the acceleration excitation. Under 2 ms^{-2} rms acceleration, the peak ischium pressure on a soft seat is 25 kPa in compression and only 8 kPa in rebound, while the corresponding variations for the rigid seat are observed to be approximately ±50 kPa. The asymmetric behavior of the soft seat thus yields mean dynamic pressure considerably larger than the corresponding static pressure.

While the soft seat yields considerably lower ischium pressure than the rigid seat, there appears to be increased pressure under the thighs on a soft seat, as illustrated by the three dimensional maps in Figure 4.1. Furthermore, the contact area and the pressure at the thigh-seat interface are strongly influenced by the magnitude of vertical vibration. Figure 4.4 presents typical time histories of the static and dynamic pressures at a single location within the interface between the thigh and the soft seat under different magnitudes of acceleration excitation, corresponding to an excitation frequency of 2.5 Hz (Subject D, ENS posture). The peak interface pressure approaches considerably high values during compression when the dynamic acceleration excitation magnitude is increased. A loss of contact between the thighs and the seat and thus zero pressure occur during the rebound cycle of vibration, under 2 m/s^2 rms acceleration. While the static thigh pressure remains constant near 4 kPa, the peak dynamic pressure approaches approximately 14 kPa under 2 ms^{-2} rms acceleration excitation. Seats, in general, are designed to yield minimal static contact pressure at the thighs in order to reduce the

loading of the soft tissues, and thus the fatigue and discomfort in blood flow and nerve conductivity that would otherwise occur under high interface pressure [57]. From the results shown in Figure 4.4, it is apparent that such a design practice based upon static pressure alone may be inadequate to achieve dynamic comfort. The high levels of dynamic thigh pressure observed during the compression cycle may cause driver discomfort and numbness. Although the peak ischium and thigh pressures in the vicinity of the resonant frequencies are illustrated in Figures 4.2 and 4.4 for a single subject, an analysis of the measured data obtained for all six subjects revealed identical trends.

4.3.3 Dynamic ischium pressure as a function of excitation frequency

While the vibration acceleration transmitted to the human body is identical to the excitation level at the base of the rigid seat due to its unity transmissibility, the magnitude of vibration transmitted to the subject seated on a soft seat is strongly dependent upon the visco-elastic properties of the seat cushion. The acceleration transmissibility of the coupled human-seat system, measured under sinusoidal excitations swept in the 0.5 to 10 Hz frequency range at a rate of 1 octave/minute has been illustrated in Figure 4.3. The magnitude of sinusoidal excitations was selected to achieve an overall rms acceleration of 1 ms^{-2} rms. The coupled cushion-human system results in considerable amplification of vibration in the 2 - 4 Hz frequency range, and significant vibration attenuation at excitation frequencies above 4 Hz. The fundamental resonant frequency of the coupled system occurs in the vicinity of 2.8 Hz. The magnitude of the transmissibility at resonance is approximately 2.2. The transmissibility characteristics also reveal a weak secondary peak near 6.3 Hz, most likely related to the structural resonance of the seat.

For other subjects, the fundamental resonant frequency and the transmissibility magnitude at resonance may vary due to inter-subject variability, however, the trend in the transmissibility and the frequency range of the vibration amplification remain similar.

The magnitude of acceleration at the interface and thus the dynamic ischium pressure further depend upon the excitation frequency. The dynamic interface pressure data measured on the soft seat were analyzed to study the variations in maximum ischium pressure (IP_{max}), the peak value of the pressure obtained from the time history, for two postures (ENS and EBS), two excitation levels (1 ms^{-2} and 2 ms^{-2} rms acceleration), and different excitation frequencies (1 to 10 Hz). While the data acquired for all the subjects revealed similar trends in IP_{max}, the important observation and trends are discussed here using the data for a single subject (subject D). Figure 4.5 illustrates that the frequency response characteristics of IP_{max} approach its peak value in the vicinity of the resonant frequency of the loaded seat (2.5 - 3 Hz), which can be attributed to the vibration amplification in this frequency range. Since the seat exhibits considerable attenuation of vibration at higher frequencies, IP_{max} varies only slightly at excitation frequencies exceeding 5 Hz, irrespective of the posture and the excitation levels. The results further show that an ENS posture yields considerably higher ischium pressure peaks at frequencies below 5 Hz than those observed with an EBS posture. The peak value of IP_{max} increases considerably with increase in the acceleration excitation for both postures, while the increase is more significant for the ENS posture.

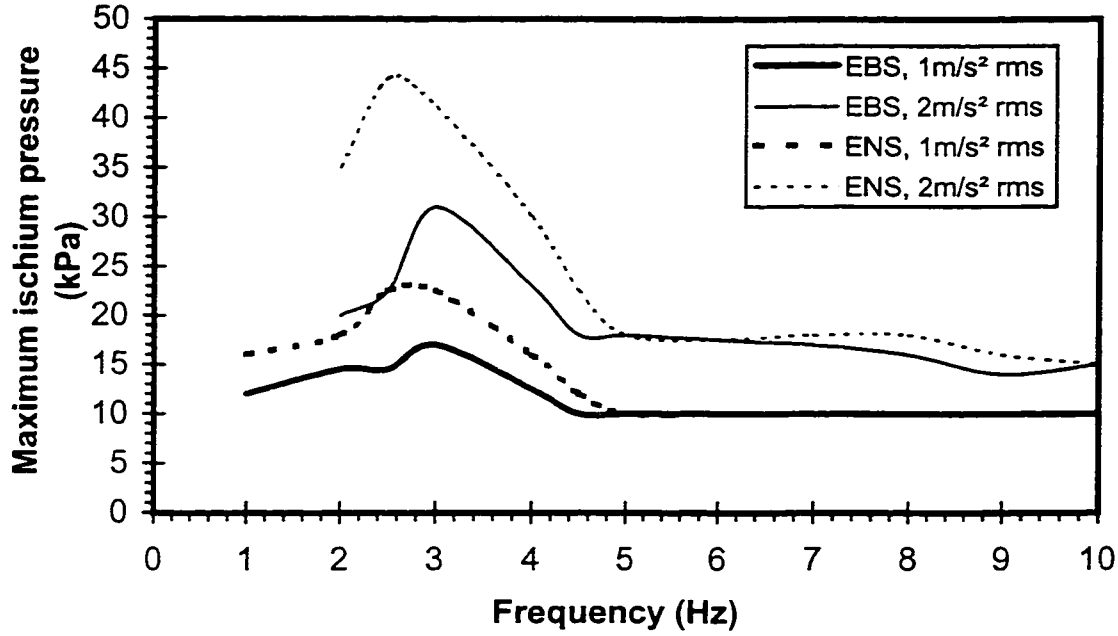

Figure 4.5: Maximum ischium pressure as a function of excitation frequency under different excitation magnitudes with the subject assuming different postures.

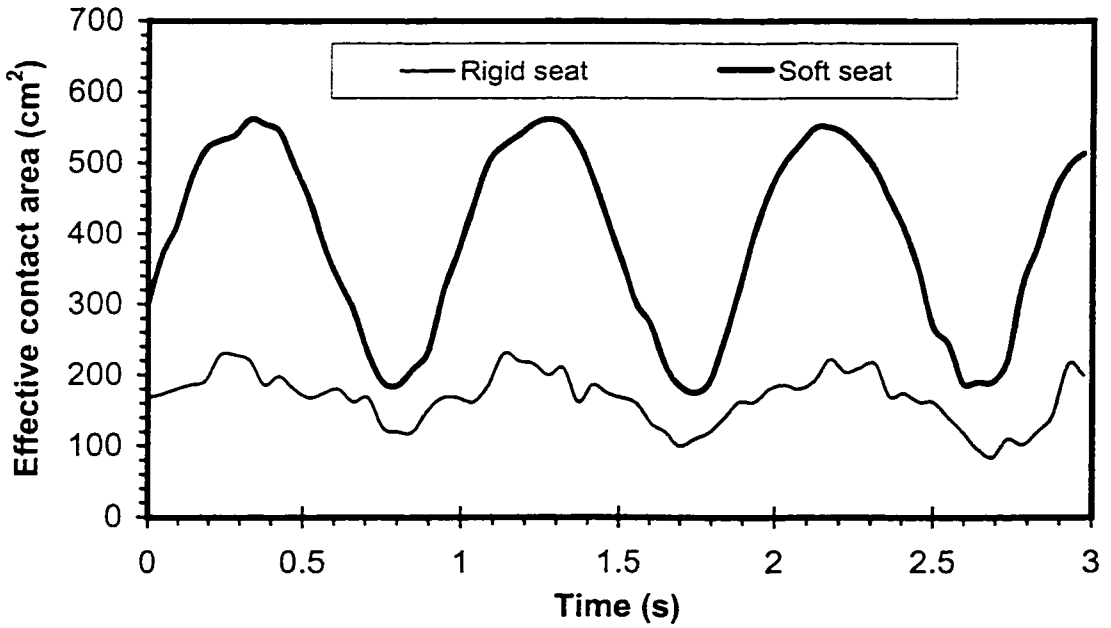

Figure 4.6: Time histories of effective contact area on both rigid and soft seats at an excitation frequency of 1 Hz (subject D, ENS posture).

4.3.4 Analysis of dynamic effective contact area

In view of the strong dependency of maximum ischium pressure (IP_{max}) on the excitation frequency and magnitude, the human-seat interface pressure was further analyzed in terms of effective contact area (ECA) and dynamic contact force. To compare the rigid and soft seat systems, a sinusoidal vibration with a magnitude of 1 ms^{-2} rms and a frequency of 1 Hz was selected, since the vibration transmissibility of the human-soft seat system is also almost unity at 1 Hz. The results show that the ECA and the variations in ECA with respect to time on the soft seat are much larger than those obtained for a rigid seat, as shown in Figure 4.6 (subject D, ENS posture). The ECA of the rigid seat is caused by the deformation of the subject's buttocks tissues alone, while that on a soft seat is caused by the deformations of both the seat and the buttocks, thereby contributing to significantly larger ECA and its variation.

Figure 4.7 further illustrates the ECA time histories on the soft seat at an excitation frequency of 2.5 Hz (subject D, ENS posture). Under dynamic conditions, the ECA varies at the same frequency as that of the excitation and the peak magnitude of ECA increases with vibration excitation magnitude. The variations in ECA are observed to be asymmetric with respect to the static value, which remains nearly constant with time. The ECA during upward or rebound motion tends to be lower than that obtained during downward or compressive motion. Large magnitude excitation may lead to loss of contact between the subject and the seat, thus inducing zero ECA. In contrast, under compression, the ECA tends to increase in a nonlinear manner due to the deformation of both the buttocks tissue and the cushion. Under 2 ms^{-2} rms acceleration, the maximum ECA is more than three times the corresponding static value. The loss of contact between

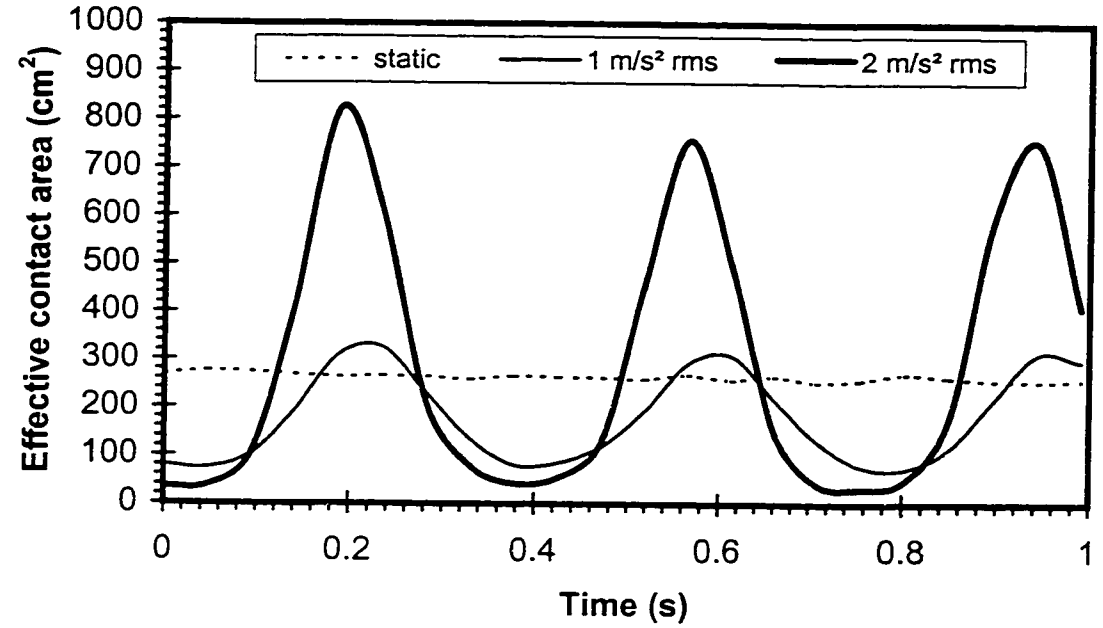

Figure 4.7: Time histories of effective contact area on the soft seat at an excitation frequency of 2.5 Hz measured with subject D under ENS posture.

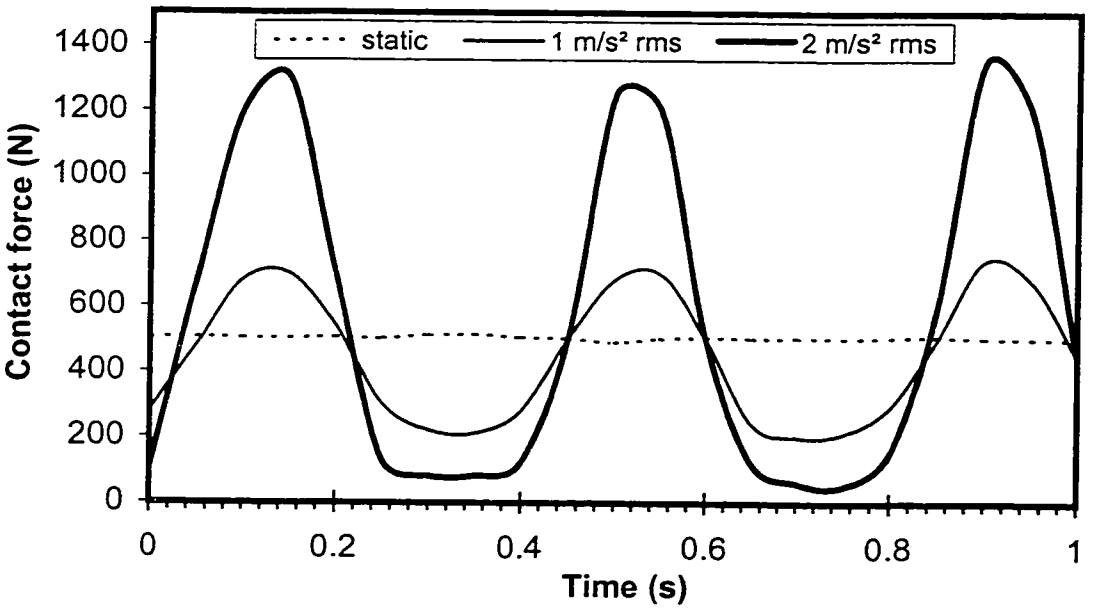

Figure 4.8: Time histories of contact force on the soft seat at an excitation frequency of 2.5 Hz measured with subject D under ENS posture.

cushion and subject begins from the thighs contact region and the areas surrounding the ischial tuberosities. The ischial tuberosities are usually the last part to lose contact with the cushion due to the largest deformation of the seat in this region. In view of the large variations in ECA under dynamic conditions, the assumption of point contact or constant area contact between the seat cushion and human body can be questionable, although such a concept has been widely used in the model development. The nonlinear behavior in ECA of the interface under the influence of vibration necessitates consideration of perhaps a nonlinear seat cushion model to account for such observed behavior.

4.3.5 Analysis of dynamic contact force

It can be expected that the dynamic contact force at the human-seat interface is also a function of the excitation magnitude and frequency, just as is the case for ischium pressure and the effective contact area. At a given excitation frequency, the value of the contact force varies at the same frequency as that of the excitation, and the contact force magnitude increases with an increase in excitation magnitude. Similar to the ischium pressure, shown in Figure 4.2, the dynamic contact force on a rigid seat has been observed to be almost symmetric, with respect to the static contact force, over the range of excitation magnitudes studied. The variation in the contact force on the soft seat, however, is significantly asymmetric, specifically under high levels of vibration transmitted to the human body. This occurs when the excitation magnitude is large and the excitation frequency is close to the resonant frequency of the human-seat system, as observed in Figure 4.8, where the time histories of contact force on the soft seat at 2.5 Hz excitation frequency are illustrated. Under 2 ms^{-2} rms acceleration, the peak dynamic

contact force on a soft seat is approximately 2.5 times the corresponding static contact force, while the minimum contact force approaches close to zero. The pattern is similar to that of the ischium pressure, shown in Figure 4.2.

The high magnitude progressively increasing contact force during compression suggests that the human-cushion system may " bottom out" , under higher magnitudes of excitation. The stiffness of the coupled system increases considerably due to deflection of the buttock tissue and seat cushion. The progressively increasing contact force during compression is also partially caused by a wrapping phenomenon during the pressure measurement, which is shown in Figure 4.9. The flexible sensing mat can only sample pressure perpendicular to the local contact surface, while the measured contact force is just a simple summation of the contact force at various locations. Therefore, the measured contact force is always higher than the vertical load when a human subject sits on a soft cushion. Large deformations of the cushion and the human buttocks causes a higher degree of wrapping, which in turn, will cause a higher error in the contact force measurement. The near zero contact force under rebound with an excitation magnitude of 2 ms^{-2} rms indicates that the seated body has nearly left the seat surface, or body hopping has almost occurred. It has been examined that under small excitation magnitude and/or at excitation frequencies far from the resonance frequency of the human-seat system (*e.g.* above 5 Hz), the contact force is almost symmetric with respect to the static body weight supported by the seat, due to the small deflection at the human-seat interface.

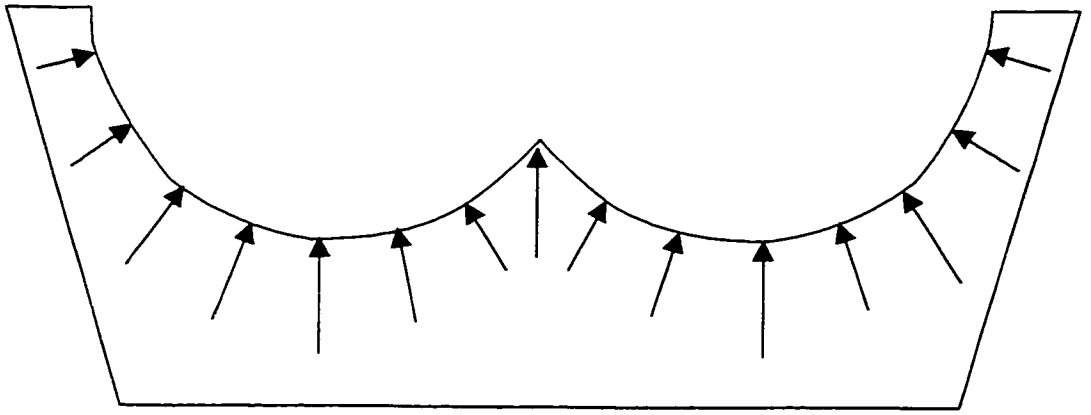

Figure 4.9: Schematic of human-seat interface illustrating the sensing mat measuring pressure perpendicular to the local interfaces.

4.4 Development and Validation of the Seat Cushion Model

The asymmetric characteristics of the contact force under high levels of excitation, shown in Figure 4.8, suggest that the contact stiffness increases progressively when the seat cushion tends to bottom out. The contact stiffness during extension may approach zero when the contact between the body and the cushion is lost or the body hop motion occurs. The nonlinear force-deflection characteristics, however, cannot be attributed solely to the nonlinear properties of polyurethane foam material, which can be measured with an indentor of a fixed area using the procedure outlined in SAE J1051 [79], as shown in Figure 4.10. The nonlinear elastic properties and the contour shape of human buttocks (thus the varying contact area at different deflection) also contribute to the nonlinear force-deflection characteristics. These factors can cause the stiffness at the human-seat interface to vary in a more progressive manner during compression. In this section, a seat cushion model is derived upon considerations of nonlinear contributions due to all the above factors.

The force-deflection properties of a seat cushion have mostly been represented by a linear stiffness element, which may be considered appropriate under small deflections in the vicinity of the static cushion equilibrium position. The force-deflection characteristics of the human-seat interface, in general, require adequate considerations of the nonlinear stiffness and stiffness gradients for different human-seat combinations. A proposed relationship between the contact force and deflection at the human-seat interface is presented in Figure 4.11, which illustrates progressively hardening and softening behaviors in the vicinity of static equilibrium position y_0 corresponding to the seated load F_{c0}. Further hardening characteristics at the onset of bottoming can be

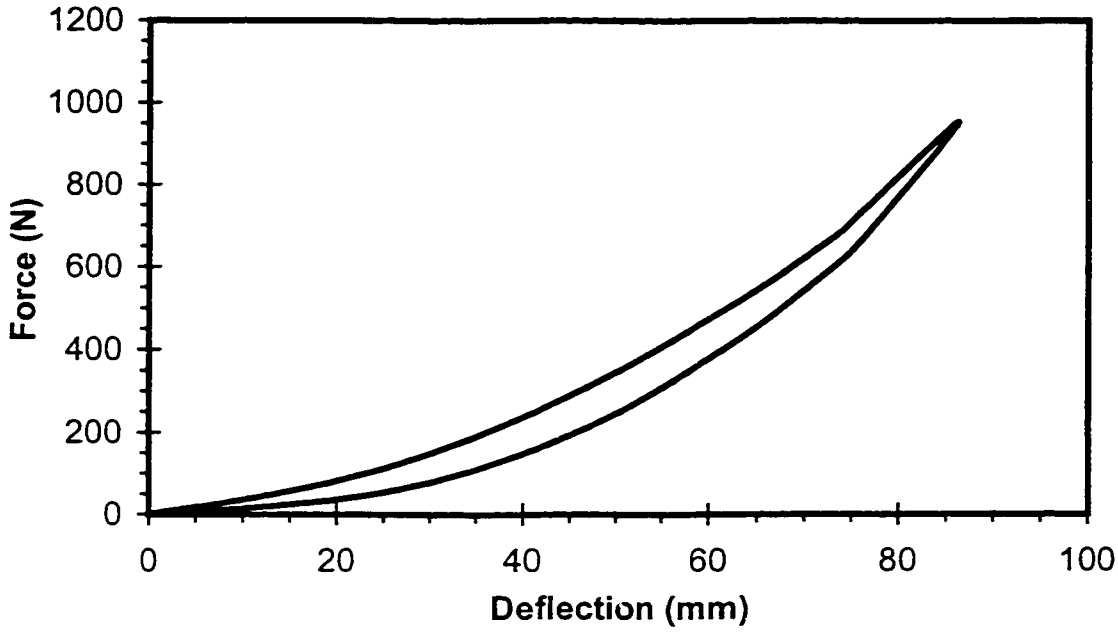

Figure 4.10: The static force-deflection characteristics of the soft seat cushion measured with an indentor.

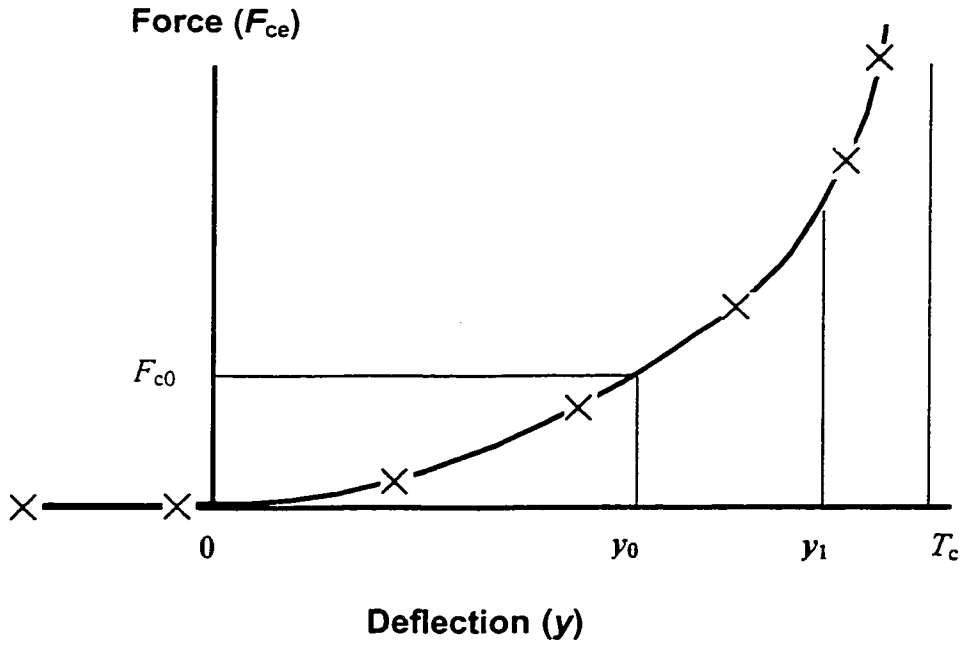

Figure 4.11: Proposed force-deflection characteristics of polyurethane foam seat cushion.

observed, when the deflection exceeds y_1. The proposed force-deflection properties also show that the contact force during extension approaches zero for $y \leq 0$. The proposed force-deflection characteristics can be expressed by the following nonlinear relation:

$$F_{ce} = \begin{cases} F_{c0} + k_{c1} \cdot (y - y_0) + f(y) + k_{c3}(y - y_1)^3 & y_1 \leq y < T_c \\ F_{c0} + k_{c1} \cdot (y - y_0) + f(y) & 0 \leq y < y_1 \\ 0 & y \leq 0 \end{cases} \qquad (4.1)$$

where F_{ce} is the cushion force associated with elastic deflections of the human-seat interface, F_{c0} is the static load on the seat cushion under which the seat cushion undergoes a static deformation of y_0. y is the deflection of the seat cushion with reference to the free thickness of the seat cushion, which should not exceed its free thickness, T_c. A compression of the cushion corresponds to positive value of deformation and a negative deflection of the seat cushion indicates the loss of contact between the human body and the seat. k_{c1} is the linear stiffness coefficient; and k_{c3} is the nonlinear progressively increasing stiffness coefficient of the human-seat system, when cushion bottoming is initiated beyond the deflection threshold of the seat cushion, y_1. The deflection threshold of the seat cushion y_1 should be greater than the cushion deflection at the equilibrium position y_0. $f(y)$ is a nonlinear force function, which mostly relates to the nonlinearity associated with body hop motion. The force function $f(y)$ and the stiffness coefficients are derived from the proposed force-deflection characteristics and the contact force model presented in Equation (4.1).

As the cushion deformation approaches its free surface ($y \approx 0$), both the contact force and its derivative with respect to the deflection must vanish:

$$\begin{cases} F_{ce}\big|_{y=0} = F_{c0} - k_{c1} y_0 + f(0) = 0 \\ \dfrac{dF_{ce}}{dy}\Big|_{y=0} = k_{c1} + \dfrac{df}{dy}\Big|_{y=0} = 0 \end{cases} \tag{4.2}$$

In the vicinity of static equilibrium position ($y=y_0$), the contact force and its derivative equal the static load F_{c0} and linear stiffness coefficient k_{c1}, respectively:

$$\begin{cases} F_{ce}\big|_{y=y_0} = F_{c0} + f(y_0) = F_{c0} \\ \dfrac{dF_{ce}(y)}{dy} = k_{c1} + \dfrac{df}{dy}\Big|_{y=y_0} = k_{c1} \end{cases} \tag{4.3}$$

From Equations (4.2) and (4.3), it can be established that the nonlinear force function $f(y)$ must satisfy the following conditions:

$$f(y) = \begin{cases} k_{c1} y_0 - F_{c0}; & y = 0 \\ 0; & y = y_0 \end{cases} \quad \text{and} \quad \frac{df(y)}{dy} = \begin{cases} -k_{c1}; & y = 0 \\ 0; & y = y_0 \end{cases} \tag{4.4}$$

A function of the following form can be used to satisfy the above condition:

$$f(y) = a_1 \sin(a_2 y + a_3) + a_4 \tag{4.5}$$

where the coefficient a_1, a_2, a_3, and a_4 can be derived from the static load F_{c0}, equilibrium position y_0 and linear stiffness coefficient k_{c1}.

$$\begin{cases} a_1 = \dfrac{k_{c1} y_0 - F_{c0}}{(-1)^n + \sin(a_3)} \\ a_2 = \dfrac{-a_3 + \dfrac{(2n-1)\pi}{2}}{y_0} \\ a_3 = \arcsin[(1 - \dfrac{F_{c0}}{k_{c1} y_0}) \cdot (a_3 + \dfrac{(1-2n)\pi}{2}) \cdot \cos(a_3) + (-1)^{n-1}] \\ a_4 = (-1)^n a_1 \end{cases} \tag{4.6}$$

where n is an integer, $-\infty < n < \infty$. Due to the periodic nature of the sinusoidal function, there exists infinite sets of solutions. When n=0, the above equation can be simplified as:

$$\begin{cases} a_1 = \dfrac{k_{c1} y_0 - F_{c0}}{1 + \sin(a_3)} \\ a_2 = -\dfrac{a_3 + \dfrac{\pi}{2}}{y_0} \\ a_3 = \arcsin[(1 - \dfrac{F_{c0}}{k_{c1} y_0})(a_3 + \dfrac{\pi}{2})\cos(a_3) - 1] \\ a_4 = a_1 \end{cases} \tag{4.7}$$

The elastic force-deflection characteristics of the human-cushion system can thus be described by Equations (4.1), (4.5) and (4.7). The dynamic stiffness properties of the polyurethane foam may further vary as a function of the excitation frequency. The dynamic stiffness, in general, tends to increase with increase in excitation frequency, from an initial value given by the stiffness of the foam matrix alone to an upper limit given by the resistance to deformation of the matrix and the contained air [80]. The dynamic stiffness of the soft cushion, described in Subsection 4.2.2 and measured using an indentor proposed in [79], is illustrated in Figure 4.12, as a function of excitation frequency. It can be observed that the dynamic stiffness tends to increase with an increase in excitation frequency. The increase, however, is relatively low at frequencies below 10 Hz. The stiffness tends to increase more rapidly at higher frequencies. Within the range of resonant frequency of the human-seat system (2.5 to 4.0 Hz), the stiffness of the cushion can be considered to be less sensitive to excitation frequencies. The stiffness characteristics of the cushion are thus considered to be independent of excitation frequency in order to reduce complexities associated with the seat cushion model.

The mechanism of energy dissipation in polyurethane foam is also quite complex. Under dynamic deformations, the energy is dissipated in open-cell foams by a viscous mechanism when air flows through the pores, as well as by the mechanical hysteresis of

the constituent material. At extremely low frequencies the air flow is slow and the viscous damping may be expected to be relatively small. The vibration energy is dissipated mainly by the mechanical hysteresis. As the excitation frequency increases, viscous damping rises due to the increased rate of flow through the pores. However, the viscous resistance increasingly constrains the air within the foam, where it undergoes volume changes in phase with the deformation. Consequently, at higher frequencies the amount of air passing through the pores diminishes and the viscous damping decreases again [80]. The equivalent viscous damping coefficient of the soft seat cushion is presented as a function of excitation frequency in Figure 4.13, as measured with an indentor specified in [79]. The figure illustrates that the equivalent viscous damping coefficient is almost a constant at frequencies above 4 Hz. Although the equivalent viscous damping coefficient at frequencies below 2 Hz is relatively high, this high damping at low frequencies is not expected to affect the vibration transmission of the human-seat system significantly. Since the resonant frequencies of the human-seat cushion system may be expected to lie between 2.5 and 4 Hz in many situations, it may be considered that the equivalent viscous damping coefficient is almost constant, without introducing any large error in the vibration transmission characteristics.

Based on the above discussions, the proposed seat cushion model consists of a parallel nonlinear spring and a linear viscous damper. The force – motion relationship at the human-seat interface of the seat cushion model can then be expressed as:

$$F_c(y) = \begin{cases} F_{c0} + k_{c1} \cdot (y - y_0) + f(y) + k_{c3}(y - y_1)^3 + c \cdot \dot{y}, & y_1 \le y < T_c \\ F_{c0} + k_{c1} \cdot (y - y_0) + f(y) + c \cdot \dot{y}, & 0 \le y < y_1 \\ 0, & y < 0 \end{cases} \tag{4.8}$$

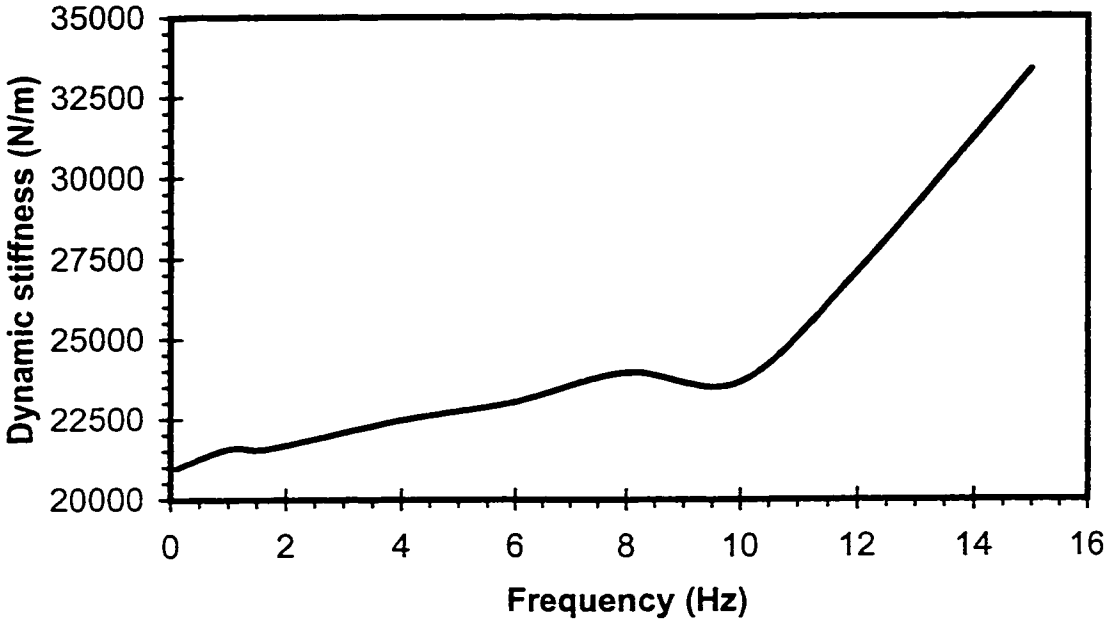

Figure 4.12: Dynamic stiffness of the soft seat cushion as a function of excitation frequency measured with an indentor (preload: 530 N; excitation amplitude: 6.35 mm).

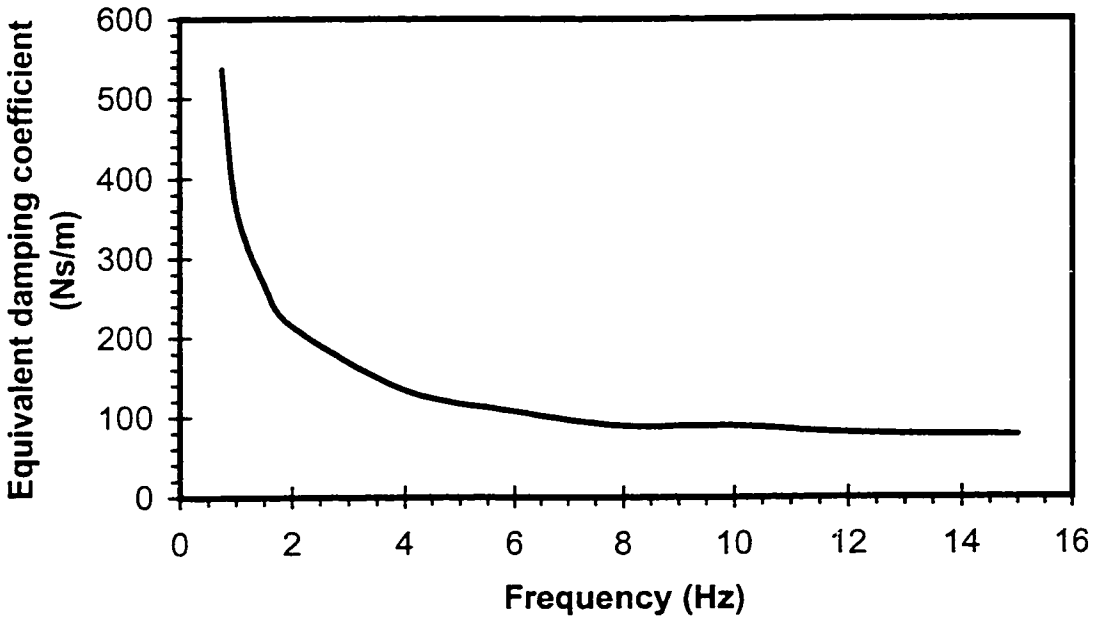

Figure 4.13: Equivalent viscous damping coefficient of the soft seat cushion as a function of frequency measured with an indentor (preload: 530 N; excitation amplitude: 6.35 mm).

where c is equivalent viscous damping coefficient which can be estimated from vibration transmission characteristics of the human-seat system. $\dot{y}$ is the relative velocity due to foam deformation. The mass of the seat cushion is further assumed to be negligible, since the density of polyurethane foam is quite low (in the order of 50 kg/m^3).

The vibration transmission characteristics of a coupled human-seat model were evaluated to examine the validity of the proposed seat cushion model. The coupled model is derived upon integrating the human body model, developed in Chapter 3, to the proposed cushion model, as illustrated in Figure 4.14, where $F_c(y)$ represents the cushion force, defined in Equation (4.8). The differential equations of the coupled human-seat cushion model are derived as:

$$\begin{cases} m_3\ddot{x}_3 = F_3 - m_3 g \\ m_2\ddot{x}_2 = F_2 - m_2 g \\ m_1\ddot{x}_1 = F_1 - F_2 - m_1 g \\ m_0\ddot{x}_0 = F_c(y) - F_1 - F_3 - m_0 g \end{cases} \tag{4.9}$$

where F_1 and F_3 are vertical forces acting between the masses m_1 and m_0, and the masses m_3 and m_0, respectively, and F_2 is the vertical forces acting between the masses m_1 and m_2, given by:

$$\begin{cases} F_3 = k_3(x_0 - x_3) + c_3(\dot{x}_0 - \dot{x}_3) + m_3 g \\ F_2 = k_2(x_1 - x_2) + c_2(\dot{x}_1 - \dot{x}_2) + m_2 g \\ F_1 = k_1(x_0 - x_1) + c_1(\dot{x}_0 - \dot{x}_1) + (m_1 + m_2) g \end{cases} \tag{4.10}$$

The dynamic deflection of the cushion, is computed from the displacement response of the body interface mass m_0 (x_0) and the excitation displacement (x_s), such that $y = x_s - x_0$. The dynamic force, developed by the cushion, may thus be rewritten as:

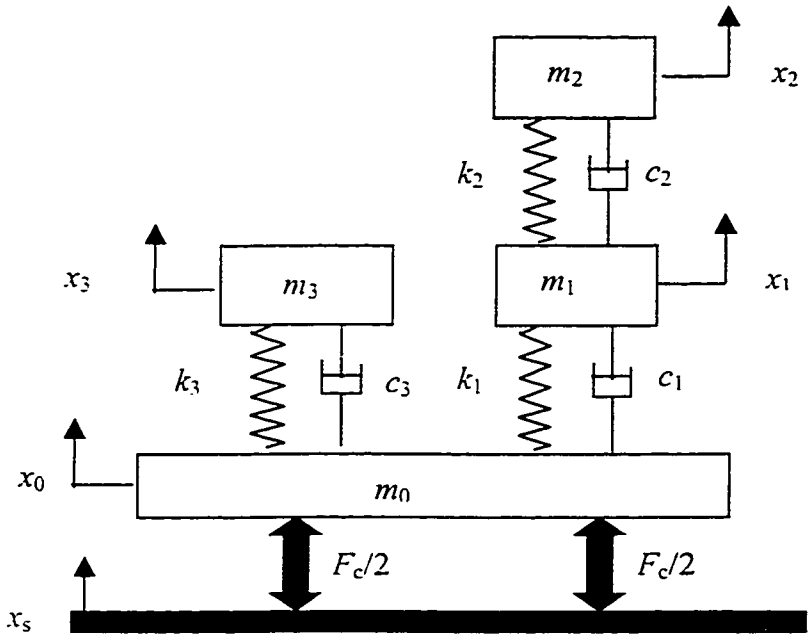

Figure 4.14: Coupled human-seat cushion model.

$$F_c(y)=\begin{cases} F_{c0}+k_{c1}(x_s-x_0-y_0)+f(x_s-x_0)+k_{c3}(x_s-x_0-y_1)^3 \\ \qquad +c(\dot{x}_s-\dot{x}_0), & y_1 \le x_s-x_0 < T_c \\ F_{c0}+k_{c1}(x_s-x_0-y_0)+f(x_s-x_0)+c(\dot{x}_s-\dot{x}_0), & 0 \le x_s-x_0 < y_1 \\ 0, & x_s-x_0 < 0 \end{cases} \tag{4.11}$$

where

$$f(x_s-x_0)=a_1\sin(a_2(x_s-x_0)+a_3)+a_4 \tag{4.12}$$

The parameters of the seat cushion model used in the simulation are listed in Table 4.2, while those for the human body model are presented in Section 3.6. The static load F_{c0} is the total mass in the human body model defined in Chapter 3. The linear stiffness coefficient k_{c1} and the static deformation y_0 under the static load were determined from the measured force-deflection characteristics of a seat cushion. The nonlinear stiffness k_{c3} and deflection threshold of bottoming y_1 were estimated from the force-deflection characteristics shown in Figure 4.10. The viscous damping coefficient c was estimated

Table 4.2: Parameters of seat cushion model.

Static load, F_{c0} (N):	527
Static deformation, y_0 (m):	0.047
Linear stiffness coefficient, k_{c1} (N/m):	2.25×10^4
Nonlinear stiffness, k_{c3} (N/m^3):	3×10^8
Deformation threshold of cushion bottoming, y_1 (m):	0.065
Free thickness of the seat cushion, T_c (m):	0.114
Viscous damping coefficient, c (Ns/m):	200
Coefficient a_1 (N)	1.4111×10^3
Coefficient a_2 (m^{-1})	-76.648
Coefficient a_3	0.3454
Coefficient a_4 (N)	1.4111×10^3

from Figure 4.13. The four parameters in the nonlinear force function $f(y)$, expressed in Equation (4.12), can be computed from static load F_{c0}, linear stiffness coefficient k_{c1} and the static deformation y_0 using Equation (4.7).

The differential equations of the coupled human-seat model were solved using the MATLAB software package. The time histories of cushion deflection, contact force and body acceleration are derived at an excitation frequency of 2.5 Hz under different excitation magnitudes, and illustrated in Figures 4.15 to 4.17, respectively. Under low excitation amplitude (1 m/s^2 rms), the dynamic cushion deflection, contact force and body acceleration are almost symmetric with respect to their static values. The symmetric response behavior is attributed to nearly linear stiffness characteristics in the vicinity of the static deformation ($y_0 = 47$ mm). An increase in the excitation amplitude to 2 m/s^2 rms causes the dynamic deformation to vary within a wider range, which results in a higher degree of asymmetry in the contact force and body acceleration. The variation in rebound deflection tends to be larger than that in compression deflection with respect to the static equilibrium position due to the progressively nonlinear cushion stiffness. The variation in contact force during rebound is thus observed to be lower than that during cushion compression. The trend is very comparable with the experimental data presented in Figure 4.8. The corresponding magnitudes of contact force, however, differ slightly. The greatest difference between measured and computed values of peak contact forces occurs during compression under an excitation of 2 m/s^2 rms acceleration. The peak measured force was obtained near 1450 N, while the proposed model revealed a peak force of approximately 1200 N. This discrepancy may be partly explained by the wrapping phenomenon during the pressure measurement, as shown in Figure 4.9. This wrapping

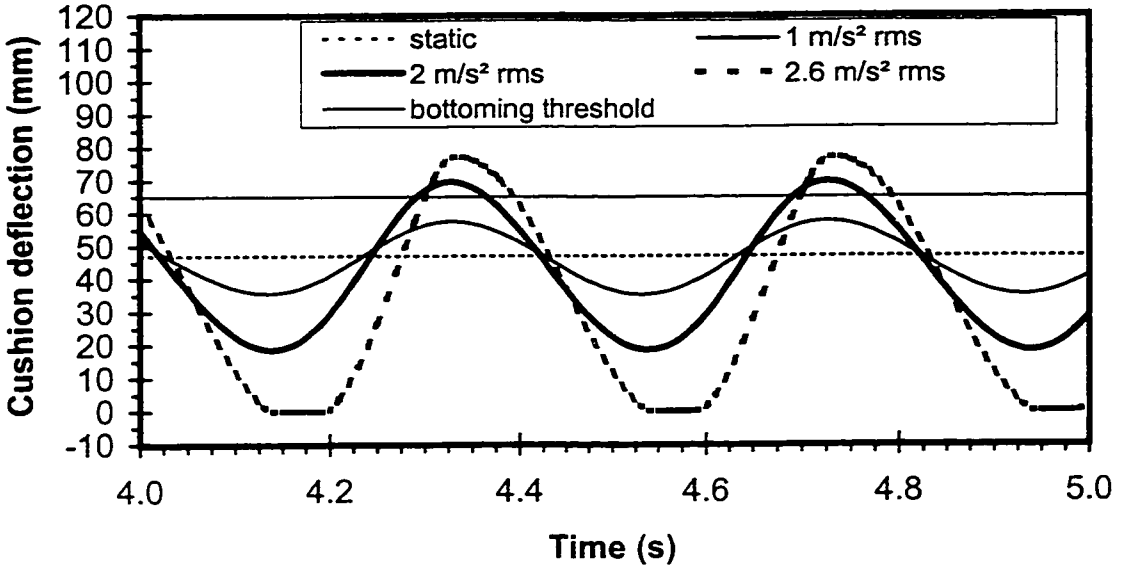

Figure 4.15: Computed time histories of cushion deflection under different excitation magnitudes at an excitation frequency of 2.5 Hz.

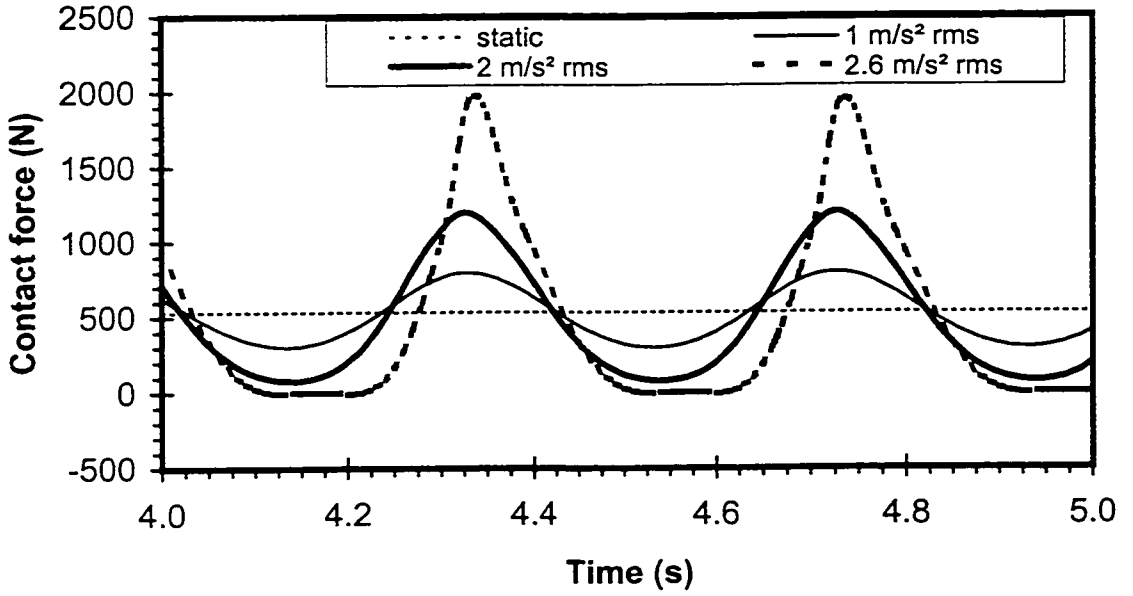

Figure 4.16: Computed time histories of contact force under different excitation magnitudes at an excitation frequency of 2.5 Hz.

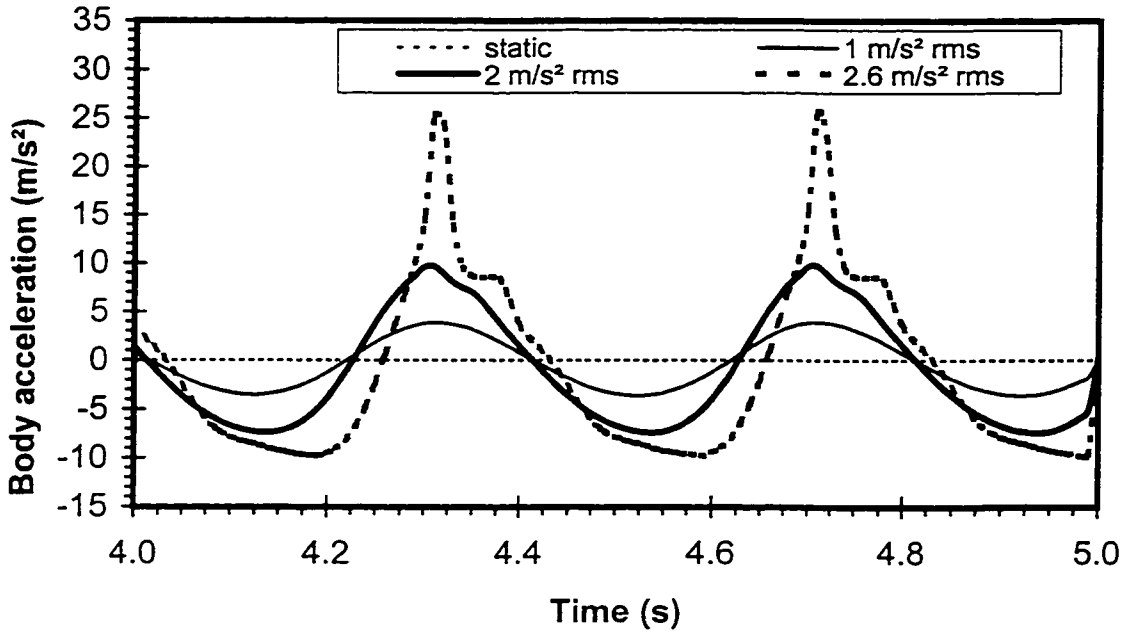

Figure 4.17: Computed time histories of body acceleration under different excitation magnitudes at an excitation frequency of 2.5 Hz.

phenomenon causes the measured contact force to be always higher than the vertical load due to a seated subject. The discrepancy between the measured and computed contact forces may be further attributed to the differences associated with the biodynamic characteristics of the individual human subject involved in the measurements and the human body model, which is based on the mean biodynamic data of a group of subjects. Upon recognizing the contributions due to above two factors, it can be concluded that the proposed seat cushion model, resulting in the curves shown in Figure 4.14, provides reasonably good prediction of the measured contact force presented in Figure 4.8.

A further increase in the excitation amplitude to 2.6 m/s^2 rms results in loss of body-seat contact and cushion bottoming, as shown in the figures. During rebound motion, the cushion deflection and contact force thus approach zero, and the body acceleration approaches a value of -1 *g*. During compression motion, both the contact force and body acceleration reach high values, while the increase in cushion deflection is limited, due to the occurrence of cushion bottoming. The acceleration level transmitted to the body can be as high as 2.5 *g*. Although body hop motion and cushion bottoming may not occur frequently during passenger car driving, they might occur more frequently during off-road vehicle operation. Large magnitude and low frequency vibration of off-road vehicle are more susceptible to cause high magnitude of impacts at the base of the seat cushion, leading to possible body hop and cushion bottoming.

The proposed seat cushion model is further verified by comparing the measured and computed acceleration transmissibility characteristics of the human-seat system. The acceleration transmissibility is derived as the ratio of acceleration response at the human-seat interface to that at the seat base. The acceleration transmissibility characteristics

derived from the measurements performed in the laboratory using a 75 kg subject under 1 m/s^2 rms acceleration excitation have been presented in Figure 4.3. The acceleration transmissibility response of the model, derived under same excitation magnitude, is compared with the measured data, as shown in Figure 4.18. Both the measured and computed transmissibility characteristics reveal almost identical resonant frequency around 2.8 Hz. While the analytical model response correlates well with the measured data at frequencies below 2.5 Hz, discrepancies are observed in the vicinity of the resonant frequency. The acceleration transmissibility response of the model is higher than transmissibility. This discrepancy may arise from that the human body model was developed on the basis of the mean biodynamic data of a group of subjects, and the measured transmissibility was obtained with a single subject of somewhat different mass (75 kg). It may also be partly attributed to errors in estimation of damping coefficient using an indentor. In view of the similar trends and comparable magnitude response, the model may be considered acceptable for predicting the dynamic characteristics of the human-seat cushion system.

4.5 Summary

The pressure distribution at the human-seat interface of both rigid and soft seats was measured using a flexible pressure sensing mat, under sinusoidal vibration of different magnitudes and frequencies. The three dimensional maps of static pressure distribution, the time histories of the ischium pressure and the effective contact area on the soft seat were compared with those measured on a rigid seat. The effects of magnitude and frequency of vibration on the pressure distribution on the soft seat were

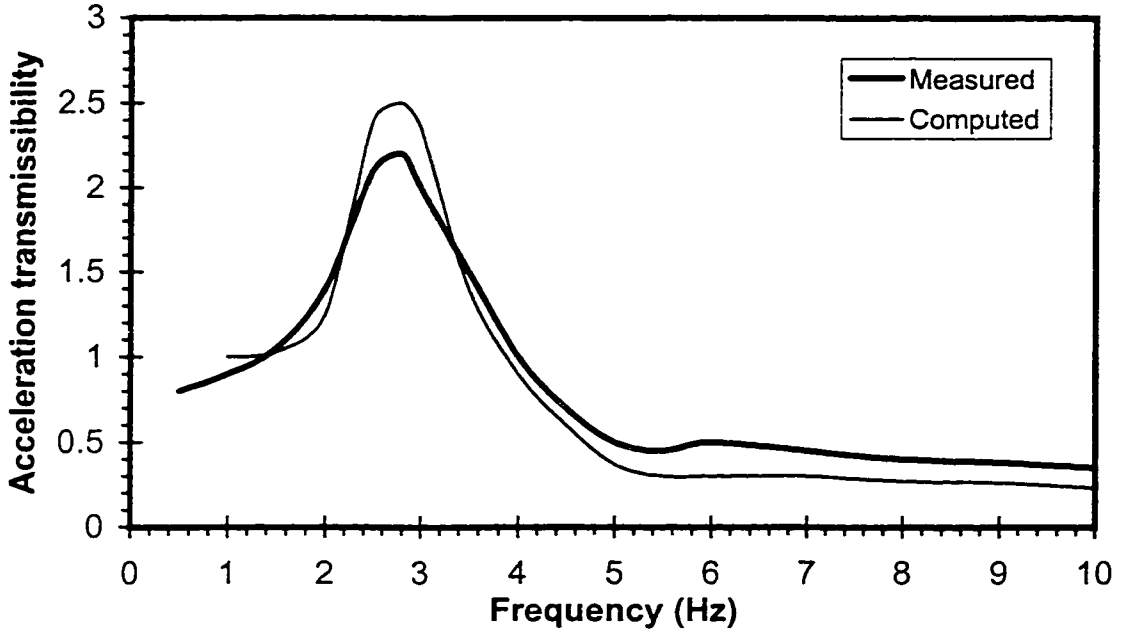

Figure 4.18: Comparison of the computed and tested human-seat system transmissibility.

investigated in terms of ischium pressure, effective contact area and contact force. The study revealed that the interface pressure on the soft seat is more evenly distributed over a larger effective contact area than on the rigid seat. Maximum pressure on a soft seat is reduced significantly compared with that on a rigid seat. Under vibration excitations, the maximum variations in the ischium pressure and the effective contact area on a soft seat are attained around the resonant frequency of the human-seat system. An increase in excitation magnitude results in higher maximum ischium pressure and maximum effective contact area around the resonant frequency of the human-seat system. The time histories of dynamic ischium pressure, effective contact area and contact force on the rigid seats are almost symmetric with respect to their static values within the range of excitation magnitudes and frequencies considered.

Based on the interface pressure measurements, a nonlinear seat cushion model was developed to account for the body hop motion and cushion bottoming, occurring under large magnitudes of vibration excitation. Although the proposed model behaves like a conventional linear element when the dynamic deflection is in the vicinity of the static equilibrium position, it demonstrates progressively hardening/softening behavior over a wider range of deflections to account for the body hop and cushion bottoming phenomena. Computed results of contact force, cushion deflection and body acceleration under different excitation magnitudes clearly demonstrate the occurrence of body hop and cushion bottoming, as well as the near linear behavior of the cushion under low excitation magnitudes. The response characteristics of proposed model, derived in terms of contact force and acceleration transmissibility characteristics, revealed reasonably good agreement with the experimental data.

CHAPTER 5

MODEL DEVELOPMENT OF HUMAN-SUSPENSION SEAT SYSTEM

5.1 Introduction

Suspension seats are employed in various vehicles in the industrial, agricultural, forestry, construction and transportation sectors to isolate the whole body vibration transmitted to the operator. For maximum vibration isolation, it has been established that the resonant frequency of the human-suspension seat system should be well below the dominant frequency of vehicle vibration and that the suspension damping ratio should be kept to be low for the suspension to provide greatest attenuation at higher vibration frequencies. The requirements for suspension design parameters have been reflected in current International Standards [32, 33, 81], describing laboratory seat testing methodology applicable to off-road machinery, agricultural tractors and general purpose seats. According to these standards, the dynamic performance of suspension seats are evaluated according to two different tests. The first test determines the maximum vibration response of the seat at a frequency close to the resonance frequency of the loaded suspension seat, with specified standard inert masses being used in place of the human subject. The second test measures the ratio of frequency-weighted rms acceleration at the seat cushion-human subject interface to the weighted rms acceleration at the seat base, referred to as SEAT value (Seat Effective Amplitude Transmissibility), where human subjects are used to define the SEAT ratio. The input motions used for this test are defined as standardised narrow-band random input spectra characterising the vehicle vibration environment in which the seat is to be used. The use of an idealised narrow-band random input spectrum in the standard tests generates low crest factors compared to the situations in vehicles. The stiffness and the

damping for the seat suspension may therefore be required to assume low values in order to maximise the isolation of the idealised spectra in the first test without the transmissibility at resonance exceeding the acceptance level given in the second test. A suspension design with soft spring and light damping yields high magnitudes of dynamic deflection of the suspension, when exposed to shocks, or low frequency vibration of high magnitude. A large deflection may cause the suspension to reach the limits of its travel and thus impacts against relatively stiff motion limits. Majority of suspension seats use rubber buffers at the extremities of the clearance provided by the suspensions to minimize the severity of these impacts. Obviously, the laboratory tests defined in current standards, only partially reflect the real operating conditions of seats and therefore do not fully predict the performance of seats when in real use. In order to achieve a reasonable compromise between steady-state vibration attenuation and end-stop impacts prevention, careful consideration must be given to the selection of the spring rate and damping of the suspension. Furthermore, end-stop buffer properties need to be optimised to minimize the severity of end-stop impacts, which has seldom been investigated previously.

In earlier studies, vertical suspension seats have often been characterized by a two degree-of-freedom dynamic system, in which the seat cushion, suspension spring and suspension damper have been simplified as linear elements, and end-stop buffer properties have seldom been considered. Analytical models incorporating nonlinearities due to shock absorber damping, Coulomb friction force and elastic limit stops have been proposed in some other studies [5, 8, 69]. These models were developed mainly to investigate the attenuation performance of suspension seats under steady state vibration excitations. In such studies, although an attempt was made to extrapolate its use to shock

type excitation in [8], the damper was either considered as an element of constant velocity squared damping force, or with a variable damping coefficient incorporating bleed and blow-off stages. Most suspension dampers provide asymmetric forces in compression and rebound, which may cause variations in suspension sprung mass mid-ride position under excitations of different magnitudes. Such variations in the mid-ride position can usually induce more frequently and more severe end-stop impacts. Furthermore, the representation of elastic limit stops as springs of linear stiffness may be considered applicable only when the end-stop buffers are subject to small deformation and when only occasional impacts are involved. When the vibration causes large deflection of the end-stop buffers and/or repeated impacts, the linear approximation may result in large errors, since the resulting vibration dose value due to end-stop impacts would account for most of the total vibration dose value. Furthermore, the force-deflection characteristics of conventional rubber buffers show progressively hardening nonlinear stiffness and hysteresis, as shown in Figure 5.1. In a human-suspension seat model developed to investigate specifically end-stop impacts, Wu and Griffin [69] simplified this progressively hardening spring with dual-linear stiffness characteristics: the lower stiffness corresponding to shorter buffer deformation and the higher stiffness corresponding to larger deformation. The hysteresis was modelled assuming linear viscous damping. Although the non-linear elastic and damping properties were taken into consideration, the model did not account for the material damping which is related to the deflection of the buffer instead of the velocity of the deformation as viscous damping. Some suspension seats employ only bottom compression buffers, while the upper displacement limit is either limited by the extension limit of the damper, or by a rigid end-stop.

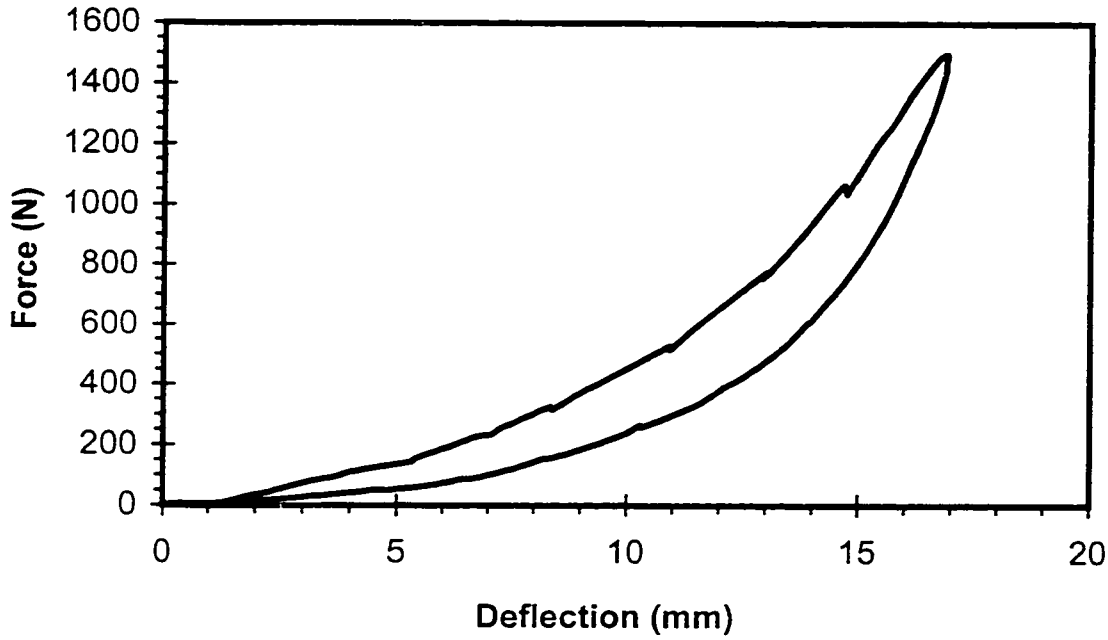

Figure 5.1: Force-deflection characteristics of a typical end-stop buffer.

In the model, therefore, the top and bottom buffers should be proposed to have different properties, in order to investigate the influence of these properties on suspension seat performance.

In this chapter, a non-linear human-suspension seat model is proposed and validated. The model incorporates the nonlinear cushion model developed in Chapter 4 and the human body model developed in Chapter 3, along with asymmetric damping characteristics, nonlinear end-stop buffer properties and Coulomb friction. The suspension seat model is first validated by comparing the computed results by using a mass in place of human model with those obtained in laboratory measurements by loading the seat with a rigid mass. The coupled human-suspension seat model is further validated by comparing the computed results, with those obtained in laboratory measurements using a human subject.

5.2 Modeling Human-Suspension Seat System

Development of an analytical suspension seat model necessitates adequate consideration of the realistic static and dynamic characteristics of the basic components including the cushion, the suspension spring, the shock absorber, the friction and the bump-stops. Dynamic characteristics of the human driver also need to be considered in order to formulate an effective driver-suspension seat model. The proposed vertical human-suspension seat system is characterized by a five degrees-of-freedom nonlinear mechanical model as shown in Figure 5.2, where m_s represents the mass due to suspension; and F_s, F_f, F_d and F_b are the suspension forces due to suspension spring, Coulomb friction, damper and end-stop buffer, respectively. The damper is mounted at an

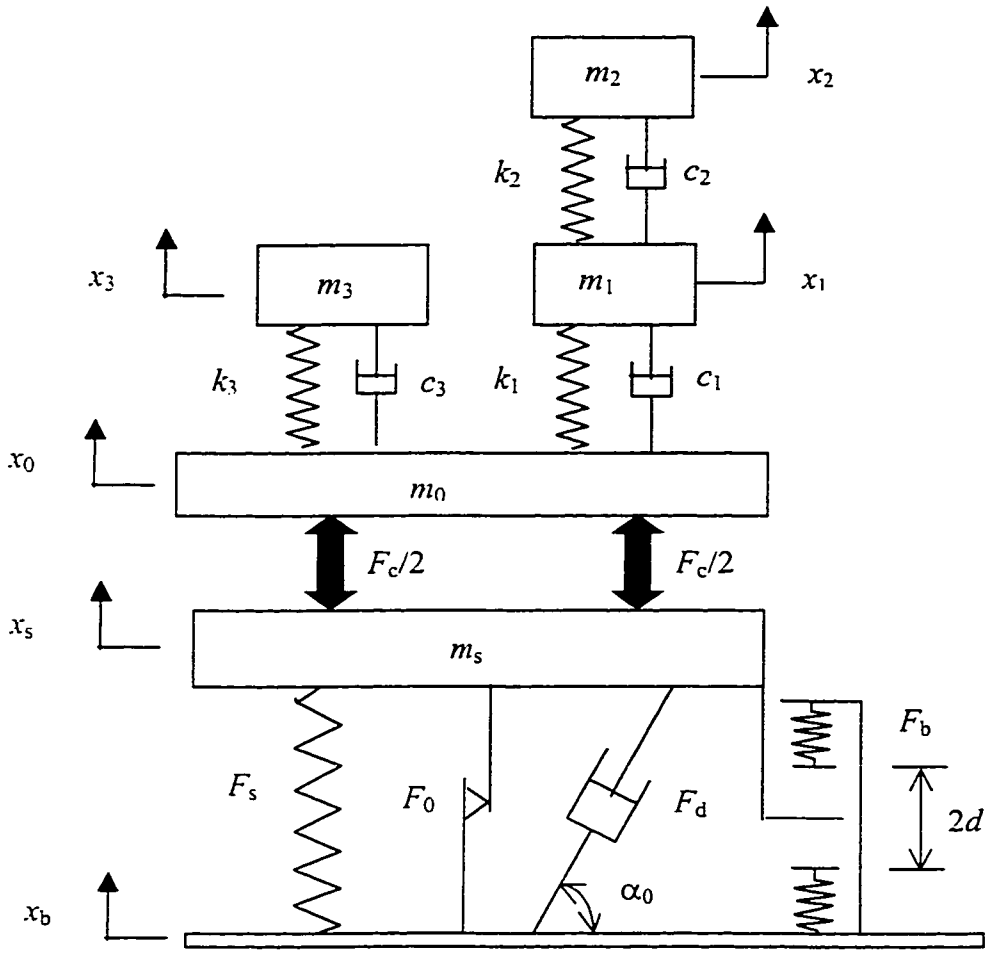

Figure 5.2: Combined human-suspension seat model.

inclination angle α_0. The total suspension free travel is expressed as $2d$, which is the clearance between the top (rebound) and bottom (compression) end-stop buffers. The displacement excitation at the base of the suspension is expressed as x_b, while the displacement response of the suspension mass is expressed as x_s. Various suspension elements are modeled in the following subsections and the simplifying assumptions associated with the model are:

i) The masses due to suspension and driver models are constrained to move along the vertical direction only;

ii) Coulomb friction due to shock absorber seals, various sliding surfaces, and linkage joints is assumed to possess ideal characteristics;

iii) The resilient means of the suspension system is modeled as a vertical spring with linear stiffness coefficient;

iv) The shock absorber is modeled as a nonlinear damper with asymmetric characteristics in rebound and compression incorporating bleed and blow-off stages;

v) End-stop buffers are modeled as progressively hardening springs with variable hysteresis;

vi) The human body is modeled as a three degrees-of-freedom system, as proposed in Chapter 3;

vii) The seat cushion is modeled as a nonlinear elastic element with linear viscous damping coefficient, as defined in Chapter 4.

5.2.1 Modeling asymmetric damper properties

A typical hydraulic damper involves operations at different velocities ranging from very low to very high. For low piston velocity, the fluid flows through the bleed orifices to yield high damping and thus to improve control of resonant vibrations. The flow modulation, using blow-off or pressure control valves, at higher piston velocity leads to low damping and thus to improved vibration isolation and ride quality at higher excitation frequencies. Furthermore, dampers are usually designed to provide a considerably larger damping force during rebound than that developed during the compression stroke. Typical force-velocity characteristics of a hydraulic damper are illustrated in Figure 5.3 [82]. The damping force developed by the suspension seat damper is thus modeled considering the multi-phase and asymmetric damping characteristics. From Figure 5.3, the damper force F_d can be expressed as:

$$F_d = \begin{cases} c_1 v; & \text{for } 0 \le v \le v_1 \\ c_1 v_1 + c_2 (v - v_1); & \text{for } v > v_1 \\ c_3 v; & \text{for } v_2 \le v < 0 \\ c_3 v_2 + c_4 (v - v_2); & \text{for } v < v_2 \end{cases} \tag{5.1}$$

where v is the relative velocity across the damper along its axis, c_1 and c_3 are high damping coefficients at low piston velocity in compression and rebound, respectively, and c_2 and c_4 are low damping coefficients corresponding to high piston velocity in compression and rebound, respectively. The transition from high to low values of damping occurs at preset velocities, v_1 and v_2 in compression and rebound, respectively.

The damping force developed by a hydraulic damper may also be expressed as:

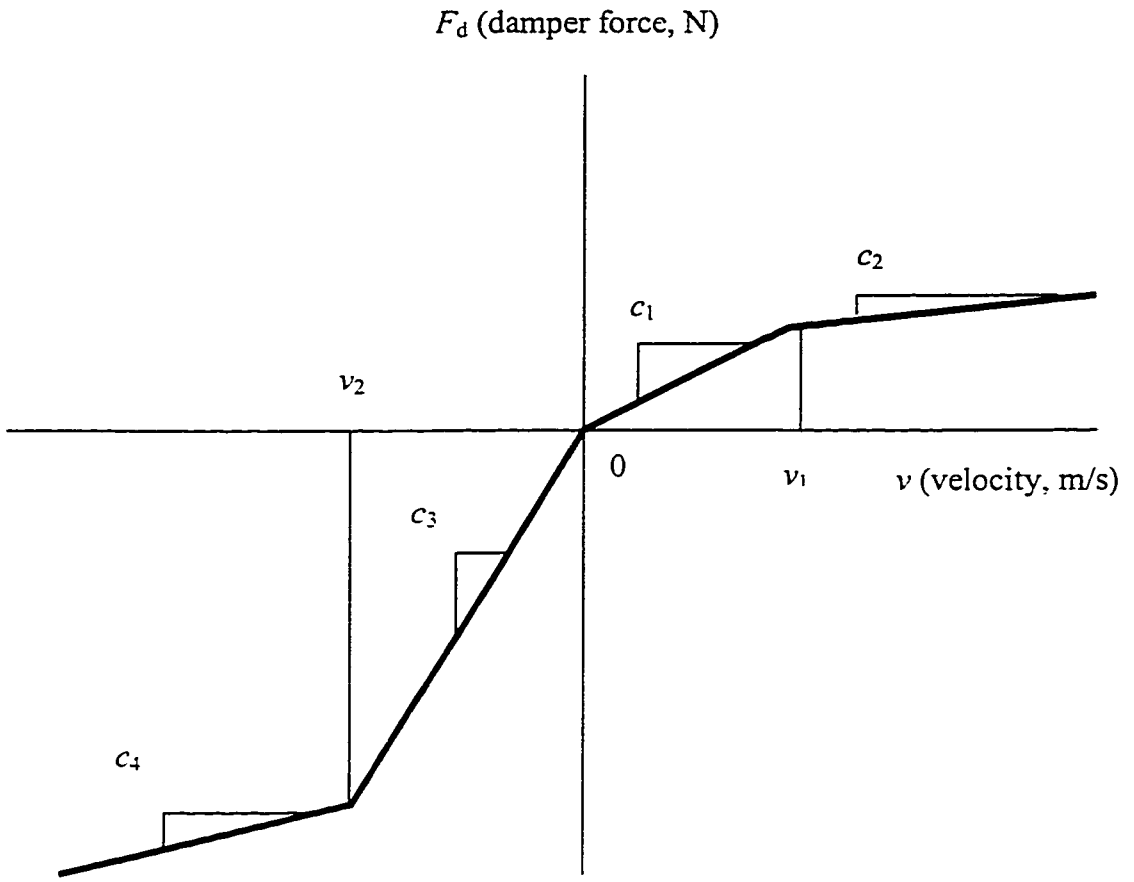

Figure 5.3: Force-velocity characteristics of a typical hydraulic damper.

$$F_d = \begin{cases} c_s v; & \text{for } 0 \le v \le v_1 \\ c_s[v_1 + \gamma_1(v - v_1)]; & \text{for } v > v_1 \\ c_s p v; & \text{for } v_2 \le v < 0 \\ c_s p[v_2 + \gamma_2(v - v_2)]; & \text{for } v < v_2 \end{cases} \tag{5.2}$$

where c_s=c_1, is the low speed compression mode damping coefficient, $\gamma_1 = c_2/c_1$ and $\gamma_2 = c_4/c_3$ are the compression and the rebound damping reduction factors, respectively, and $p = c_3/c_1$ is the asymmetry factor, which describes the ratio of low speed rebound to low speed compression damping.

In various seat suspension linkages, hydraulic dampers are usually installed with inclination angle, α_0. For the commonly used cross-linkage shown in Figure 5.4, the vertical component of damping force developed by the shock absorber is related to the relative velocity of the suspension, $\dot{z}_s = \dot{x}_b - \dot{x}_s$, and its instantaneous angle of inclination, α. The instantaneous inclination angle of the damper is related to the initial inclination angle α_0 at mid-ride position H_0, the instantaneous suspension relative displacement z_s, and the horizontal distance between the attachment points of the damper, B:

$$\alpha = \tan^{-1}[\tan(\alpha_0) - \frac{z_s}{B}] \tag{5.3}$$

The vertical component of damping force developed by the hydraulic damper can thus be expressed as:

$$F_d = \begin{cases} c_s \dot{z}_s \sin^2\alpha; & \text{for } 0 \le \dot{z}_s \sin\alpha \le v_1 \\ c_s[v_1 + \gamma_1(\dot{z}_s \sin\alpha - v_1)]\sin\alpha; & \text{for } \dot{z}_s \sin\alpha > v_1 \\ c_s p \dot{z}_s \sin^2\alpha; & \text{for } v_2 \le \dot{z}_s \sin\alpha < 0 \\ c_s p[v_2 + \gamma_2(\dot{z}_s \sin\alpha - v_2)]\sin\alpha; & \text{for } \dot{z}_s \sin\alpha < v_2 \end{cases} \tag{5.4}$$

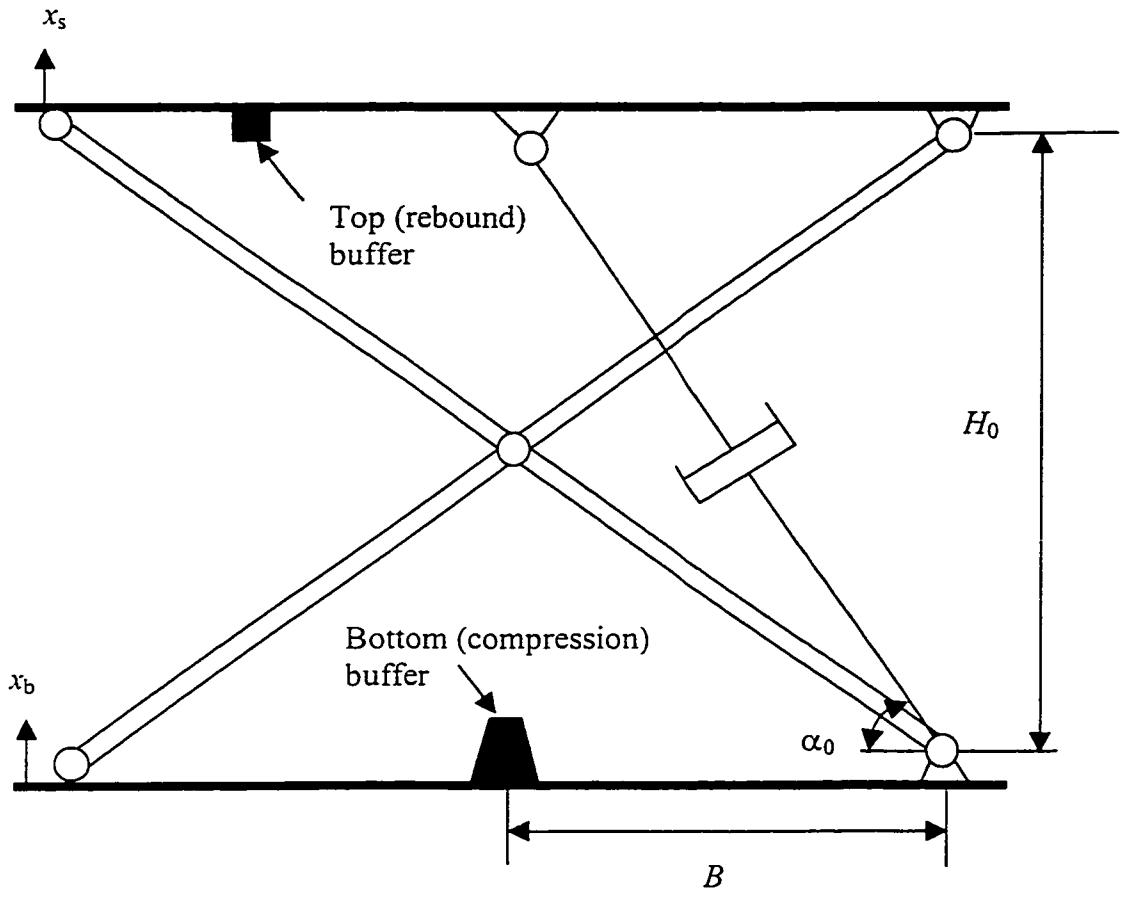

Figure 5.4: Cross linkage mechanism of seat suspension.

The damper force described in Equation (5.4) can also be applied to other linkage mechanisms with some modifications. In a behind-the-seat linkage mechanism, the instantaneous inclination angle α remains constant during the motion.

5.2.2 Modeling of the elastic end stops

Suspension seats are designed with end-stops or rubber buffers to limit the excessive relative motion of soft suspension that may occur under high levels of excitation. Figure 5.4 illustrates the location of compression and extension end-stop buffers. The elastic buffers, invariably, exhibits nonlinear force-deflection characteristics and hysteresis characteristics, similar to those illustrated in Figure 5.1. Such buffers can be modeled as nonlinear clearance springs and the force-deflection characteristics can be presented as shown in Figure 5.5. The force due to an end-stop buffer (F_b) is related to the suspension clearance ($2d$) and relative displacement response of the suspension mass (z_s). The elastic buffers experience deformation beyond the suspension clearance. The effective suspension travel thus includes the maximum deflections. Let $d_m^{(b)}$ and $d_m^{(t)}$ represent the maximum suspension travel in compression and extension, respectively, with respect to the mid-ride position, as shown in Figure 5.5. The differences between the maximum and free travels, $(d_m^{(b)}-d)$, and $(d_m^{(t)}-d)$ thus represent the maximum deformations due to compression and extension buffers, respectively. They also represent the thickness of bottom and top buffers, respectively. The hysteresis due to the buffers yields displacement lags, $h^{(b)}$ and $h^{(t)}$, due to compression (bottom) and extension (top) buffers, given by:

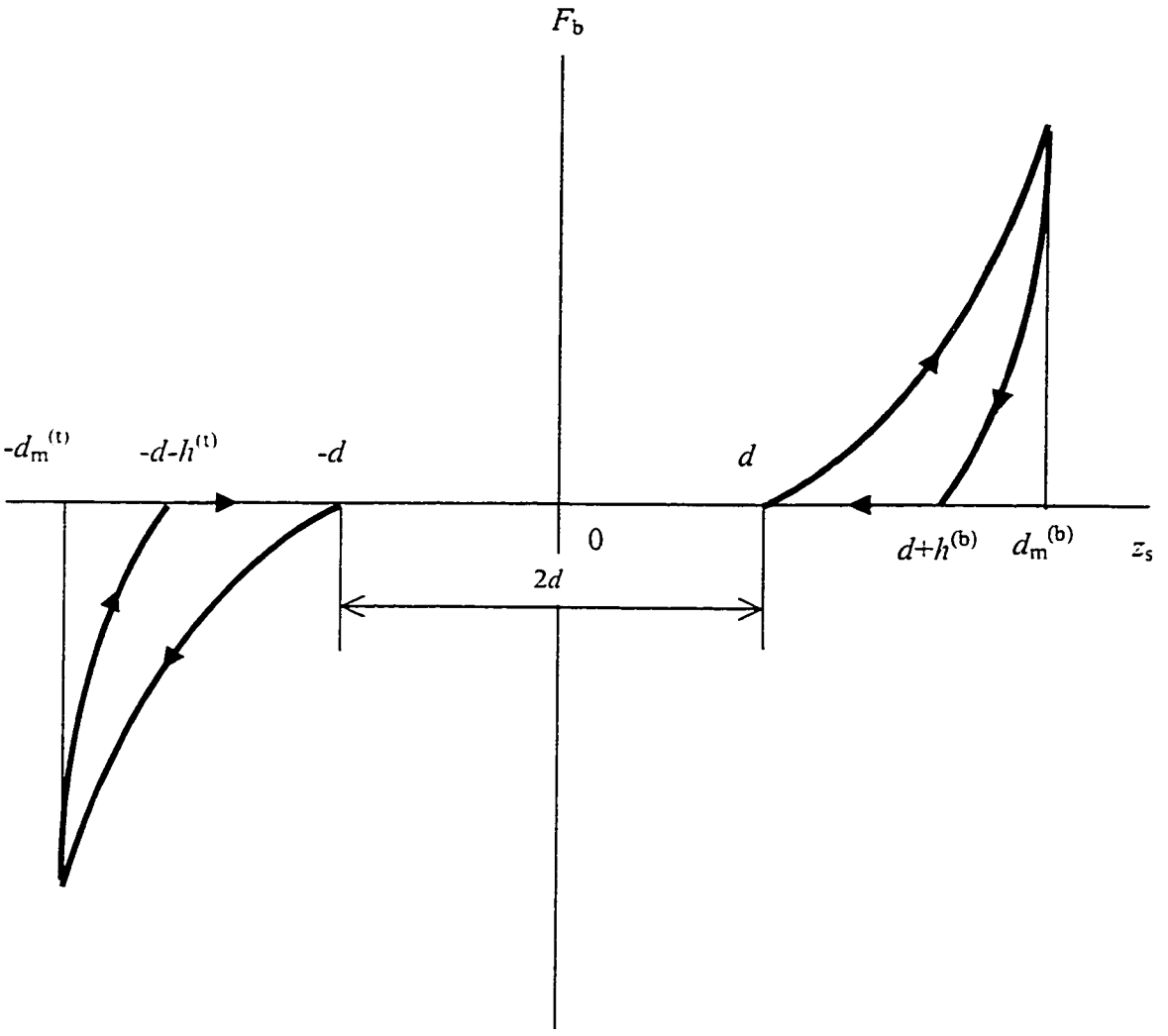

Figure 5.5: Proposed buffer force representation as a function of relative suspension displacement.

$$\begin{cases} 0 \le h^{(b)} \le d_m^{(b)} - d; & \text{for } z_s > 0 \\ 0 \le h^{(t)} \le d_m^{(t)} - d; & \text{for } z_s < 0 \end{cases} \tag{5.5}$$

The progressively hardening properties of the buffers may be expressed as a cubic function of the deformation. The bottom end-stop characteristics during loading and unloading stages are thus expressed as:

$$F_b^{(b)} = \begin{cases} k_{b1}^{(b)}(z_s - d) + k_{b2}^{(b)}(z_s - d)^3; & \text{for } z_s > d \text{ and } \dot{z}_s > 0 \\ k_{b3}^{(b)}[z_s - (d + h^{(b)})] + k_{b4}^{(b)}[z_s - (d + h^{(b)})]^3; & \text{for } z_s > d \text{ and } \dot{z}_s < 0 \end{cases} \tag{5.6}$$

where $k_{b1}{}^{(b)}$ and $k_{b2}{}^{(b)}$ are the linear and cubic stiffness coefficients of the bottom buffer during loading, respectively, and $k_{b3}{}^{(b)}$ and $k_{b4}{}^{(b)}$ are the linear and cubic stiffness coefficients of the bottom buffer during unloading, respectively. $F_b{}^{(b)}$ is the force developed by the bottom buffer due to impacts. Similarly, the force developed by top buffer ($F_b{}^{(t)}$), under an impacts with the top buffer may be expressed as follows:

$$F_b^{(t)} = \begin{cases} k_{b1}^{(t)}(z_s + d) + k_{b2}^{(t)}(z_s + d)^3; & \text{for } z_s < -d \text{ and } \dot{z}_s < 0 \\ k_{b3}^{(t)}[z_s + (d + h^{(t)})] + k_{b4}^{(t)}[z_s + (d + h^{(t)})]^3; & \text{for } z_s < -d \text{ and } \dot{z}_s > 0 \end{cases} \tag{5.7}$$

where $k_{b1}{}^{(t)}$ and $k_{b2}{}^{(t)}$ are the linear and cubic stiffness coefficients of the top buffer during loading, and $k_{b3}{}^{(t)}$ and $k_{b4}{}^{(t)}$ are the corresponding coefficients during unloading, respectively.

The suspension force developed by elastic end-stops, in general, may be expressed as:

$$F_b = \begin{cases} 0; & \text{for } |z_s| \le d \\ F_b^{(b)}; & \text{for } z_s > d \\ F_b^{(t)}; & \text{for } z_s < -d \end{cases} \tag{5.8}$$

The force-deflection characteristics illustrated in Figure 5.5 suggest that the buffer forces during loading and unloading approach identical values corresponding to

maximum deformation, $d_m^{(b)}$ or $d_m^{(t)}$. The force-deflection characteristics, expressed in Equations (5.6) and (5.7), must satisfy the following:

$$\begin{cases} k_{b1}^{(b)}(d_m^{(b)}-d)+k_{b2}^{(b)}(d_m^{(b)}-d)^3 = k_{b3}^{(b)}[d_m^{(b)}-(d+h^{(b)})]+k_{b4}^{(b)}[d_m^{(b)}-(d+h^{(b)})]^3 \\ k_{b1}^{(t)}(d_m^{(t)}+d)+k_{b2}^{(t)}(d_m^{(t)}+d)^3 = k_{b3}^{(t)}[d_m^{(t)}+(d+h^{(t)})]+k_{b4}^{(t)}[d_m^{(t)}+(d+h^{(t)})]^3 \end{cases} \quad (5.9)$$

5.2.3 Seat cushion model

The vertical force developed by the cushion is derived from the nonlinear cushion model developed in Chapter 4. The model incorporates the dynamics associated with body hop motion and the cushion bottoming. The cushion force is derived from Equations (4.11) and (4.12), as a function of relative deflection, $y = x_s - x_0$, and velocity, $\dot{y} = \dot{x}_s - \dot{x}_0$.

5.2.4 Modeling of spring and friction forces

The effective suspension spring rate is affected by the stiffness of spring elements and the suspension linkage. The magnitude of friction force is attributed to shock absorber seals, various sliding contact surfaces and linkage joints. The effective spring rate and hysteresis due to the suspension can be characterized from force-deflection characteristics measured during uploading and downloading. The force-deflection properties, however, must be measured for the suspension adjusted to its mid-ride position under the preload due to the operator. The measurements performed in earlier studies have revealed nearly linear effective spring rate, k_s, of the suspension [13]. The measured data have further been used to determine the magnitude of total friction force,

F_0. Assuming linear spring rate and ideal friction characteristics, the components of suspension and Coulomb friction forces can be expressed as:

$$F_s = \mathrm{k}_s z_s + (\mathrm{m}_0 + \mathrm{m}_1 + \mathrm{m}_2 + \mathrm{m}_3 + \mathrm{m}_s)\mathrm{g} \tag{5.10}$$

$$F_f = F_0 \,\mathrm{sgn}(\dot{z}_s) \tag{5.11}$$

where F_s and F_f are component forces developed by suspension spring and friction, respectively, and the function *sgn*(.) is given by:

$$\mathrm{sgn}(.) = \begin{cases} +1; & if(.) \geq 0 \\ -1; & if(.) < 0 \end{cases} \tag{5.12}$$

5.2.5 Differential equations of motion of the human-suspension seat system model

The differential equations of motion of the total human-suspension seat system can be written as:

$$\begin{cases} m_3\ddot{x}_3 = F_3 - m_3 g \\ m_2\ddot{x}_2 = F_2 - m_2 g \\ m_1\ddot{x}_1 = F_1 - F_2 - m_1 g \\ m_0\ddot{x}_0 = F_c - F_1 - F_3 - m_0 g \\ m_s\ddot{x}_s = F_s + F_f + F_d + F_b - F_c - m_s g \end{cases} \tag{5.13}$$

where F_s, F_f, F_d, and F_b are suspension component forces defined in Equations (5.4) to (5.12), respectively. The cushion force F_c has been presented in Equations (4.11) and (4.12). The forces acting between the masses of human body model, F_1, F_2 and F_3, have been expressed in Equations (4.10).

5.3 Human-Suspension Seat Model Validation

The analytical model of the human-suspension seat system, described in Equations (5.3) to (5.13), is analyzed under deterministic and random vehicle vibration. The response characteristics are compared with those derived from laboratory measurements to examine the validity of the model. The nonlinear model of the suspension seat coupled with a rigid mass is first evaluated and the response characteristics are compared with those measured with a rigid mass. The validity of the nonlinear human-suspension seat model is then examined by comparing its results with those measured using a human subject as the load, whose seated mass was equivalent to that defined by the mass model parameters. Both acceleration transmissibility and power spectral density response characteristics at the cushion interface were measured and analyzed under identical excitation signals.

5.3.1 Determination of model parameters

A suspension seat with behind-the-seat suspension was used for performing the model validation. The parameters of some of the suspension components were taken to be those previously identified from the static and dynamic laboratory measurements and reported in an earlier study [83]. The reported force-deflection and force-velocity characteristics are further analyzed to derive the static deflection y_0, stiffness coefficients k_{c1}, k_{c3} and bottoming threshold deflection of the cushion y_1. The cushion damping coefficient c_c is identified from the measured dynamic characteristics of the cushion. The coefficients a_1, a_2, a_3 and a_4 of the force function $f(y)$ are computed from static load F_{c0}, linear stiffness coefficient k_{c1} and the static deformation, y_0 using Equation (4.7). The

measured force-deflection properties of the suspension system were further analyzed to derive stiffness coefficients of the elastic limit stops in compression and extension, while the damping properties of the shock absorber were estimated from the reported force-velocity characteristics. Various parameters of the suspension seat model are summarized in Table 5.1.

5.3.2 Excitation signals

Sinusoidal excitations and two random type excitations defined in International Standard ISO 7096 [32] were employed for performing the model validation, as used in the respective experiments. Sinusoidal excitation was used to derive the acceleration transmissibility of the human-suspension seat system at discrete frequencies. The harmonic excitation possesses a constant displacement amplitude of 25 mm between 0.5 to 2 Hz, and a constant acceleration amplitude of 3.95 m/s^2 (2.8 m/s^2 rms) between 2 to 10 Hz. The harmonic excitation was initially designed to limit the extremely large displacement requirement of the WBVVS at very low frequencies during the experiments. International Standard ISO 7096 defines Class I for tractor-scrapers without primary suspension or vibration absorber and Class II for tractor-scrapers with either front axle suspension or vibration absorber hitch. The acceleration PSD characteristics of these classes of excitations are given in terms of filter equations:

Class I $$PSD = 5.30(HP_{24})^2(LP_{24})^2 \quad (5.14)$$

Class II $$PSD = 2.72(HP_{24})^2(LP_{24})^2 \quad (5.15)$$

where $(LP)_{24}$ and $(HP)_{24}$ characterize low- and high-pass filters respectively with 24 dB/octave attenuation. The filter transfer functions are given by:

Table 5.1: Parameters for the suspension seat model.

Description		Symbol	Value
Cushion	Static Load (N)	F_{c0}	5.27×10^{2}
	Static deflection (m)	y_0	2.5×10^{-2}
	Linear stiffness (N/m)	k_{c1}	8.23×10^{4}
	Cubic stiffness (N/m^3)	k_{c3}	2.10×10^{8}
	Deflection threshold of bottoming (m)	y_1	3.8×10^{-2}
	Cushion damping (Ns/m)	c_c	300
	Coefficient (N)	a_1	1.1405×10^{3}
	Coefficient (1/m)	a_2	-76.78
	Coefficient	a_3	0.3487
	Coefficient (N)	a_4	1.1405×10^{3}
Damper	Low speed compression damping coefficient (Ns/m)	c_s	8.92×10^{2}
	Compression damping reduction factor	γ_1	0.43
	Rebound damping reduction factor	γ_2	0.53
	Compression transition velocity (m/s)	v_1	1.12×10^{-2}
	Rebound transition velocity (m/s)	v_2	-3.32×10^{-2}
	Asymmetry factor	p	1.47
	Inclination angle (degrees)	α_0	70
End-stop buffers	Total travel between end-stop buffers (m)	$2d$	0.1
	Compression travel limit (m)	$d_m^{(b)}$	0.06
	Rebound travel limit (m)	$d_m^{(t)}$	0.06
	Bottom buffer loading linear stiffness (N/m)	$k_{b1}^{(b)}$	1.2×10^{5}
	Bottom buffer loading cubic stiffness (N/m^3)	$k_{b2}^{(b)}$	1.3×10^{9}
	Bottom buffer unloading linear stiffness (N/m)	$k_{b3}^{(b)}$	1.8×10^{5}
	Bottom buffer unloading cubic stiffness (N/m^3)	$k_{b4}^{(b)}$	2.1×10^{9}
	Bottom buffer hysteresis displacement lag (m)	$h^{(b)}$	2.0×10^{-3}
	Top buffer loading linear stiffness (N/m)	$k_{b1}^{(t)}$	1.0×10^{5}
	Top buffer loading cubic stiffness (N/m^3)	$k_{b2}^{(t)}$	1.5×10^{9}
	Top buffer unloading linear stiffness (N/m)	$k_{b3}^{(t)}$	1.2×10^{5}
	Top buffer unloading cubic stiffness (N/m^3)	$k_{b4}^{(t)}$	3.0×10^{9}
	Top buffer hysteresis displacement lag (m)	$h^{(t)}$	2.0×10^{-3}
Others	Suspension spring stiffness (N/m)	k_s	5.33×10^{3}
	Suspension sprung mass (kg)	m_s	10
	Coulomb friction force (N)	F_0	15

$$(LP)_{24} = \frac{1}{s^4 + 2.6315s^3 + 3.414s^2 + 2.6315s + 1} \tag{5.16}$$

$$(HP)_{24} = \frac{s^4}{s^4 + 2.6315s^3 + 3.414s^2 + 2.6315s + 1} \tag{5.17}$$

where $s = jf/f_c$; f is the excitation frequency and f_c is the cut-off frequency in Hz. The cut-off frequency for the HP_{24} filter is 1.5 Hz for both classes of vehicles, while that for the LP_{24} is 2.5 Hz for Class I and 3.0 Hz for Class II excitation. The peak acceleration PSD of Class I excitation is 4.13 $(ms^{-2})^2$/Hz occurring at a frequency of 1.85 Hz, while the peak acceleration PSD of Class II excitation is 2.4 $(ms^{-2})^2$/Hz occurring at a frequency of 2.1 Hz. Figure 5.6 illustrates the acceleration PSD of Class I and Class II excitations. The rms accelerations corresponding to Class I and Class II excitations are 2.35 and 2.05 m/s^2 rms, respectively.

5.3.3 Validation of the suspension seat model

The suspension seat model and the coupled human-suspension seat model are validated by comparing the computed results with the measured data reported in [8]. The analytical model of the suspension seat is initially validated in conjunction with a rigid mass in place of the human body model. The equations of motion for the model are solved under deterministic and random excitations using the MATLAB software. The acceleration time histories of floor vibration were generated first by passing a white noise signal (with a unity rms value) through a given band-limiting filter applicable to the selected excitation classes. The band-limiting filtered acceleration time histories were then integrated to yield displacement and velocity time histories to be used as excitation signals in the computation. The differential equations of motion were solved in the time

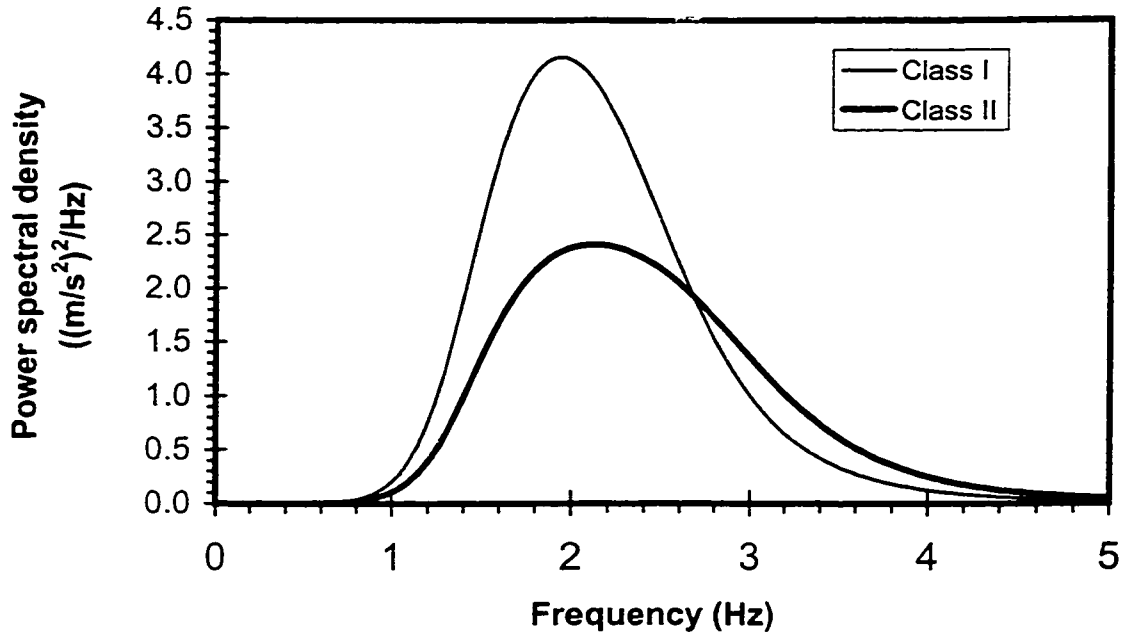

Figure 5.6: Acceleration power spectral density of Class I and Class II excitations in the vertical direction as defined in ISO 7096 [32].

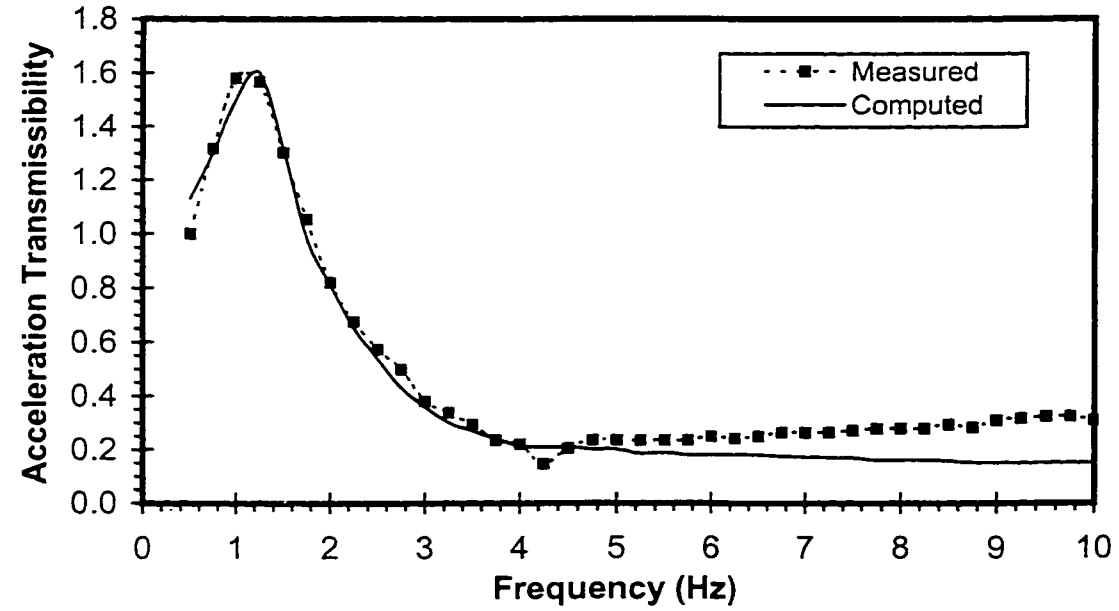

Figure 5.7: Comparison of measured and computed acceleration transmissibility of suspension seat system loaded with a rigid mass.

domain for each type of vibration excitation using Runge-Kutta integration method to evaluate the acceleration response at the load-cushion interface. Fast Fourier Transform (FFT) techniques are then applied to derive the vibration acceleration PSD and/or the acceleration transmissibility.

The response characteristics of the suspension seat model are compared to those established from the laboratory measured data, obtained by loading the seat with a mass of 63.6 kg. Figure 5.7 illustrates a comparison of measured and computed seat acceleration transmissibility with a rigid mass. A good agreement between the computed and measured transmissibility characteristics can be observed at frequencies below 5 Hz. The resonant frequency of the analytical model of the load-suspension seat system correlates very well with that obtained from the measured data. Above 5 Hz, however, the measured transmissibility is observed to be consistently higher than the computed data. The discrepancy between the computed and measured response at higher frequencies of excitation is attributed to the contact vibrations caused by clearance between the seat base and the mounting rails.

Figures 5.8 to 5.9 further illustrate the comparison of measured and computed acceleration PSD response at the seat interface when loaded with a rigid mass and subjected to random excitations due to Class I and Class II vehicles, respectively. Compared with those of the excitation spectra illustrated in Figure 5.6, the peak frequencies of response spectra have been shifted towards lower values due to the fact that the mass-seat system amplifies vibration below 2 Hz and attenuates vibration at frequencies above 2 Hz. The results show that the model provides good agreement with

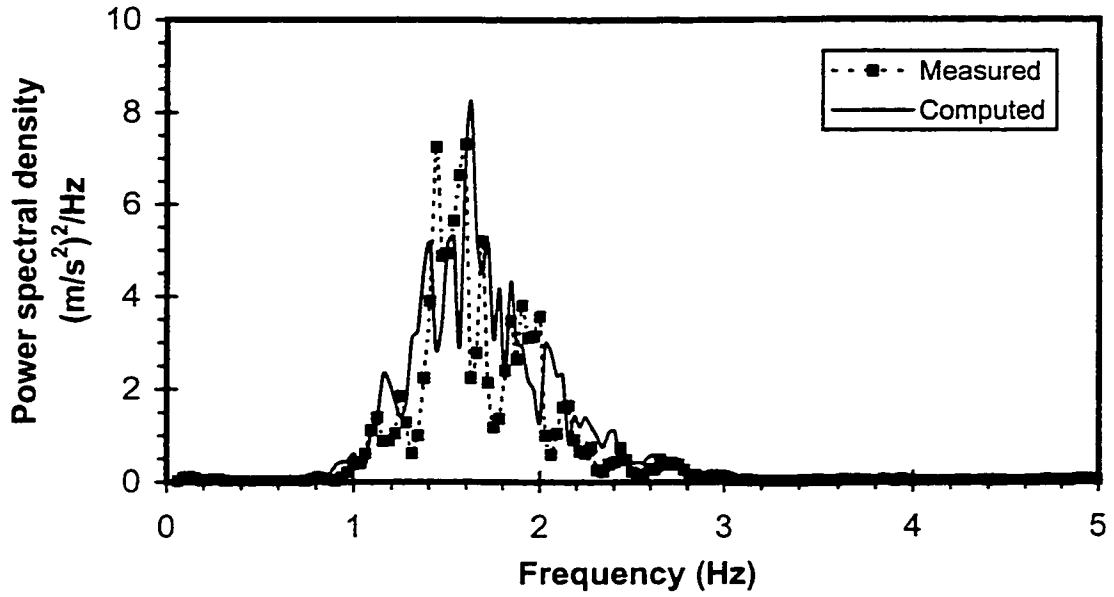

Figure 5.8: Comparison of measured and computed suspension seat acceleration PSD responses loaded with a rigid mass under Class I of random excitation.

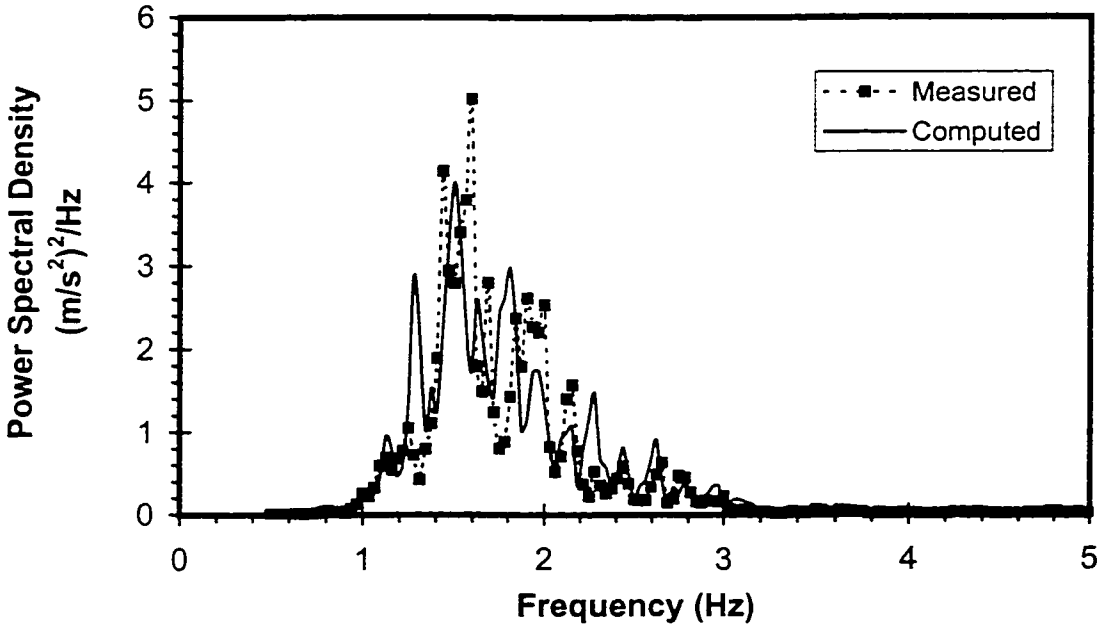

Figure 5.9: Comparison of measured and computed suspension seat acceleration PSD responses loaded with a rigid mass under Class II of random excitation.

the measured response under both classes of excitation over most of the frequency range investigated. The discrepancies observed in the acceleration transmissibility at high frequencies do not have significant influence on the PSD response under the two classes of excitations, attributed to the lack of excitation energy at these frequencies. In view of the high level of difficulty involved in determining the model parameters related to cushion and suspension damping, the degree of correlation between computed and measured response is considered relatively good under the excitations selected. The suspension seat model can thus be considered as a useful tool to further study the behavior of coupled driver-suspension seat system, the influence of the suspension parameters on the vibration attenuation performance, and the optimal suspension design to minimize whole body vibration exposure.

5.3.4 Validation of the human-suspension seat model

Upon validating the suspension seat model, the combined human-suspension seat model is further validated by comparing the measured results obtained while using a human subject as the seat load (total mass 73.2 kg; 55.6 kg on the seat) with the computed results, as illustrated in Figure 5.10. The total mass on the seat due to the human body model ($m_0+m_1+m_2+m_3$=53.8 kg) is quite comparable to that due to the human subject (55.6 kg). The figure illustrates reasonably good agreement between the measured and computed acceleration transmissibilities of the seat loaded with a human subject. The comparison reveals good agreement in terms of the resonant frequency, which occurs at around 1.3 Hz, and the trends in acceleration transmissibility. The measured and computed transmissibilities, however, demonstrate larger discrepancies

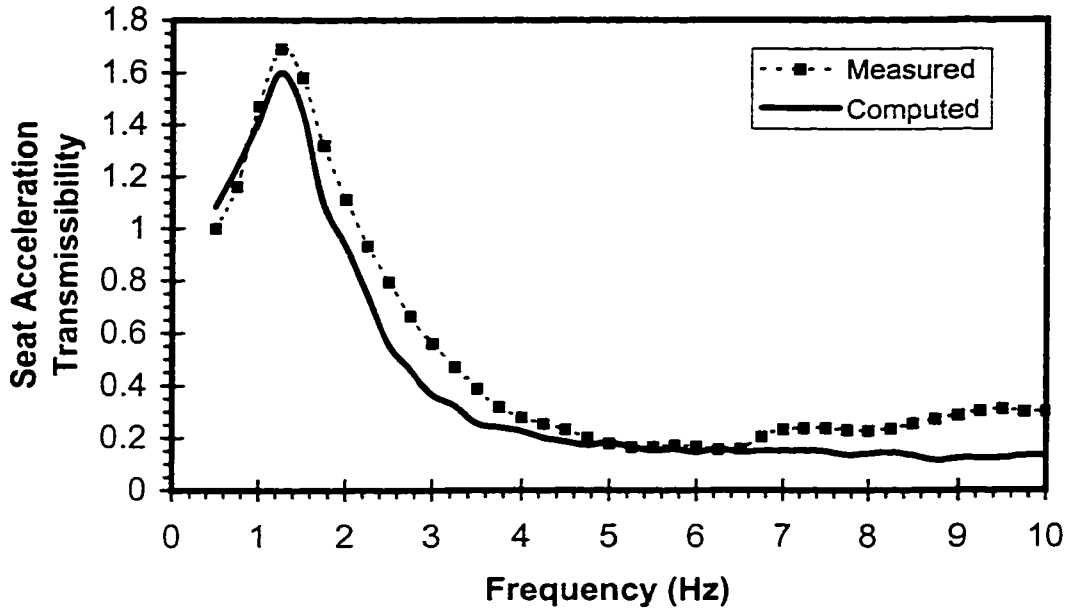

Figure 5.10: Comparison of measured and computed acceleration transmissibility of human-suspension seat system loaded with a human subject.

between 1 to 5 Hz and at frequencies above 7 Hz. The measured values are observed to be consistently higher than the computed values in most of the frequency range. As observed from the previous validation using a rigid mass, the measured transmissibility at high frequencies are also higher than the computed values. This difference is mostly attributed to the contact vibration caused by clearance between the seat base and mounting rails. It should be further noted that the human body model in this study is developed on the basis of the biodynamic response characteristics of a group of subjects, while the measurements were performed with one subject only. The proposed model may thus be expected to yield dynamic characteristics different from those of the single subject.

The validity of the coupled human-suspension seat model is further examined under random excitations due to Class I and Class II vehicles. The PSD of acceleration response at the driver model-seat interface, derived under both excitations, are compared with those established from the measured response. Figures 5.11 and 5.12 illustrate the comparison between PSD of computed and measured acceleration response under Class I and II excitations, respectively. The results, in general, show reasonably good agreement between the measured and model response under both excitations.

5.4 Summary

A combined nonlinear human-suspension seat model is developed by integrating the seated human body model proposed in Chapter 3, and the seat cushion model developed in Chapter 4 to the suspension seat model. The coupled human-suspension seat model incorporates nonlinear and asymmetric properties of the damper, cushion and end-

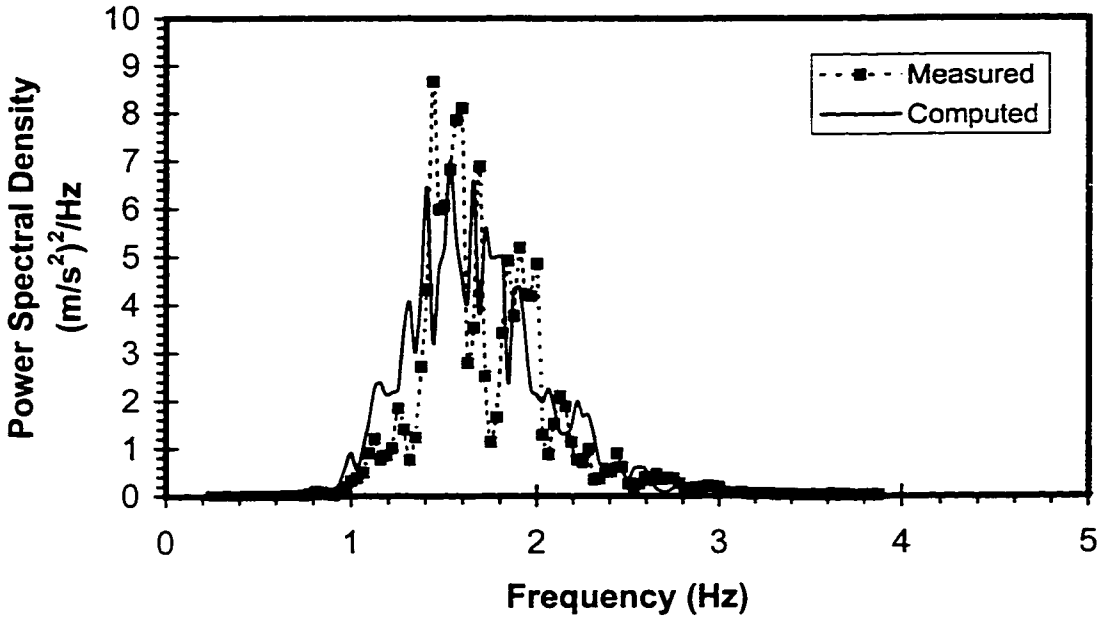

Figure 5.11: Comparison of measured and computed acceleration PSD response of the human-suspension system subject to Class I of random excitation.

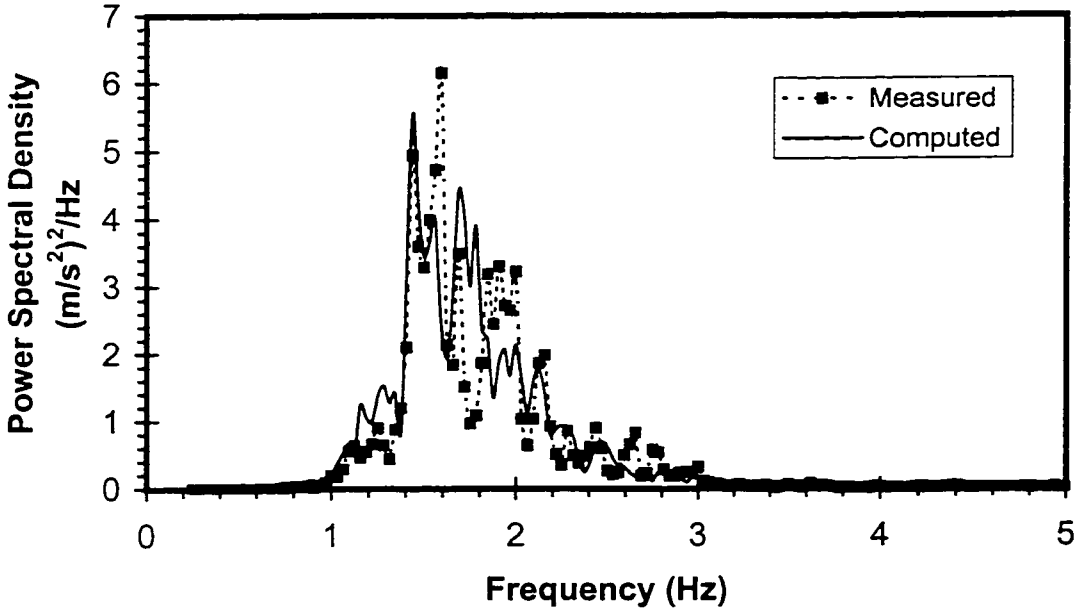

Figure 5.12: Comparison of measured and computed acceleration PSD response of the human-suspension system subject to Class II of random excitation.

stops. The combined human-suspension seat model is analyzed under sinusoidal and random excitations. The response characteristics in terms of acceleration transmissibility and PSD response are compared with those obtained from the laboratory measurements performed using a rigid mass and a human subject. The comparison revealed reasonably good agreement between the computed and measured response under both sinusoidal and random excitations. The proposed model is thus considered to serve as a valid analytical tool for design and assessment studies. The model is further utilized to design optimal parameters under steady state vibration and to minimize the severity of end-stop impacts in Chapters 6 and 7.

CHAPTER 6

STEADY-STATE VIBRATION PERFORMANCE OF HUMAN-SUSPENSION SEAT SYSTEM

6.1 Introduction

The dynamic performance of the nonlinear human-suspension seat system, defined in Chapter 5, depends on system parameters, including the suspension travel, the spring stiffness, the damping coefficient, the asymmetry and reduction factors in damping, the transition velocity, the damper inclination angle, the suspension mass, the Coulomb friction force, and the seat cushion and end-stop buffer properties. The effectiveness of the system also heavily depends on the frequency contents and magnitude of vibration excitation as well as on the applicable frequency weighting function, which defines the vibration frequency sensitivity of the human body. While the system design parameters and the excitation magnitude have a significant effect on the acceleration transmissibility of the human-suspension seat system, it is predominantly the frequency components of the excitation and the frequency weighting function that determine how severely the human body is exposed to vibration through the human-suspension seat system.

The performance of a human-suspension seat system can be characterised in three categories based upon the excitation magnitude. When the excitation acceleration is too low to overcome suspension friction, the suspension mechanism exhibits lock-up behaviour and the sprung part of the seat, including the body, moves in phase with the seat base. Under such low vibration excitation levels, the influence of vibration on the human body may be regarded as being not significant. With increased acceleration, or

within the second category, the suspension begins to move relative to its base, resulting in amplification and/or attenuation of vibration depending on the suspension design parameters and frequency components of the excitation. Further increase in excitation magnitude causes the suspension to reach the limits of the available free travel resulting in collision with the end-stop buffers. Within this third category, increased vibration and shock is transmitted to the human body. It has been discussed in the literature that improved attenuation performance of the system under steady-state vibration and the prevention of severe end-stop impacts pose contradictory requirements on the suspension design parameters [8, 84]. It is a challenging task to realize a generally optimum suspension seat performance under excitations of different steady-state floor spectra, let alone satisfying the contradictory requirements for steady-state and shock excitations. It is therefore essential to divide the problem of suspension design into two steps: (i) optimizing the seat suspension and seat cushion properties with constrained suspension travel under given steady-state floor spectra not likely to cause severe end-stop impacts; and (ii) optimizing the end-stop buffer properties once the seat suspension and seat cushion properties have been fixed to minimize the severity of end-stop impacts under excitations likely to cause end-stop impacts.

In this chapter, the frequency weighting function defined for vertical vibration exposure for a seated subject and criteria for evaluating the dynamic performance of the human-suspension seat system are firstly introduced. The influence of variations in various design factors on the performance characteristics is investigated and an optimal suspension design under steady-state vibration is attempted.

6.2 Frequency Weighting Function

Vibration discomfort assessment of drivers is primarily based on laboratory evaluations of subjects' judgment when exposed to various vibration stimuli. Equivalent sensitivity contours express the vibration magnitude required to produce equivalent discomfort for each vibration frequency, axis and input position. Frequency weighting functions are defined to express the differences in discomfort at different vibration frequencies and axes for a given and fixed measurement position.

The most widely used standard for evaluating human exposure to whole-body vibration and shock is the International Standard ISO 2631/1 [85], which replaces several older versions. For the assessment of health and comfort effects due to vertical vibration transmitted at the seat level, a frequency weighting function, W_k, is defined in the 0.5 to 80 Hz frequency range. The frequency weighting function is defined from a combination of a band-limiting filter and a network weighting filter. Mathematically, the transfer function of the band-limiting filter is expressed as:

$$H_b(s) = \frac{\omega_2^{\,2} s^2}{(s^2 + \sqrt{2}\omega_1 s + \omega_1^{\,2})(s^2 + \sqrt{2}\omega_2 s + \omega_2^{\,2})} \tag{6.1}$$

where $\omega_1 = 2\pi f_1$ and $\omega_2 = 2\pi f_2$; f_1 and f_2 are the band-pass corner frequencies (f_1 = 0.4 Hz and f_2 = 100 Hz), and $s = j\omega$. The transfer function of the network weighting filter is given by:

$$H_w(s) = \frac{\omega_4^{\,2}(s + \omega_3)(s^2 + \frac{\omega_5}{Q_5} s + \omega_5^{\,2})}{\omega_3(s^2 + \frac{\omega_4}{Q_4} s + \omega_4^{\,2})(s^2 + \frac{\omega_6}{Q_6} s + \omega_6^{\,2})} \tag{6.2}$$

where $\omega_3 = 2\pi f_3$, $\omega_4 = 2\pi f_4$, $\omega_5 = 2\pi f_5$ and $\omega_6 = 2\pi f_6$; $f_3 = f_4 = 12.5$ Hz, $f_5 = 2.37$ Hz, $f_6 = 3.35$ Hz. $Q_4 = 0.63$, $Q_5 = Q_6 = 0.91$. The transfer function of the total weighting filter is then obtained from:

$$W_k(s) = H_b(s)H_w(s) \tag{6.3}$$

6.3 Criteria for Evaluating the Dynamic Performance of Human-Suspension Seat System

The criteria for evaluating the dynamic performance of the human-suspension seat system depend on the crest factor, which separates steady-state vibration from shock-type vibration. The crest factor is defined as the ratio of peak value of frequency-weighted acceleration to frequency-weighted rms acceleration [85]. For a crest factor below 9, the vibration can be considered as steady-state vibration and the vibration exposure level can be expressed using the frequency-weighted rms acceleration:

$$a_{w,rms} = \sqrt{\frac{1}{t_1}\int_0^{t_1} a_w^2(t)dt} \tag{6.4}$$

where $a_{w,rms}$ is the overall frequency-weighted rms acceleration, $a_w(t)$ is the frequency-weighted acceleration and t_1 is the exposure duration. A SEAT value (Seat Effective Amplitude Transmissibility) is further defined to measure the efficiency of a seat in isolating the body from vibration [1]. It represents the ratio of the frequency-weighted rms acceleration measured on the seat to the frequency-weighted rms acceleration measured at the seat base along the same direction. A SEAT value lower than unity suggests that the human-suspension seat system is effective in reducing vibration exposure, while a SEAT value greater than unity suggests that the human-suspension seat system amplifies the vibration exposure. Mathematically, the SEAT is defined as:

$$SEAT\ (\%) = \frac{a_{w,rms}\ of\ seat\ vibration}{a_{w,rms}\ of\ base\ vibration} \times 100 \qquad (6.5)$$

When the crest factor is larger than 9, the vibration can be considered as shock-type vibration and the exposure is characterized by both the frequency-weighted rms acceleration and a vibration dose value (VDV) according to the ISO 2631-1 [85]. The VDV relies on the fourth power of the frequency-weighted acceleration, thus providing greater emphasis on large instantaneous acceleration values which may arise from shocks. The VDV method thus appears to be appropriate for evaluating the severity of end-stop impacts caused by high level excitation. The vibration dose value is not only influenced by the most severe shock, it accumulates in value according to the magnitude and duration of the frequency-weighted acceleration time histories. The VDV value is used to provide guidance on exposures to vibration or shocks that may cause injury [85, 86], defined as:

$$VDV = [\int_0^T a_w^4(t)dt]^{1/4} \qquad (ms^{-1.75}) \qquad (6.6)$$

A VDV ratio may be defined to measure the efficiency of a seat in isolating the body from shock-type vibration or preventing severe end-stop impacts [84]. The VDV ratio is defined as the ratio of the frequency-weighted VDV measured on the seat to the VDV measured at the seat base along the same direction. The VDV ratio is expressed as:

$$VDV\ ratio\ (\%) = \frac{VDV\ of\ seat\ vibration}{VDV\ of\ base\ vibration} \times 100 \qquad (6.7)$$

6.4 Parametric Sensitivity Analysis on the Basis of Vibration Transmissibilities

The steady-state vibration transmission characteristics of a human-suspension seat system can be conveniently evaluated in terms of acceleration transmissibility and relative displacement transmissibility in the frequency range of interest. The vibration transmissibility response can provide significant information related to vibration attenuation characteristics and probable frequency range of vibration isolation. The acceleration transmissibility is defined as the ratio of acceleration magnitude transmitted to the human-seat interface to the magnitude of excitation acceleration at the base. The relative displacement transmissibility is defined as the ratio of magnitude of relative displacement across the suspension mechanism to the excitation displacement at the base. Occasionally, suspension acceleration transmissibility is also used to demonstrate the performance of the suspension mechanism, defined as the ratio of suspension mass acceleration to the excitation acceleration at the base. The vibration transmissibility characteristics are known to be influenced by many design and operating parameters, such as suspension spring rate, friction, damping, and cushion properties, and magnitude of excitation. A study of the influence of variations in such parameters on the vibration transmission performance can yield significant insight into the most desirable design parameters for a suspension seat. In this section, the influence of variations in a single parameter at one time on the acceleration transmissibility is investigated under a nominal excitation level of 1.4 m/s^2 rms, except where otherwise stated. All the other suspension parameters are held at their nominal values listed in Table 5.1.

6.4.1 Influence of excitation magnitude

The vibration transmission performance of a human-suspension seat system is strongly affected by the excitation magnitude due to its nonlinear properties arising from force-velocity characteristics of the damper, Coulomb friction, end-stops and cushion. The equations of motion for the human-suspension seat model are solved under harmonic excitations of constant acceleration magnitude at discrete frequencies. The response characteristics are analysed to derive the acceleration transmissibility of the driver mass interfacing with the seat (m_0) and the suspension mass (m_s), and the relative displacement transmissibility of the suspension. Figures 6.1 to 6.3 illustrate the acceleration transmissibility of the suspension and driver masses, and relative displacement transmissibility under different excitation magnitudes, ranging from 0.1 to 2.1 m/s^2 rms. Under very low excitation magnitude (0.1 m/s^2 rms), the excitation acceleration is too low to overcome the friction force in the suspension. The suspension mechanism experiences 'lock-up' and the sprung part of the seat moves in phase with the seat base. The 'lock-up' behaviour of the suspension mechanism is examined using the following condition:

$$\left|m_s\ddot{x}_s + m_0\ddot{x}_0 + m_1\ddot{x}_1 + m_2\ddot{x}_2 + m_3\ddot{x}_3\right| \le F_0 \qquad (6.8)$$

where m_s, m_0, m_1, m_2 and m_3 are the system masses, $\ddot{x}_s, \ddot{x}_0, \ddot{x}_1, \ddot{x}_2$ and $\ddot{x}_3$ are their corresponding acceleration responses, as illustrated in Figure 5.2. Under lock-up condition, the suspension acceleration transmissibility approaches a value of almost unity, while the acceleration transmissibility of the system reflects the vibration transmissibility of the seat cushion only. The peak acceleration transmissibility occurs near 6 Hz, which is the resonant frequency of the human-cushion subsystem. An increase in excitation magnitude, in general, yields higher peak acceleration and relative displacement transmissibility

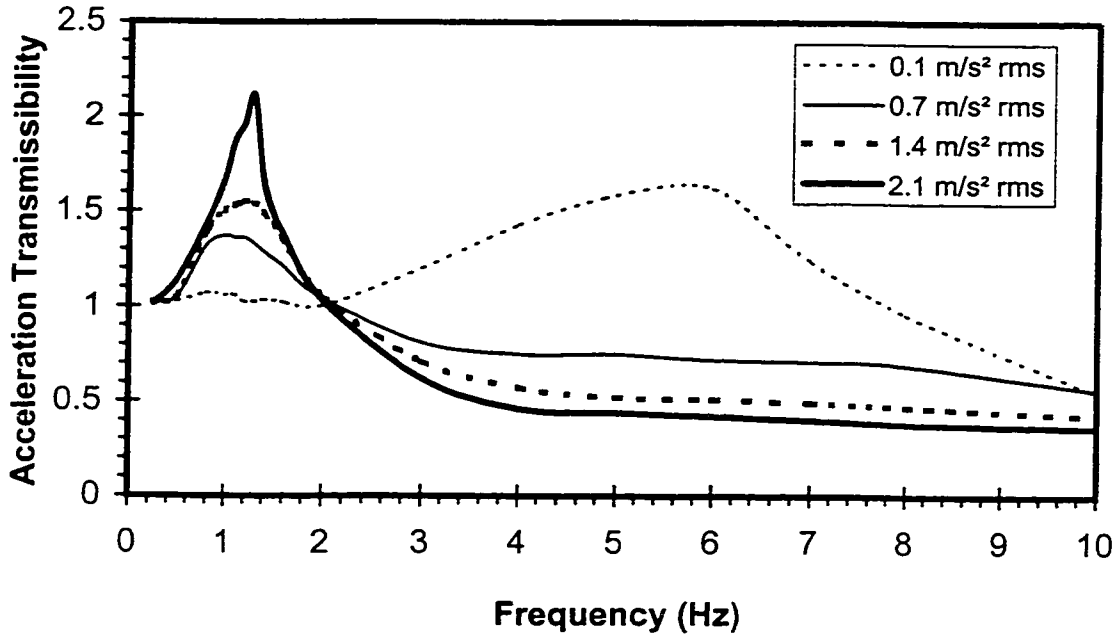

Figure 6.1: Influence of excitation magnitude on the seat acceleration transmissibility.

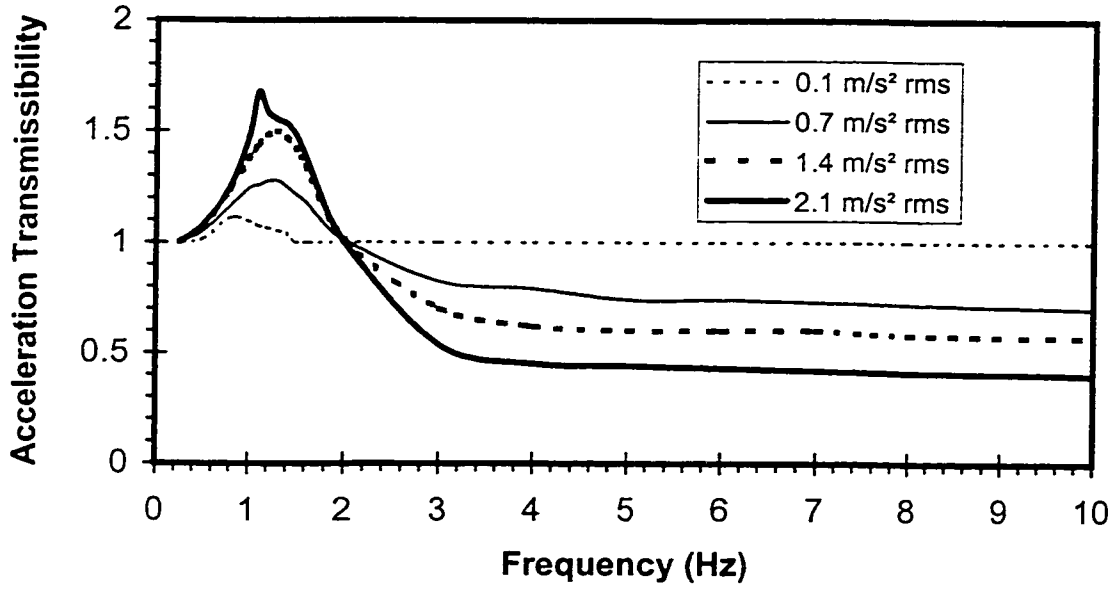

Figure 6.2: Influence of excitation magnitude on the suspension acceleration transmissibility.

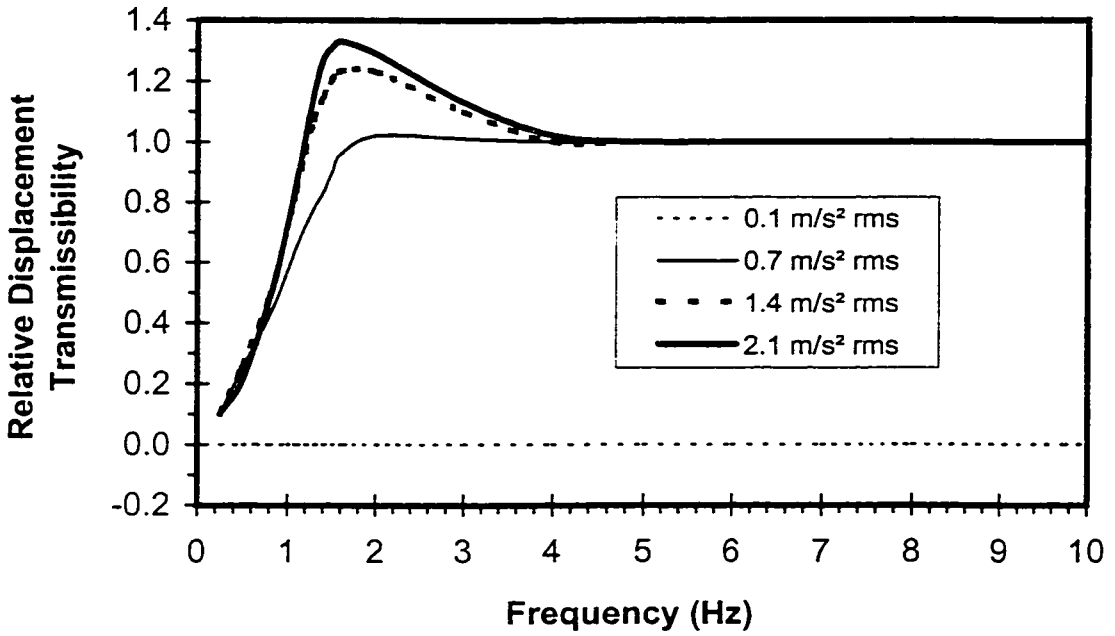

Figure 6.3: Influence of excitation magnitude on the relative displacement transmissibility of the suspension mass.

response, and improved vibration attenuation at frequencies above 2 Hz. This may be attributed to two factors: (i) the damper tends to operate in both bleed and blow-off stages, which leads to lower equivalent damping coefficient; and ii) the equivalent damping coefficient due to a constant Coulomb friction force decreases with increase in the relative motion, when the excitation level is increased [87]:

$$c_{eq} = \frac{4F_0}{\pi\omega|z_s|} = \frac{4F_0\omega}{\pi|\ddot{z}_s|} \tag{6.9}$$

where c_{eq} is the equivalent viscous damping coefficient, F_0 is the constant Coulomb friction force, ω is the excitation frequency, and $|z_s|$ and $|\ddot{z}_s|$ are the magnitudes of relative displacement and relative acceleration of suspension mass, respectively.

A further increase in the excitation magnitude (2.1 m/s^2 rms) causes the suspension to reach the limits of the available travel, which results in collisions with the end-stop buffers. Body hop motion and cushion bottoming may also occur under such large magnitude of vibration excitation, as evident in the significant increase in the peak seat and suspension acceleration transmissibility characteristics, shown in Figures 6.1 and 6.2. The peak relative displacement response does not increase as significantly when the magnitude is increased from 1.4 to 2.1 m/s^2 rms, as illustrated in Figure 6.3, which is attributed to the effective operation of the end-stop buffers.

The results presented in Figures 6.1 to 6.3 suggest that the performance characteristics of the human-seat system are directly affected by the vibration levels of the vehicle. It is thus vital to tune the suspension parameters for specific vehicle vibration environment. In view of the strong dependence of the system performance on excitation

level, the parametric analyses presented in the following sections are restricted to only one excitation magnitude, 1.4 m/s^2 rms.

6.4.2 Influence of Coulomb friction

The magnitude of Coulomb friction force affects the suspension performance mainly under low level excitation. The friction may cause suspension lock-up at extremely low excitation frequencies due to relatively low inertia forces, and stick-slip motion at higher frequencies, when the excitation levels are relatively low. The influence of variations in friction force, in most of the frequency range of interest, can be best described as a variation in the viscous damping as evident in Equation (6.9). Figure 6.4 illustrates the influence of variation in the friction force on the seat acceleration transmissibility under 1.4 m/s^2 rms acceleration excitation. The seat does not exhibit lock-up behavior due to relatively higher excitation level. An increase in friction force, however, yields lower peak transmissibility magnitude and higher acceleration response in the range of vibration isolation (above 2 Hz).

6.4.3 Influence of suspension spring rate

Under a given vibration excitation, the dynamic performance of the human-suspension seat system heavily depends on its spring rate k_s. The variations in spring stiffness coefficient affect the resonant frequency of the system, the frequency range of vibration isolation, the relative displacement response, and the frequency and potential of impacts against the end-stop buffers. The variations may also affect the static mid-ride height in seats, where a height-compensation mechanism is not available. The influence

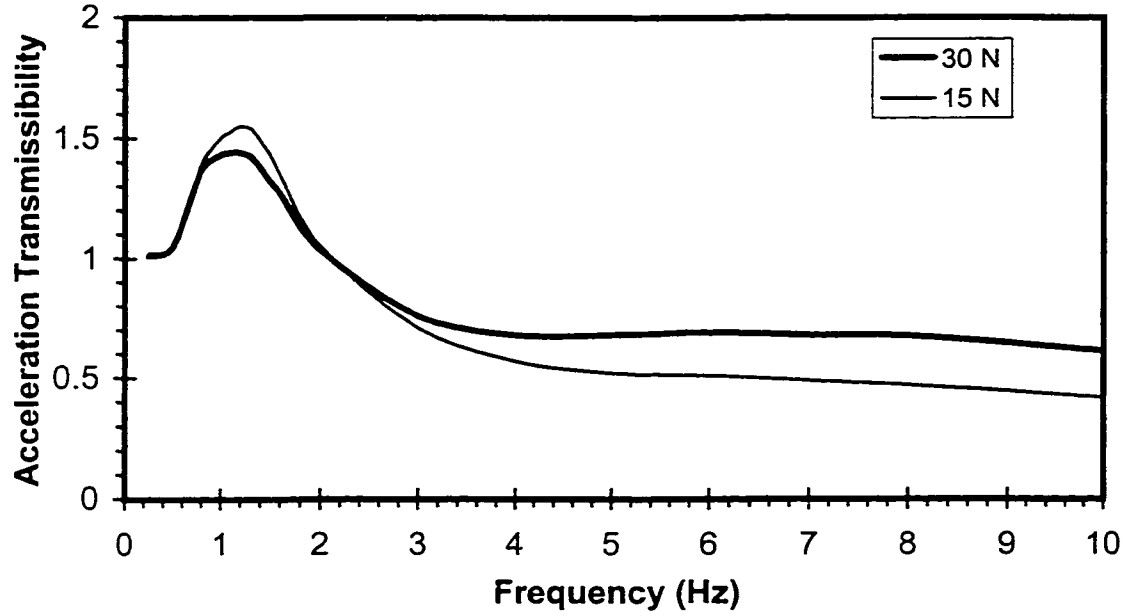

Figure 6.4: Influence of Coulomb friction on the seat acceleration transmissibility.

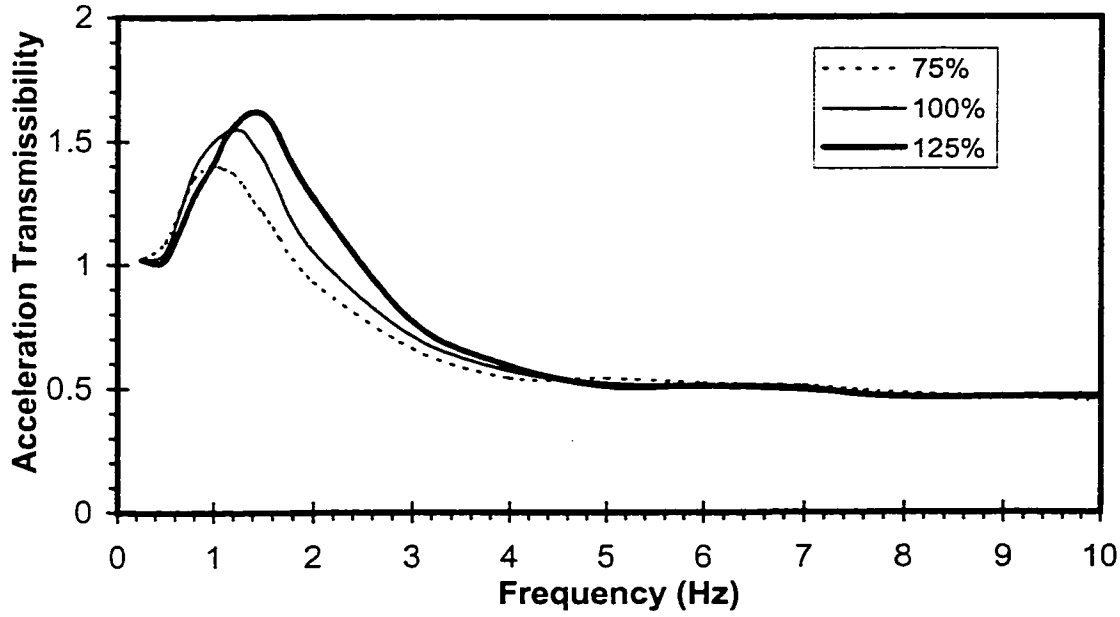

Figure 6.5: Influence of variation in suspension stiffness on the acceleration transmissibility of the seat.

of the spring rate on the acceleration transmissibilities of the human-suspension seat system is investigated by varying the suspension spring stiffness k_s by ±25% of its nominal value, while all other parameters assume their nominal values. Figure 6.5 illustrates the influence of such variations on the acceleration transmissibility of the seat. The results show that an increase in suspension spring stiffness yields increase in both the resonant frequency and the acceleration transmissibility at resonance. The effective damping ratio also tends to decrease with increase in the spring stiffness. The resonant response thus tends to increase with higher spring rate suspension. The vibration transmissibility at frequencies greater than 4.6 Hz, however, remains almost unaffected due to ±25% variations in the spring rate. The results show that suspension seats with low suspension stiffness can greatly attenuate vehicular vibration over a wide frequency range. Soft suspension seats, however, induce large dynamic deflection of the suspension, that may cause more frequent and severe end-stop impacts. Since most wheeled off-road vehicles have dominant whole-body ride vibration in the 1.8 to 2.6 Hz frequency range, it is desirable to select lower suspension spring rate.

6.4.4 Influence of suspension damping parameters

The suspension damping affects the suspension performance in a most significant and complex manner, since the damping properties are expressed in terms of various design parameters (asymmetry factor, reduction factors, transition velocities and low speed compression mode damping coefficient). A parametric study is performed in a systematic manner to highlight the influence of each variable with appropriate coupling among different variables.

The influence of variations in low speed compression damping coefficient c_s on acceleration transmissibility of the human-suspension seat system is initially investigated, as illustrated in Figure 6.6. It should be noted that a variation in c_s causes changes in all the damping coefficients associated with low speed damping in compression and rebound, as evident from Subsection 5.2. Figure 6.6 illustrates the influence of ±25% variations in c_s from its nominal value, on the seat acceleration transmissibility. The high speed compression mode damping coefficient (c_2), and low and high speed rebound mode damping coefficients (c_3 and c_4), thus also vary by ±25%. While an increase in suspension damping coefficient decreases the transmissibility at resonance, the acceleration transmissibility at frequencies above 2 Hz increases. The contributions of damping to the overall vibration attenuation performance of the system thus depend on the frequency components of vibration excitations. A high value of low speed compression damping coefficient c_s may be desirable, when the excitation vibrations predominate around lower frequencies close to the suspension resonant frequencies or when excessive relative motions are anticipated.

The symmetric damping properties in rebound and compression are expressed by the asymmetry factor p, as the ratio of low speed rebound damping coefficient to low speed compression damping coefficient. A variation in p value thus causes considerable variation in the rebound mode damping coefficients (c_3 and c_4), since the values of c_s and γ_1 are held constant. Figure 6.7 illustrates the influence of variations in p on the seat acceleration transmissibility, for three values of p: 0.5, 1.0 and 2.0. Such variations are realized by selecting rebound mode damping coefficient c_2, as: 446, 892, 1784 Ns/m, respectively. The results show that p=0.5 (rebound damping lower than the compression

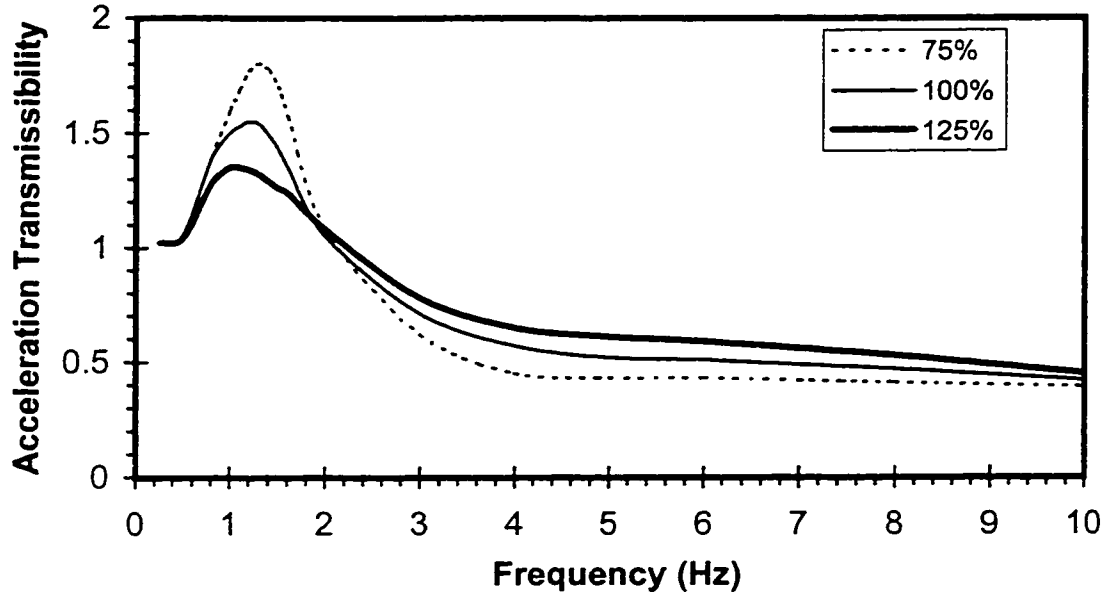

Figure 6.6: Influence of low speed compression damping coefficient on acceleration transmissibility.

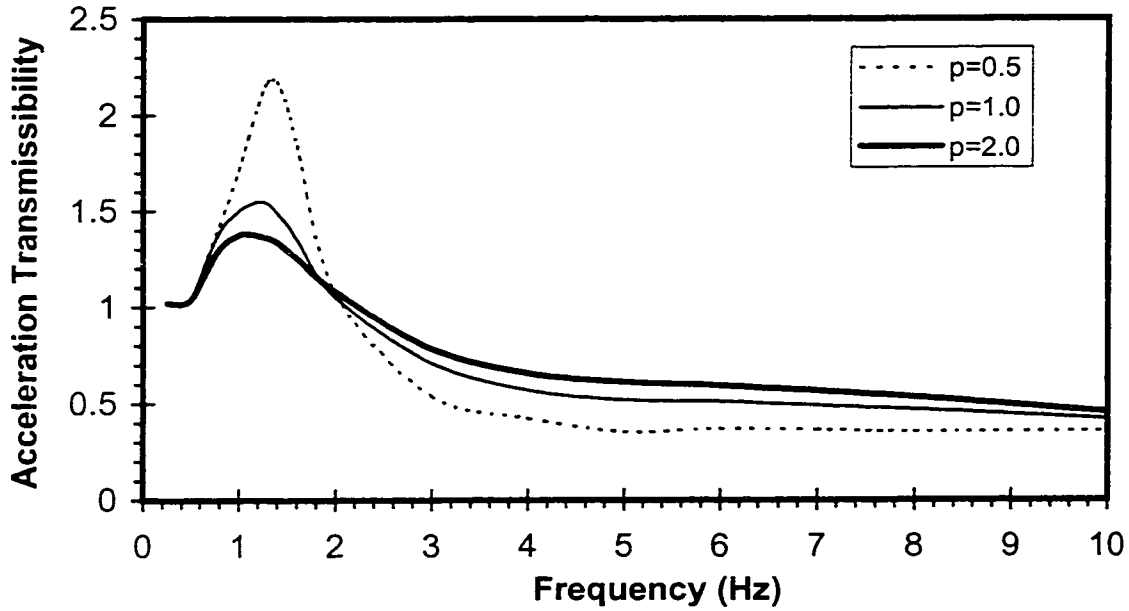

Figure 6.7: Influence of asymmetric factor on the acceleration transmissibility (c_s=892 Ns/m).

mode damping) yields significant increase in resonant transmissibility and improved vibration attenuation performance in the isolation range. A high value of p (p=2, rebound damping higher than the compression damping) tends to effectively suppress the resonant peak with poor vibration attenuation performance at frequencies above 2 Hz. Symmetric damping properties yield a compromise response between the two types of asymmetry. The above results can be considered valid only when c_s is held fixed at its nominal value.

Alternatively, variations in asymmetry factor may be realized by selecting the c_s values, as: 1784, 892, 446 Ns/m. Figures 6.7 to 6.9 illustrate the influence of variations in both c_s and p, on the seat acceleration transmissibility. It should be noted that a low p value yields a lower equivalent damping coefficient for the system, which is demonstrated by the respective high resonant response and lower response at frequencies above 2 Hz, irrespective of the low speed compression damping coefficient. A high p value, however, is desirable when the low speed compression damping coefficient assumes a low value, as evident in Figure 6.8, where both p values of 0.5 and 1.0 relate to high peaks in acceleration transmissibility around resonance, indicating that severe end-stop impacts and/or cushion bottoming have occurred due to low equivalent damping coefficient. On the other hand, a low p value may be preferable when the low speed compression damping coefficient assumes a high value, as evident in Figure 6.9, where both p values of 1.0 and 2.0 relate to high magnitudes at frequencies above 2 Hz, where the dominant vibration excitation energy is expected. This severely deteriorates the vibration attenuation performance of the system due to high equivalent damping coefficient. The dampers, in general, provide p value greater than unity to prevent the

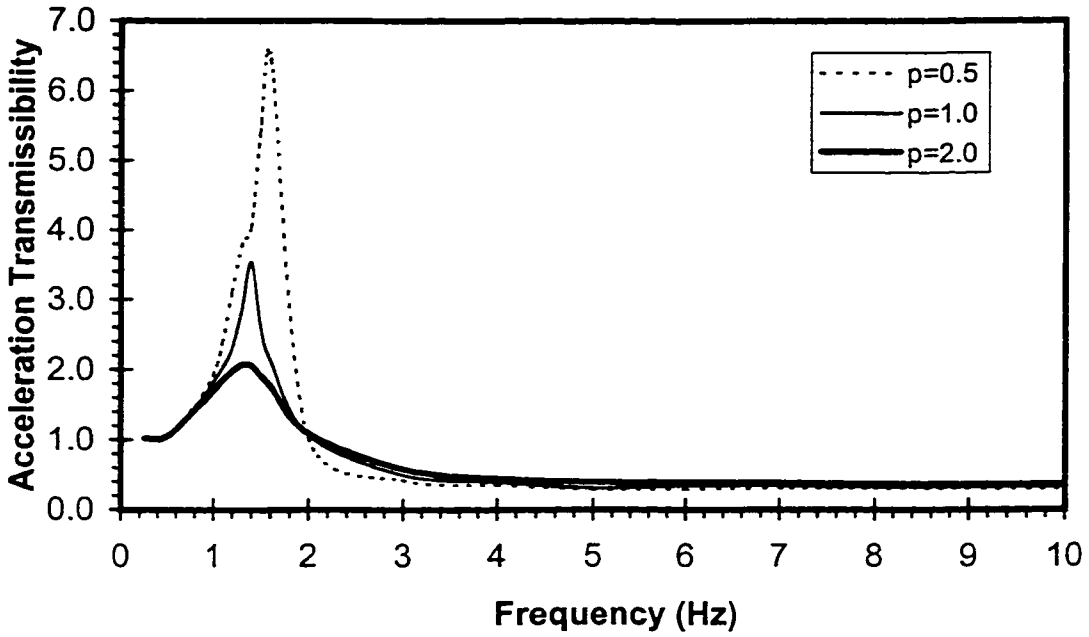

Figure 6.8: Influence of asymmetric factor on acceleration transmissibility (c_s=446 Ns/m).

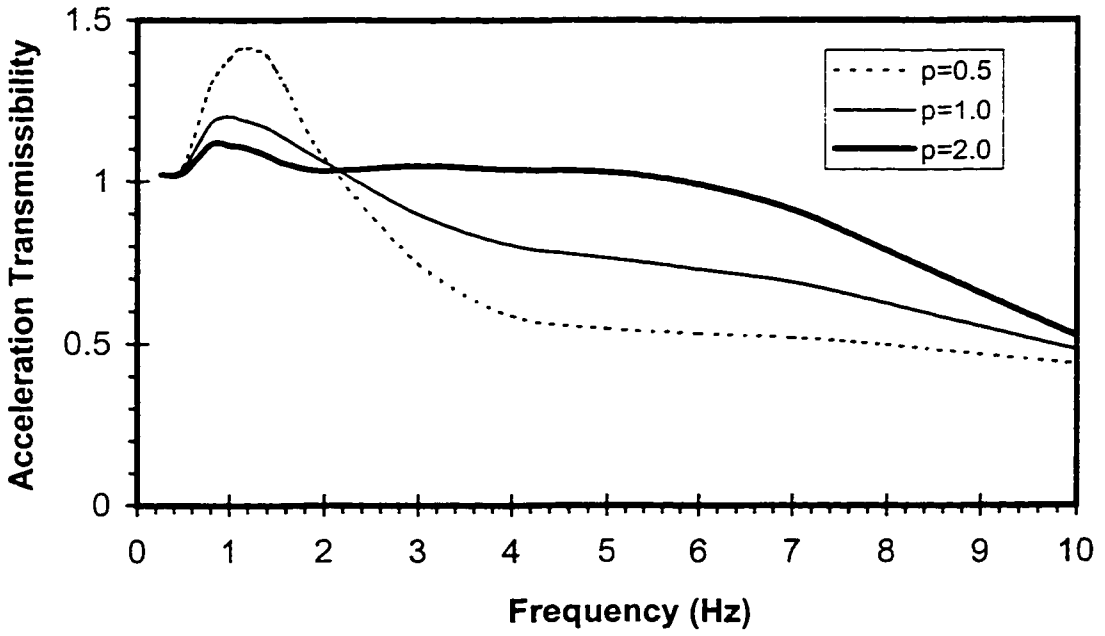

Figure 6.9: Influence of asymmetric factor on acceleration transmissibility (c_s=1784 Ns/m).

suspension to hit the top buffers, which may cause body hop motion resulting in interference with the vehicle controls.

The damping reduction factors in compression and rebound, γ_1 and γ_2, express the ratio of the blow-off stage damping coefficient to the bleed stage damping coefficient. A low value of γ implies that the damper provides low damping effect at high velocity. The influence of reduction factors on the acceleration transmissibility, when both the factors are varied by ±25%, is illustrated in Figure 6.10. An increase in reduction factor reduces the transmissibility at resonance with only a slight increase in the acceleration transmissibility at frequencies above 2 Hz. A two-stage damper is thus desirable for applications in seat suspension. At low piston velocity, related with low frequency vibration components, fluid flows through the bleed orifices to yield high damping and thus improved control of resonant vibrations. At higher piston velocity, related with high frequency vibration components, the flow modulation using blow-off or pressure control valves leads to low damping and thus improved vibration isolation.

The transition velocities v_1 and v_2 determine the condition when the damper changes from 'bleed' to 'blow-off' stage. Zero or infinite transition velocities imply only single stage damping. The influence of variations in transition velocities (±25% variations with respect to their nominal values) on the acceleration transmissibility is illustrated in Figure 6.11. The influence is observed to be relatively insignificant for the nominal parameters of the suspension seat listed in Table 5.1. An increase in transition velocity slightly suppresses the transmissibility at resonance, and causes an insignificant increase in acceleration transmissibility at high frequencies.

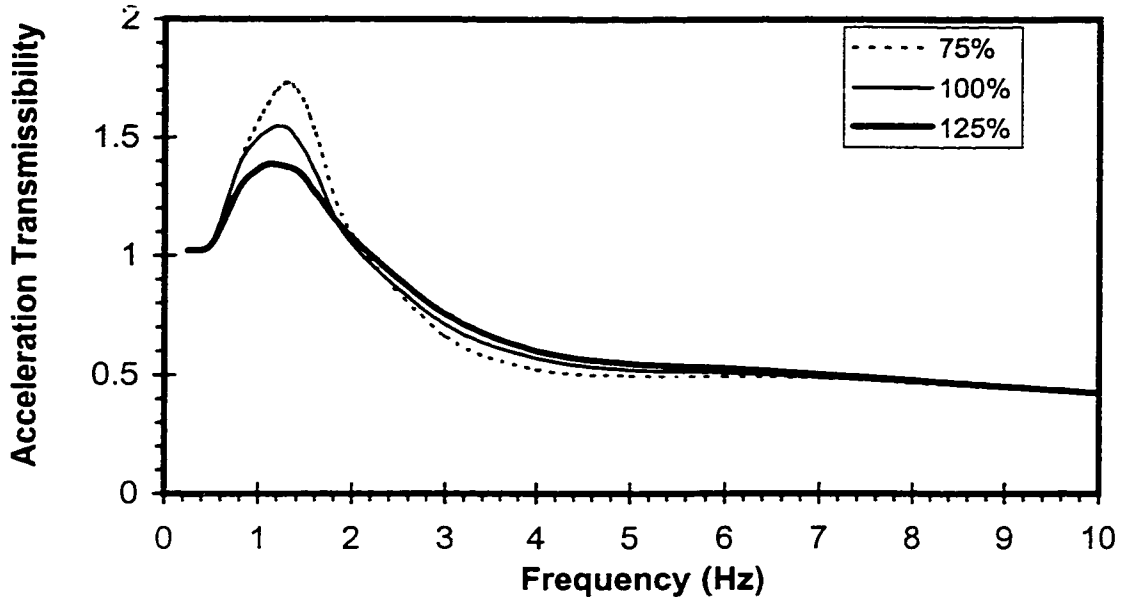

Figure 6.10: Influence of reduction factor on the acceleration transmissibility.

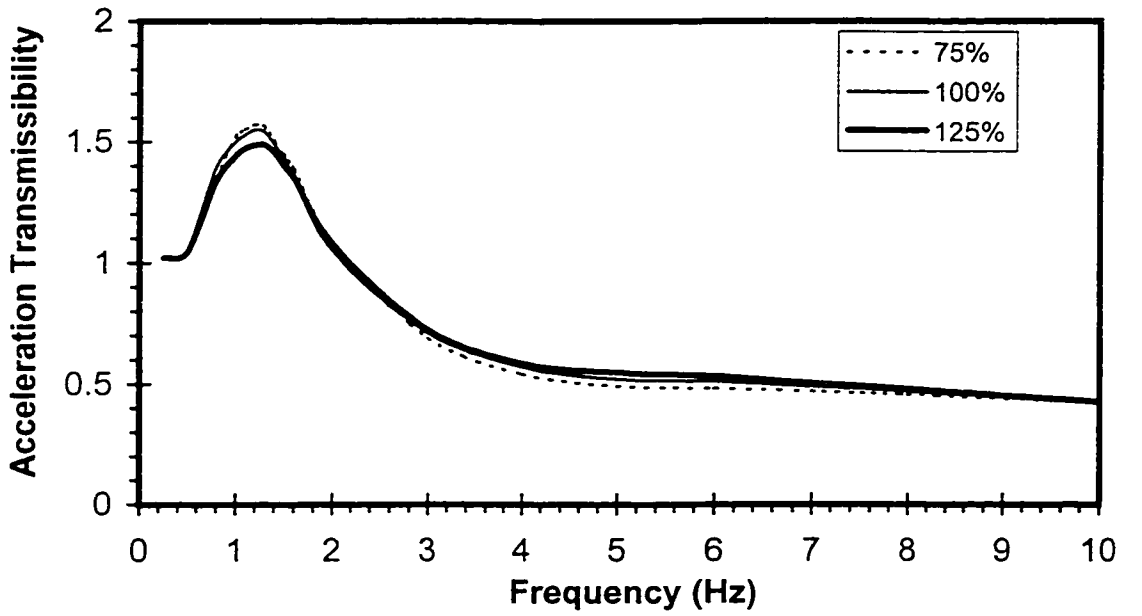

Figure 6.11: Influence of variation in transition velocities on the acceleration transmissibility.

The variations in damper inclination angle α_0 affect the vertical component of the damper force, as shown in Equations (5.3) and (5.4). An increase in the inclination angle causes an increase in vertical damper force, resulting in lower resonant transmissibility and higher response at frequencies above 2 Hz, as shown in Figure 6.12, which is similar to that observed for variations in c_s.

6.4.5 Influence of suspension mass

The suspension mass m_s is usually low compared to drivers' weight supported by the seat. Its influence on seat acceleration transmissibility can thus be expected to be insignificant. Variations in the suspension mass, however, may affect the critical damping coefficient and the resonant frequency of the coupled system. Figure 6.13 illustrates the influence on the acceleration transmissibility of the system when the suspension mass is varied from 5 to 15 kg. An increase in suspension mass causes the resonant frequency to shift towards a slightly lower value, and the resonant transmissibility to increase slightly. The vibration attenuation performance of the human-suspension seat system, however, improves slightly, when the dominant excitation frequency components are above 2 Hz.

6.4.6 Influence of seat cushion parameters

Relatively hard cushions are frequently used in suspension seats to provide controlled seated posture. The influence of cushion properties are usually considered insignificant. A significantly soft cushion may cause similar resonant frequencies associated with deflection of the suspension mass and the seated body. Soft cushions can thus yield increase in acceleration transmissibility at resonance, and lower magnitude at

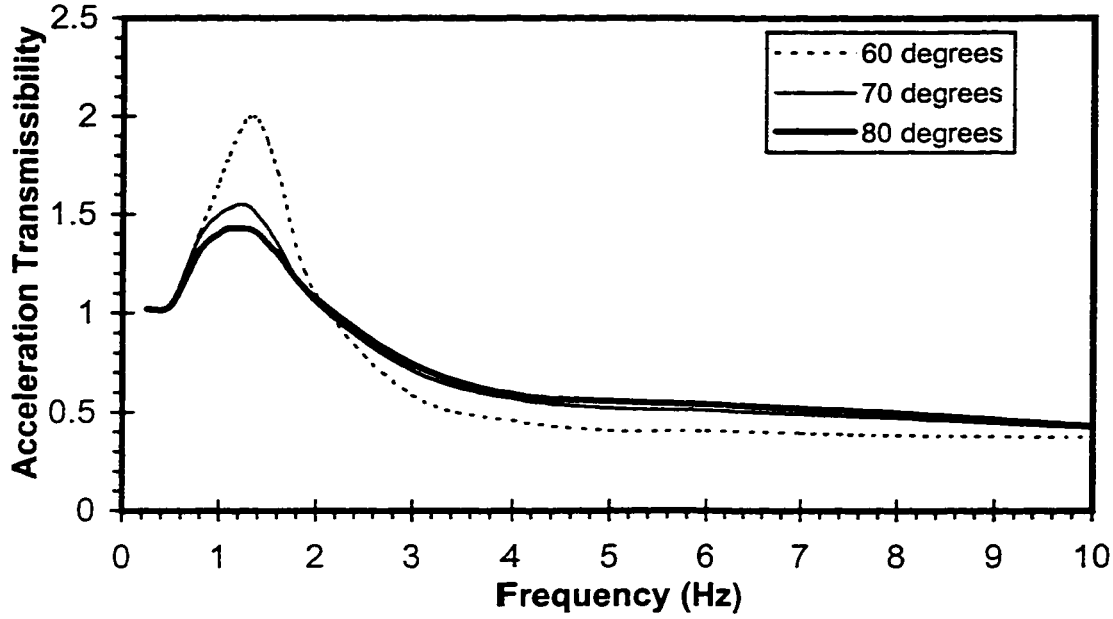

Figure 6.12: Influence of variation in damper inclination angle on acceleration transmissibility.

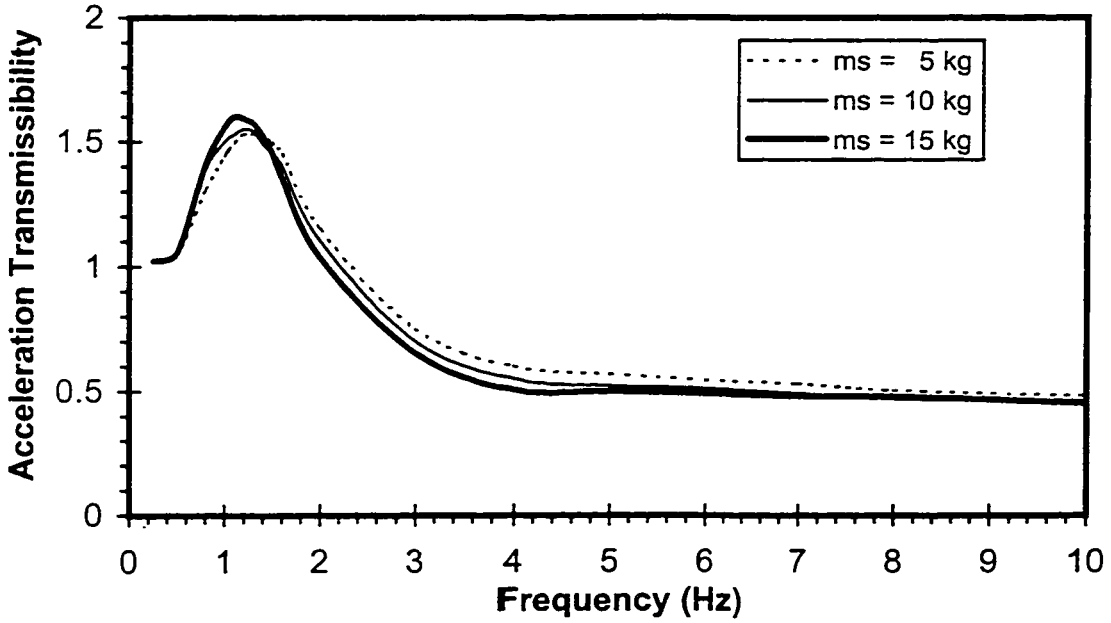

Figure 6.13: Influence of variation in suspension mass on the seat acceleration transmissibility.

higher frequencies, as illustrated in Figure 6.14. It should be mentioned that a variation in the cushion linear stiffness coefficient also causes the variations in parameters a_1, a_2, a_3 and a_4, as evident from Equation (4.7). Since the parametric study is performed under relatively lower levels of sinusoidal excitations, the variations in nonlinear cushion parameter k_{c3} does not influence the acceleration transmissibility of the human-cushion system.

Since foam cushions offer very light damping, the variations in its damping coefficient are known to have very little influence on the acceleration transmissibility at the primary resonant frequency of the system. A higher cushion damping coefficient, however, relates to lower magnitude of acceleration transmissibility, attributed to the suppression of the resonance of the human-cushion subsystem, at a frequency around 6 Hz, as illustrated in Figure 6.15.

6.5 Parametric Sensitivity Analysis on the Basis of SEAT Values

Although the influence of variations in suspension seat parameters on acceleration transmissibility of the system has been shown clearly in Figures 6.1 to 6.15, the quantitative sensitivity of any parameter variation can not be determined for a given excitation spectrum without computing its SEAT value under a specific excitation. A quantitative parametric sensitivity analysis is thus performed for excitations arising from Class I and Class II vehicles, while the parameters are varied by ±25% about their respective nominal values. Figures 6.16 and 6.17 illustrate the variations in SEAT values caused by ±25% variations in individual suspension seat parameters under Class I and Class II excitation spectra, respectively. The variations in parameters are expressed in

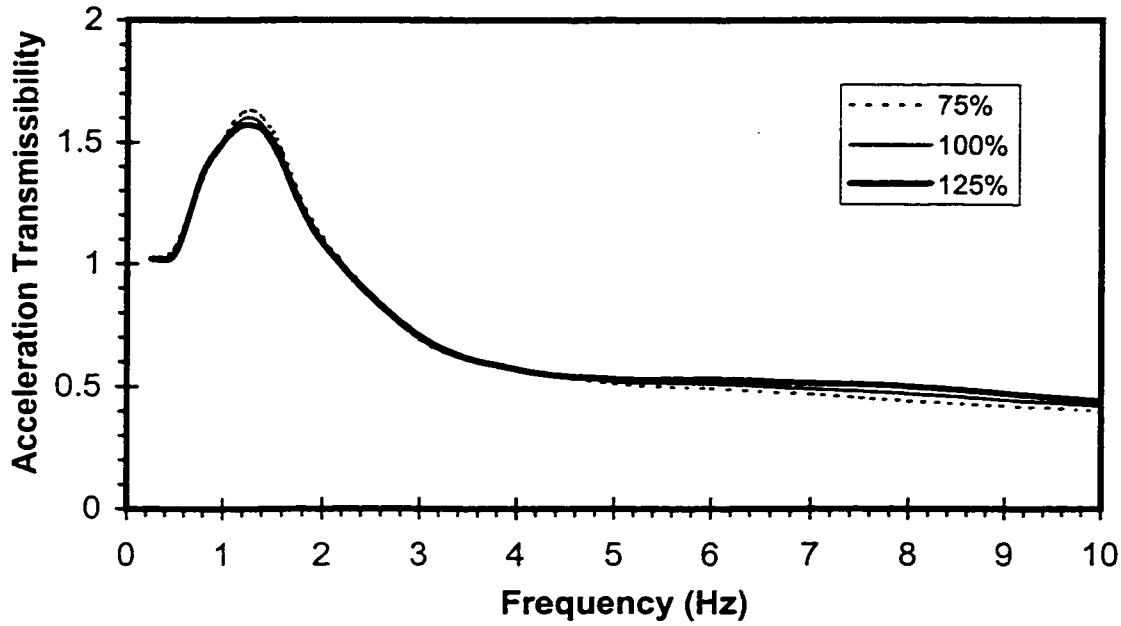

Figure 6.14: Influence of cushion linear stiffness k_{c1} on acceleration transmissibility.

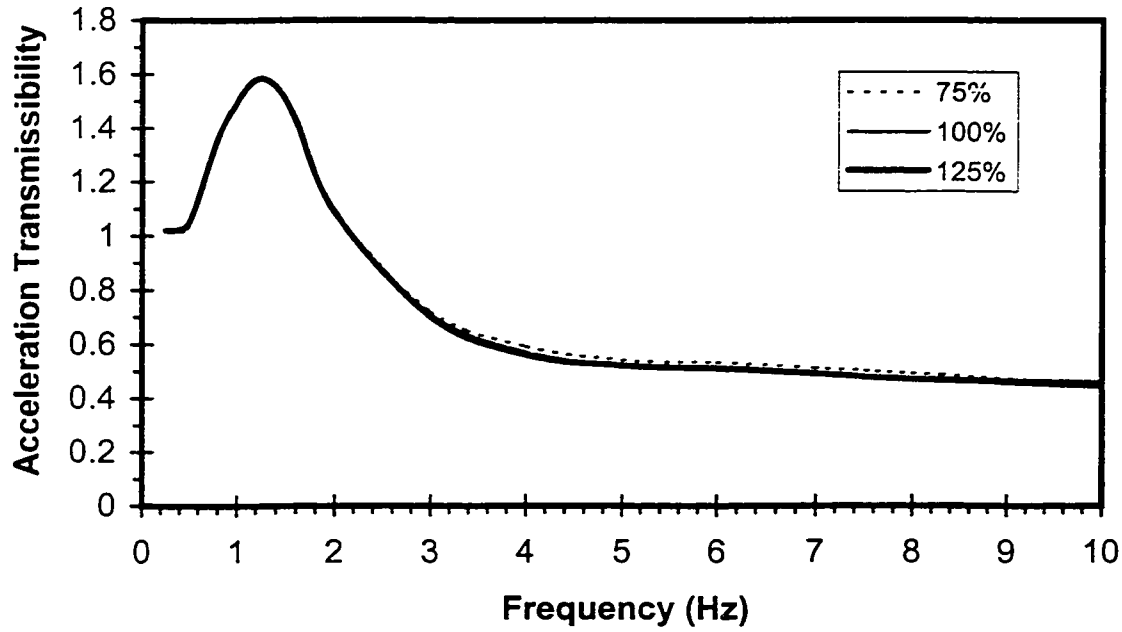

Figure 6.15: Influence of cushion damping coefficient on the acceleration transmissibility.

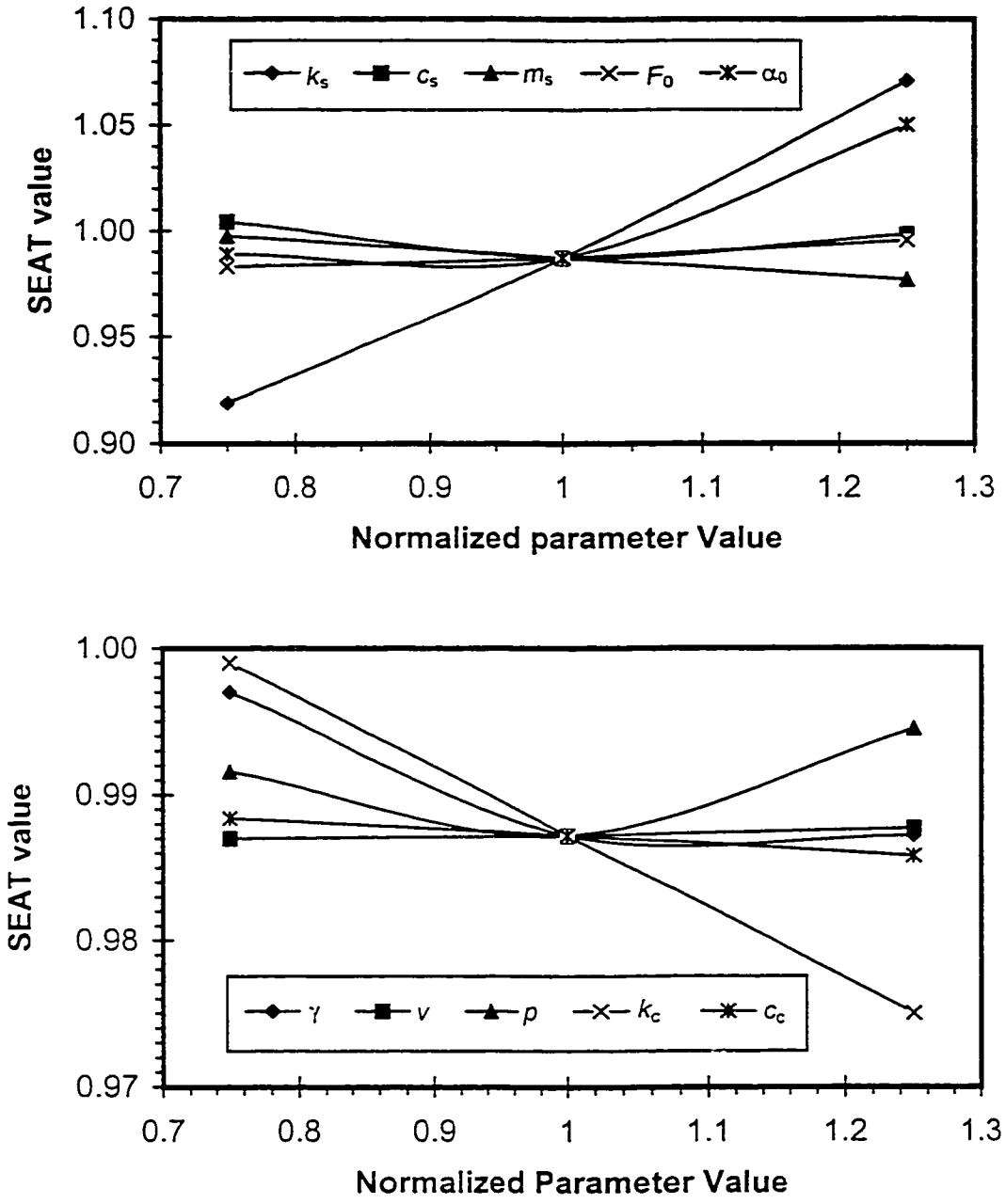

Figure 6.16: The SEAT values as functions of normalized parameter values for Class I excitation spectrum.

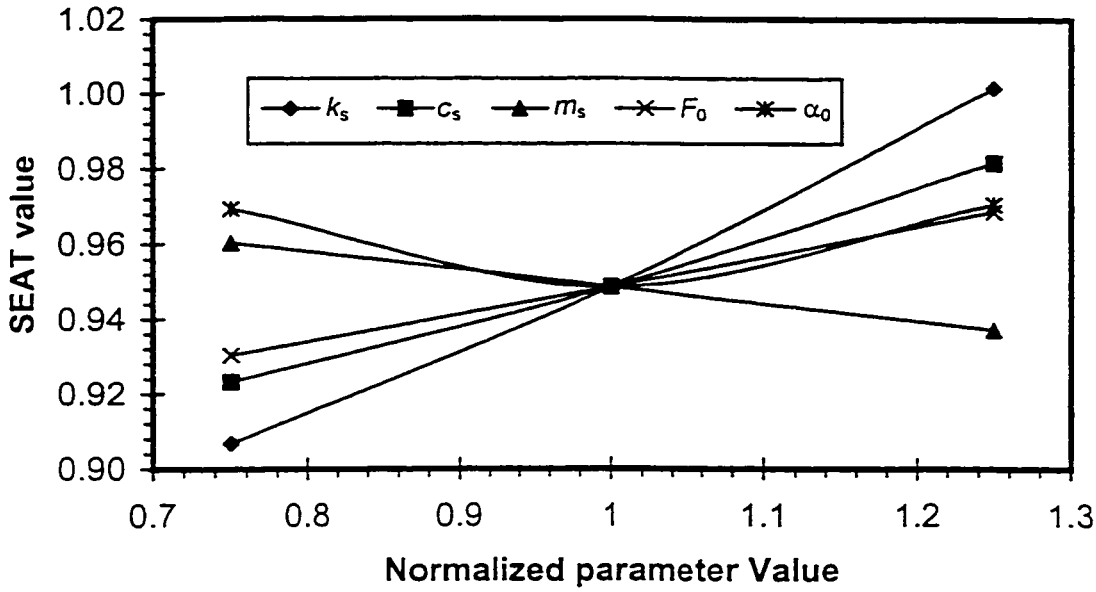

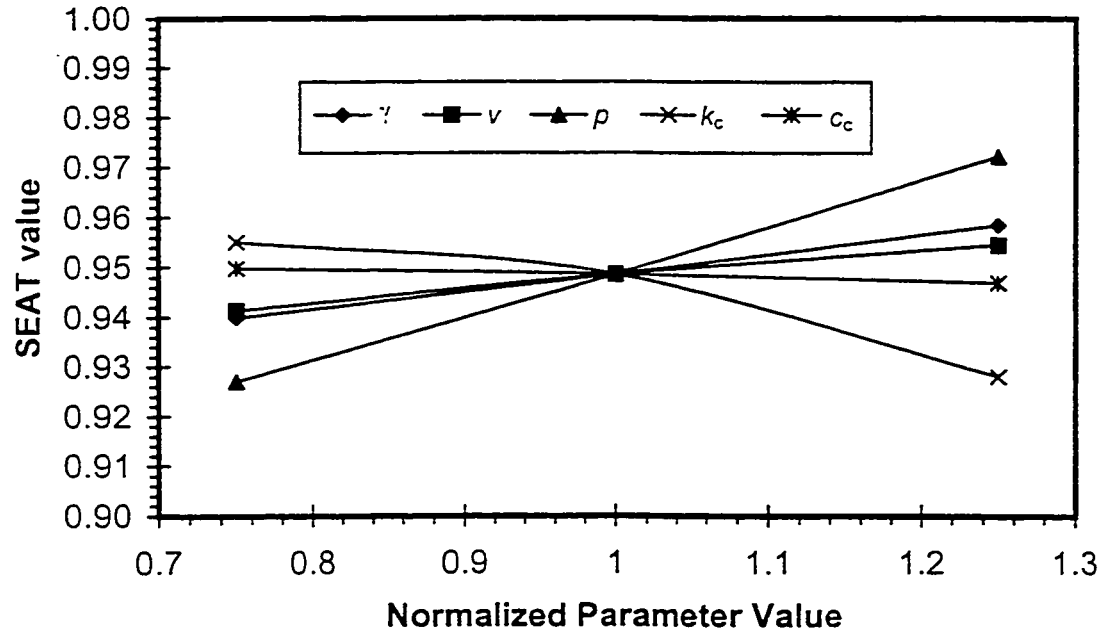

Figure 6.17: The SEAT values as functions of normalized parameter values for Class II excitation spectrum.

terms of percent change normalized with the nominal parameter value. The percentage variations in SEAT values attained for ±25% variations in the parameters are further summarized in Table 6.1. The variation in SEAT value caused by -25% change in a parameters is expressed as 100% to 75% SEAT value variation, and that caused by +25% change in a parameters is defined as 100% to 125% SEAT value variation, respectively:

$$100\%\text{ to }75\%\text{ SEAT value variation }(\%) = \frac{SEAT_{75\%} - SEAT_{100\%}}{SEAT_{100\%}} \times 100 \qquad (6.9)$$

$$100\%\text{ to }125\%\text{ SEAT value variation }(\%) = \frac{SEAT_{125\%} - SEAT_{100\%}}{SEAT_{100\%}} \times 100 \qquad (6.10)$$

where $SEAT_{75\%}$, $SEAT_{100\%}$ and $SEAT_{125\%}$ refer to the SEAT values corresponding to a parameter assuming 75%, 100% and 125% of its nominal values, respectively, while all other parameters assume their nominal values.

Table 6.1: Variation in SEAT value caused by parameter variations.

Excitation Classes	**Variation in parameters**	**Parameter variations**									
		k_s	c_s	m_s	F_0	α_0	γ_1 γ_2	ν_1 ν_2	p	k_{c1}	c_c
		Percentage change in SEAT value									
Class I	**100% to 75 %**	-6.9	1.7	1.0	-0.4	0.2	1.0	0.0	0.4	1.2	0.1
	100% to 125 %	8.5	1.1	-1.1	0.8	6.4	0.1	0.1	0.7	-1.2	-0.1
Class II	**100% to 75 %**	-4.4	-2.7	1.2	-1.9	2.2	-0.9	-0.8	-2.3	0.7	0.1
	100% to 125 %	5.6	3.5	-1.2	2.1	2.3	1.0	0.6	2.5	-2.2	-0.2

From both Figures 6.16 and 6.17, and Table 6.1, it can be observed that the influence of variations in most of the parameters on the SEAT value is similar under both

excitation spectra. The variations in a few parameters, however, yield contradictory influence on the SEAT value. The first group of these parameters includes the suspension spring stiffness k_s, Coulomb friction F_0 and transition velocities v_1 and v_2. An increase in those values causes an increase in the SEAT value, or worsened vibration attenuation performance. The second group of these parameters includes the suspension mass m_s, cushion linear stiffness k_c and damping coefficient c_c. An increase in values of these parameters causes a decrease in the SEAT values, or improved vibration attenuation performance. For both excitation spectra, both an increase and a decrease in the damper inclination angle α_0 from the nominal value cause higher SEAT values, which means that the nominal value of inclination angle α_0 may be near optimal for the excitation spectra considered.

Although for Class I excitation spectrum, both an increase and a decrease in the low speed compression damping coefficient c_s, reduction factors γ_1 and γ_2, and asymmetric factor p cause an increase in the SEAT value, which means that the nominal value of these parameters may be considered near optimal. An increase in these parameters of the suspension seat subject to Class II excitation, however, causes an increase in the SEAT value. An examination of the acceleration transmissibility characteristics related with the last three parameters (Figures 6.6, 6.7 and 6.10) suggests that an increase in their values suppress the transmissibility magnitude at resonance, and increase the transmissibility magnitude at frequencies above 2 Hz. Since Class II excitation spectrum exhibits a higher peak frequency (2.15 Hz) compared to Class I excitation spectrum (1.85 Hz), Class II excitation spectrum is more likely to be in the attenuation region of the human-suspension seat system. For Class I excitation spectrum,

benefits derived from lower values of last three parameters, resulting in low acceleration magnitude at above 2 Hz, may outweigh the vibration attenuation loss near the resonant frequency. The results show that SEAT values range from approximately 0.92 to 1.07 and 0.91 to 1.00 under Class I and II excitations, respectively, for all the variations considered. These SEAT values reflect poor vibration attenuation performance under these classes of excitation.

The sensitivity of the overall suspension seat to variations in a given parameter can be conveniently derived from the percentage change in SEAT value. For Class I excitation spectrum, suspension spring stiffness k_s, suspension mass m_s and cushion linear stiffness k_{c1}, are among the parameters which pose significant influence on the SEAT values. The low speed compression damping coefficient c_s, asymmetric factor p, Coulomb friction F_0 and damper inclination angle α_0 are further added to the above list of parameters, which show significant influence on the SEAT value under Class II excitation spectrum. The variations in reduction factors γ_1 and γ_2, transition velocities v_1 and v_2, and cushion damping coefficient c_c are considered to have insignificant influence on the SEAT values under both classes of excitation spectra.

6.6 Optimization of Suspension Seat Parameters under Steady-State Vibration Excitations

The attenuation of steady-state vibration and transient or shock-type excitation poses contradictory design requirements for the suspension seats. While the steady-state vibration isolation performance of a suspension seat mostly relates to the suspension seat parameters, the attenuation of shock-type excitation is mostly affected by the limited suspension travel and properties of the end-stop buffers. The attenuation of shock

excitations can be ideally attained through relaxation of the free travel and/or with design of adequately damped stiff suspension. Such design variations, however, will significantly deteriorate the suspension performance under continuous excitations. In view of such contradictory design requirements, design optimization in this study is attempted in two sequential stages. In the initial stage, optimal suspension seat parameters are derived by minimizing the SEAT value under a given vibration excitation, and limiting the relative suspension displacement within the free travel of the suspension mechanism. These optimal suspension seat parameters are further employed as fixed parameters in the second stage, where the end-stop buffer characteristics are optimized by minimizing the VDV ratio under high level vibration excitations, which cause successive end-stop impacts. This approach is expected to provide an optimal design to yield improved isolation of vibration and reduced severity of impacts under high magnitude transient excitations. It should be noted that the vibration spectra of most vehicles comprise of continuous vibration arising from tire-terrain interactions with occasional high magnitude jolts caused by sudden unevenness in the terrain. Such a design methodology is thus considered appropriate, which will ensure optimal isolation of continuous vibration encountered during most of the operation, and reduced frequency and severity of occasional impacts.

6.6.1 Formulation of optimization problem

From the results of the parametric study, presented in Section 6.5, it is apparent that suspension spring stiffness k_s, low speed compression damping coefficient c_s, suspension mass m_s, Coulomb friction F_0, damper inclination angle α_0, asymmetric factor

p, and cushion linear stiffness k_{c1}, affect the suspension performance in the most considerable manner. The optimization problem for suspension seat parameters under steady-state vibration excitations is thus formulated to include these design parameters. The optimization problem is formulated to minimize the SEAT value, and expressed as:

$$U(\chi) = \text{minimize}[\ \text{SEAT}] \tag{6.12}$$

where $U(\chi)$ is the objective function and χ is the vector of parameters to be optimized, given by:

$$\chi = \{k_s, c_s, m_s, F_0, \alpha_0, p, k_{c1}\}^T \tag{6.13}$$

where 'T' designates the transpose. The optimal vibration isolation or SEAT values under steady-state vibration attenuation can be attained by limiting the dynamic suspension deflection within its free travel. The optimization function is thus subject to the following constraint:

$$|z_s| \leq \beta d \tag{6.14}$$

where z_s is the suspension relative displacement response, d is half the free travel of the suspension, and a scaling factor $\beta \leq 1.0$ is introduced to ensure that the impacts with the end-stop buffers do not occur under continuous vibration.

Apart from the above constraint, limit constraints are imposed on the design parameters, to achieve more feasible optimal solutions. The suspension stiffness k_s and low speed compression rebound damping coefficient c_s are limited by their nominal values to prevent the convergence to very high values, which may produce near unity transmissibility and SEAT values. The suspension stiffness k_s is limited to a lower limit of 2000 N/m to ensure somewhat realistic spring rate of the suspension. The suspension mass is limited to an upper value of 20 kg to limit the total weight of the optimal

suspension seat. The inclination angle of the hydraulic damper is limited to values below 85^0 and above 45^0. The value of F_0 is limited to a maximum value of 25 N to ensure availability of maximum travel. Finally, an upper limit of cushion linear stiffness is imposed to provide reasonable pressure distribution, while a lower limit is provided to prevent the resonance of the human-cushion subsystem to occur at a frequency in the vicinity of the resonant frequency of the human-suspension seat system. The limit constraints posed on the design parameters are summarized below:

$$2000 \leq k_s \leq 5330 \text{ N/m}$$
$$0 \leq c_s \leq 892 \text{ Ns/m}$$
$$1 \text{ kg} \leq m_s \leq 20 \text{ kg}$$
$$45^0 \leq \alpha_0 \leq 85^0$$
$$p \geq 1$$
$$0 \leq F_0 \leq 25 \text{ N}$$
$$5\times10^4 \leq k_{c1} \leq 1\times10^5 \text{ N/m}$$

6.6.2 Results

The constrained optimization problem was solved using the MATLAB software. The optimization was performed with different values of starting design vector, and the resulting function values were examined to identify the existence of a global optimum. The results of various solutions revealed convergence to similar design vector. It should be noted that the excitation signals (Class I and Class II) used in the optimization study were generated from narrow-band excitation spectra representing the motions of specific vehicles. Both classes of excitations reveal near-Gaussian amplitude distributions, with crest factor ranging from 3.2 to 3.9. Actual vehicle floor motions often include occasional high accelerations with crest factors ranging from 4.3 for a tractor operating on a farm road

to 8.5 for a hay turning tractor [1]. The occasional high accelerations cause large magnitude relative displacement of the seat suspension. The relative displacement response is thus constrained to be well below the available free travel to account for relatively low crest factors of the synthesized excitation signals. The relative displacement is constrained by selecting β=0.8. The results of the optimisation study under Class I and II excitations are summarised in Table 6.2.

Table 6.2: Optimal parameters under the excitations of Class I and Class II spectra.

Parameters	k_s (N/m)	c_s (Ns/m)	m_s (kg)	α_0 (degrees)	p	F_0 (N)	k_{c1} (N/m)
Nominal	5330	892	10	70	1.47	15	82300
Optimal for Class I	3605	531	20	72	1.2	0	100000
Optimal for Class II	2000	0	20	-	-	0	100000
Recommended	3600	530	20	70	1.2	15	100000

It can be observed that for both excitation spectra, suspension mass m_s and cushion linear stiffness k_{c1} converge to their upper limits, while Coulomb friction F_0 converges to its lower limit, to allow for maximum vibration attenuation. For Class I spectrum, the optimal values of suspension spring stiffness k_s, low speed compression damping coefficient c_s and asymmetry factor p are lower than the respective nominal values. Although Table 6.1 shows that under Class I excitation spectrum a decrease in low speed compression damping coefficient c_s causes an increase in SEAT value for the nominal parameters, the significantly lower value of spring rate k_s tends to shift the resonant frequency well below the dominant frequency of Class I excitation spectrum. A lower value of c_s is thus attained to achieve effective attenuation of such vibration energy. The optimal damper inclination α_0 is also observed to be close to its nominal value. The

solution of the optimization problem is most significantly affected by the relative displacement constraint, expressed in Equation (6.14). The convergence achieved corresponds to the limiting value of the allowable relative motion for Class I excitation. The optimization under Class II excitation, however, converges to lower limits of k_s and c_s, where the peak relative travel remains below βd. The convergence to such values is due to relatively lower level and higher frequency excitation of Class II excitation spectrum. The c_s value converges to zero, due to relatively low excitation in the vicinity of suspension resonance. This suggests that the suspension seat can be designed to provide excellent vibration attenuation performance without causing any end-stop impacts under this excitation class. Since the results of optimization suggest that a damper is not needed for the vibration attenuation of Class II spectrum, the corresponding optimal asymmetry factor p and damper inclination α_0 are not relevant. Since the Class I excitation exhibits a lower central frequency and higher peak value of acceleration PSD than the Class II excitation, the suspension needs to be designed with relatively stiffer spring and heavier damping to limit the relative displacement within the permissible travel. The resulting SEAT value is thus considerably higher than that observed under Class II excitation.

Since the Class I vibration excitation is more severe among the two classes considered, the optimal parameters obtained corresponding to Class I excitation are recommended for the optimal seat design, as listed in Table 6.2. Although the solution converges to zero value of Coulomb friction force, a value of 15 N is recommended to account for friction inherent to the linkages and pin joints. This recommended design vector is considered as optimal parameter vector in the investigation of suspension seat

end-stop impacts, to be performed in Chapter 7. The SEAT values corresponding to the nominal, optimal and recommended parameter values under the two excitation classes are illustrated in Figure 6.18. The optimal parameter values can be observed to reduce the SEAT values significantly from those obtained using the nominal values. It can be observed that the optimal design yields a SEAT value of 0.73 under Class I excitation, which is 26% lower than that obtained with nominal design. The optimal design under Class II excitation yields a SEAT value of 0.3, which is 68% lower than that obtained from the nominal design (0.95). The optimal design attained under Class II excitation, however, can not be considered adequate due to the associated undamped and extremely soft suspension. Such a suspension will yield excessively high levels of vibration under occasional transient motions. It is thus recommended to adapt the optimal parameters attained under Class I excitation. This recommended design vector, however, yields SEAT value, which is significantly higher than that obtained for the optimal design under Class II excitation. Figure 6.18 illustrates that the SEAT value of the recommended design is nearly 120% larger than the optimal, but nearly 30% lower than that of the nominal design. Under Class I excitation, the recommended design, however, yields SEAT value similar to that obtained for the optimal design. The suspension seat designed using the recommended parameter values may be implemented in vehicles with floor vibration spectra similar to those defined in Class I and Class II excitation.

6.7 Summary

A comprehensive parametric study is performed to quantify the influence of various parameters on the overall vibration attenuation performance of the coupled

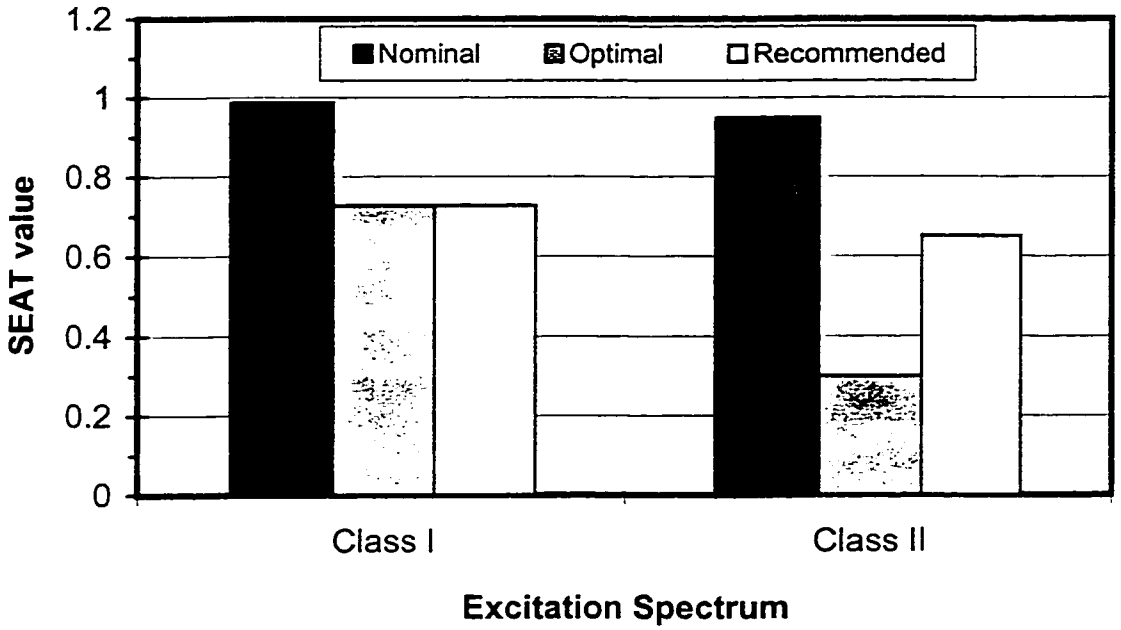

Figure 6.18: SEAT values as functions of nominal, optimal and recommended parameters under two excitation classes.

human-suspension seat system, in terms of both the vibration transmissibility and SEAT value. Under the two classes of excitations defined in this chapter, suspension spring rate, low speed compression damping coefficient, suspension mass, Coulomb friction, shock absorber inclination angle, asymmetry factor and cushion linear stiffness were found to be the factors, which most significantly influence the steady-state vibration attenuation performance. Optimization techniques are employed to derive the optimal values of these parameters, through minimizing the SEAT value and limiting the relative displacement of the suspension within its free travel. A set of recommended design parameters is derived, from the optimal design vectors obtained under two classes of excitation. The proposed design vector is considered as the optimal design vector for attenuation of steady-state vibration in vehicles with floor vibration spectra similar to those defined in Class I and Class II excitation. These parameter values will be further used in Chapter 7 to optimize the end-stop buffer characteristics under vibration excitations of large magnitudes.

CHAPTER 7

ANALYSIS OF DRIVER SUSPENSION SEAT SYSTEM UNDER END-STOP IMPACTS

7.1 Introduction

It is believed that severe shocks and vibration encountered by some off-road vehicle drivers may induce various disorders in the human body, particularly low back injury [1]. Although the intensity of these shocks and vibration transmitted to the driver can often be reduced by incorporating a properly adapted suspension seat, the end-stop impacts occurring under exposure to low frequency high magnitude motion may result in an increased risk of injury. Adjustments to the stiffness and damping of the suspension mechanism so as to minimize the occurrence of end-stop impacts may involve a compromise in the vibration isolation efficiency provided by the suspension under conditions where end-stop impacts do not occur.

There is currently no mandatory requirement or standard aimed at measuring the performance of a suspension seat, when end-stop impacts occur. In current seat designs, it is common to use rubber end-stop buffers to limit the suspension displacement to within a fixed clearance. Some of these seats, however, use relatively hard buffers, which result in high magnitude shocks during end-stop impacts. The optimization of suspension seats should thus involve recognition that both the motions transmitted to the human body caused by terrain roughness and also the shocks arising from end-stop impacts are relevant to the health of drivers. The vibration dose value is used to provide guidance on exposures to vibration or shocks that may cause injury, or when the excitations due to terrain roughness are characterized by a crest factor value larger than 9. A VDV ratio has

been defined in Chapter 6 to evaluate the dynamic performance of suspension seats when end-stop impacts occur.

In this chapter, the effects of end-stop buffer force-deflection characteristics and buffer hysteresis on end-stop impacts are investigated be means of analysis and optimization techniques, using the coupled human-suspension seat model developed in Chapter 5. The optimal buffer force-deflection characteristics and buffer thickness are examined under both sinusoidal and random excitations of different magnitudes. The general guidance of buffer design is recommended on the basis of the above analysis.

7.2 Optimization Methodology

It has been illustrated in Figure 6.1 that a suspension seat subject to high magnitude vibration excitation can induce high magnitude of resonant acceleration transmissibility due to end-stop impacts. Such impacts may also cause possible loss of contact between the driver and seat. The attenuation of continuous vibration, however, is considered to be of utmost importance, since the vehicle-terrain interactions yield ride vibration of such nature over majority of the operations. The suspension seat design is thus optimized in Chapter 6, under vibration excitation of two different classes of vehicles. The recommended optimal design, however, does not incorporate the transmission of vibration due to occasional end-stop impacts. The proposed design thus can not be considered truly optimal, since the realistic vibration environment of a vehicle comprises both continuous vibration of low crest factors, and high magnitude transient vibration. An analysis of the optimal suspension seat subject to excitation levels that are twice the magnitude of Class I excitation revealed that the SEAT value of the 'optimal'

suspension seat increases from its optimal value of 0.73 to 2.24. The significant deterioration of the suspension seat performance is primarily attributed to the occurrence of end-stop impacts. It is therefore necessary to further optimize the buffer design to improve the overall performance of the seat.

A second stage optimization study is thus performed with an objective to minimize the VDV ratio, by reducing the severity of end-stop impacts. The relative displacement of a suspension seat, in general, is constrained by physical limits described by the geometry of the suspension and end-stop buffers. The suspension travel between the free thickness of end-stop buffers is defined as its free travel. For a given buffer thickness, the optimization problem can be defined as to select the proper buffer force-deflection characteristics to minimize the VDV ratio of the seated body with respect to a given vibration excitation. The optimization may thus be expressed as:

$$U(\chi) = \text{minimize}[VDV\ ratio]$$
$$\text{subject to } |z_s| \le \frac{d_m^{(t)} + d_m^{(b)}}{2} \tag{7.1}$$

where $U(\chi)$ is the objective function, and $d_m^{(t)}$ and $d_m^{(b)}$ are the suspension travel limits corresponding to compression of the buffers, as described in Figure 5.5. χ is the vector of design parameters. The design optimization in the second stage is attempted to derive the buffer parameters only, while the suspension parameters are taken as the recommended values to ensure optimal vibration isolation. The design vector in Equation (7.1) may include various stiffness coefficients due to top and bottom buffers ($k_{bi}^{(t)}$ and $k_{bi}^{(b)}$, i=1 to 4), hysteresis properties ($h^{(t)}$ and $h^{(b)}$) and the effective travel determined from the thickness of the buffers ($2d$). The optimization problem thus involves a large number of nonlinear design parameters, given by:

$$\chi = \left\{ k_{b1}^{(b)}, k_{b2}^{(b)}, k_{b3}^{(b)}, k_{b4}^{(b)}, h^{(b)}, k_{b1}^{(t)}, k_{b2}^{(t)}, k_{b3}^{(t)}, k_{b4}^{(t)}, h^{(t)}, d \right\}^T \quad (7.2)$$

The contributions due to various parameters are carefully examined to derive a reduced design vector comprising the most significant parameters. The influence of various design parameters on the VDV ratio is investigated under harmonic excitation near the resonant frequency of the coupled human-suspension seat system. Such an excitation of varying magnitudes is considered to represent the most severe situation that will most likely cause repetitive impacts against the end-stop buffers. The contributions due to various parameters are investigated upon considering the set of recommended design parameters, listed in Table 6.2, for achieving optimal vibration isolation. The remaining design parameters are considered to assume their former nominal values. Table 7.1 summarizes the above parameters, considered as the nominal values for the study of end-stop impacts.

7.3 Influence of Hysteresis due to End-Stop Buffers on the VDV Ratio

The severity and frequency of end-stop impacts have been directly related to the magnitude and frequency contents of the excitations. The elastic and hysteretic properties, and the allowable travel of a suspension seat also affect the severity of the resulting impacts. It has been established that a lightly damped suspension is highly desirable to achieve improved vibration isolation. Such lightly damped suspension, however, yields more frequent and severe end-stop impacts under high magnitude excitation due to the associated high dynamic relative displacement response. High suspension damping is thus considered desirable to dissipate vibration energy associated with shock motions.

Table 7.1: Nominal parameter values considered for study of end-stop impacts performance.

Description		Symbol	Value
Cushion	Static Load (N)	F_{c0}	5.27×10^{2}
	Static deflection (m)	y_0	2.5×10^{-2}
	Linear stiffness (N/m)	k_{c1}	1.0×10^{5}
	Cubic stiffness (N/m^3)	k_{c3}	2.1×10^{8}
	Deflection threshold of bottoming (m)	y_1	3.8×10^{-2}
	Cushion damping (Ns/m)	c_c	300
	Coefficient (N)	a_1	1.374×10^{3}
	Coefficient (m^{-1})	a_2	-80.782
	Coefficient	a_3	0.4488
	Coefficient (N)	a_4	1.374×10^{3}
Damper	Low speed compression damping coefficient (Ns/m)	c_s	530
	Compression damping reduction factor	γ_1	0.43
	Rebound damping reduction factor	γ_2	0.53
	Compression transition velocity (m/s)	v_1	1.12×10^{-2}
	Rebound transition velocity (m/s)	v_2	-3.32×10^{-2}
	Asymmetry factor	p	1.2
	Inclination angle (degrees)	α_0	70
End-stop buffers	Total free travel between end-stop buffers (m)	$2d$	0.1
	Compression travel limit (m)	$d_m^{(b)}$	0.06
	Rebound travel limit (m)	$d_m^{(t)}$	0.06
	Bottom buffer loading linear stiffness (N/m)	$k_{b1}^{(b)}$	1.2×10^{5}
	Bottom buffer loading cubic stiffness (N/m^3)	$k_{b2}^{(b)}$	1.3×10^{9}
	Bottom buffer unloading linear stiffness (N/m)	$k_{b3}^{(b)}$	1.8×10^{5}
	Bottom buffer unloading cubic stiffness (N/m^3)	$k_{b4}^{(b)}$	2.1×10^{9}
	Bottom buffer hysteresis displacement lag (m)	$h^{(b)}$	2.0×10^{-3}
	Top buffer loading linear stiffness (N/m)	$k_{b1}^{(t)}$	1.0×10^{5}
	Top buffer loading cubic stiffness (N/m^3)	$k_{b2}^{(t)}$	1.5×10^{9}
	Top buffer unloading linear stiffness (N/m)	$k_{b3}^{(t)}$	1.2×10^{5}
	Top buffer unloading cubic stiffness (N/m^3)	$k_{b4}^{(t)}$	3.0×10^{9}
	Top buffer hysteresis displacement lag (m)	$h^{(t)}$	2.0×10^{-3}
Others	Suspension spring stiffness (N/m)	k_s	3.6×10^{3}
	Suspension sprung mass (kg)	m_s	20
	Coulomb friction force (N)	F_0	15

The high vibration energy may also be dissipated by hysteresis due to the elastic end-stop buffers, which would ensure optimal suspension performance in terms of vibration isolation. The coupled human-suspension seat model is analyzed for elastic buffers with zero and maximum hysteresis to explore the potential for such hysteresis to reduce the severity of end-stop impacts. It should be noted that maximum hysteresis represents an extreme situation, involving dissipation of the entire energy absorbed by the buffer. The maximum hysteresis is realized by letting the unloading forces approach zero, such that the entire energy absorbed by the buffer is dissipated. Equations (5.6) to (5.8), describing the force-deflection properties of top and bottom buffers, can thus be simplified as:

$$F_b = \begin{cases} 0; & \text{for } |z_s| \le d \\ k_{b1}^{(b)}(z_s - d) + k_{b2}^{(b)}(z_s - d)^3; & \text{for } z_s > d \text{ and } \dot{z}_s > 0 \\ 0; & \text{for } z_s > d \text{ and } \dot{z}_s < 0 \\ k_{b1}^{(t)}(z_s + d) + k_{b2}^{(t)}(z_s + d)^3; & \text{for } z_s < -d \text{ and } \dot{z}_s < 0 \\ 0; & \text{for } z_s < -d \text{ and } \dot{z}_s > 0 \end{cases} \tag{7.3}$$

where $k_{b1}^{(b)}$ and $k_{b2}^{(b)}$ are the linear and cubic stiffness coefficients of the bottom buffer during loading, respectively; and $k_{b1}^{(t)}$ and $k_{b2}^{(t)}$ are the linear and cubic stiffness coefficients of the top buffer during loading, respectively.

The zero hysteresis due to a buffer is realized by letting the unloading forces equal to the loading forces, such that the buffer does not dissipate any energy. Equations (5.6) to (5.8) are thus simplified as:

$$F_b = \begin{cases} 0; & \text{for } |z_s| \le d \\ k_{b1}^{(b)}(z_s - d) + k_{b2}^{(b)}(z_s - d)^3; & \text{for } z_s > d \\ k_{b1}^{(t)}(z_s + d) + k_{b2}^{(t)}(z_s + d)^3; & \text{for } z_s < -d \end{cases} \tag{7.4}$$

The resulting VDV ratio with the zero and maximum hysteresis are evaluated and compared as a function of harmonic excitation magnitudes, as illustrated in Figure 7.1. The results show a constant VDV ratio of 1.7 for excitation magnitudes ranging from 0.7 to 1.25 m/s^2 rms. This high value of VDV is attributed to the excitation near the resonant frequency of the coupled human-suspension seat system. The VDV ratio increases rapidly to a value above 5.0 due to occurrence of end-stop impacts under excitation magnitudes exceeding 1.25 m/s^2 rms. The extreme buffer hysteresis yields only slightly lower values of VDV ratio over the entire range of excitation magnitude. The elastic buffers, in general, offer low hysteresis rate, and thus relatively negligible potential for reducing the severity of suspension seat end-stop impacts. It can thus be concluded that the severity of end-stop impacts can not be significantly reduced through hysteretic properties of passive buffers. High end-stop damping, however, may be realized through semi-active and active control of an electro-rheological fluid damper. The performance of such an actively controlled end-stop damper in reducing the severity of impacts has been shown to be promising [88].

In view of the negligible contribution due to hysteresis, the simplified force-deflection characteristics of the nonlinear buffer, described in Equation (7.4), may be considered appropriate. This simplification eliminates the consideration of stiffness coefficients $k_{b3}^{(t)}$, $k_{b4}^{(t)}$, $k_{b3}^{(b)}$ and $k_{b4}^{(b)}$, associated with the unloading curve, and the hysteresis coefficients $h^{(t)}$ and $h^{(b)}$.

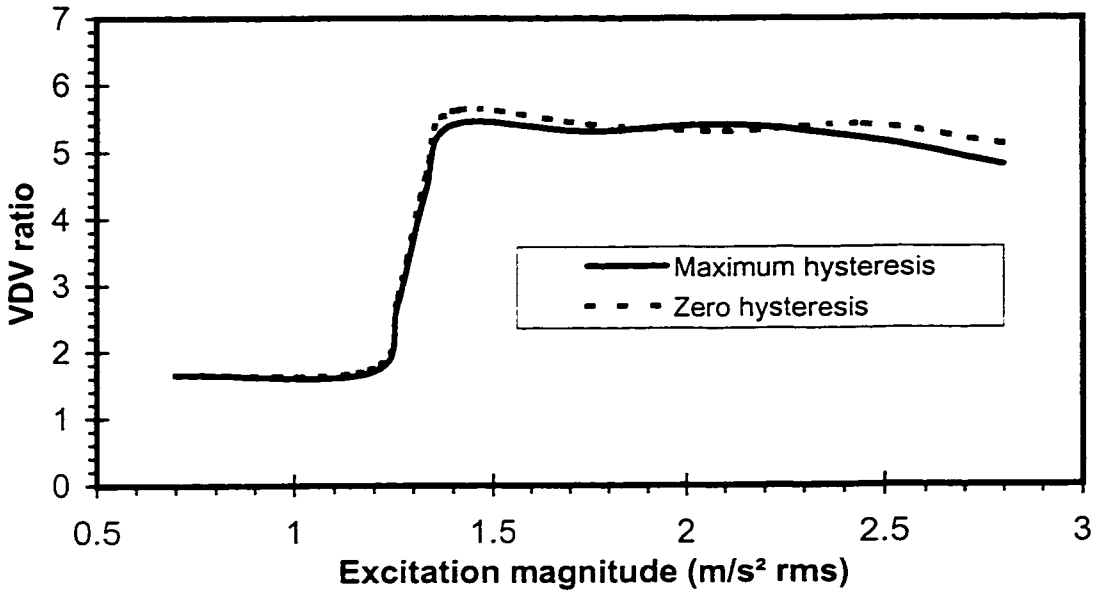

Figure 7.1: The influence of buffer hysteresis on the VDV ratio.

7.4 Design Optimization for Minimizing End-Stop Impacts

The optimization problem, described in Equation (7.1), is solved using the force-deflection relationship for end-stop impacts. The force-deflection characteristics of the buffers are further simplified by assuming symmetric behavior due to compression (bottom) and extension (top) buffers. The force-deflection characteristics are thus simplified by letting $k_{b1}^{(t)}=k_{b1}^{(b)}=k_{b1}$ and $k_{b1}^{(t)}=k_{b1}^{(b)}=k_{b1}$, such that:

$$F_b = \begin{cases} 0; & \text{for } |z_s| \le d \\ k_{b1}(z_s - d) + k_{b2}(z_s - d)^3; & \text{for } z_s > d \\ k_{b1}(z_s + d) + k_{b2}(z_s + d)^3; & \text{for } z_s < -d \end{cases} \tag{7.5}$$

where k_{b1} and k_{b2} are the linear and cubic stiffness of both the top and bottom buffers, respectively. The top and bottom buffers are also considered to yield identical maximum deflection, which is related to their thickness. Considering $d_m^{(t)}=d_m^{(b)}=d_m$, the optimization problem defined in Equation (7.1) may be expressed as:

$$\begin{aligned} U(\chi) &= \text{minimize}[VDV\ ratio] \\ &\text{subject to } |z_s| \le d_m \end{aligned} \tag{7.6}$$

where the design vector includes only linear and cubic stiffness coefficient of the elastic buffers and suspension free travel, given by:

$$\chi = \{k_{b1}, k_{b2}\}^T \tag{7.7}$$

It should be noted that the maximum possible travel d_m comprises half the free travel of the suspension (d) and the buffer thickness T_b (i.e. $d_m=d+T_b$). In current suspension design, the free travel and the buffer thickness are limited to ensure adequate control by the driver. A lower value of free travel may cause more frequent impacts, while a larger free travel will cause larger magnitude of relative motion of the driver. In the study, two different values of free travel are selected (d = ±40 and d = ±50 mm),

which conform with most modern suspension designs. This results in two different buffer thickness (20 and 10 mm) to achieve the nominal maximum possible travel of $d_m = \frac{d_m^{(t)} + d_m^{(b)}}{2} = 60\,\text{mm}$.

7.5 VDV Ratio of Optimal Buffers

The performance characteristics of human-suspension seat with optimal end-stop buffers are investigated under harmonic excitations of varying magnitudes at a frequency of 1.3 Hz. The influence of optimal buffer stiffness attained under different levels of excitations on the VDV ratio is initially investigated. For the nominal free travel (± 50 mm), which corresponds to buffer thickness of 10 mm, the optimum buffer force-deflection curves are illustrated in Figure 7.2 under different excitation magnitudes. An increase in excitation magnitude (1.4 to 2.8 m/s^2 rms) requires an increase in the optimal buffer stiffness. In other words, a stiffer buffer is needed to prevent the suspension from exceeding the constrained possible maximum travel, when the excitation magnitude is increased. The results further show that the optimal buffers utilize the maximum available travel (d_m=60 mm) to reduce the severity of impacts.

The influence of variations in the free travel (or buffer thickness) on the force-deflection characteristics of the buffers is further illustrated in Figure 7.3 under an excitation magnitude of 1.4 m/s^2 rms acceleration. The results show that an increase in buffer thickness (from 10 mm to 20 mm) causes a decrease in the optimal buffer stiffness. A thicker and softer buffer is thus considered desirable to reduce the severity of impacts by transmitting relatively lower magnitude of buffer forces to the suspension mass.

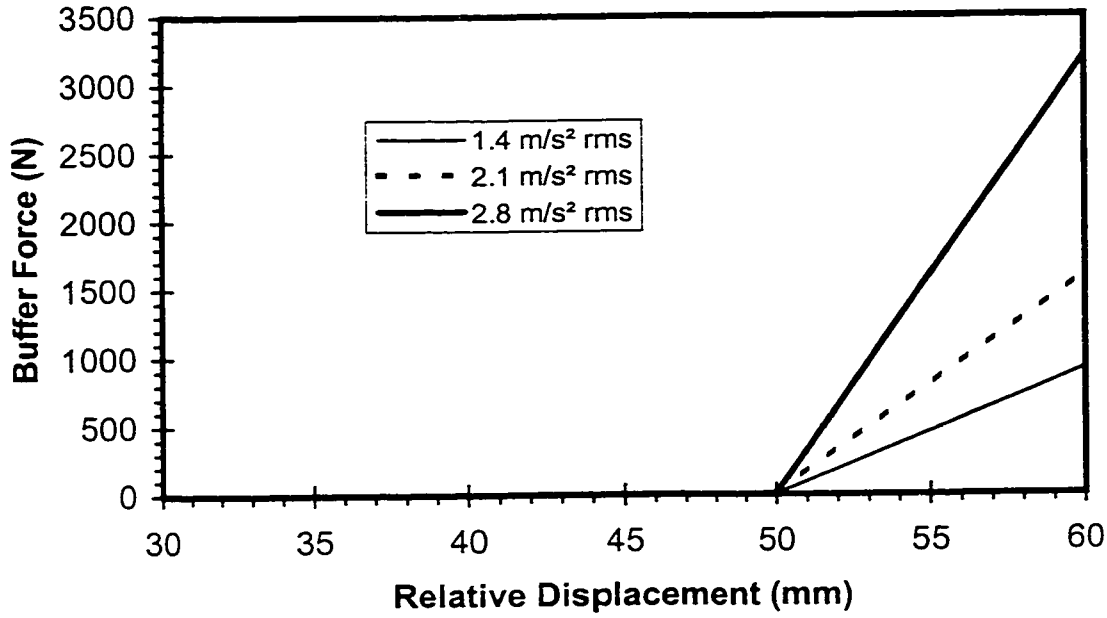

Figure 7.2: The optimum buffer force-deflection curves under various excitation amplitudes ($2d$=100 mm).

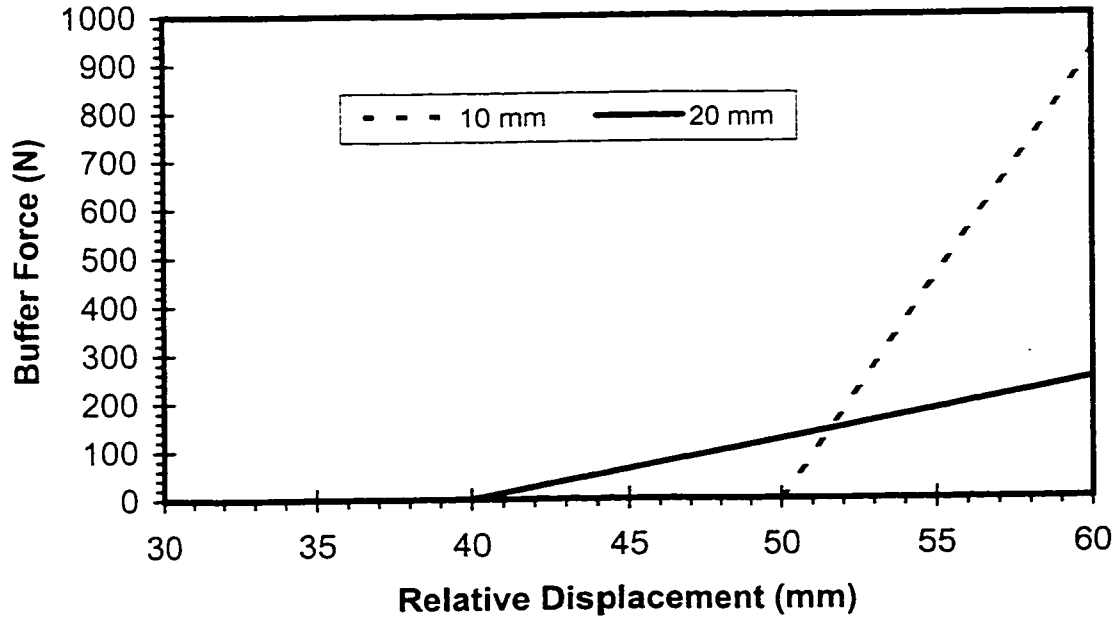

Figure 7.3: The optimum buffer force-deflection curves for various suspension free travels under a given excitation amplitude (1.4 m/s² rms).

Upon recognizing the significant influence of excitation magnitude on the optimal stiffness values, the optimization problem is further solved for a wide range of excitation magnitudes, ranging from 0.7 to 2.8 m/s^2 rms acceleration. The corresponding optimal stiffness values are used to demonstrate the influence of excitation magnitude and buffer thickness on the VDV values. It has been observed that the optimal buffers always possess only a linear stiffness coefficient, while the cubic stiffness coefficient converges to zero, irrespective of the buffer thickness and excitation magnitude. The optimization study thus suggests that linear elastic buffers provide optimal VDV response, when contribution due to hysteresis are considered negligible. In all cases, the optimal solution converges to the lowest possible value of linear stiffness in order to minimize the severity of impacts. The buffers thus undergo their maximum deflection or full thickness, irrespective of the excitation magnitudes.

The VDV ratio and optimal linear buffer stiffness obtained as functions of the excitation magnitude are illustrated in Figures 7.4 and 7.5 for two values of buffer thickness. The results show that excitation magnitudes lower than 1.2 m/s^2 rms acceleration do not cause end-stop impacts. The suspension operates within its free travel leading to nearly constant VDV ratio for different thickness values of the buffers, as shown in Figure 7.4. The absence of end-stop impacts is further shown in Figure 7.5, where the corresponding optimal buffer thickness is shown to be zero. An increase in excitation magnitude from 1.2 to 1.3 m/s^2 causes a considerable increase in the VDV ratio for a buffer thickness of 20 mm. This considerable increase in the VDV ratio occurs at a slightly higher excitation magnitude, from 1.3 to 1.4 m/s^2, for the thinner buffer (10 mm thickness). The results thus show that end-stop impacts with thick buffer occur under

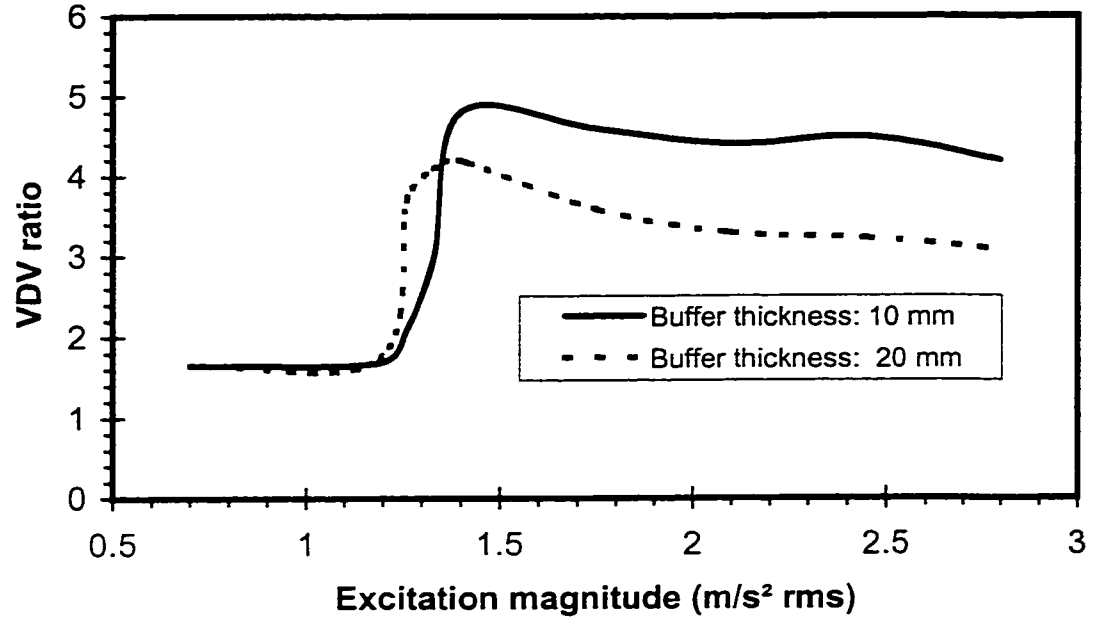

Figure 7.4: The optimal VDV ratio as functions of the input amplitudes.

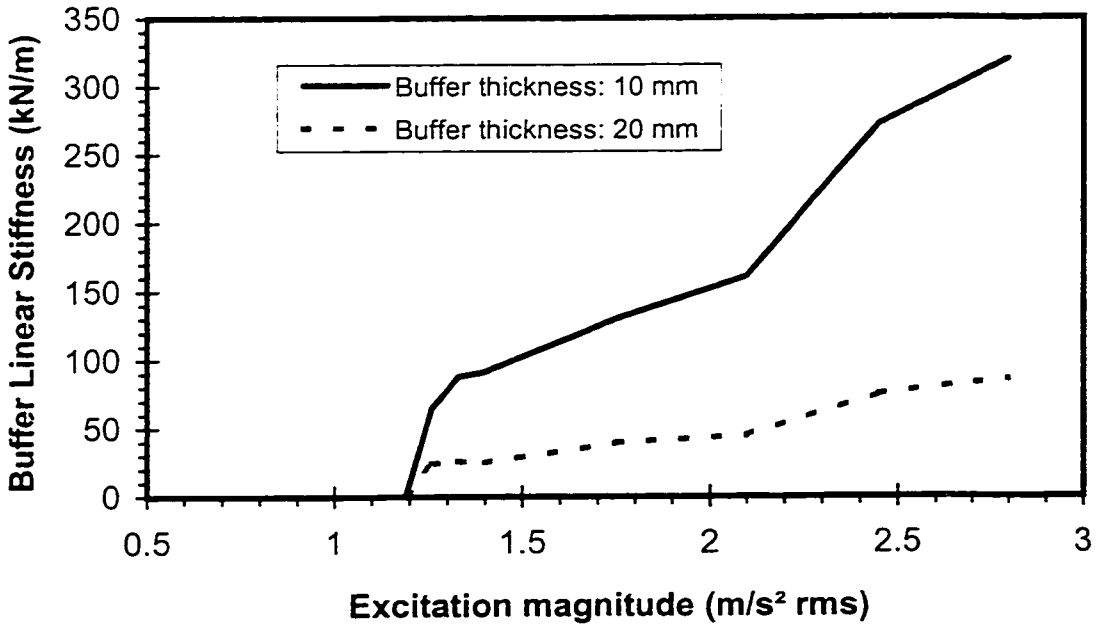

Figure 7.5: The optimum buffer linear stiffness as functions of the input amplitude.

a slightly lower excitation magnitude, due to reduced free travel. The corresponding optimal buffer stiffness, shown in Figure 7.5, suggests that a much lower stiffness is required for the thicker buffer to prevent severe end-stop impacts. When the excitation magnitude is greater than 1.3 to 1.4 m/s^2 rms, the VDV ratio decreases slightly for both values of buffer thickness. An examination of the time histories of body acceleration under different excitation magnitudes and buffer thickness, T_b=10 mm, illustrated in Figure 7.6, reveals that an excitation magnitude greater than 1.4 m/s^2 rms acceleration results in body hop motion. This body hop phenomenon induces slightly lower VDV ratio shown in Figure 7.4. The true VDV value derived from the body acceleration response, however, will continue to increase with an increase in excitation magnitude.

The results of the optimization study, presented in Figures 7.2 to 7.6, suggest that use of thick and soft buffers with linear stiffness characteristics can lead to lower VDV ratio response. Although thick buffers may cause more frequent impacts due to reduced travel, their low stiffness tends to reduce the severity of impacts considerably. The situations involving excessively high magnitudes of ride vibration necessitate high buffer stiffness to limit the deflection. The resulting severity of impacts may be reduced by relaxing the free suspension travel. Although the optimization study converges to linear stiffness properties, it may be desirable to introduce slightly progressively hardening properties, which is inherent in the elastic buffers. A very soft linear buffer may cause extremely higher impact forces under high excitation magnitude, when the suspension displacement tends to exceed the maximum travel or the linear range.

Very similar trends have been reported in an experimental study [23], in which a suspension seat was tested with different rubber buffers. The force-deflection properties

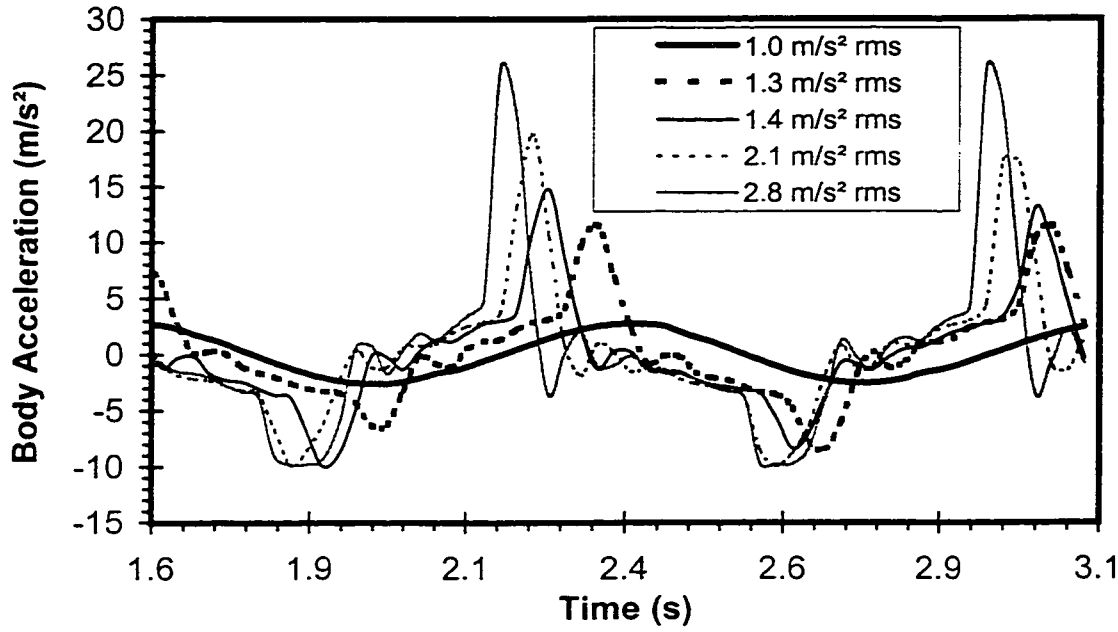

Figure 7.6: Time histories of body aceleration on the seat cushion under various input amplitude.

of two buffers, referred to as '*O*' and '*B*' are illustrated in Figure 7.7. The buffer '*O*' exhibits strongly non-linear progressively hardening force-deflection characteristics, and higher stiffness than buffer '*B*', which possesses nearly linear stiffness over a wide range of deflection. The thickness of buffer '*B*' is considerably larger than that of buffer '*O*'. The proposed buffers were fitted into a suspension seat with resonant frequency of 1.6 Hz and free travel of ±50 mm. The VDV ratio response of the seat fitted with two buffers, were evaluated experimentally, under different harmonic excitation magnitudes at the resonant frequency. Figure 7.8 illustrates the VDV ratio response of the seat incorporating two different buffers as a function of the excitation magnitudes. The results show the absence of end-stop impacts, when the excitation magnitude is less than 0.5 m/s^2 rms. The suspension mechanism seems to be locked up, resulting in a unity VDV ratio response. When the excitation magnitude is greater than 0.6 ms^{-2} rms, the VDV ratio increases significantly. The softer and thicker buffer '*B*' yields considerably lower VDV ratio than the thinner and stiffer buffer '*O*' under high excitation magnitudes.

7.6 Optimal Buffer Design under Random Excitations

The optimal elastic properties of the buffers, presented in the previous sections, were derived under resonant excitations of the suspension system. The excitations used thus represent the most severe type of excitation resulting in end-stop impacts. The ride vibration of most vehicles predominates in a frequency range, which is higher than the resonant frequency of the suspension. Although the results obtained from the optimization study yields considerable insight into the design of buffers, it is vital to investigate the optimal designs under more realistic vehicular vibration excitations.

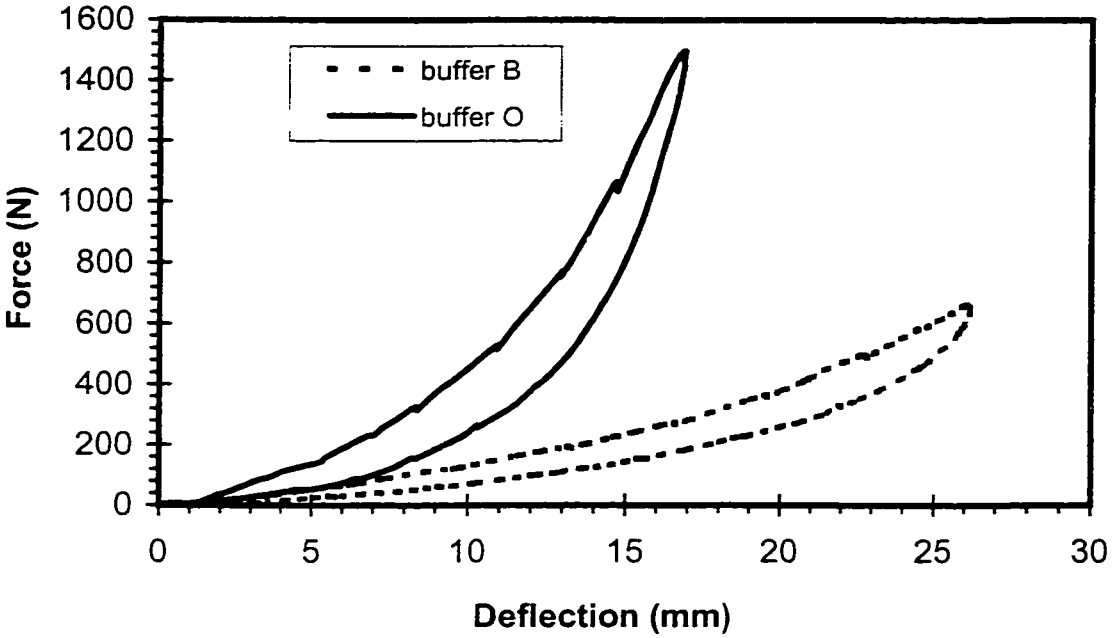

Figure 7.7: Force-deflection characteristics of end-stop buffers [23].

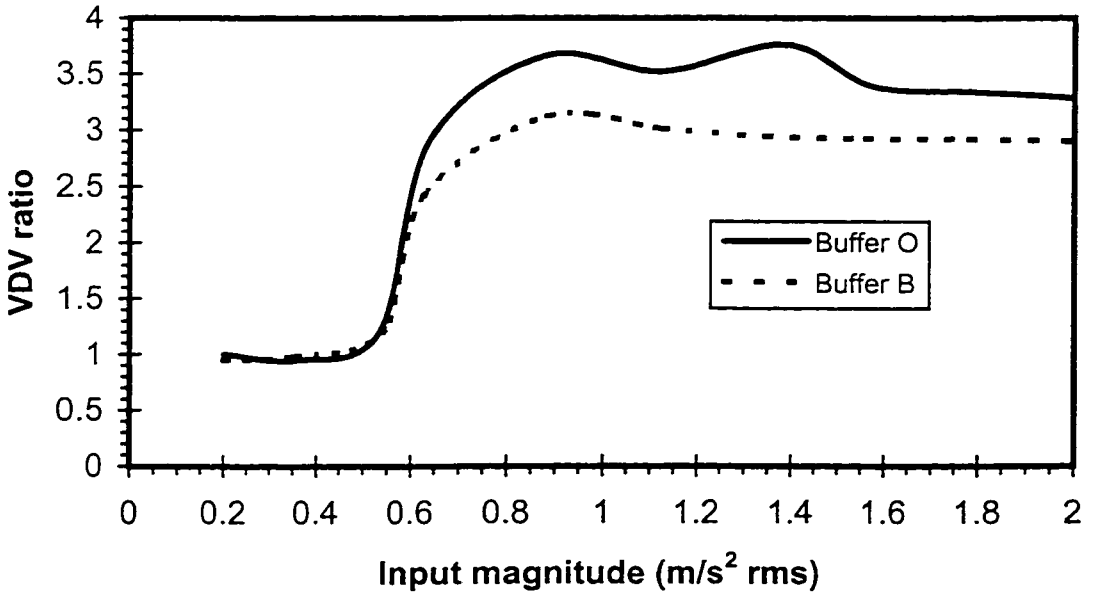

Figure 7.8: Effect of buffer force-deflection characteristics on VDV ratio [23].

From the results presented in Section 6.6, it is apparent that Class I excitation is more likely to cause end-stop impacts, due to its lower central frequency and higher magnitude than Class II spectrum. The optimization problem, derived in Equations (7.6) and (7.7), is thus solved under excitations arising from Class I spectrum. The synthesized Class I excitation, however, yields crest factors known to be considerably lower than those obtained from field measured data. The optimization is thus performed under three different excitation spectra, synthesized by amplifying the Class I excitation. The time histories of acceleration excitation are amplified by factors of 1.0, 1.5, and 2.0, to realize three different spectra. The optimization problem is solved to derive optimal values of k_{b1} and k_{b2} for two different values of free travel, ±50 and ±40 mm, corresponding to 10 and 20 mm thick buffers, respectively.

Similar to the sinusoidal excitations, the optimal buffer force-deflection characteristics under random excitations also converge to linear stiffness properties. The optimal stiffness properties are attained to allow the maximum use of available deflection, as observed earlier under harmonic excitations. Figure 7.9 illustrates the VDV ratio response of the suspension seat employing optimal buffer stiffness for two different values of buffer thickness. The figure shows the VDV ratio under three excitation spectra with acceleration levels of 2.35, 3.53 and 4.70 m/s^2 rms, indicated by 100%, 150% and 200% excitation magnitude. The VDV ratio response of the suspension seat with nominal buffer characteristics is also evaluated and compared with the optimal response in the figure. The figure also shows the VDV ratio response of an unsuspended cushion under the three excitation spectra considered. The optimal buffers, irrespective of the thickness, yield VDV ratio almost identical to that of the nominal buffer under 100% and 150%

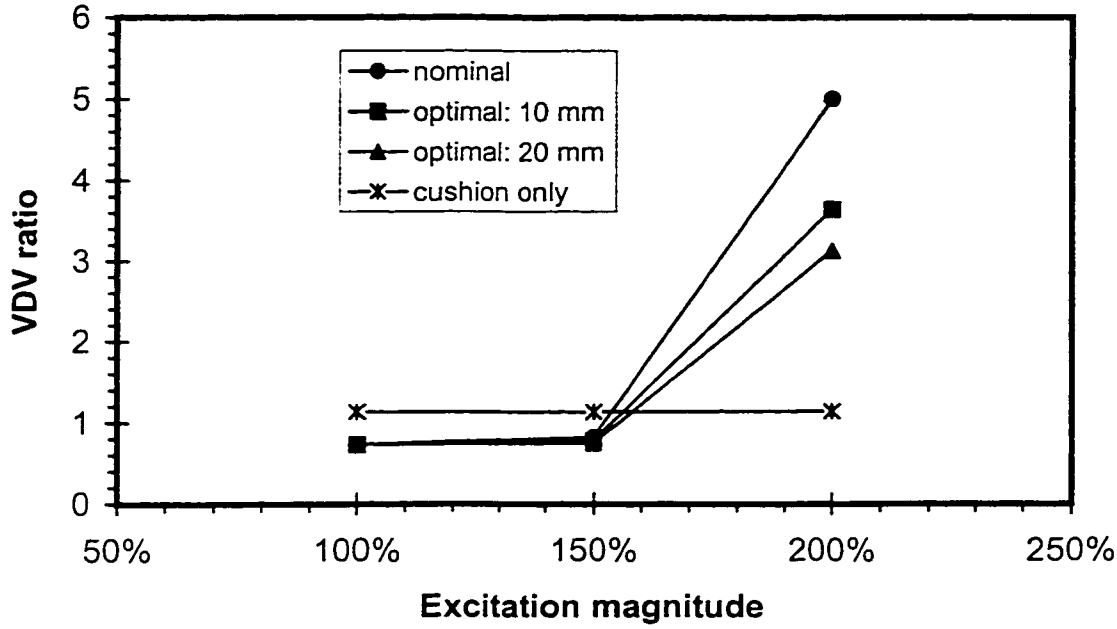

Figure 7.9: The VDV ratios as functions of vibration magnitudes under Class I excitation obtained using the the nominal and optimal buffer properties as well as the cushion only.

excitation spectra. The identical response of the nominal and optimal buffers is attributed to the absence of end-stop impacts under these excitations. Both buffers yield VDV ratio of approximately 0.73. It should be noted that both buffers yield a slight increase in VDV ratio under 150% excitation spectrum, which may be attributed to occasional impacts. The VDV ratio response of the nominal buffer approaches a value as high as 5, under 200% excitation spectra. The corresponding increase in the VDV ratio response of 10 mm and 20 mm thick optimal buffers with linear stiffness coefficients of 1.6×10^{5} and 4.5×10^{4} N/m, are obtained as 3.6 and 3.1 respectively. The results show trends similar to those observed for the optimal design under harmonic excitations, which further suggests the use of thick and soft buffers to minimize the severity of impacts.

7.7 General Design Guidelines for End-Stop Buffers

The results from the optimization studies suggest that soft end-stop buffers that can provide nearly linear stiffness over a large deflection are highly desirable to reduce the severity of end-stop impacts. The stiffness coefficient of the buffer, however, should be sufficiently high to prevent the buffer from being compressed to its high stiffness range, under motions most likely encountered in a specific vehicle where the seat is employed. This could be realized by implementing relatively thick buffers with low stiffness. Thicker buffers, however, reduce the suspension free travel and thus may increase the probability of end-stop impacts. The selection of buffer thickness thus involves a compromise between its impact absorption capabilities and available effective travel. The travel and stiffness requirements are further dependent upon the magnitude and frequency contents of vehicular vibration. The design of end-stop buffers thus,

ideally, involves optimization corresponding to the specific application of a suspension seat. It may be recommended that the physical suspension travel limits ($d_m^{(t)}$ and $d_m^{(t)}$) be relaxed to allow for the installation of thicker and softer buffers in order to reduce the severity of end-stop impacts, without increasing the frequency of their occurrence.

From the results of the optimization study, it is evident that optimal elastic buffers yield less severe end-stop impacts than those encountered with the nominal buffer coefficients. The performance benefits of the optimal buffer are clearly illustrated in terms of its VDV ratio response, which is considerably lower than that with conventional buffers. The VDV ratio of the seat with optimal buffers under large magnitude of excitation, however, is considerably higher than unity, suggesting that the suspension seat amplifies the vibration transmitted to the seated driver. Under such excitations, an unsuspended seat (cushion only) yields a VDV ratio of 1.14, which is considerably lower than that due to seat with optimal buffer. This low VDV ratio may not be achieved with a suspension seat with any optimal buffer design. Under low magnitude excitations (below 150%), however, an unsuspended seat results in VDV ratio larger than that due to the optimal suspension seat (1.13 versus 0.72). It is therefore reasonable to recommend that the suspension seat operate only when end-stop impacts occur occasionally. Under vibration excitations inducing repetitive and severe end-stop impacts, it is preferable to lock up the suspension mechanism manually or automatically. The threshold of suspension lock-up, however, would depend on the specific application of the seat.

7.8 Summary

Conventional suspension seats use rubber buffers to reduce the severity of end-stop impacts. Many of the buffer designs induce severe end-stop impacts. The severity of end-stop impacts is strongly related to the stiffness and thickness of rubber buffers, and the magnitude and frequency contents of the excitation. An optimization problem is formulated to identify optimal stiffness characteristics of the buffer as functions of excitation magnitude, free travel or buffer thickness. A parametric study is performed to demonstrate the negligible contributions due to buffer hysteresis to the overall suspension response. The solution of an optimization problem under both harmonic and random vibration excitations revealed that relatively soft and thick buffers are desirable to minimize the severity of impact, measured in terms of VDV ratio. The solution also converged to buffer design with linear stiffness characteristics, irrespective of type and magnitude of excitation, and the available travel. The results show that optimal thick buffers yield VDV ratio response, which is nearly 38% lower than that caused by the conventional suspension seat design. Although end-stop buffers can be optimized to some degree through selection of stiffness and thickness, the VDV ratio response under large magnitudes of excitation invariantly remains higher than unity. On the other hand, an unsuspended seat yields considerably lower VDV ratio under relatively high magnitude excitation. Under such excitations, a suspension seat with passive elastic buffers and travel limits, will always yield large values of VDV ratio. It is therefore recommended that the suspension seat only operate when end-stop impacts do not occur or occur occasionally. Under vibration excitations inducing repetitive and severe end-stop impacts, it is preferable to lock up the suspension mechanism.

CHAPTER 8

CONCLUSIONS AND RECOMMENDATIONS FOR FUTURE WORK

8.1 General

Many vehicles employed in industrial, agricultural, forestry and transport sectors pose vertical vibration and shock of comprehensive magnitude in the 1 to 20 Hz frequency range. The magnitude of such whole-body vibration is known to be especially significant in the 1 to 5 Hz frequency range. Prolonged exposure to such vibration and shocks is known to contribute to the degradation of health and comfort of drivers. Suspension seats, with a suspension mechanism mounted below or behind the seat cushion, have been developed to attenuate such low frequency vibration. The suspension mechanisms are designed with low stiffness to achieve effective vibration isolation performance, but limited travel so as not to impede drivers' interactions with the controls. Suspensions with low stiffness yield a large dynamic deflections when exposed to shocks, or low frequency and high magnitude vibration. Large magnitude relative deflection response often causes the suspension to reach its travel limits, and produce an impact against end-stop buffers. The operator is thus subject to repetitive shock motions, and exposure to such motion is known to be more detrimental to operator health and safety, than that due to the steady-state vibration. The thesis research was formulated to develop an analytical human-suspension seat model to effectively analyze the system and provide design guidelines to enhance driver protection under representative off-road vehicle vibration environments.

8.2 Highlights of the Study

The study of suspension seats, and transmission of vibration and shock motion to the driver involves biodynamic characterization of the seated driver, and analyses of suspension seat and coupled human-suspension seat systems. The thesis research is therefore carried out in systematic phases: (i) synthesis of biodynamic response characteristics of seated drivers and development of a seated human body model; (ii) development and validation of a coupled human-suspension seat system model; and (iii) parametric sensitivity analyses and optimization of the coupled dynamic system to maximize isolation of steady-state vibration and minimize the severity of end-stop impacts. The major highlights of this investigation are summarized as follows:

Factors Influencing the Biodynamic Response Characteristics of Seated Drivers

The human body exhibits complex biodynamic response characteristics, which are affected by many factors, including posture, mass, and vibration magnitude and frequency. The biodynamic response data reported in published study is thoroughly analyzed in an attempt to characterize the contributions due to these factors. Although body size and mass can have a definite influence on the driving-point mechanical impedance (DPMI) or apparent mass (APMS) and seat-to-head transmissibility (STHT), it is changes in the body posture (i.e. back support, torso inclination, muscle tension, feet support, etc.) that often cause the largest variations. The STHT, in general, is found to be more sensitive to changes in seated posture than the APMS or DPMI. Excitation levels, if varied within a wide range, can cause the resonant frequency of the seated body and the magnitudes of DPMI/APMS and STHT to shift towards lower values. The analysis of the

reported data clearly reviewed highly complex contributions due to variations in the test conditions, and subject characteristics. A generalized range of biodynamic response characteristics may be identified, when variation in test conditions are controlled within acceptable bounds. For applications involving vehicular whole-body vibration and shock environment, it is vital to identify a range of representative working conditions under which the limits of biodynamic response behavior may be established.

Data Synthesis of Biodynamic Response Characteristics of Seated Drivers

Due to the significant variations in subject population and posture, and magnitude and types of excitations used in different studies, the reported data in the literature differ considerably in magnitude and phase response in terms of DPMI/APMS and STHT. The measured biodynamic data acquired from 22 different studies, were examined in view of the test conditions, subject population and biodynamic measures. The data sets acquired under conditions considered to be representative of vehicular vibration and shock were further analyzed to derive a range of idealized biodynamic response characteristics. A synthesis of selected data grouped under similar test conditions was performed to characterize the DPMI/APMS and STHT of the seated subjects with feet supported, and exposed to vibration excitation levels lower than 5 ms^{-2} in the 0.5 to 20 Hz frequency range. The variations among the selected data sets were further reduced by excluding outliers and odd-behaved data sets based on the standard deviation analysis. The data that fall within the proposed range of idealized values are considered to provide acceptable representation of the seated human body's biodynamic response behavior under the specific range of conditions.

Relationship between Biodynamic Response Functions

The driving-point mechanical impedance (DPMI) or apparent mass (APMS) and seat-to-head transmissibility (STHT) have been extensively used to characterize whole-body dynamic response to vibration. While both the DPMI and APMS describe the force-motion relationship at the human-seat interface, different studies have employed these functions interchangeably assuming that they represent the data equivalently. Relationships between the two functions and between the functions and STHT, are investigated through an analysis of measured data and selected human body models. Both the experimental data and theoretical analyses, revealed that the APMS tends to yield smaller variations in the primary resonant frequency than those obtained from the DPMI data. The primary resonant frequency derived from the APMS data most likely represents the damped natural frequency of the biodynamic system, while the DPMI data yields considerably higher resonant frequency. It has been concluded that the wide range of variation in the primary resonant frequency is inherent in the biodynamic measure based upon DPMI. Although not related by definition, the similarities between the normalized APMS and STHT were clearly established, especially in view of the primary resonant frequency.

From the analysis of four different biodynamic models, it was concluded that both the APMS and STHT functions yield primary resonant frequency close to the damped natural frequency of the dynamic system. The results suggest the possibility of developing a simple and unique human body model based on both the APMS and STHT response characteristics.

Human Body Model Development

Majority of the human body models reported in the literature have been derived on the basis of APMS/DPMI or STHT. Such models thus do not correlate well with both 'to the body' and 'through the body' functions. It is proposed that the uniqueness of the human body model can be significantly enhanced by curve-fitting the magnitude and phase response characteristics of both the 'to the body' and 'through the body' biodynamic behavior of the seated subject in terms of the APMS and STHT functions. Only a few models have been derived on the basis of DPMI/APMS and STHT data. However, these models were derived based on DPMI/APMS and STHT data measured separately and/or under vaguely defined test conditions. In view of the influence of various test conditions on the measured responses, a human body model should be based on APMS and STHT data measured under identical test conditions, which represent the typical conditions encountered in heavy road or off-road vehicle driving.

Laboratory tests were performed to measure the STHT and APMS response of a group of subjects under selected test conditions. The inertia and pitch corrections were performed to derive the mean and range of APMS and STHT data for the test subjects. A three degree-of-freedom linear human body model is proposed and its parameters are identified from both the measured APMS and STHT data using multi-parameter optimization techniques. A generally good agreement between the computed and measured biodynamic response characteristics was obtained under the representative test conditions. The proposed model is thus considered applicable for the study of seating dynamics in off-road vehicles.

Investigation of Dynamic Pressure Distribution at the Human-Seat Interface

The pressure distribution at the human-seat interface affects the comfort of vehicle drivers. While some studies reported the measurements of pressure distribution under static seating, the dynamic pressure distribution on automotive seats has not been investigated. The effects of magnitude and frequency of vibration on the pressure distribution on both rigid and soft seats are investigated in terms of ischium pressure, effective contact area and contact force. The measured data is analyzed to examine the effectiveness of analytical representation of a seat cushion.

The study revealed that under vibration excitation, the maximum variations in the ischium pressure and the effective contact area on a soft seat occur around the resonant frequency of the human-seat system. An increase in excitation magnitude causes increased maximum ischium pressure and maximum effective contact area around the resonant frequency of the human-seat system. The time histories of dynamic ischium pressure, effective contact area and contact force on the rigid seats are almost symmetric with respect to their static values within the ranges of excitation magnitude and frequency considered in the study. Those measured on the soft seat, however, revealed significant asymmetry, when the excitation magnitude is large and the excitation frequency is in the vicinity of the resonant frequency of the human-seat system. The asymmetric response characteristics of the cushion are mostly attributed to the nonlinear force-deflection properties of polyurethane foam materials, contour shape of human buttocks, body-hop motion and cushion bottoming tendencies. The results suggest that a nonlinear cushion model may need to be developed to account for these behaviors.

Development of a Nonlinear Seat Cushion Model

Based on the study of dynamic pressure distribution, a nonlinear seat cushion model is developed and validated. The nonlinear analytical model is analyzed to derive contact force and acceleration transmissibility, which are compared with the corresponding measured data. The comparison revealed good agreement between the model response and measured data in terms of contact force and acceleration transmissibility. The model is further analyzed to demonstrate the occurrence of body hop motion and cushion bottoming under high magnitudes of excitation, which may occur in off-road vehicle operation.

Development of a Human-Suspension Seat System Model

A coupled human-suspension seat system models is derived upon integrating the proposed human body and cushion models to a nonlinear suspension model. The suspension seat model is developed incorporating nonlinear and asymmetric force-velocity and force-deflection properties of the damper and elastic end-stops. The Coulomb friction due to suspension linkages is represented by an ideal friction force. The coupled human-suspension seat system model was analyzed under harmonic and random excitations of two different classes of vehicles. Laboratory tests were performed and the measured data was analyzed to derive the acceleration transmissibility and PSD of acceleration. The validity of the proposed combined human-suspension seat model was demonstrated by comparing the computed acceleration transmissibility and dynamic response characteristics under given vibration excitations, with the measured data. The combined model revealed a close agreement with the measured data under both

excitations. The proposed model is thus considered a valid and effective tool to study the steady-state vibration and end-stop impacts performance of suspension seats.

Optimization of Human-Suspension Seat System for Vibration Attenuation

Suspension seats are generally designed to attenuate steady-state vibration, which is strongly affected by many design factors in a complex manner. A parametric sensitivity analysis was thus conducted to identify the factors that affect the vibration isolation performance most significantly. Suspension spring rate and damping coefficients were found to be two key factors influencing the vibration attenuation performance, and a soft spring and a light damping generally resulted in improved vibration attenuation performance. The results of the study further revealed that attenuation of continuous and transient vibration imposes conflicting design requirements. It is proposed to optimize the suspension design to maximize the attenuation performance under steady-state vibration, while the severity of impacts be minimized through design of end-stop buffers. An optimization function was thus formulated to minimize the SEAT value under excitation arising from two different classes of vehicles. The peak relative displacement was constrained to be lower than the permissible travel to minimize the occurrence of occasional end-stop impacts. For the specified excitation spectra defined in ISO 7096, a set of design parameters were recommended for optimal attenuation of steady-state vibration, by limiting the relative displacement of suspension within a predefined constraint range. These optimal design parameters are considered to be applicable to suspension seats used in vehicles whose floor vibration spectra are similar to those defined in the standard.

Analysis of Suspension Seat End-Stop Impacts

Suspension seat end-stop impacts occur when the suspension approaches the end of its travel during exposure to shocks or low frequency high magnitude excitations. Exposure to such repetitive impacts may result in an increased risk of injuries among drivers. While the severity of such impacts may be reduced through appropriate selection of suspension stiffness and damping properties, such adjustments involve a compromise in view of vibration isolation performance. Current designs of suspension seats, invariably, employed elastic end-stop buffers to limit the suspension displacement to within a fixed clearance, while some seat designs use stiff buffers resulting in transmission of high magnitude shock motions arising from end-stop impacts. A comprehensive analytical model of elastic buffer is proposed to incorporate its nonlinear force-deflection and energy dissipation properties. A second stage optimization is performed to minimize the severity of impacts by minimizing the vibration dose value (VDV) ratio of the human-suspension seat system. The optimization is performed under both harmonic and random excitations of different magnitudes to identify desirable force-deflection characteristics of buffers. The results of the optimization study revealed that soft and thick buffers with linear stiffness characteristics over a large range of deflection, are highly desirable for reducing the severity of end-stop impacts.

8.3 Conclusions

On the basis of the studies conducted in this dissertation, the following major conclusions are drawn:

- The biodynamic response behavior of seated subjects is invariably described in terms of the driving-point mechanical impedance (DPMI) or apparent mass

(APMS) and seat-to-head transmissibility (STHT). Both the DPMI and APMS describe 'to the body' biodynamic response, while STHT describes 'through the body' biodynamic response.

- From study of reported biodynamic characteristics, it is apparent that DPMI/APMS and STHT are influenced by many factors related to subject characteristics and test conditions.

- The DPMI or APMS of seated subjects is affected primarily by the body mass and factors affecting the seated posture, such as presence or absence of back support, backrest inclination, muscle tension and feet support.

- The STHT is affected primarily by the seated postures, including head position, torso inclination, backrest contact and muscle tension. The 'through the body' or STHT biodynamic function revealed significant sensitivity to variations in postural factors, than 'to the body' or DPMI/APMS functions.

- The DPMI/APMS and STHT are affected by the excitation magnitude only if the magnitude is varied considerably.

- The DPMI/APMS magnitude exhibits peaks near 5 Hz and 10 Hz, which are considered as the resonances associated with deflections of the chest and spinal supporting structure, and caused by the contact between the thighs and the seat pan, respectively.

- In view of extensive variations in the reported biodynamic functions and complexities associated with identification of sources of variability, it is proposed that limits of biodynamic response functions be established for a specific application. A range of representative working conditions applicable to vehicle driving can be identified under which the limits of biodynamic response behavior must be derived.

- The target values and envelopes of the DPMI/APMS and STHT are derived, by limiting the selection of data sets measured under identified test conditions commonly encountered during off-road vehicle driving, and further by excluding outliers and odd-behaved data sets based on standard deviation analysis.

- Representation of 'to the body' functions in terms of DPMI and APMS revealed that APMS reveals considerably less variations in primary resonant frequency than that observed in DPMI.

- Analysis of selected biodynamic models revealed certain similarities in the magnitude and phase response of normalized APMS and the STHT, specifically in terms of primary resonant frequency. The analysis revealed considerable variations and discrepancies when DPMI function is considered. The DPMI function further revealed higher sensitivity to variations in model parameters. It is

thus recommended to describe 'to the body' biodynamic response in terms of APMS.

- The APMS and the STHT of six subjects are measured under test conditions specified in the criteria. The measured vertical acceleration of the head revealed significant contribution due to its pitch motion, which can be corrected through measurement of pitch acceleration and consideration of pitch oscillation center.

- A reasonable agreement is found between the measured data and the idealized values determined in the data synthesis. Analysis of the measured data further demonstrated the similarity between the APMS and STHT biodynamic functions, especially in terms of primary resonant frequency.

- Biodynamic models developed on the basis of one biodynamic function, in general, yield poor agreement with the other biodynamic function. The uniqueness and validity of the seated body model can be considerably enhanced upon appropriate consideration of magnitude and phase components of both 'to the body' and 'through the body' biodynamic functions. A three degree-of-freedom seated human body model, derived on the basis of both APMS and STHT data for drivers maintaining an ENS posture, resulted in good agreement with both the measured APMS and STHT data.

- The pressure distribution at the human-seat interface under static and dynamic seating was measured on both a rigid and a soft seat. While the rigid seat yields high concentration of interface pressure near the tuberosities, the soft seat tends to distribute the contact force over a wider contact area. The soft seat, however, causes relatively high pressure in the thigh-cushion contact area, which may cause operator discomfort. The magnitude of contact force and ischium pressure approaches peak values under vibration excitation near the resonant frequency of the coupled human-seat system, irrespective of the seat characteristics, posture and body weight.

- The dynamic ischium pressure, the dynamic contact force and the effective contact area at the human-cushion interface exhibit strong asymmetries with respect to their static values under large excitation magnitude and at frequencies near the resonant frequencies of the human-suspension seat system, contributed by nonlinear properties of the seat cushion and buttocks tissue, and contour shape of the buttocks.

- A nonlinear and asymmetric seat cushion model is developed which accounts for the body hop motion and the cushion bottoming. The analytical model revealed good agreement with the measured data in terms of acceleration transmissibility, contact force, and cushion bottoming and body hop tendencies.

- The design and assessment of shock and vibration attenuation performance of suspension seats necessitate analysis of seating dynamics coupled with

biodynamic response characteristics of the seated body. A coupled human-suspension seat model, developed upon incorporating the proposed three degree-of-freedom seated body and nonlinear cushion models, can serve as an effective design and assessment tool. The nonlinear suspension model was developed upon incorporating multi-stage asymmetric damping, and nonlinear force-deflection characteristics due to elastic end-stop buffers.

- A comparison of the response characteristics of the analytical human-suspension seat model with the laboratory measured data revealed high degree of validity of the model under both harmonic and random vehicular vibration.

- The influence of variations in design parameters of the coupled human-suspension seat model is investigated in terms of seat acceleration transmissibility and SEAT (Seat Effective Amplitude Transmissibility) value under both harmonic and random excitations defined for two different classes of vehicles. The results of parametric sensitivity analyses revealed that variations in suspension spring rate, low speed compression damping coefficient, suspension mass, friction, damper inclination angle and cushion stiffness affect the seat performance considerably.

- Attenuation of continuous and transient or shock type excitation poses conflicting design requirements for the suspension seats. High magnitude transient excitations cause severe end-stop impacts due to travel limits of the suspension. While attenuation of continuous vibration requires soft and lightly damped suspension, the control of shock motion can be achieved through high damping and relaxed travel limits. Since continuous vibration predominate the whole-body vehicular vibration environment encountered during majority of the operations, it is desirable to design suspension seats for maximum vibration isolation. The severity of end-stop impacts can be reduced through optimal design of elastic buffers.

- The optimal design of suspension seats for isolation of vibration can be realized by minimizing SEAT value, while limiting the peak dynamic deflection below the free travel limits. The optimal design under Class I excitation, predominant around 1.85 Hz, consisted of lighter damping, softer spring rate, lower degree of damping asymmetry and larger suspension mass, than the nominal design. The optimal design resulted in SEAT value of 0.73 under Class I excitation, which is 26% lower than that obtained with nominal suspension. The optimal design for Class II excitation, predominant about 2.1 Hz, converged towards undamped and low spring rate suspension. The resulting SEAT value was obtained to be 0.3, which is 68% lower than that obtained for the nominal suspension.

- An optimal design vector based upon Class I excitation is recommended, since this class represents more severe excitation among the two classes considered.

- The suspension performance under high magnitude excitations involving end-stop impacts can be best assessed in terms of VDV (Vibration Dose Value) ratio. The severity of end-stop impacts may thus be related to the VDV ratio.

- The design optimization for reducing the end-stop impact severity is performed by minimizing the VDV ratio under both harmonic and random excitations of varying magnitudes. Since the results of an analytical study revealed negligible contributions due to hysteresis of buffers, the design optimization studies thus focus on the elastic force-deflection properties of end-stop buffers. The optimization studies, invariably, converged towards elastic buffers with linear stiffness characteristics, irrespective of magnitude and type of excitation.

- It is concluded that the severity of impacts or VDV ratio can be best minimized by introducing thick and soft buffers with linear stiffness properties. Sufficiently high stiffness, however, is vital to prevent the suspension approaching its maximum available travel.

- Relaxed free travel can further reduce the VDV ratio response.

- Although thick buffers may lead to more frequent impacts, their low stiffness properties tend to reduce the severity of impacts.

- The suspension seat equipped with optimal elastic buffers resulted in VDV ratios of 3.5 and 3.1 with two values of buffer thickness, respectively, under random excitation synthesized as 200% of the magnitude of Class I excitation. The values are nearly 70% and 62% of that attained with nominal buffer suspension. Although the optimal designs result in lower values of VDV ratio, the response still tends to be considerably large.

- Under high vibration excitation levels, when repetitive and severe end-stop impacts occur, it is preferable to lock up the suspension mechanism. A cushion seat yields considerably lower value of VDV ratio, when compared to that of the suspension seat under such excitations.

8.4 Recommendations for Future Studies

The following areas are recommended for future research:

- The human body model developed in this study is actually a mathematical curve-fitting model. In order to develop anatomical subsystem model describing accurately the body dynamics, more measurements on the seat-to-body segments transmissibility are needed to understand the way vibration is transmitted through the human body. The measurements should include the vibration transmission along the pitch direction, and the model may have degrees-of-freedom in the pitch mode.

- The human body model developed in this study is primarily applicable to the study of off-road vehicle driver seating, where the seated posture is usually an ENS posture. Errors may be expected, when the model is applied to study the seating dynamics in vehicles where the driver usually assumes an EBS posture. The human body model parameters should thus be identified to characterize the biodynamic response for the EBS posture.

- A more accurate seat cushion model may be needed to account for the load and frequency dependencies of the stiffness and damping coefficient.

- Comprehensive criteria need to be developed to evaluate the overall performance of suspension seats, including attenuation of steady state vibration, prevention of end-stop impacts, and the frequency of occurrence of end-stop impacts and body hop motion.

- The threshold of vibration excitation above which a suspension mechanism is undesirable needs to be examined based on the field measurements of vehicle vibration. A control mechanism may be proposed to lock-up the suspension based upon feedback from the frequency of impacts and VDV ratio.

REFERENCES

1. Griffin, M.J. (1990) "Handbook of Human Vibration", Academic Press Limited, London.

2. Marsh, J.A. (1965) "A case for engineered vehicle suspension seating and a review of current developments", The Institution of Body Engineers, Institute Bulletin 29, 607.

3. Suggs, C.W. and Huang, B.K. (1969) "Tractor cab suspension design and scale model simulation", Transactions of the American Society of Agricultural Engineers, 14, 283-289.

4. Stikeleather, L.F. Hall, G.O. and Radke, A.O. (1972) "A study of vehicle vibration spectra as related to seating dynamics", SAE Paper 720001, Automotive Engineering Congress, Detroit, 10-14, January, Society of Automotive Engineers, Detroit, Michigan.

5. Rakheja, S. (1983) "Computer-aided dynamic analysis and optimal design of suspension systems for off-road tractors", Ph.D. Thesis, Concordia University, Montreal, Canada.

6. Stiles, M.A. (1994) "A farmer's daily dose - part II, Result of the tractor ride vibration survey", The UK Informal Group Meeting on Human Response to Vibration, INM, Gosport, 19-21 September.

7. Burdoff, A. and Swuste, P. (1993) "The effect of seat suspension on exposure to whole-body vibration of professional drivers", Annals of Occupational Hygiene, 37(1), 45-55.

8. Boileau, P.-É. (1995) "A study of secondary suspension and human driver response to whole-body vehicular vibration and shock", Ph.D., Thesis, Concordia University, Montreal, Canada.

9. Stikeleather, L.F. and Suggs, C.W. (1970) "An active seat suspension system for off-road vehicles", Transactions of the American Society of Agricultural Engineers, 13, 99-106.

10. Rakheja, S. and Sankar, S. (1985) "Vibration and shock isolation performance of a semi-active 'on-off' damper", Transactions of the ASME, Journal of Vibration, Acoustics, Reliability in Design, 107.

11. Stein, G.J. and Ballo, I. (1991) "Active vibration control system for the driver's seat for off-road vehicles", Vehicle System Dynamics, 20, 57-78.

12. Coermann R.R. (1962) "The mechanical impedance of the human body in sitting and standing position at low frequencies", Human Factors, 227-253.

13. Rakheja, S., Ahmed, A.K.W., *et al* (1991) "Ride performance characteristics of seat-suspension systems and influence of the seated driver", ASAE Paper No. 917569, Chicago, Illinois.

14. Corbridge, C. (1987) "Vertical vibration transmission through a seat: effects of vibration input, subjects' postures and subjects' physical characteristics", The UK informal Group Meeting on Human Response to Vibration, Royal Military College of Science, Shrivenham, England, 21-22 September.

15. Hinz, B., Menzel, G., Bluthner, R. and Seidel, H. (1998) "Laboratory testing of operator seat vibration with 37 subjects – Critical comment on ISO/DIS 7096", Journal of Sound and Vibration, 215(4), 977-988.

16. Suggs, C.W., Abrams, C.F. and Stikeleather, L.F. (1969) "Application of a damped spring-mass human vibration simulator in vibration testing of vehicle seats", Ergonomics, 12, 79-90.

17. Fairley T. E. and Griffin M.J. (1989) "The apparent mass of the seated human body: vertical vibration", Journal of Biomechanics, 22, 81-94.

18. Muksian, R. and Nash, C. D. A., (1974) "A model for the response of seated humans to sinusoidal displacements of the seat", Journal of Biomechanics, 7, 209-215.

19. Amirouche, F. M. L. and Ider, S. K. (1988) "Simulation and analysis of a biodynamic human model subjected to low accelerations - a correlation study", Journal of Sound and Vibration, 123, 281-292.

20. Patil, M. K. and Palanichamy, M. S. (1988) "A mathematical model of tractor-occupant system with a new seat suspension for minimization of vibration response", Applied Mathematical Modeling, 12, 63-71.

21. Mertens H. (1978) "Nonlinear behavior of sitting humans under increasing gravity", Aviation, Space, and Environmental Medicine, 287-298.

22. International Standard for Standardisation (1993) "Mechanical driving point impedance and transmissibility of the human body", Draft CD 5982.

23. Wu, X. and Griffin, M.J. (1998) "The influence of end-stop buffer characteristic on the severity of suspension seat end-stop impacts", Journal of Sound and Vibration, 215(4), 989-996.

24. Vogt, H.L., Coermann, R.R. and Fust, H.D. (1968) "Mechanical impedance of the sitting human under sustained acceleration", Aerospace Medicine, 39, 675-679.

25. Miwa T. (1975) "Mechanical Impedance of Human Body in Various Postures", Industrial Health, 13, 1-22.

26. Griffin, M.J., Lewis, C.H., Parsons, K.C. and Whitham, E.M. (1979) "The biodynamic response of the human body and its application to standards", AGARD Conference Proceedings No. 253, Paris, France.

27. Donati, P.M. and Bonthoux, C. (1983) "Biodynamic response of the human body in the sitting position when subjected to vertical vibration", Journal of Sound and Vibration, 90, 423-442.

28. Hinz, B. and Seidel, H. (1987) "The nonlinearity of the human body's dynamic response during sinusoidal whole body vibration", Industrial Health, 25, 169-181.

29. Holmlund P., Lundström R. and Lindberg L. (1995) "Whole-body vibration mechanical impedance of human body in the vertical direction", Proceedings of the UK Informal Group Meeting on Human Response to Vibration, Silsoe, United Kingdom.

30. Seidel, H. (1996) "A contribution to the revision of ISO 5982 «Mechanical driving point impedance and transmissibility of the human body»", Personal Communications to A.J. Brammer.

31. Boileau, P.-É. and Rakheja S. (1998) "Whole-body vertical biodynamic response characteristics of the seated vehicle driver: Measurement and model development", International Journal of Industrial Ergonomics, 22, 449-472.

32. International Standard for Standardisation (1994) "Earth-moving machinery – operator seat – transmitted vibration", ISO 7096.

33. International Organization for Standardization (1987) "Agricultural wheeled tractors - operator's seat - laboratory measurement of transmitted vibration", ISO/DIS 5007.

34. Paddan, G.S. and Griffin, M.J. (1988) "The transmission of translational seat vibration to the head – I. Vertical seat vibration", Journal of Biomechanics, 21, 191-197.

35. Zimmermann, C.L. and Cook, T.M. (1997) "Effects of vibration frequency and postural changes on human responses to seated whole-body vibration exposure", Archives of Occupational and Environmental Health, 69, 165-179.

36. Magnusson, M., Pope, M., Rostedt, M. and Hansson, T. (1993) "Effect of backrest inclination on the transmission of vertical vibrations through the lumbar spine", Clinical Biodynamics, 8, 5-12.

37. Cooper, A.J. (1986) "Effect of head inclination on transmission of vertical vibration to the heads of seated subjects", Proceedings U.K. Informal Group Meeting on Human Response to Vibration, Loughborough University of Technology, 22-23, September.

38. Messenger, A.J. and Griffin, M.J. (1989) "Effects of anthropometric and postural variables on the transmission of whole-body vertical vibration from seat to head", Institute of Sound and Vibration Research, University of Southampton, ISVR Technical Report No. 172.

39. Griffin, M.J. and Whitham, E.M. (1978) "Individual variability and its effect on subjective and biodynamic response to whole-body vibration", Journal of Sound and Vibration, 58, 239-250.

40. Edwards, R.G. and Lange, K.O. (1964) "A mechanical impedance investigation of human response to vibration", AMRL-TR-64-91 Aerospace Medical Research Laboratories, Wright-Patterson Air Force Base, Ohio.

41. Fairley T.E. and Griffin M.J. (1990) "The apparent mass of the seated human body in the fore-and-aft and lateral directions", Journal of Sound and Vibration, 139, 299-306.

42. Smith, S.D. (1993) "Comparison of the driving -point impedance and transmissibility techniques in describing human response to whole-body vibration", Proceedings U.K. Informal Group Meeting on Human Response to Vibration, APRE, Farnborough, The United Kingdom.

43. Fairley, T.E. and Griffin, M.J. (1983) "Application of mechanical impedance methods to seat transmissibility", International Conference on Noise Control Engineering, Edinburgh, 533-536.

44. Fairley, T.E. and Griffin, M.J. (1986) "A test method for predicting of seat transmissibility", Society of Automotive Engineer International Congress and Exposition, Detroit, 24-28 February, SAE 860046.

45. Sandover, J. (1982) "Measurements of the frequency response characteristics of man exposed to vibration", Ph.D. Thesis, Loughborough University of Technology.

46. Griffin, M.J., Lewis, C.H., Parsons, K.C. and Whitham, E.M. (1978) "The biodynamic response of the human body and its application to standards", AGARD Conference Proceedings No. 253, Paris, France.

47. Allen, G. (1978) "A critical look at biodynamic modeling in relation to specifications for human tolerance of vibration and shock", Paper A25-5, AGARD Conference Proceedings No. 253, Paris, France, 6-10 November.

48. Society of Automotive Engineers (1980) "Determining operator seat location on off-road work machines", SAE J1163.

49. Society of Automotive Engineers (1988) "Operator's seat dimension for off-road self-propelled work machines", SAE J899, December.

50. Society of Automotive Engineers (1987) "Devices for use in defining and measuring vehicle seating accommodation", SAE J826, May.

51. Smith, S.D. (1992) "Nonlinear response behavior in the human exposed to whole-body vibration", Proceedings of the 63rd Shock and Vibration Symposium, I, 27-29, October, Las Cruces, NM, 13-22.

52. Paddan, G.S. and Griffin, M.J. (1998) "A review of the transmission of translational seat vibration to the head", Journal of Sound and Vibration, 215(4), 863-882.

53. Matsumoto and Griffin (1998) "Movement of upper-body of seated subjects exposed to vertical whole-body vibration at the principal resonance frequency", Journal of Sound and Vibration, 215(4), 743-762.

54. The MATH WORKS Inc. (1997) "MATLab application toolbox—users' manual".

55. Kumar, A., Bush, N.J. and Thakurta, K. (1994) "Characterization of occupant comfort in automotive seats", IBEC 94, Automotive Body Interior and Safety Systems.

56. Lindan, O., Greenway, R.W. and Piazza, J.M. (1965) "Pressure distribution on the surface of the human body: I. Evaluation in lying and sitting positions using a bed of springs and nails", Archive of Physical Medicine and Rehabilitation, 378-385, May.

57. Treaster, D. (1987) "Measurement of seat pressure distribution", Human Factors, 29(5), 563-575.

58. Key, A.G., ChB, M.B., Manley, M.T., and Wakefield, E. (1978-79) "Pressure redistribution in wheelchair cushion for paraplegics: its application and evaluation", Paraplegia, 16, 403-412.

60. Sanders, M.S. and McCormick, E.J. (1987) "Human Factors in Engineering Design", McGraw-Hill, New York.

61. Ng, D., Cassar, T. and Gross, C.M. (1995) "Evaluation of an intelligent seat system", Applied Ergonomics, 26, 2, 109-116.

62. Bowers-Carnahan, R., Carnahan, T., Tallis-Crump, R., Crump, R., Faulkner, D., Martin, P., Sanford, L., and Walters, J. (1995) "User perspectives on seat design", International Truck and Bus Meeting and Exposition, Winston-Salem, North Carolina, 13-15 November, SAE No. 952679.

63. Thakurta, K., Koester, D., Bush N. and Bachle, S. (1995) "Evaluating short and long term seating comfort", International Congress and Exposition, Detroit, Michigan, February 27-March 2, SAE Paper No. 950144.

64. Hilyard, N.C., Collier, P. and Care, C.M. (1983) "Dynamic mechanical behaviour of flexible foam cushion materials and its influence on ride comfort", The UK informal Group Meeting on Human Response to Vibration, the National Institute of Agricultural Engineering, Silsoe, Bedfordshire, England, 14-16 September.

65. Ebe, K. (1993) "Effect of composition of polyurethane foam on the vibration transmissibility of automotive seat", The UK informal Group Meeting on Human Response to Vibration, Ministry of Defense, Farnborough, Hampshire, England, 20-22 September.

66. Ebe, K. (1997) "Effect of thickness on static and dynamic characteristics of polyurethane foams", The UK informal Group Meeting on Human Response to Vibration, ISVR, University of Southampton, Southampton, England, 17-19 September.

67. Ebe, K. and Griffin, M.J. (1994) "Effect of polyurethane foam on dynamic sitting comfort", InterNoise 94, Pacifico Yokohama, Japan, 29-31, August.

68. Smith, S.D. (1994) "The effect of military aircraft seat cushion on human vibration response", The UK informal Group Meeting on Human Response to Vibration, the Institute of Naval Medicine, Alverstoke, Gosport, Hants, England, 19-21 September.

69. Wu, X. and Griffin, M.J. (1995) "Simulation study of factors influencing the severity of suspension seat end-stop impacts", The United Kingdom Informal Group Meeting on Human Response to Vibration, Silsoe Research Institute, Wrest Park, Silsoe, Bedford MK45 4HS, 18-20 September.

70. Swearingen, J.J., Wheelwright, C.D. and Garner, J.D. (1962) "An analysis of sitting areas and pressure of man (Report 62-1)", Oklahoma City, OK: Civil AeroMed. Research Institute.

71. Frisina, W. and Lehneis, H.R. (1970) "Pressure mapping: a preliminary report", Journal of Biomechanics, 3, 526.

72. Mooney, V., Einbund, J.J., Rogers, J.E. and Stauffer, E.S. (1971) "Comparison of pressure distribution qualities in seat cushions", Bulletin of Prosthetics Research, BPR, 10-16, 129-143.

73. Garber, S.L., Krouskop, T.A. and Carter, R.E. (1978) "A system for clinically evaluating wheelchair pressure relief cushions", American Journal of Occupational Therapy, 32, 565-570.

74. Bush, C.A. (1969) "Study of pressures on skin under ischium tuberosities and thighs during sitting", Archives of Physical Medicine and Rehabilitation, 60, 207-213.

75. Drummond, D.S., Narechania, R.G., Rosenthal, A.N., Breed, A.L., Lange, T.A. and Drummond, D.K. (1982) "A study of pressure distribution measured during balanced and unbalanced sitting", Journal of Bone and Joint Surgery, 64, 1034-1039.

76. Piché, A., Rakheja, S. Gouw, G.J. and Sankar, T.S. (1988) "Development of an elastic human-seat interface pressure sensing system", ICAART '88, Montreal, 118-119.

76. Gurram, R., Rakheja, S. and Gouw, G.J. (1995) "A study of hand grip pressure distribution and EMG of finger flexor muscles under dynamic loads", Ergonomics, 38, 4, 684-699.

77. Wu, X., Rakheja, S. and Boileau, P.-É. (1998) "Study of human-seat interface pressure distribution under vertical vibration", International Journal of Industrial Ergonomics, 21, 433-449.

78. Wu, X., Rakheja, S. and Boileau, P.-É. (1998) "Distribution of human-seat interface pressure on a soft automotive seat under vertical vibration", International Journal of Industrial Ergonomics, (awaiting for publication).

79. Society of Automotive Engineers (1988) "Force deflection measurements of cushioned components of seats for off-road work machines", SAE J1051, December.

80. Gent, A.N. and Thomas, A.G. (1963) "Mechanics of foamed elastic materials", The Proceedings of the 7th Annual Technical Conference of the Cellular Plastics, Division of the Society of the Plastics, New York.

81. "International Organisation for Standardisation (1992) Mechanical Vibration - laboratory method for evaluating seat vibration - part 1: basic requirement", ISO 10326-1.

82. Ahmed, A.K.W. and Rakheja, S. (1991) "An equivalent linearization technique for the frequency response analysis of asymmetric dampers", Journal of Sound and Vibration, 153(3), 537-542.

83. Rakheja, S., Sankar, S. and Afework, Y. (1989) "Vibration transmission performance of vertical seat suspension systems", Report submitted to IRSST, CONCAVE, 114.

84. Wu, X and Griffin, M.J. (1996) "Towards the standardization of a testing method for the end-stop impacts of suspension seats", Journal of Sound and Vibration, 192(1), 307-319.

85. International Standard for Standardisation (1997) "Evaluation of human exposure to whole-body vibration-part I: General requirements", ISO 2631/1 - Part 1: General requirements.

86. British Standard Institute (1987) "Measurement and evaluation of human exposure to whole-body mechanical vibration and repeated shock", BS 6841.

87. Thomson, W.T. (1993) "Theory of Vibration with Applications", 4th edition, Prentice-Hall Inc., New Jersey.

88. Wu, X. and Griffin, M.J. (1997) "A semi-active control policy to reduce the occurrence and severity of end-stop impacts in a suspension seat with an electrorheological fluid damper", Journal of Sound and Vibration, 203, 781-793.

89. Boileau, P.-É., Wu, X. and Rakheja, S. (1998) Definition of a range of idealized values to characterize seated body biodynamic response under vertical vibration.